February 7, 2022

Memo: Scientific Basis for Possible Revision of the Stipulated Order of Abatement (SOA)

From: Scientific Advisory Group (SAG)

To: Jon O'Brien, California Department of Parks and Recreation (CDPR)
Gary Willey, San Luis Obispo County Air Pollution Control District (SLOAPCD)

Cc: Sarah Miggins, California Department of Parks and Recreation (CDPR)
Liz McGuirk, California Department of Parks and Recreation (CDPR)

Executive Summary

Background. Since publication of the 2020 Annual Report and Work Plan (ARWP), the Scientific Advisory Group (SAG), in consultation with staff from the California Department of Parks and Recreation (CDPR) and the San Luis Obispo County Air Pollution Control District (SLOAPCD), has been reexamining the initial target set by the Stipulated Order of Abatement (SOA) for reducing emissions of PM10 (particulate matter with an aerodynamic diameter of less than 10 microns) from the Oceano Dunes State Vehicular Recreation Area (ODSVRA). The goal of the SAG's work has been to determine whether the initial SOA PM10 emissions reduction target appropriately reflects the contribution of off-highway vehicle (OHV) activity to emissions of PM10 dust at the ODSVRA, as determined by the difference between the 2013 baseline and conditions prior to OHV disturbance. The SAG's analysis of the SOA target is motivated, in part, by recent studies indicating that areas within the current OHV Riding Area formerly experienced lower PM10 emissions and higher protective vegetation cover than in the present day.

In tandem with its reexamination of the initial SOA target, the SAG has also been revisiting the procedures for determining the effectiveness of dust mitigation treatments toward achieving PM10 emissions reductions. This work is intended to assess the accuracy of current approaches to model the effect of existing and planned dust mitigation treatments on PM10 emissions reductions. Recent studies that explore certain effects of existing treatments, such as the downwind sheltering effect of the 48-acre foredune restoration project, are currently overlooked in modeling of PM10 reductions. In addition, the current assumption that all dust control treatments produce no dust emissions may overestimate the effectiveness of such control measures.

Summary of SAG findings. In this report, the SAG offers advice to guide a potential revision of the SOA. The SAG's findings are informed by ongoing research and monitoring of dust emissions and dune dynamics at the ODSVRA. At the recommendation of the SAG, CDPR commissioned several new studies to inform this work. These new studies are included as attachments to this report. Here, the SAG summarizes its two key findings on the SOA:

1. **SOA target.** If the management objective is to reduce emissions of PM10 from the ODSVRA to a level consistent with dust emissions prior to significant OHV disturbance, then there is a strong scientific justification based on recent modeling for adjusting the

PM10 emissions reduction target in the SOA from the initial 50% reduction to a value of 40.7%. This potential new SOA target would represent a reduction from 182.8 to 108.4 metric tons per day of PM10 emissions, as modeled for the existing 10 baseline days scenario applied to the ODSVRA Riding Area. This potential new target is based on modeling of a 1939 pre-disturbance emissions scenario, offering the more conservative (i.e., lower emissions) target among two modeled pre-disturbance scenarios (1939 and 1966). The 1939 scenario also shows a substantial reduction in ambient PM10 concentrations at the CDF and Mesa2 receptor sites relative to the 2013 baseline. It is important to note that, given the naturally dusty nature of the Oceano Dunes, exceedances of the California ambient PM10 air quality standard are unlikely to be eliminated for the existing SOA PM10 emission reduction target or for a refined value based on these pre-disturbance scenarios. *The SAG emphasizes that elimination of all California PM10 air quality exceedances would likely require a reduction in PM10 emissions far below what existed in the 1939 pre-disturbance scenario and would present a formidable engineering and management challenge.*

2. **PM10 emissions modeling framework.** To more accurately account for the effectiveness of dust mitigation treatments, the SAG advises that the 2022 ARWP adopt a revised approach to accounting for PM10 emissions reductions. The proposed framework for this revised accounting approach, which is informed by ongoing data collection and recent scientific studies on PM10 emissions within the ODSVRA, is described in detail in this report. Relative to the current accounting approach, some changes would increase credited PM10 emissions reductions, while other changes would decrease credited emissions reductions. The specific net effect of the proposed new PM10 emissions accounting framework, in terms of the overall acreage needed to meet the SOA target, would need to be determined via full implementation of this framework in tandem with preparation of the upcoming 2022 ARWP.

Scientific basis. The SAG's advised new PM10 emissions reduction target of 40.7% (relative to the 2013 baseline) was obtained by using the Desert Research Institute (DRI) emission-dispersion model to estimate the total mass emissions (metric tons per day of PM10 emissions) using an emissions grid that the SAG determined to best represent the emissivity within the ODSVRA in the absence of OHV activity. This pre-disturbance emissions grid uses a distribution of vegetation cover that is equivalent to that which existed prior to the present-day levels of OHV activity (1939 and 1966), and it uses meteorology of the 10 days of highest emissions in 2013, consistent with existing approaches to determining the baseline emission value of 182.8 metric tons per day of PM10 emissions, as defined in the current SOA.[1] Defining a dust mitigation target based on modeled mass emissions for a standard set of 10 high wind days (rather than observed airborne PM10 concentrations at specific receptor sites) retains the approach of the current SOA target, and it directly addresses the *total* impact of OHV disturbance on degraded air quality in a manner that is unaffected by wind variability from year to year.

[1] Mejia, J., Gillies, J. A. (January 10, 2022). "Model-Derived Estimates of Mass Emissions of PM10 for Pre-OHV Disturbance and Past Vegetation Scenarios" *[see Attachment 1 of this report]*

Key aspects of the SAG's approach to determining a new PM10 emissions reduction target are informed by extensive data collection and modeling built on peer-reviewed scientific findings. First, creation of the pre-disturbance emissions grid is based on multiple years of emissivity data obtained using the PI-SWERL (Portable In-Situ Wind Erosion Laboratory) instrument, the effectiveness of which has been documented in multiple peer-reviewed scientific studies. Analyses of these emissivity data, including a peer-reviewed study demonstrating a difference in emissivity between Riding and Non-Riding Areas,[2] address the effects of OHVs as well as an observed north-south emissions gradient across the ODSVRA. Second, modeling of PM10 emissions associated with this pre-disturbance grid utilizes the peer-reviewed DRI emission-dispersion model,[3] which is already the basis for SOA modeling efforts in the PMRP and ARWPs, and the predictions of which have shown excellent agreement with observations of PM10 concentrations within and downwind of the ODSVRA. Third, the vegetation maps representing the years 1939 and 1966 within the model were developed using aerial photographic images that were subject to quality assurance and intense scrutiny by CDPR and the SAG.[4] Ongoing speciation studies to determine the specific constituents of PM10 dust at the ODSVRA are also expected to provide useful information toward pinpointing mechanisms of PM10 generation; however, the approach described here addresses the total impact of OHV-related disturbance on all sources of PM10, not just specific constituents.

The SAG notes that its proposed new SOA target is designed to achieve a specific management objective: reducing PM10 emissions to levels associated with conditions prior to present-day levels of OHV disturbance, as represented by a 1939 emissions scenario. The SAG's analysis and proposed 40.7% emissions reduction target account for quantifiable uncertainties within this scenario. However, the SAG acknowledges the existence of unquantifiable uncertainties associated with defining a "natural" background condition. The Oceano Dunes are a dynamic system that has responded to changes in climate, sea level, and human activity over millennia, as documented in the geologic record.[5] Over the past few decades, dramatic growth of invasive weeds outside of ODSVRA Riding Areas has reduced the footprint of open sand surfaces that produce PM10 emissions, including at the Oso Flaco site upon which the current 50% emissions reduction target is based.[6] Therefore, the current 50% target likely represents a reduction of PM10 emissions to levels substantially below what existed prior to significant OHV disturbance. Even with such influence of invasive weeds, exceedances of the California PM10 ambient air quality standard are still known to occur at the Oso Flaco monitoring site, suggesting that complete elimination of California PM10 exceedances would require even further reductions in PM10 emissions beyond the current 50% target.

---

[2] Gillies, J. A., Furtak-Cole, E., Nikolich, G., Etyemezian, V. (2022). "The role of off-highway vehicle activity in augmenting dust emissions at the Oceano Dunes State Vehicular Recreation Area, Oceano, CA," *Atmospheric Environment: X, 13*, https://doi.org/10.1016/j.aeaoa.2021.100146

[3] Mejia, J. F., Gillies, J. A., Etyemezian, V. Glick, R. (2019). "A very-high resolution (20 m) measurement-based dust emissions and dispersion modeling approach for the Oceano Dunes, California," *Atmospheric Environment*, *218*, https://doi.org/10.1016/j.atmosenv.2019.116977

[4] Swet, N., Hilgendorf, Z., Walker, I. (February 2022). "UCSB Historical Vegetation Cover Change Analysis (1930-2020) within the Oceano Dunes SVRA" *[see Attachment 2 of this report]*

[5] Cooper, W. S., 1967. *Coastal Dunes of California*. Geological Society of America Memoir 104.

[6] Swet, N., Hilgendorf, Z., Walker, I. (February 2022). "UCSB Historical Vegetation Cover Change Analysis (1930-2020) within the Oceano Dunes SVRA" *[see Attachment 2 of this report]*

Next steps and timeline. If CDPR and SLOAPCD agree to adopt a new PM10 emissions reduction target and modeling framework, as proposed by the SAG, this would likely change the acreage goal for further dust mitigation treatments at the ODSVRA. According to the current modeling framework, a PM10 emissions reduction target of 40.7% (i.e., 59.3% of 2013 levels) would probably require an additional 75-100 acres of treatment areas beyond the 412.5 cumulative acres already planned for full implementation by July 31, 2022.[7] Adoption of a new PM10 emissions modeling framework would also affect the determination of additional acres needed. Within the context of a new SOA target, the overall acreage goal would depend on the specific locations and types of planned dust mitigation treatments, as well as the specific implementation of the new PM10 emissions modeling framework. Such implementation, leading to a specific acreage target, could be undertaken through the process of preparing the upcoming 2022 ARWP. If it turns out that achieving this specific acreage target is not feasible within the timeframe of the current SOA (i.e., by 2023), then this shortfall could be addressed either by extending the timeframe for completion of dust mitigation projects or by implementing permanent OHV exclosures that would bridge the emissions reduction gap. Per acre, such OHV exclosures are expected to be less effective at reducing PM10 emissions than active dune restoration options (such as planting vegetation), but they could be deployed with minimal effort. Analysis of the 2020 ODSVRA closure indicates that areas exclosed from OHV activity experienced significant PM10 emissions reductions within a few months of closure.

In addition to considering the timeline for achieving PM10 emissions reductions, the SAG also advises CDPR and SLOAPCD to carefully consider plans for long-term monitoring and assessment of the effectiveness of existing dune restoration and dust emissions mitigation treatments. These treatments take time to establish and develop, as does their effect on mitigating dust emissions. For example, the 2020 foredune restoration site could take several years to decades to develop a sustainable morphology and plant communities. Accordingly, the onsite and downwind effectiveness of the foredune for reducing dust emissions will take time, and it may require adaptive management interventions and continued monitoring to ensure effectiveness. Continued monitoring and assessment for several years beyond implementation of dust control measures could inform any future course corrections, if needed.

A complete description and scientific basis for the SAG's advice on the SOA target is provided in Section I of this report, and its advice on the PM10 emissions modeling framework is provided in Section II.

Respectfully,
The Scientific Advisory Group

Dr. Raleigh Martin (Chair of SAG); Dr. William Nickling; Dr. Ian Walker; Ms. Carla Scheidlinger; Mr. Earl Withycombe; Mr. Mike Bush, Dr. John A. Gillies

[7] Desert Research Institute (October 1, 2021). "Additional treatment area to reach the Stipulated Order of Abatement (SOA) 50% goal" *[see 2021 ARWP Conditional Approval Draft, Attachment 18]*

I. Detailed SAG Analysis of SOA Target

Background. In 2018, the San Luis Obispo County Air Pollution Control District (SLOAPCD) and California Department of Parks and Recreation (CDPR) agreed to a Stipulated Order of Abatement (SOA), approved by the SLOAPCD Hearing Board, to reduce emissions of PM10 (particulate matter with an aerodynamic diameter of less than 10 microns) from the Oceano Dunes State Vehicular Recreation Area (ODSVRA).[8] SOA provision 2c calls for "establishing an initial target of reducing the maximum 24-hour PM10 baseline emissions by fifty percent (50%), based on air quality modeling based on a modeling scenario for the period May 1 through August 31, 2013." The SOA also states, "The estimate of emission reductions identified in 2c may be modified based on air quality modeling conducted by CARB or other modeling subject to the review of the SAG."

The 2020 Annual Report and Work Plan (ARWP) prompted discussions among members of the Scientific Advisory Group (SAG), in consultation with CDPR and SLOAPCD, of possible scientifically informed revisions to the existing SOA target of reducing PM10 mass emissions by 50% relative to the 2013 baseline.[9] As a first step, the SAG examined the approach that was used to establish the initial 50% emissions reduction target. The initial target, which was developed by SLOAPCD staff, was derived based on a comparison between measurements at the California Department of Fire (CDF) air quality monitoring station, which is directly downwind of OHV-impacted sections of the ODSVRA, and an air quality monitoring station downwind of the Oso Flaco section of the ODSVRA, which experiences negligible disturbance from off-highway vehicles (OHVs). SLOAPCD staff estimated that a 50% reduction in maximum 24-hour PM10 baseline emissions from the ODSVRA Riding Area would be required to achieve a similar frequency of PM10 exceedances at CDF as at Oso Flaco.

In initial discussions following publication of the 2020 ARWP, the SAG expressed basic support for SLOAPCD's approach to establishing the initial SOA target, but the SAG also noted that the SOA target could potentially be refined to more accurately reflect the amount by which OHV activity had caused an elevation in PM10 emissions and concentrations relative to natural background levels.[10] To derive a refined SOA target, the SAG recommended a modeling approach whereby PM10 emissions and airborne concentrations for a "pre-disturbance emissions scenario," reflecting dust emissions prior to OHV disturbance, would be compared to PM10 mass emissions and concentrations for the "baseline" 2013 scenario, which reflects elevated dust emissions due to OHV disturbance but prior to implementation of significant dust mitigation measures.

To determine the feasibility of this new approach, the SAG requested (and CDPR agreed) to commission preliminary modeling by the Desert Research Institute (DRI) of a pre-disturbance emissions scenario. Noting that the intensity of PM10 mass emissions is significantly higher within ODSVRA Riding Areas (i.e., areas impacted by significant OHV activity) than within Non-Riding Areas (i.e., areas where OHV activity is non-existent), the SAG recommended that

[8] SLOAPCD Hearing Board (May 4, 2018). "Case No. 17-01, Stipulated Order of Abatement"
[9] CDPR (September 30, 2020). "2020 Annual Report and Work Plan: Fourth Draft"
[10] SAG (December 18, 2020). "Reevaluating the Stipulated Order of Abatement (SOA) Oceano Dunes PM10 dust mitigation target" *[see Attachment 3 of this report]*

DRI model PM10 emissions and concentrations resulting from a scenario in which the PM10 emissivity of all ODSVRA Riding Areas is replaced with the mean emissivity of Non-Riding Areas. In response, DRI utilized its emission-dispersion model[11] and available data on PM10 emissivity within the ODSVRA (collected via PI-SWERL from 2013 to 2019) to estimate PM10 emissions and concentrations under this pre-disturbance scenario.[12]

DRI's preliminary modeling showed that, for this preliminary pre-disturbance emissions scenario, the mean value of PM10 mass emissions is 118.2 metric tons per day. This is 35.3% lower than the modeled 2013 baseline PM10 emissions of 182.8 metric tons per day, but the difference is significantly less than the 50% reduction currently required by the SOA. In a review of the DRI preliminary model results,[13] the SAG offered two key points. First, DRI's modeling confirmed the unambiguous impact of OHV activity on increased PM10 emissions within the ODSVRA. Second, DRI's preliminary modeling confirmed the plausibility of the pre-disturbance emissions scenario modeling approach, a refined version of which could potentially be used as a tool for determining a new PM10 emissions reduction target.

Based on these preliminary findings, the SAG recommended that, should CDPR choose to move forward with further modeling toward modifying the SOA target, three key refinements should be made to modeling of the pre-disturbance emissions scenario. First, the pre-disturbance scenario should be refined to account for a noticeable north-south gradient in PM10 emissivity, which was not included in the preliminary modeling. Second, the pre-disturbance emissions scenario should be refined to account for historical vegetation coverage, which may have significantly exceeded vegetation cover in 2013. Third, uncertainties associated with the inputs to this refined pre-disturbance emissions scenario should be appropriately quantified.

In response to SAG's analysis of the preliminary DRI modeling results, CDPR chose to move forward with efforts to refine the pre-disturbance emissions scenario and to (potentially) propose a new SOA target. The key steps in this work are described in the 2021 ARWP, which was developed in consultation with the SAG.[14] Proposed model refinements to address the north-south gradient in PM10 emissivity are relatively straightforward, but refinements to model historic vegetation cover are more complicated. For this latter task, CDPR commissioned an analysis by the University of California, Santa Barbara (UCSB), in consultation with ODSVRA staff, to analyze historic air photos of vegetation cover at the ODSVRA.[15] Refinements to address model uncertainty are primarily related to uncertainty in this historical vegetation analysis.

---

[11] Mejia, J. F., Gillies, J. A., Etyemezian, V. Glick, R. (2019). "A very-high resolution (20 m) measurement-based dust emissions and dispersion modeling approach for the Oceano Dunes, California," *Atmospheric Environment*, *218*, https://doi.org/10.1016/j.atmosenv.2019.116977

[12] Gillies, J. A., Mejia, J., Furtak-Cole, E. (April 27, 2021). "Report to the SAG and Parks Evaluating the Potential for Developing a New Baseline Mass Emissions Rate and Target Reduction within the SOA" *[see Attachment 4 of this report]*

[13] SAG (April 30, 2021). "Scientific Advisory Group (SAG) Review of *Report to the SAG and Parks Evaluating the Potential for Developing a New Baseline Mass Emissions Rate and Target Reduction within the SOA*" *[see 2021 ARWP Conditional Approval Draft, Attachment 12]*

[14] CDPR (October 1, 2021). "2021 Annual Report and Work Plan: Conditional Approval Draft"

[15] Swet, N., Hilgendorf, Z., Walker, I. (February 2022). "UCSB Historical Vegetation Cover Change Analysis (1930-2020) within the Oceano Dunes SVRA" *[see Attachment 2 of this report]*

Upon receipt of results from the historic vegetation study, the CPDR, in consultation with the SAG, directed DRI to model PM10 emissions resulting from two refined pre-disturbance emissions scenarios for comparison to the 2013 baseline scenario. For comparability of scenarios, the same wind condition (from the 2013 top 10 days) was applied for all modeling scenarios, and the resulting PM10 mass emissions within the ODSVRA Riding Area boundaries were compared. These modeling scenarios are summarized in Table 1 and described in further detail in the sections below.

Table 1. Parameters for refined pre-disturbance emissions scenarios, in comparison to existing 2013 baseline scenario:

	2013 Baseline Scenario	**Pre-disturbance Scenario 1**	**Pre-disturbance Scenario 2**
PM10 emissivity of open sand areas	Use 2013 PI-SWERL grid	Use mean emissivity of adjacent Non-Riding Areas, subdivided into 3 zones (north, central, south)	Use mean emissivity of adjacent Non-Riding Areas, subdivided into 3 zones (north, central, south)
Vegetation cover	2013 vegetation islands (as indicated through 2014 air photos)	Vegetation cover estimated from 1939 air photo (from UCSB study)	Vegetation cover estimated from 1966 air photo (from UCSB study)

Modeling PM10 emissivity for the SOA target. Over the past decade, DRI has conducted extensive field campaigns to determine PM10 emissivity across the ODSVRA. These campaigns have utilized an instrument known as the PI-SWERL (Portable In-Situ Wind Erosion Laboratory).[16] The PI-SWERL is placed on an open patch of dune surface, and then a flat rotating circular blade within the PI-SWERL chamber generates wind stress on the surface at defined levels. By measuring the resulting PM10 emissions, the PI-SWERL can determine how much PM10 dust is emitted at a given wind speed. This wind-dust relationship is known as the PM10 emissivity, and it varies significantly across the ODSVRA. The higher the emissivity, the more a location will emit PM10 dust for any given wind stress.

A recent study by DRI showed that surfaces within the ODSVRA Riding Area experience significantly higher PM10 emissivity than Non-Riding Areas.[17] (Results of this study were first presented in the 2021 ARWP[18] and subsequently published as a peer-reviewed publication.) This finding of elevated PM10 emissivity in Riding Areas, along with the discovery that Riding Areas experienced a significant reduction in PM10 emissivity during a temporary park closure in 2020,

[16] Etyemezian, V., Nikolich, G., Ahonen, S., Pitchford, M., Sweeney, M., Purcell, R., Gillies, J., Kuhns, H. (2007). "The Portable In Situ Wind Erosion Laboratory (PI-SWERL): A new method to measure PM10 windblown dust properties and potential for emissions," *Atmospheric Environment, 41*, 18. https://doi.org/10.1016/j.atmosenv.2007.01.018

[17] Gillies, J. A., Furtak-Cole, E., Nikolich, G., Etyemezian, V. (2022). "The role of off-highway vehicle activity in augmenting dust emissions at the Oceano Dunes State Vehicular Recreation Area, Oceano, CA," *Atmospheric Environment: X, 13*, https://doi.org/10.1016/j.aeaoa.2021.100146

[18] Gillies, J. A., Furtak-Cole, E., Nikolich, G., Etyemezian, V. (August 1, 2021). "Examining Dust Emissions and OHV Activity at the ODSVRA" *[see 2021 ARWP Conditional Approval Draft, Attachment 10]*

strongly support the idea that intensive vehicular activity within the ODSVRA has caused an increase in PM10 emissions relative to previously undisturbed conditions. These results also support the idea that PM10 emissivity within Non-Riding Areas can provide a reasonably good approximation for such pre-disturbance conditions.

One additional finding, indicated in the results of the DRI study, is that there is a general gradient of decreasing PM10 emissivity from north to south across the ODSVRA, both within and outside the Riding Area.[19] This gradient likely reflects a general coarsening of dune sands from north to south, which increases the minimum wind speed required to move sand grains and cause PM10 dust emissions.

Based on these two findings – lower PM10 emissivity outside the Riding Area, and an overall north-south gradient of declining PM10 emissivity – the SAG advised DRI to adopt the following approach to modeling PM10 emissivity for pre-disturbance scenarios, which is summarized in Table 1. The open sand area within the ODSVRA Riding Area and Non-Riding Area were each respectively subdivided into 3 latitudinal zones – north, central, and south. For each of the 3 Riding Area zones, a PM10 emissivity curve for pre-disturbance conditions was estimated by taking the average PM10 emissivity value for the closest Non-Riding Area (at a similar latitude). By subdividing the ODSVRA into zones, the modeling of pre-disturbance scenarios accounts for the natural north-south gradient in emissivity. Areas outside the Riding Area extent retained PM10 emissivities from the 2013 PI-SWERL grid.

Modeling vegetation cover for the SOA target. What has been described thus far is the approach to modeling PM10 emissions for open sand areas within the ODSVRA. However, in the past and present, small but significant portions of the ODSVRA Riding Area extent have been covered with vegetation. A reasonable assumption, which has been utilized throughout the modeling that supports the SOA process, is that vegetation shelters the dune surface and thus PM10 emissions are negligible within these areas. Thus, modeling of pre-disturbance PM10 emissions must account for the difference between historical and present-day vegetation cover, and the associated effects of this vegetation cover on PM10 emissions.

As described above, CDPR commissioned a study by UCSB of vegetation cover through time at the ODSVRA, as determined through analysis of historic air photos.[20] This analysis extends back to the 1930s, the earliest time for which such air photos are available. Looking specifically at vegetation cover within the ODSVRA Riding Area boundaries, the UCSB report indicates three distinctive time periods in the history of vegetation cover. First, from the 1930s to the late 1960s, vegetation cover remained stable at about 10-12% of the Riding Area. Second, from the late 1960s into the 1980s, vegetation cover experienced a dramatic decline down to below 5% of the Riding Area. Third, from the 1980s into the early 2010s, vegetation cover remained relatively low (mostly below 7%), increasing only in recent years with the installation of dust mitigation measures.

---

[19] Gillies, J. A., Furtak-Cole, E., Nikolich, G., Etyemezian, V. (2022). "The role of off-highway vehicle activity in augmenting dust emissions at the Oceano Dunes State Vehicular Recreation Area, Oceano, CA," *Atmospheric Environment: X, 13*, https://doi.org/10.1016/j.aeaoa.2021.100146

[20] Swet, N., Hilgendorf, Z., Walker, I. (February 2022). "UCSB Historical Vegetation Cover Change Analysis (1930-2020) within the Oceano Dunes SVRA" *[see Attachment 2 of this report]*

Although the exact history of management practices at the ODSVRA is unknowable, the fact that vegetation cover remained relatively stable from the 1930s through the 1960s indicates that this is a reasonable period from which to estimate a "pre-disturbance" condition for vegetation cover. The UCSB report cites evidence that significant OHV activity at the ODSVRA began in the 1950s.[21] Vegetation cover maps from 1939 and 1966 roughly bracket this period of high vegetation cover within the current Riding Area extent, providing a range of possible pre-disturbance conditions in terms of both the spatial distribution and percentage cover of vegetation within the current ODSVRA Riding Area boundaries.

Based on this finding that 1939 and 1966 represent a reasonable range of pre-disturbance vegetation cover, the SAG advised DRI to adopt the following approach to modeling the effects of vegetation cover for two pre-disturbance scenarios. This approach is summarized in Table 1. Based on the 1939 and 1966 historic air photo analyses, vegetation cover masks were generated and incorporated into the modeling of these two pre-disturbance emissions scenarios. In each of these scenarios, PM10 emissions from areas not covered with vegetation were modeled as described in the previous section. PM10 emissions from areas that were covered with vegetation were modeled as having zero PM10 emissions. The difference between modeled PM10 emissions for the 1939 and 1966 scenarios thus provided an estimate of the uncertainty resulting from the range in vegetation cover observed between the 1930s and 1960s.

Results from modeling pre-disturbance scenarios. DRI modeled the 1936 and 1966 pre-disturbance scenarios as recommended by the SAG.[22] The results of this modeling are summarized in Table 2 below. The 2013 baseline scenario, which has been the subject of extensive previous modeling, produces an average of 182.8 metric tons per day of PM10 mass emissions for the 10 baseline wind days. In comparison, the 1939 and 1966 scenarios produce 108.4 and 108.9 metric tons per day of PM10 emissions, respectively, for these 10 reference wind days. These represent 40.7% and 40.4% reductions, respectively for 1939 and 1966, relative to previously modeled values for PM10 emissions for the 2013 baseline scenario. Averaging between these two pre-disturbance scenarios and using the difference between the two scenarios as a proxy for uncertainty, the modeled pre-disturbance PM10 mass emissions are 108.7 ± 0.3 metric tons per day of PM10 mass emissions, or a 40.5% ± 0.2% reduction relative to the 2013 baseline scenario.

Table 2. Results of modeling pre-disturbance scenarios:

	2013 Baseline Scenario	**Pre-disturbance Scenario 1 (1939)**	**Pre-disturbance Scenario 2 (1966)**
PM10 mass emissions (metric tons per day)	182.8	108.4	108.9
Percentage reduction from baseline	N/A	40.7%	40.4%

[21] Swet, N., Hilgendorf, Z., Walker, I. (February 2022). "UCSB Historical Vegetation Cover Change Analysis (1930-2020) within the Oceano Dunes SVRA" *[see Attachment 2 of this report]*

[22] Mejia, J., Gillies, J. A. (January 10, 2022). "Model-Derived Estimates of Mass Emissions of PM10 for Pre-OHV Disturbance and Past Vegetation Scenarios" *[see Attachment 1 of this report]*

Although this estimate of the difference between 2013 and pre-disturbance PM10 mass emissions reflects modeling based on the best available information about PM10 emissivity and vegetation cover under pre-disturbance conditions, two additional sources of possible uncertainty in this analysis should be noted. First, though averages of PM10 emissivities within present-day Non-Riding Areas should provide a reasonable approximation of PM10 emissivities within pre-disturbance surfaces within Riding Area boundaries, there is in fact quite a bit of natural variability in PM10 emissivity. This variability arises from variations in topography, particle size, soil moisture conditions, and other factors. Assigning pre-disturbance emissivity values based on latitudinal zones helped to reduce some of this variability, but it is impossible to account for all factors. Second, the 2013 baseline scenario uses a vegetation mask derived from CDPR image analysis, whereas the 1939 and 1966 pre-disturbance scenarios use a vegetation mask derived from UCSB image analysis.[23] CDPR and UCSB employed slightly different methods to derive vegetation cover. But it is noteworthy that the UCSB report finds a negligible difference (<0.1%) between CDPR and UCSB vegetation cover analyses for 2014, which is the closest year to 2013 for which air photo imagery is available.[24] Despite these unavoidable uncertainties, the SAG notes that the approach described here is a significant refinement over the approach used to determine the initial SOA target of reducing PM10 emissions by 50%.

SAG advice on SOA target. If the management objective is to reduce emissions of PM10 from the ODSVRA to a level consistent with dust emissions prior to significant OHV disturbance, then there is a strong scientific justification for adjusting the PM10 emissions reduction target in the SOA from the initial 50% reduction to a new target of 40.5% ± 0.2%, representing the range of values from the modeled 1939 and 1966 pre-disturbance scenarios. In light of the uncertainties described above, the SAG advises picking a new target on the conservative end of this uncertainty range, i.e., using the 40.7% emissions reduction value from the 1939 pre-disturbance scenario, which produced lower PM10 emissions than the 1966 scenario. Specifically, a new 40.7% SOA target would represent a reduction from 182.8 to 108.4 metric tons per day of PM10 emissions, as modeled for the existing 10 baseline days scenario applied to the ODSVRA Riding Area. These values are summarized in Table 3 below.

Table 3. Comparison of modeled PM10 mass emissions for initial SOA target versus pre-disturbance scenario.

	2013 baseline	**Initial SOA target (current approach)**	**Uncertainty range for new SOA target based on pre-disturbance scenario**	**Proposed new SOA target based on lower emissions end of uncertainty range (1939 scenario)**
PM10 mass emissions (metric tons per day)	182.8	91.4	108.7 ± 0.3	108.4
Percentage reduction relative to 2013	N/A	50%	40.5% ± 0.2%	40.7%

[23] SAG (December 15, 2021). Personal communication with Jack Gillies.
[24] Swet, N., Hilgendorf, Z., Walker, I. (February 2022). "UCSB Historical Vegetation Cover Change Analysis (1930-2020) within the Oceano Dunes SVRA" *[see Attachment 2 of this report]*

Scientific basis for new SOA target. The SAG's advised new PM10 emissions reduction target of 40.7% (relative to the 2013 baseline) was obtained by using the DRI emission-dispersion model to estimate the total mass emissions (metric tons per day of PM10) using an emission grid that the SAG determined to best represent the emissivity within the ODSVRA in the absence of OHV activity. This pre-disturbance emissions grid uses a distribution of vegetation cover that is equivalent to that which existed prior to the present-day levels of OHV activity (1939 and 1966), and it uses meteorology of the 10 days of highest emissions in 2013, consistent with existing approaches to determining the baseline emission value of 182.8 metric tons per day of PM10 as defined in the current SOA. The SAG provides the following points to highlight the defensibility of the proposed percent emission reduction target relative to the 2013 baseline:

1. Multiple years of emissivity data of the Non-Riding Areas across the spatial extent of the entire ODSVRA measured with the PI-SWERL instrument,[25,26,27] which has been used widely to quantify emissivity across a variety of surfaces,[28,29,30,31,32] are used to define emissivity relationships for the Riding Areas within the model to represent pre-disturbance conditions existing prior to significant OHV impacts.

2. The emissivity grid used to represent pre-disturbance PM10 emissions from within the ODSVRA accounts for both the removal of OHV impacts within the Riding Area extent and the observed gradient of emissivity in the Non-Riding and Riding Areas (emissivity decreases from north to south in both). The methods used to develop and test the validity of the latitudinally-dependent emissivity relationships in the ODSVRA have been subject to peer review and published in the scientific literature.[33]

---

[25] Sweeney, M., Etyemezian, V., Macpherson, T., Nickling, W., Gillies, J., Nikolich, G., McDonald, E. (2008). "Comparison of PI-SWERL with dust emission measurements from a straight-line field wind tunnel," Journal of Geophysical Research, 113, F01012, https://doi.org/10.1029/2007JF000830

[26] Etyemezian, V., Nikolich, G., Ahonen, S., Pitchford, M., Sweeney, M., Purcell, R., Gillies, J., Kuhns, H. (2007). "The Portable In Situ Wind Erosion Laboratory (PI-SWERL): A new method to measure PM10 windblown dust properties and potential for emissions," *Atmospheric Environment, 41*, 18, https://doi.org/10.1016/j.atmosenv.2007.01.018

[27] Etyemezian, V., Gillies, J. A., Shinoda, M., Nikolich, G., King, J., Bardis, A. R. (2014). "Accounting for surface roughness on measurements conducted with PI-SWERL: Evaluation of a subjective visual approach and a photogrammetric technique," *Aeolian Research, 13,* 35-50, https://doi.org/10.1016/j.aeolia.2014.03.002

[28] King, J., Etyemezian, V., Sweeney, M., Buck, B. J., Nikolich, G. (2011). "Dust Emission Variability at the Salton Sea, California, USA," *Aeolian Research, 3*, 67-79, https://doi.org/10.1016/j.aeolia.2011.03.005

[29] Sweeney, M. R., McDonald, E. V., Etyemezian, V. (2011). "Quantifying dust emissions from desert landforms, eastern Mojave Desert, USA," *Geomorphology, 135,* 21-34, https://doi.org/10.1016/j.geomorph.2011.07.022

[30] Sweeney, M. R., Lu, H., Cui, M., Mason, J. A., Feng, H., Xu, Z. (2016). "Sand dunes as potential sources of dust in northern China," *Science China Earth Sciences, 59*, 760-769, https://doi.org/10.1007/s11430-015-5246-8

[31] Etyemezian, V., Gillies, J. A., Mastin, L. G., Crawford, A., Hasson, R., Van Eaton, A. R., Nikolich, G. (2019). "Laboratory experiments of volcanic ash resuspension by wind," *Journal of Geophysical Research: Atmospheres, 124,* 9534–9560, https://doi.org/10.1029/2018JD030076

[32] von Holdt, J. R. C., Eckardt, F. D., Baddock, M. C., Wiggs, G. F. S. (2019). "Assessing landscape dust emission potential using combined ground-based measurements and remote sensing data. *Journal of Geophysical Research: Earth Surface, 124*, https://doi.org/10.1029/2018JF004713

[33] Gillies, J. A., Furtak-Cole, E., Nikolich, G., Etyemezian, V. (2022). "The role of off-highway vehicle activity in augmenting dust emissions at the Oceano Dunes State Vehicular Recreation Area, Oceano, CA," *Atmospheric Environment: X, 13*, https://doi.org/10.1016/j.aeaoa.2021.100146

3. The emission and dispersion model used to generate the total mass emission estimates and PM10 concentrations at key receptor sites for the pre-OHV impact scenario has been peer reviewed and published in the scientific literature,[34] and its use is accepted by the SOA, as demonstrated by usage of this model in the PMRP and ARWPs. The model predicted values of PM10 concentrations compared to measurements of PM10 both in the ODSVRA[35] and downwind of the ODSVRA[36] show excellent agreement. This provides a high degree of confidence that a developed emission grid, combined with the meteorological and dispersion components, provide realistic predictions of total mass emissions and PM10 concentrations.

4. The vegetation maps representing the years 1939 and 1966 were developed using aerial photographic images that were subject to very high levels of scrutiny and quality assurance to produce classified vegetation raster data sets that were converted to GIS shapefiles.[37] These shapefiles were used in the modeling to represent areas from which emissions of PM10 would be zero due to the presence of the vegetation.

Other factors in PM10 attribution. A recent study led by Dr. Lynn Russell of the Scripps Institution of Oceanography found that only a small percentage of airborne PM10 collected via gravimetric sampling at the CDF monitoring station can be attributed to mineral dust.[38] Based on these findings, Dr. Russell argued that only a small fraction of the airborne PM10 measured at CDF is potentially attributable to the ODSVRA and associated OHV activity. On this basis, some have argued that CDPR's responsibility should therefore be limited to reducing this small increment of increased PM10 that can be directly tied to OHV-sourced mineral dust.

As documented in the SAG's review of the Scripps study[39] and its open letter to the Off Highway Motor Vehicle Recreation (OHMVR) Commission,[40] the SAG disputes the main arguments of the Scripps study that seek to minimize the role of OHV in producing PM10. In addition, the SLOAPCD has disputed the filter sampling methods utilized in the Scripps study.[41] Irrespective of its specific concerns about the Scripps study, the SAG notes that its approach to modeling pre-disturbance PM10 emissions, which is based on determining the *total* effect of

---

[34] Mejia, J. F., Gillies, J. A., Etyemezian, V. Glick, R. (2019). "A very-high resolution (20 m) measurement-based dust emissions and dispersion modeling approach for the Oceano Dunes, California," *Atmospheric Environment*, *218*, https://doi.org/10.1016/j.atmosenv.2019.116977

[35] Gillies, J. A., Mejia, J. (July 2020). "Model Verification Based on 2013 Measurements and 2013 Emission Grid and 2013 Wind Field for the 10 Baseline Days," Report prepared for CDPR by DRI *[see Attachment 5 of this report]*

[36] Mejia, J. F., Gillies, J. A., Etyemezian, V. Glick, R. (2019). "A very-high resolution (20 m) measurement-based dust emissions and dispersion modeling approach for the Oceano Dunes, California," *Atmospheric Environment*, *218*, https://doi.org/10.1016/j.atmosenv.2019.116977

[37] Swet, N., Hilgendorf, Z., Walker, I. (February 2022). "UCSB Historical Vegetation Cover Change Analysis (1930-2020) within the Oceano Dunes SVRA" *[see Attachment 2 of this report]*

[38] Russell, L. M. (November 8, 2021). "Scripps/UCSD Interim Report 2021: Preliminary Results from May 2021 Aerosol Measurements"

[39] SAG (October 20, 2021). "Memo: SAG Review of Scripps/UCSD "Interim Report 2021: Preliminary Results from May 2021 Aerosol Measurements""

[40] SAG (December 1, 2021). "Re: "Scripps/UCSD Interim Report 2021: Preliminary Results from May 2021 Aerosol Measurements""

[41] SLOAPCD (November 2, 2021). "APCD Review of "Scripps/UCSD Interim Report 2021""

human disturbance on elevated PM10 emissions, is agnostic to the specific chemical composition of the emitted PM10 dust. The approach presented here aligns with the federal and state PM10 ambient air quality standards motivating the SOA, which regulate the total airborne PM10, not just specific constituents.

Effects of SOA target on PM10 ambient air quality. Both the initial SOA target (50%) and the potential new SOA target (40.7%) are based on a management framework in which the goal is to reduce PM10 emissions commensurate with the estimated effect of human disturbance on elevating these PM10 emissions. These PM10 emissions reductions will also significantly reduce airborne PM10 concentrations. DRI modeling of the 1939 pre-disturbance scenario, upon which the proposed new SOA target is based, produced average PM10 concentrations of 88 $\mu g/m^3$ and 71 $\mu g/m^3$ at CDF and Mesa2, respectively. Modeling of the 1966 pre-disturbance scenario produced comparable average PM10 concentrations of 87 $\mu g/m^3$ and 76 $\mu g/m^3$ at CDF and Mesa2, respectively. In both pre-disturbance scenarios, modeled PM10 concentrations are substantially lower than those modeled for the 2013 baseline: 124 $\mu g/m^3$ and 98 $\mu g/m^3$ at CDF and Mesa2, respectively.[42]

For reference, modeling of expected dust controls installed through 2022 produces average top 10 day PM10 concentrations of 66.4 $\mu g/m^3$ and 65.5 $\mu g/m^3$ at CDF and Mesa2, respectively.[43] A likely reason why average modeled PM10 concentrations are already lower than for pre-disturbance conditions, despite the fact that PM10 mass emissions reductions expected as of 2022 are only 31.7%,[44] is the contribution of invasive weeds to substantial expansion of vegetation cover within Non-Riding Areas in recent decades.[45] Increasing Non-Riding Area vegetation cover has the effect of suppressing PM10 emissions from these areas, thus lowering the contribution of these areas to overall PM10 concentrations at receptor sites.

The SAG notes that, while PM10 air quality is substantially improved for the pre-disturbance scenarios relative to the 2013 baseline, PM10 concentrations for these scenarios still substantially exceed the 50 $\mu g/m^3$ California PM10 air quality standard. These results reflect the fact that the ODSVRA is a naturally dusty environment, even in the absence of OHV activity. For context, the California PM10 standard is occasionally exceeded at the Oso Flaco monitoring site, which is assumed to be unaffected by human disturbance (and which may in fact have levels of PM10 emissions lower than pre-disturbance conditions, due to the widespread presence of invasive weeds). Therefore, a management approach seeking to completely eliminate exceedances of the California PM10 standard would likely require reducing PM10 emissions far below what existed prior to OHV disturbance. Ultimately, the selection of the PM10 target will depend on the management objectives of the CDPR, the SLOAPCD, and other governing bodies.

---

[42] Mejia, J., Gillies, J. A. (January 10, 2022). "Model-Derived Estimates of Mass Emissions of PM10 for Pre-OHV Disturbance and Past Vegetation Scenarios" *[see Attachment 1 of this report]*

[43] CDPR (October 1, 2021). "PMRP Evaluation Metrics – Annual Record 2020-21" *[see 2021 ARWP Conditional Approval Draft, Attachment 02]*

[44] CDPR (October 1, 2021). "PMRP Evaluation Metrics – Annual Record 2020-21" *[see 2021 ARWP Conditional Approval Draft, Attachment 02]*

[45] Swet, N., Hilgendorf, Z., Walker, I. (February 2022). "UCSB Historical Vegetation Cover Change Analysis (1930-2020) within the Oceano Dunes SVRA" *[see Attachment 2 of this report]*

II. Detailed SAG Analysis of PM10 Emissions Reduction Modeling

Background. In parallel with efforts to revisit the initial 50% PM10 mass emissions reduction target under the SOA, the SAG has consulted with CDPR and SLOAPCD on methods by which the effects of dust mitigation actions within the ODSVRA are credited via metrics for evaluating progress toward achieving this target. As described in the 2021 ARWP[46] and the SLOAPCD[47] and SAG[48] responses to this ARWP, there is a mutually held interest in improving the accuracy of accounting for PM10 emissions reductions.

The ultimate purpose of this effort, in tandem with reexamining the SOA target, is to determine the amount of acreage of dust mitigation treatments required to achieve the air quality goals of the SOA. The 2019 Particulate Matter Reduction Plan (PMRP) estimated that about 500 acres of dust control measures would be needed to achieve the goals of the SOA,[49] whereas an analysis accompanying the 2021 ARWP increased this estimate to roughly 600 acres,[50] due to differences between the expected and actual placement of dust mitigating treatments amidst significant spatial variation in PM10 emissivity. For comparison, 412.5 acres of dust mitigation treatments are currently planned by July 31, 2022, assuming full implementation of the current 2021 ARWP work plan and building cumulatively on existing treatments.

Within the past year, CDPR has commissioned multiple studies that can inform the accounting for PM10 emissions reductions. These studies and their key findings are summarized below:

1. **DRI Increments of Progress.**[51] This study shows that, as dust control measures within the ODSVRA have increased over time, airborne PM10 concentrations (normalized by wind power density, a proxy for wind strength) have declined at the CDF receptor site. In contrast, the Mesa2 receptor site, up to 2020, has not seen the same level of reduction in PM10 concentrations (relative to wind power density) over this period. These empirical findings mostly align with existing model predictions of PM10 reductions resulting from dust mitigation measures, including the fact that such reductions have been larger at CDF than at Mesa2. This study indicates that the current approach to modeling PM10 emissions reductions is generally sound, though model refinements could further improve the accuracy of the model.

2. **DRI Role of OHV.**[52] Among its findings, this study (which was also mentioned in the previous section of this report) shows that a temporary moratorium on OHV activity in

[46] CDPR (October 1, 2021). "2021 Annual Report and Work Plan: Conditional Approval Draft"
[47] SLOAPCD (August 24, 2021). "San Luis Obispo County Air Pollution Control District Comments on August 2, 2021 Draft ARWP"
[48] SAG (August 16, 2021). "Memo: SAG Review of CDPR "DRAFT 2021 ODSVRA ARWP" (dated August 2, 2021)"
[49] CDPR (June 2019). "Oceano Dunes State Vehicular Recreation Area Draft Particulate Matter Reduction Plan"
[50] Desert Research Institute (DRI) (October 1, 2021). "DRI Estimate of Additional Treatment Area to Reach the Stipulated Order of Abatement 50% Goal" *[see 2021 ARWP Conditional Approval Draft, Attachment 18]*
[51] Gillies, J. A., Furtak-Cole, E., Etyemezian, V. (August 1, 2021). "Increments of Progress Towards Air Quality Objectives - ODSVRA Dust Controls" *[see 2021 ARWP Conditional Approval Draft, Attachment 10]*
[52] Gillies, J. A., Furtak-Cole, E., Nikolich, G., Etyemezian, V. (2022). "The role of off-highway vehicle activity in augmenting dust emissions at the Oceano Dunes State Vehicular Recreation Area, Oceano, CA," *Atmospheric Environment: X, 13*, https://doi.org/10.1016/j.aeaoa.2021.100146

2020 caused PM10 concentrations (relative to wind power density) to decline steadily over time at monitoring stations within the ODSVRA Riding Area, as well as at receptor sites downwind of Riding Areas, such as CDF. In addition, PI-SWERL measurements collected within the Riding Area during the ODSVRA closure showed a reduction in PM10 emissivity relative to pre-closure levels. This study suggests that the simple act of fencing off an area to OHV activity, without any other management changes, can lead to a significant reduction in PM10 emissions within a few months. The current approach to modeling PM10 emissions reductions does not account for OHV exclosures; model refinements in the future that account for the PM10-mitigating effects of such exclosures could therefore also improve model accuracy.

3. **DRI / UCSD CFD Study.**[53] This study utilizes computational fluid dynamics (CFD) modeling to understand how foredune topography affects the spatial distribution of surface shear stress within and downwind of coastal foredunes at the ODSVRA. This modeling shows that, compared to a flat unvegetated surface, a partially vegetated foredune produces substantial reductions in shear stress (a proxy for wind strength) both within the foredune and downwind of the foredune, with associated reduction in, although not elimination of, PM10 emissions. In contrast, the current approach to modeling foredune-related PM10 emissions reductions is to assume a total elimination of PM10 emissions within the foredune, but no reduction in PM10 emissions downwind of the foredune. Model refinements in the future that better account for the actual variations in shear stress both within and downwind of the foredune could therefore improve model accuracy.

In addition to these recent studies, ongoing monitoring efforts also help to inform understanding of how management actions affect PM10 emissions:

1. **PI-SWERL monitoring.** In addition to the 2013 PI-SWERL campaign, which is the basis for the existing PM10 emissivity grid currently used to model dust emissions at the ODSVRA, additional PI-SWERL campaigns have been conducted in subsequent years, including a comprehensive campaign in 2019.[54]

2. **Sand flux monitoring.** Within treatment areas (including wind fences, straw treatments, and revegetation areas), arrays of BSNE sand traps have been set up to document reductions in wind-driven sand flux relative to areas outside the treatment areas.[55] These normalized sand flux (NSF) measurements demonstrate that treatments significantly reduce (but do not eliminate) sand transport, with associated reductions in PM10 emissions expected.

[53] Furtak-Cole, E., Gillies, J., Walker, I., Hilgendorf, Z. (December 2, 2021). "Quantifying the value of a coastal foredune for wind erosion and dust emissions through numerical simulation" *[see Attachment 6 of this report]*
[54] CDPR (September 30, 2020). "2020 Annual Report and Work Plan: Fourth Draft"
[55] Desert Research Institute (DRI) and University of California, Santa Barbara (UCSB) (August 1, 2021). "Saltation flux measurements – Temporary Sand Fences Arrays and Foredune Restoration Areas" *[see 2021 ARWP Conditional Approval Draft, Attachment 7]*

Assessment of current approach to PM10 emissions modeling. The current approach to modeling PM10 emissions at the ODSVRA takes a simple binary view. For areas that are vegetated or subject to temporary dust controls, PM10 emissions are assumed to be zero. For all other areas, PM10 emissions are determined based on applying wind conditions for the SOA 10 baseline days to a static PM10 emissivity map that was determined through a comprehensive 2013 PI-SWERL campaign. Though this simple approach has proven to be reasonably effective at modeling emissions reductions (as demonstrated, for example, by the DRI Increments of Progress study), it overlooks important factors that could also be influencing PM10 emissions. Some of these factors are described below:

1. **Open sand areas.** Currently, the PM10 emissivity of open sand areas is modeled based on a PM10 emissivity map obtained through a comprehensive 2013 PI-SWERL campaign. However, subsequent PI-SWERL campaigns (e.g., 2019) have shown significant changes in the spatial distribution of PM10 emissivity. Such changes may reflect the natural evolution of the dune field as well as changes in OHV riding patterns resulting from installation of dust controls that reduce the available area for OHV use. These changes in PM10 emissivity patterns are not currently accounted for in modeling of PM10 emissions reductions.

2. **Foredune shadow zone.** Currently, dust mitigation treatments are assumed to affect PM10 emissions only within the immediate footprint in which they are installed. However, the CFD study showed that shear stress is also reduced in the downwind shadow of foredunes. Such indirect effects of foredune treatments are not currently accounted for in modeling of PM10 emissions reductions.

3. **Temporary dust mitigation treatments and developing foredune.** Currently, dust mitigation treatments are assumed to have complete control effectiveness, i.e., PM10 emissions are zero within the footprint of such treatments. Though this is a reasonable assumption for densely vegetated back dune areas, it may not be an appropriate assumption for sparsely vegetated foredunes (as modeled in the CFD study) or for temporary non-vegetative treatments (as shown by reduced but nonzero NSF values within these treatments).

4. **Permanently exclosed areas.** Currently, exclosed areas are assumed to have the PM10 emissivity that existed at the time of the 2013 PI-SWERL campaign. This is a reasonable approach for temporary exclosures, which are expected to quickly revert to full PM10 emissions levels when they are reopened to OHV activity. However, in light of the recent findings that areas exclosed from OHV riding experience significant reductions in PM10 emissions within a few months of closure, installation of permanent exclosures may be considered as a management option in the future. However, the current approach to modeling PM10 emissions reductions does not account for the dust mitigating effects of such exclosures.

Suggested refinements to PM10 emissions modeling. Based on the above findings, the SAG suggests several refinements to modeling PM10 emissions reductions to account for these factors.

1. **Emissivity of open sand areas.** Instead of the PM10 emissivity grid derived from the 2013 PI-SWERL campaign, utilize an emissions grid derived from the most recent comprehensive PI-SWERL campaign (i.e., 2019).

2. **Emissivity of foredune shadow zone.** Instead of assuming PM10 emissions as derived from the 2013 PI-SWERL campaign, utilize the updated PI-SWERL emissivity grid and then reduce the shear stress applied to this surface as determined by the CFD study.

3. **Emissivity within temporary dust mitigation treatments and developing foredune.** Instead of assuming total control effectiveness (i.e., zero PM10 emissions) within the developing foredune and temporary dust mitigation treatment areas, calculate partially reduced (but nonzero) PM10 emissions values based on information from normalized sand flux (NSF) measurements and CFD modeling.

4. **Emissivity of exclosed areas.** Instead of assuming that permanently exclosed areas retain the emissivity that existed in the PM10 emissions grid derived from the 2013 PI-SWERL campaign, utilize information from the recent study on the effect of the 2020 ODSVRA closure to model reduced PM10 emissions values within such exclosures.

Table 4. Comparison of current and proposed new approaches to modeling reductions in PM10 mass emissions and airborne concentrations resulting from ODSVRA management changes.

Surface Type	***Approach to modeling PM10 emissions***		
	2013 baseline	**Simplified modeling of PM10 emissions reductions (current approach)**	**Refined modeling of PM10 emissions reductions (possible new approach)**
Open sand areas	2013 PI-SWERL grid	2013 PI-SWERL grid	Most recent PI-SWERL grid
Foredune shadow zone	N/A	2013 PI-SWERL grid	Reduced PM10 emissions as determined by CFD modeling applied to most recent PI-SWERL grid
Temporary dust mitigation treatments and developing foredune	N/A	No emissions	Low (but nonzero) PM10 emissions as determined from measured sand flux reductions and CFD study
Permanent exclosures	N/A	N/A	Reduced PM10 emissions as determined by the 2020 ODSVRA closure study

The SAG advises that CDPR, in consultation with SAG and SLOAPCD, adopt a new, refined approach to modeling PM10 emissions reductions for the upcoming 2022 ARWP, as summarized in Table 4 above. The SAG notes that these suggested refinements do not apply to modeling of the 2013 baseline. In this case, the 2013 PI-SWERL grid is the appropriate source of

PM10 emissivity information, and the absence of a foredune restoration zone, temporary treatments, or permanent exclosures in 2013 make consideration of these modified factors not applicable to modeling of this baseline scenario.

Overall scientific basis for new PM10 emissions modeling framework. As described above, the PMRP and ARWPs currently follow a simple approach to modeling reductions in PM10 emissions and airborne concentrations resulting from dust mitigating treatments. Areas without dust controls are assumed to produce PM10 emissivity at levels measured in 2013. Areas with dust controls are assumed to produce no PM10 emissions. There are a few potential issues with this approach. First, post-2013 measurements indicate that the spatial distribution of PM10 emissivity in the Riding Area has changed over time (both positively and negatively). Second, CFD modeling shows that the sheltering effect of the foredune restoration zone reduces wind speeds and thus PM10 emissions in parts of the Riding Area located immediately downwind of the foredune. Third, sand flux measurements indicate small but quantifiable rates of sand transport within temporary dust mitigation treatments and the developing foredune, indicating that these areas produce small but quantifiable PM10 emissions (contrary to the current assumption of no emissions within these zones). Fourth, PM10 emissivity measurements during the 2020 temporary park closure show that OHV-impacted surfaces experience a substantial reduction in PM10 emissions once they are exclosed, even if no other mitigation treatments are applied. The SAG's proposed new PM10 emissions refined modeling framework will address all of these factors.

Next steps and timeline. What has been presented here is merely a framework for improving the accuracy of PM10 emissions modeling and the effects of dust mitigation measures at the ODSVRA. Subject to the agreement by CDPR and SLOAPCD to adopt these proposed changes, the next step would be to determine the specific implementation of these modeling refinements. Such implementation could be carried out in tandem with preparation of the 2022 ARWP, and it would take into account the specific type and location of future dust mitigation treatments. Though full analyses to determine the effect of these modeling changes have not yet been carried out, the SAG is confident that sufficient data and modeling resources exist to execute these refinements prior to publication of the 2022 ARWP. For example, a narrowly defined campaign of PI-SWERL and sand flux measurements could be performed in the coming months to estimate those factors for which sufficient information on emissivity changes does not currently exist.

One important outcome of potential changes to the SOA target and PM10 emissions modeling process would be determination of a new acreage goal for dust mitigating treatments. According to the current emissions accounting framework, a PM10 emissions reduction target of 40.7% (i.e., 59.3% of 2013 levels) would probably require an additional 75-100 acres of treatment areas beyond the 412.5 cumulative acres planned for full implementation by July 31, 2022.[56] A new PM10 emissions accounting framework may change this acreage target, though the specific effect of this change is unclear at this time. A specific acreage goal would be determined once the new emissions accounting framework is implemented as part of the 2022 ARWP. This new goal would need to account for the specific location and type of planned dust mitigation treatments, which have not yet been determined.

[56] Desert Research Institute (October 1, 2021). "Additional treatment area to reach the Stipulated Order of Abatement (SOA) 50% goal" *[see 2021 ARWP Conditional Approval Draft, Attachment 18]*

Based on the current pace of dune restoration activities (about 90 acres of new treatments per year), it seems feasible that the proposed new PM10 emissions reduction target could be attained roughly within the timeframe of the current SOA (i.e., by 2023). However, if it turns out that attainment of this target is not feasible at the current pace, then the SAG offers two options for consideration. One option would simply be to extend the timeline for completion of dust mitigation projects under the SOA. A second option would be to implement additional permanent OHV exclosures to close the gap between the expected effect of dust mitigation treatments and the PM10 emissions reduction target. Per acre, such exclosures are expected to be less effective at reducing PM10 emissions than other dune restoration options (such as planting vegetation), but they could be deployed with minimal effort. Analysis of the 2020 ODSVRA closure indicates that areas exclosed from OHV activity experienced significant PM10 emissions reductions within a few months of closure. Other exclosed areas, such as the seasonal bird nesting exclosure and other sites fenced off to vehicle activity since 1982 (e.g., North Oso Flaco), have also shown appreciable vegetation re-establishment and dune development that aid in dust emissions reductions.

Long-term monitoring to maintain progress. An additional consideration when planning future dust control measures is to allow for continued monitoring and assessment of the effectiveness of existing restoration and dust emissions mitigation treatments. These treatments take time to establish and develop, as does their effect on mitigating dust emissions. Some examples of dust restoration activities that require further tracking are described below.

1. **Foredune restoration site.** The 2020 foredune restoration site could take several years to decades to develop a sustainable morphology and plant communities. Accordingly, the onsite and downwind effectiveness of the foredune for reducing dust emissions will take time and might require adaptive management interventions and continued monitoring to ensure effectiveness.

2. **Back dune treatments.** Currently, revegetation is the primary dune restoration strategy to show long-term viability for PM10 emissions reductions. In contrast, straw treatments and wind fences are typically described as "temporary," because their dust mitigating capacity decreases over time as they are overtaken by actively migrating dune surfaces. Continued monitoring of plant survivorship, morphological characteristics, and PM10 emissivity of revegetated dune surfaces could help to inform assessments of long-term effectiveness of such treatments.

3. **Exclosures.** One long-term management option may be to permanently close off areas that were previously impacted by OHV riding. Analysis of the 2020 ODSVRA closure provides information on short-term changes in PM10 emissions resulting from such exclosures, but the long-term effects are not yet known.

Continued monitoring and assessment for several years beyond implementation of dust control measures could inform any future course corrections, if needed.

List of Attachments

Attachment 1: Mejia, J., Gillies, J. A. (January 10, 2022). "Model-Derived Estimates of Mass Emissions of PM10 for Pre-OHV Disturbance and Past Vegetation Scenarios"

Attachment 2: Swet, N., Hilgendorf, Z., Walker, I. (February 2022). "UCSB Historical Vegetation Cover Change Analysis (1930-2020) within the Oceano Dunes SVRA"

Attachment 3: SAG (December 18, 2020). "Reevaluating the Stipulated Order of Abatement (SOA) Oceano Dunes PM10 dust mitigation target"

Attachment 4: Gillies, J. A., Mejia, J., Furtak-Cole, E. (April 27, 2021). "Report to the SAG and Parks Evaluating the Potential for Developing a New Baseline Mass Emissions Rate and Target Reduction within the SOA"

Attachment 5: Gillies, J.A., Mejia, J. (July 2020). "Model Verification Based on 2013 Measurements and 2013 Emission Grid and 2013 Wind Field for the 10 Baseline Days," Report prepared for CDPR by DRI

Attachment 6: Furtak-Cole, E., Gillies, J., Walker, I., Hilgendorf, Z. (December 2, 2021). "Quantifying the value of a coastal foredune for wind erosion and dust emissions through numerical simulation"

ATTACHMENT 1

Mejia, J., Gillies, J. A. (January 10, 2022). "Model-Derived Estimates of Mass Emissions of PM10 for Pre-OHV Disturbance and Past Vegetation Scenarios"

Model-Derived Estimates of Mass Emissions of PM10 for Pre-OHV Disturbance and Past Vegetation Scenarios

J. Mejia and J.A. Gillies

The Science Advisory Group (SAG) requested, and California State Parks agreed, that DRI use available PI-SWERL emissivity data and the DRI emission/dispersion model to evaluate an alternative method to determine the target for mass emission reductions in the Stipulated Order of Abatement (SOA). The first stage of this evaluation was the estimation of mass emissions from the ODSVRA for the 10 baseline days if the emissivity of the riding area was represented by the mean emissivity relationship for all non-riding areas, with the non-riding area emissivity remaining as it was based on the 2013 PI-SWERL data. The assumption was that the mean non-riding area emissivity better represents the conditions for a non-OHV impacted dune system than is currently represented in the SOA. The mass emissions target defined in the SOA is based solely on PM_{10} and wind data downwind of the Oso Flaco/southern dune preserve area.

The initial examination of the alternative method first involved comparing the non-riding area emissivity distribution with the riding area emissivity distribution for the PI-SWERL emissivity data collected between 2013 and 2019. PI-SWERL tests made within the seasonal plover exclosure were excluded as this area has a period that allows OHV activity and period that excludes OHV activity.

The mass emissions rate expressed in metric tons of PM_{10} emitted in 24 hours for the ODSVRA based on the 2013 emissivity data and the mean non-riding emissivity relationship and the 10 baseline days of meteorology and the distribution of the emissions across space are shown in Fig. 1 (Gillies et al., 2022). The only masking done to identify zones of zero emissivity was for the vegetation islands that currently exist. The vegetation mask layer was received from Parks (T. Carmona, personal communication).

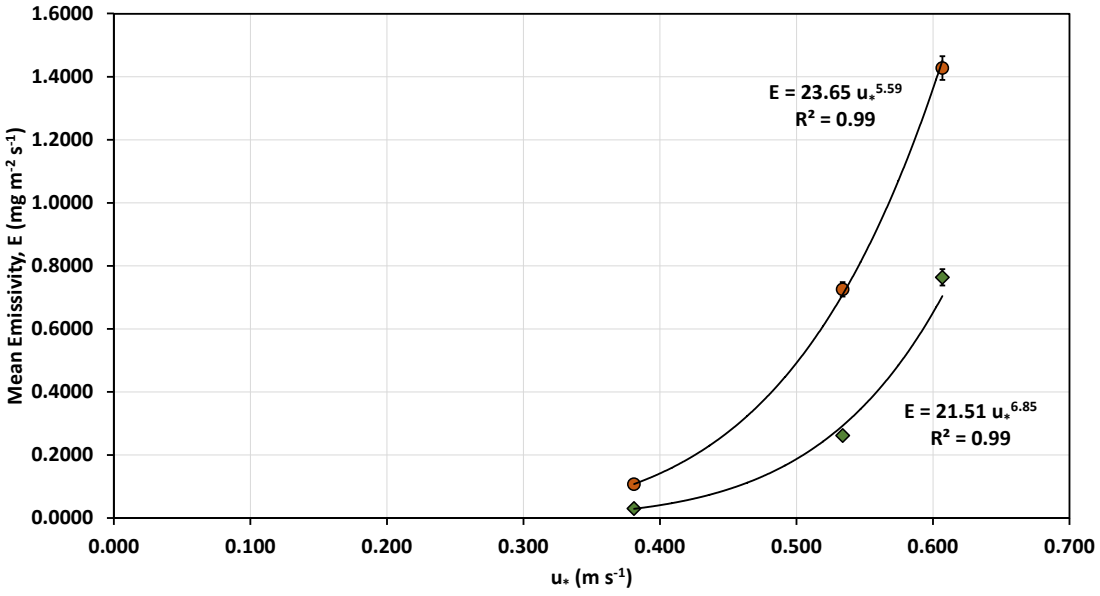

Figure 1. The relation between mean E (mg m^{-2} s^{-1}) and u_* (m s^{-1}) for the amalgamated data from 2013 to 2019 for the riding (orange circles) and non-riding areas (green diamonds). Error bars represent the standard error of the estimate (standard deviation/(#observations-1)$^{0.5}$) (from Gillies et al., 2022).

The modeled mass emissions for the 2013 PI-SWERL emissions grid for the ODSVRA (riding area grid cells) was 182.8 metric tons day^{-1} (refer to Table 4-2, 2021 ARWP) and for the alternative emissions grid (i.e., riding area represented by non-riding mean emissivity) was 118.2 metric tons day^{-1}. The difference is 64.6 metric tons day^{-1}, which represents a percentage difference of 35.3% (lower) compared with the 2013 total mass emissions.

The modified emission grid and the 10 baseline days of meteorology were also used to model the 24-hour mean PM_{10} concentrations at the two key receptor sites CDF and Mesa2. The PM_{10} 24-hour mean concentrations for the 10 baseline days (measured and modeled) for the 2013 emission grid and the alternative emission grid for CDF and Mesa2 are shown in Table 1. For the meteorology of the 10 baseline days and the alternative grid, the modeled 24-hour mean PM_{10} concentrations for both measurement sites are still above the State standard of 50 μg m^{-3}.

Table 1. Measured and modeled 24-hour mean PM_{10} at CDF and Mesa2 for the two emission grids for the 10 baseline days.

CDF	PM_{10} (μg m^{-3})	% Change (lower than obs.)
Observed	128	
Modeled (2013 grid)	124	
Modified grid	80	37.5
Mesa2		
Observed	95	
Modeled (2013 grid)	98	
Modified grid	73	23.2

As part of the initial evaluation DRI also examined the available PI-SWERL emissivity data to characterize the observed north to south gradient in emissivity. There is strong evidence of a decrease in emissivity moving from north to south in the riding and non-riding areas of the ODSVRA (Gillies et al., 2022).

The mean emissivity relations for riding and non-riding areas (Fig. 2) were disaggregated to examine for geographic influence on the emissivity across space. The emissivity data for the non-riding areas can be grouped as: northern dune preserve, areas east of the riding/non-riding boundary in the middle zone of the ODSVRA, and the southern dune preserve (Fig. 2). For each of the three zones an ANOVA test was done on the paired data for each set-point u_*. The ANOVA tests indicated that the mean emissivity values for each test u_* are significantly different between the geographic locations at the P=0.05 level, with the north having higher emissivity than the east and the south, and east higher than the south. The gradient of increasing emissivity towards the north in the non-riding area also was observed in the emissivity data for the riding area of the ODSVRA.

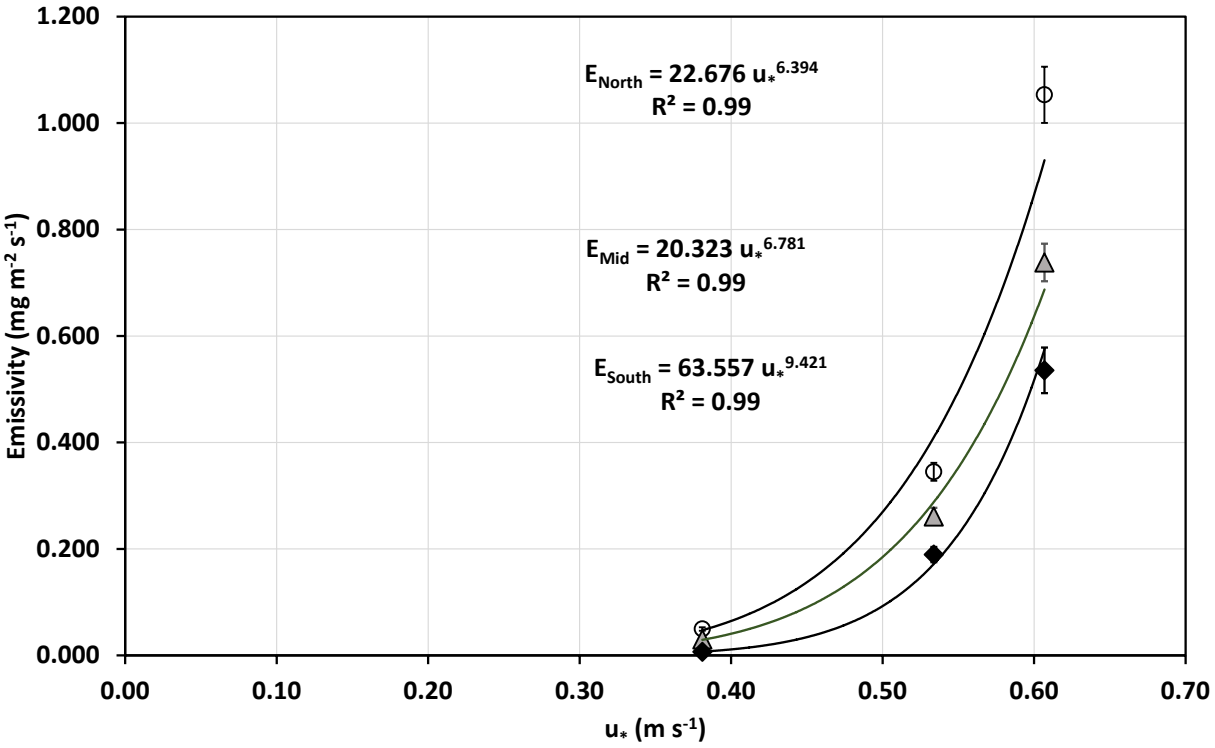

Figure 2. The relation between mean E (mg m^{-2} s^{-1}) and u_* (m s^{-1}) compared by geographic position for the non-riding areas: white circle, north; grey triangle, middle, black diamond, south. Error bars represent the standard error of the estimate (standard deviation/(#observations-1)$^{0.5}$) (from Gillies et al., 2022).

The SAG requested, and Parks agreed, that DRI carry out additional modeling to define a pre-OHV impact scenario using the latitudinally influenced emissivity relations shown in Fig. 2. For modeling, the emission grid was divided into three latitudinal zones: north, middle, and south. For each case the emissivity is assigned within the latitude range and across the west-east expanse of the riding areas. The non-riding area grid cells maintained their 2013 emissivity.

In addition, DRI was provided with two vegetation distribution scenarios developed by Swet et al. (2021) that were developed from analysis of aerial photographs from 1939 (Fig. 3) and 1966 (Fig. 4). These were agreed upon by Parks and the SAG to be the best representation available that characterize vegetation patterns for a much less impacted ODSVRA.

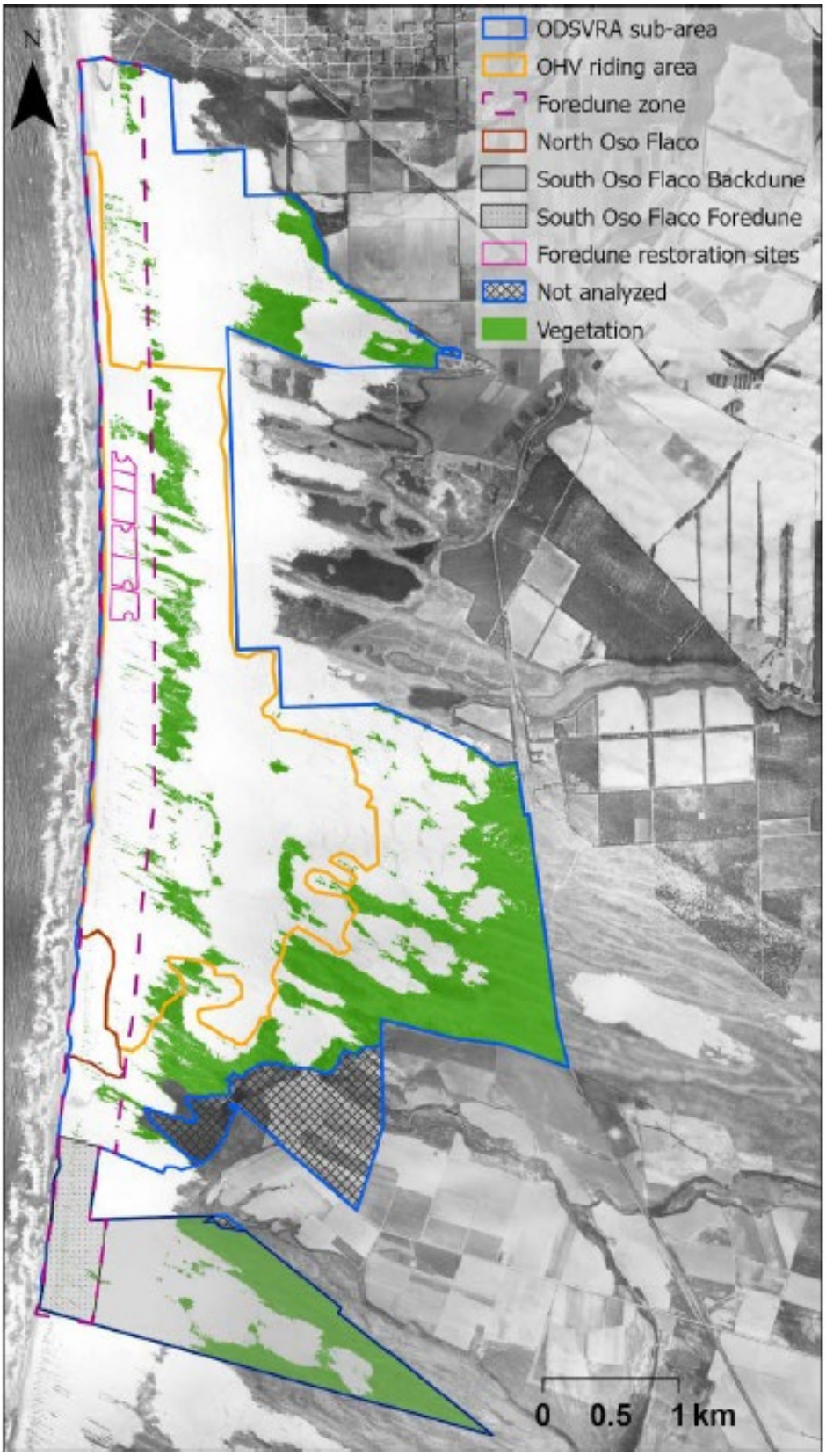

Figure 3. Vegetation cover map, 1939 (from Swet et al., 2021).

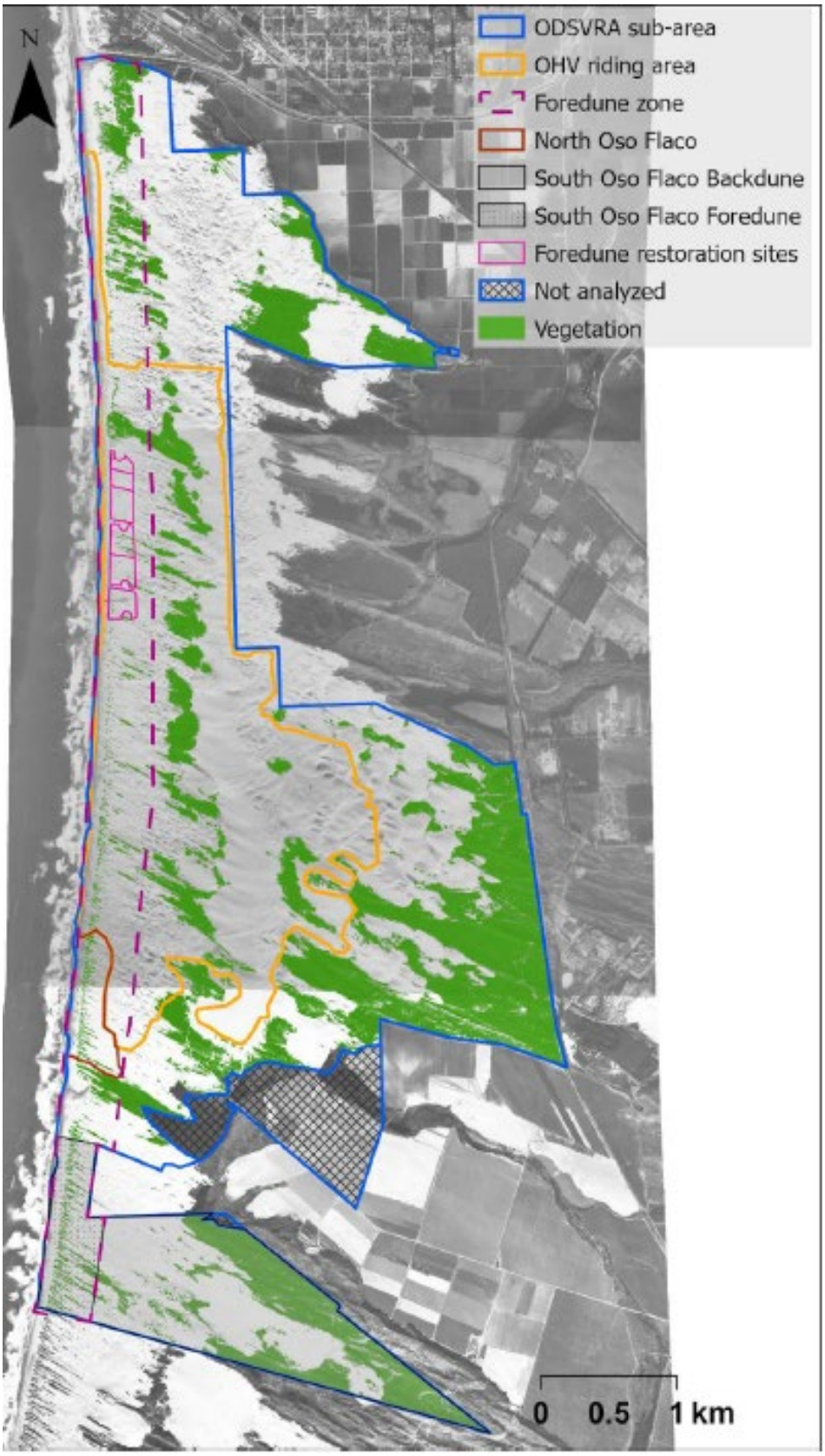

Figure 3. Vegetation cover map, 1966 (from Swet et al., 2021).

Model Results

The emission grid was first modified to fill in the established vegetation islands with grid cells represented by the emissivity relations shown in Fig. 2, depending on the latitudinal position of the vegetation islands representing the vegetation distribution of 2013. The pre-disturbance emission grid (vegetation removed) is shown with the 2013 emission grid as currently and previously used to develop emission scenarios in Fig. 5.

The vegetation masks for 1939 and 1966 were then used to create the emission grid for each of these years. The emissivity was set to zero for the parts of the surface covered by the vegetation mask. The total mass emission was then calculated by using the meteorology that represents the 10 baseline days of 2013. It should be noted that the 1939 and 1966 vegetation are overlain onto the topography of 2013. We do not have topographical data for these two earlier years.

The maps of emissions (g m^{-2} day^{-1}) for the two vegetation masks are shown in Fig. 6. Note that the scale bars are different between Figures 5 and 6, which allows for more detail to be shown for the spatial patterning in the pre-disturbance vegetation scenarios. The spatial distribution of the emissions is a function of the assigned emissivity relations to each grid cell and the model-derived values of shear velocity (u_*, m s^{-1}) generated by CALMET on the underlying topography.

The modeled emissions (metric tons day^{-1}) for the 1939 and 1966 vegetation scenarios estimated for the riding area only for the meteorology of the 10 highest emission days in 2013 are 108.4 metric tons day^{-1} and 108.9 metric tons day^{-1}, respectively.

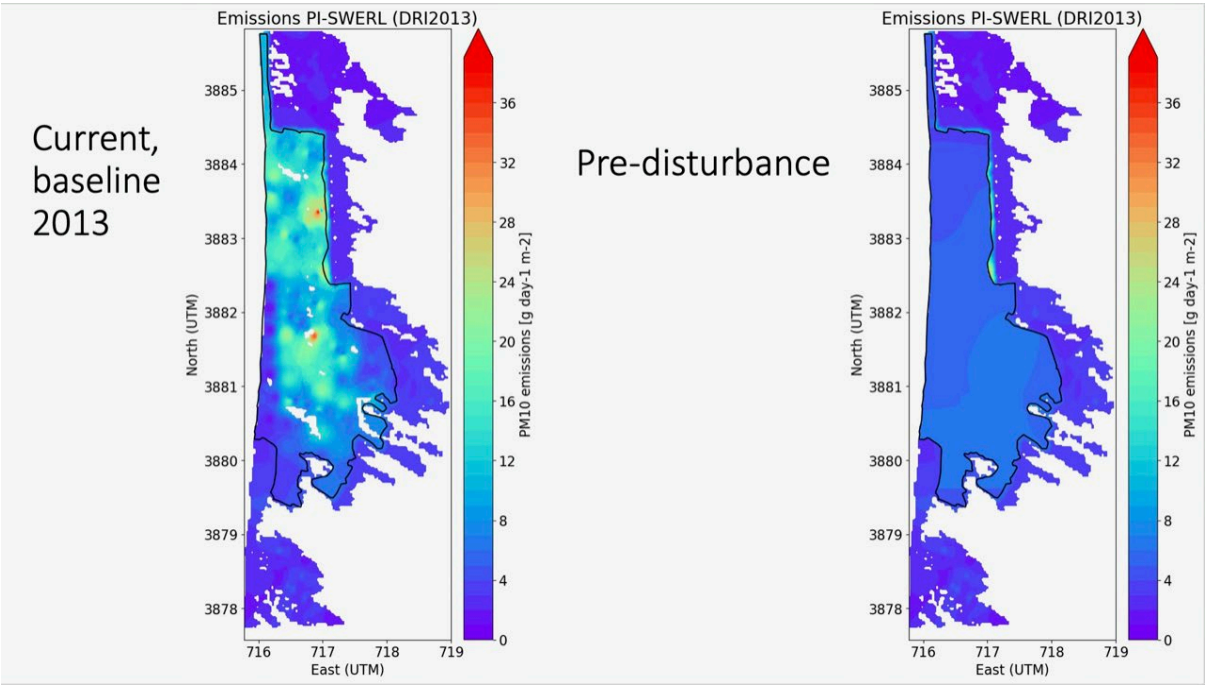

Figure 5. The baseline emission map for 2013 (left panel) and the pre-disturbance emission grid (right panel) where the vegetation within the riding areas has been replaced with the appropriate latitudinal dependent emission relation.

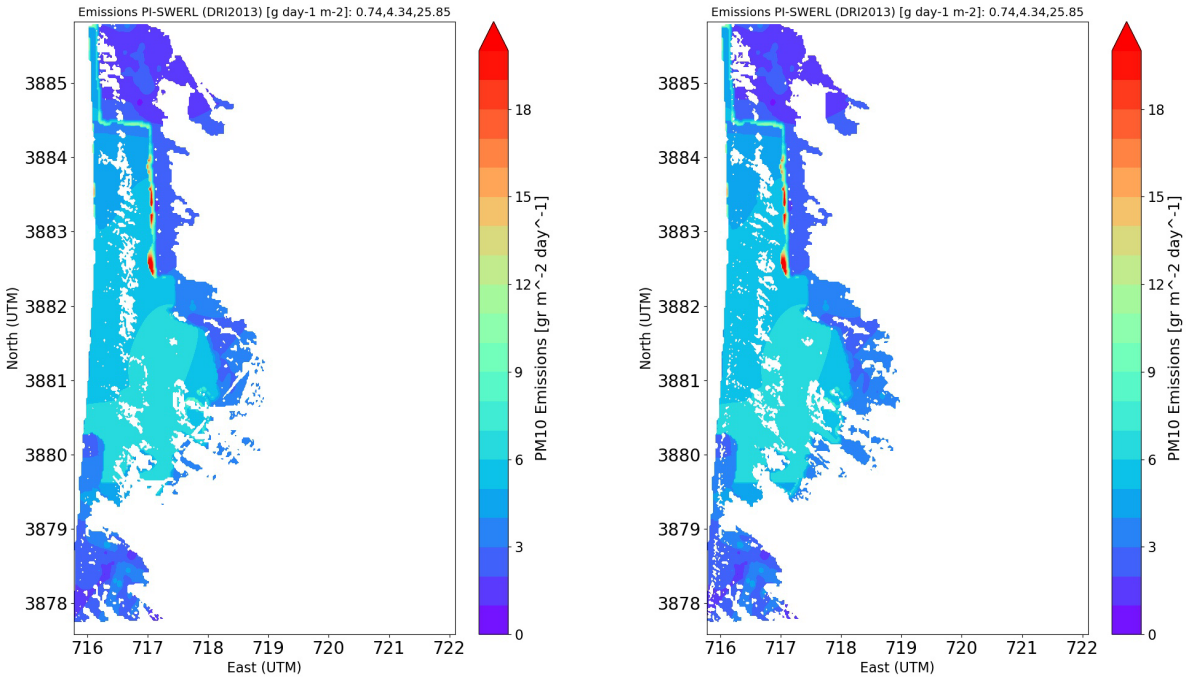

Figure 6. The baseline emission maps for 1939 (left panel) and 1966 (right panel) for the 2013, 10 baseline days meteorology and the respective vegetation masks.

The model estimates for mass emissions up to July 2022 with 412.5 acres of dust control were presented in Table 3-1 of the 2021 Annual Report and Workplan, which is reproduced here as Table 1. Based on the total mass emissions estimate of 131.2 metric tons day^{-1} accounting for the dust controls in place by July 2022 within the riding and camping areas, the riding area would be producing 22.1 and 22.3 more metric tons day^{-1} than the 1939 and 1966 vegetation scenarios, which is approximately 16.9% and 17.0% greater than these pre-disturbance baseline values for 1939 and 1966, respectively.

The pre-impact OHV scenario modeled here suggests that the potential emission target for the SOA be increased to approximately 108 metric tons day^{-1} from 91.4 metric tons day^{-1} that is the current SOA target. The modified SOA target of 108 metric tons day^{-1} represents a percent reduction from the baseline value of 182.8 metric tons day^{-1} of 40.9%.

Table 1. Modeled Estimated Reductions of PM_{10} for the ODSVRA Riding Area.

Table 3-1. Modeled PM_{10} Mass Emissions Reductions – 2021/2022 Dust Control Projects

Scenario/Evaluation	Cumulative Area Controlled (Acres)	ODSVRA – All Areas		ODSVRA – Open Riding and Camping Area Only	
		PM_{10} Mass Emissions (Metric Tons/Day)	Percent Reduction in PM_{10} Mass Emissions	PM_{10} Mass Emissions (Metric Tons/Day)	Percent Reduction in PM_{10} Mass Emissions
2013 Modeled Baseline Emissions from Open Riding and Camping Area (No Dust Control Measures in Place)	0	182.8(A)	0%	182.8(A)	0%
Cumulative Dust Control Measures in Place as of July 31, 2021	322.5	142.0 (-40.8)(B)	-22.3%(B)	145.2 (-37.6)	-20.6%
New Dust Control Measures to be Installed between August 1, 2021 and July 31, 2022	*90.0*	*124.9 (-17.1)(C)*	*-9.4%(C)*	*131.2 (-14.0)*	*-7.7%*
Cumulative Totals - All Dust Control Measures in Place as of July 31, 2021	**412.5**	**124.9 (-57.9)(D)**	**-31.7%(D)**	**131.2 (-51.6)**	**-28.2%**
SOA Condition 2.c Goal	**--**	**91.4(E)**	**50%**	**91.4**	**50%**

Source: DRI, 2021 (see Attachment 17), modified by State Parks.

(A) Pursuant to the SOA, the 2013 modeled baseline for mass emissions is based on emissions from the ODSVRA open riding and camping area only; however, the mass emissions reductions needed to comply with the SOA, as amended, may occur from both inside and outside the open riding and camping area.

(B) The cumulative dust control measures in place throughout the ODSVRA as of July 31, 2021 reduced 2013 modeled baseline mass emission from 182.8 metric tons per day to 142.0 metric tons per day, a reduction of 40.8 metric tons per day, which equals a 22.3% reduction in 2013 modeled baseline emissions (40.8/182.8 = 22.3%). Most of the mass emissions reductions (37.6 out of 40.8 metric tons per day, or 92.2% of mass emissions reductions) are achieved by dust control measures installed inside the open riding and camping area. Note table values for ODSVRA – All Areas may differ slightly (less than 1.0 metric ton per day) from values contained in Attachment 17 due to rounding and model tolerances.

(C) The new dust control measures installed throughout the ODSVRA between August 1, 2020 and July 31, 2021 reduced 2013 modeled baseline mass emissions from 153.1 (as of July 31, 2020) to 142.0 metric tons per day, a reduction of 11.1 metric tons per day, which equals 6.1% of 2013 modeled baseline emissions levels (11.1/182.8 = 6.1%). Most of the mass emissions reductions (10.1 out of 11.1 metric tons per day, or 91.0% of mass emissions reductions) are achieved by dust control measures installed inside the open riding and camping area. Note table values for ODSVRA – All Areas may differ slightly (less than 1.0 metric ton per day) from values contained in Attachment 17 due to rounding and model tolerances.

(D) The cumulative dust control measures in place throughout the ODSVRA as of July 31, 2021 reduced 2013 modeled baseline mass emission from 182.8 metric tons per day to 142.0 metric tons per day, a reduction of 40.8 metric tons per day, which equals a 22.3% reduction in 2013 modeled baseline emissions (40.8/182.8 = 22.3%). Most of the mass emissions reductions (51.6 out of 57.9 metric tons per day, or 89.1% of mass emissions reductions) are achieved by dust control measures installed inside the open riding and camping area. Note table values for ODSVRA – All Areas may differ slightly (less than 1.0 metric ton per day) from values contained in Attachment 17 due to rounding and model tolerances.

(E) A 50% reduction in 2013 modeled baseline mass emissions (182.8 metric tons per day) equals 91.4 metric tons per day.

Downwind PM_{10} at CDF and Mesa2 for the Vegetation Scenarios and 10 Baseline Days Meteorology

Dispersion modeling for the two vegetation scenarios was carried out to provide estimates of the PM_{10} mass concentrations (µg m^{-3}) that would be observed at the APCD monitoring stations CDF and Mesa2 (Table 2).

The modeled values of 24-hour mean PM_{10} at CDF for the pre-OHV impact emission grid and vegetation masks for 1939 and 1966 are 31.3% and 32.0% lower than the 2013 Observed baseline value of 128 µg m^{-3}. The modeled values of 24-hour mean PM_{10} at Mesa2 for the pre-OHV impact emission grid and vegetation masks for 1939 and 1966 are 25.2% and 20.0% lower than the 2013 Observed baseline value of 95 µg m^{-3}.

The modeled values of 24-hour mean PM_{10} at CDF and Mesa2 are above the State Standard of 50 µg m^{-3} for the pre-OHV impact and both vegetations scenarios. This suggests that even in a pre-OHV impacted condition this area could produce PM_{10} concentrations on the Nipomo Mesa that exceed the current State standard 24 hour mean PM_{10} concentration.

Table 2. Measured and modeled 24-hour mean PM_{10} at CDF and Mesa2 for the two vegetation scenarios for the 10 baseline days meteorology.

CDF	PM_{10} (µg m^{-3})	% Change (lower than obs.)
Observed	128	
Modeled (2013 grid)	124	
1939 Vegetation, pre-impact emission grid	88	31.3
1966 Vegetation, pre-impact emission grid	87	32.0
Mesa2		
Observed	95	
Modeled (2013 grid)	98	
1939 Vegetation, pre-impact emission grid	71	25.2
1966 Vegetation, pre-impact emission grid	76	20.0

References

Gillies, J.A., E. Furtak-Cole, G. Nikolich, V. Etyemezian (2022). The role of off highway vehicle activity in augmenting dust emissions at the Oceano Dunes State Vehicular Recreation Area, Oceano CA. *Atmospheric Environment: X*, 13, 100146, doi: 10.1016/j.aeaoa.2021.100146.

Gillies, J.A., J. Mejia, E. Furtak-Cole (2021). Report to the SAG and Parks Evaluating the Potential for Developing a New Baseline Mass Emissions Rate and Target Reduction within the SOA. Report prepared for California State Parks by Desert Research Institute, Reno, NV, March 2021.

Swet, N., Z. Hilgendorf, I. Walker (2021). UCSB Historical Vegetation Change Analysis (1930-2020) within the Oceano Dunes SVRA. Report prepared for California State Parks by University California, Santa Barbara, CA, December 2021.

ATTACHMENT 2

Swet, N., Hilgendorf, Z., Walker, I. (February 2022). "UCSB Historical Vegetation Cover Change Analysis (1930-2020) within the Oceano Dunes SVRA"

UCSB Historical Vegetation Cover Change Analysis

(1930-2020) within the Oceano Dunes SVRA

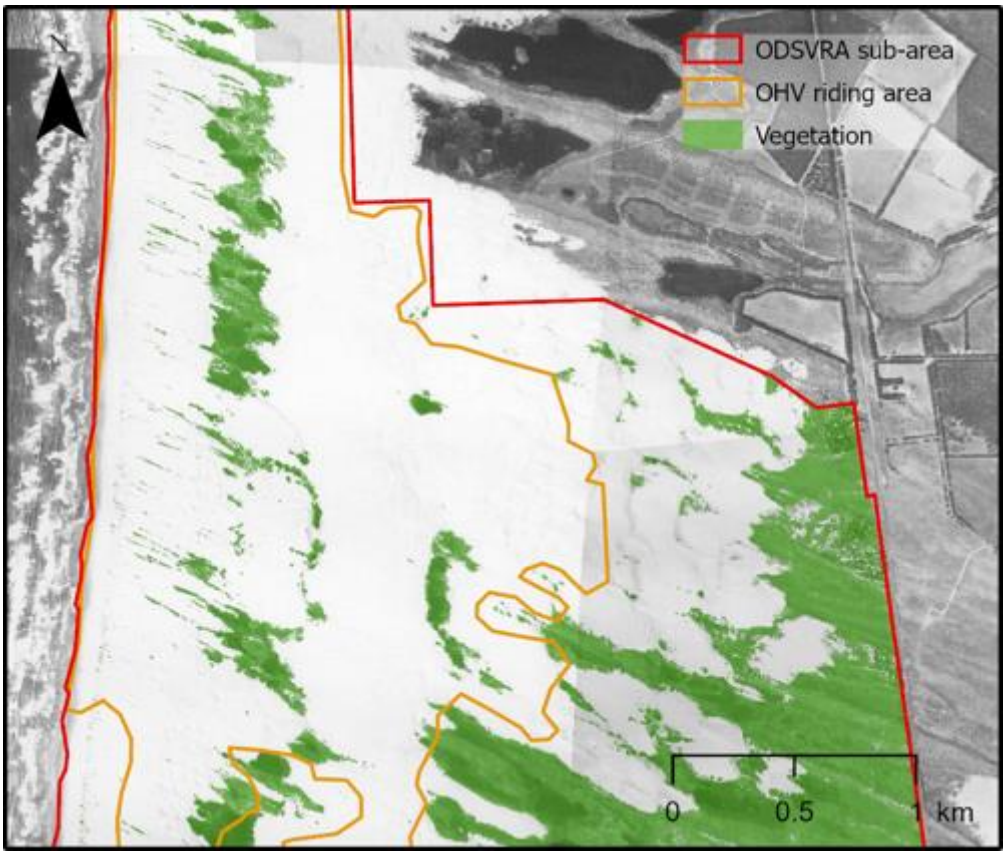

Map of vegetation cover (green) derived from historical 1939 aerial photography of the southern portion of the Oceano Dunes SVRA

Prepared by: Nitzan Swet[1], Zach Hilgendorf[1,2] and Ian Walker[1,3]

[1] Department of Geography, University of California Santa Barbara

[2] School of Geographical Sciences and Urban Planning, Arizona State University

[3] Member of the Oceano Dunes Scientific Advisory Group

February 2022

EXECUTIVE SUMMARY

This report examines 90 years of historical changes in vegetation cover within the ODSVRA as requested by CDPR for the 2020 ARWP. Trends in plant cover are mapped and quantified using a Geographic Information System (GIS) and best available aerial photography obtained from CDPR, UCSB Library's Geospatial Collection, and the National Agriculture Imagery Program (NAIP), from 16 years with sufficient coverage of ODSVRA between 1930 and 2020.

To examine and interpret vegetation cover trends and allow comparison between different regions of the ODSVRA, the report focuses on:

- the overall ODSVRA, located south of Arroyo Grande Creek (~75% of the total area of ODSVRA), presented here as ODSVRA sub-area,
- the OHV riding area (c. 2013),
- the North Oso Flaco foredune complex, which serves as a reference site for foredunes closed to OHV activity since 1982,
- the South Oso Flaco dune complex within the ODSVRA boundary, including both foredune and backdune areas, which serves as a reference site for mature foredunes and backdunes that have not seen OHV activity since 1982,
- the foredune zone of each of the areas above, or the area in which foredune vegetation would typically exist in the region, that extends ~400 m eastward/inland from the high-water mark,
- the new (2020) foredune restoration sites, located within the foredune zone of the OHV riding area between post markers 4-6.

Plant cover maps and calculations (area and percentage) were obtained for each analytical zone across all image years.

Resulting maps were analyzed for locations and extents of change between all years. In addition, changes between 4 specific time periods that relate to different land management intervals were interpreted:

1. 1939-1985: landscape responses preceding the management of ODSVRA by CDPR, which began in 1982,
2. 1985-2012: landscape changes during the management of ODSVRA by CDPR up to adoption of SLO-APCD Rule 1001 (2011) and related particulate matter reduction plans (PMRP),
3. 2012-2020: landscape responses following implementation of PMRP mitigation efforts resulting from Rule 1001 (2011) and the eventual Stipulated Order of Abatement (SOA) in 2018, and
4. 1939-2020: total landscape change over the historic aerial photo record that compares a time prior to widespread OHV riding and the current state of vegetation cover.

Plant cover trends within ODSVRA have varied over time and differ notably between the analytical zones. Within the broader ODSVRA sub-area, vegetation change generally increased over time, from approximately 25% in 1939, to a peak of 37% in 2012, to just over 35% in 2020. In the OHV riding area, vegetation cover has been comparatively low across all years and declined appreciably from a peak of 12% in 1966 to 8% in 2020. After 1966, plant cover decreased to a low of 3.9% in 1985 and remained low (<5%) until the early 2000's when vegetation cover gradually began to increase to 2020 levels following revegetation efforts by CDPR. In the South Oso Flaco area, plant cover changes are similar to those in the broader ODSVRA sub-area, but with generally higher values. Vegetation cover at South Oso Flaco decreased from 26% in 1939 to a historic low of 24% in 1949, then more than doubled to a peak of 66% in 2012. Following this, plant cover declined slightly but remained >60% to 2020.

Similar trends occur within the foredune zone in each analytical area, albeit with generally less plant cover. The foredune zone at the South Oso Flaco reference site had very low plant cover (2.3%) in 1939, but increased by an order of magnitude to over 30% in the 2010s. For comparison, foredune vegetation in the OHV riding area also had low cover (2.6%) in 1939, rose to a peak of 5.3% in 1966, but steadily declined to very low values ~1% from 1985 to 1998. Since 2005, plant cover increased slightly in the riding area to 2.4% by 2020, mostly due to new plants on the margins of fenced vegetation islands and in the seasonal bird nesting enclosures. At North Oso flaco, foredune vegetation cover was extremely low (<1%) in the 1930s, less than in the OHV riding area, but after 1985 the values increased to over 24% in 2012.

Broader ecological and climatic conditions aside, observed patterns and differences in vegetation trends across these areas is largely attributable to three main factors: 1) the presence of camping and OHV riding (sanctioned or otherwise) activities in the dunes, 2) widespread and targeted removals of invasive grass species in some areas (e.g., South Oso Flaco), and 3) land management and plant restoration efforts by CDPR since establishment of the park in 1982 and in response to PMRPs associated with Rule 1001 (2011) and the 2018 SOA.

Interpretation of positive (vegetation gain) and negative (vegetation loss) changes over the four reference time periods indicates the following:

- 1939-1985: a general decline in plant cover in the foredune and backdune zones of the OHV riding area (from 11% to 4%) while vegetation in the broader ODSVRA increased notably from 1939-1966, then declined until 1985. In the riding area, overall change is characterized by 10% negative change (plant losses) and only 2% positive gains,
- 1985-2012: mostly increasing plant cover with over 15% gains in the broader ODSVRA sub-area, mainly around existing vegetation and other targeted restoration areas, particularly between 2005 and 2012.

- 2012-2020: a general decline in plant cover across the ODSVRA and South Oso Flaco areas compared to previous intervals with 8% total change in the ODSVRA sub-area. Some of this decline reflects removal of invasive plants by CDPR. Within the OHV riding area, plant cover remained steady at ~8% during this time.

1. Introduction

Vegetation plays a vital role in the development and maintenance of certain dune types and related ecosystems common in the central coast of California (e.g., nebkha and shadow dunes, foredunes, blowouts, parabolic dunes) as well as in the stabilization of sand surfaces to reduce sand drift, wind erosion, and dust emissions. In areas of high recreation activity, natural windblown (aeolian) and related dune ecological processes often become challenged. In turn, this can result in a loss of vital ecosystem services provided by coastal dunes including mitigating sand transport and dust emissions, buffering coastal erosion and flooding, facilitating groundwater recharge, and providing important habitat for a wide range of endemic, migratory, threatened, and endangered plant and animal species.

This report provides a thorough review of historical changes in vegetation cover within the Oceano Dunes State Vehicular Recreation Area (ODSVRA) as requested by the California Department of Parks and Recreation (CDPR) for the 2020-2021 Annual Report and Work Plan (2020 ARWP). Vegetation cover from historical aerial photographs from the 1930s to 2020 was analyzed to interpret changes from the earliest photo records. As such, the analysis documents landscape changes through decades of unsanctioned OHV activity prior to establishment and management of ODSVRA by CDPR in 1982 and through almost another 40 years following. Changes during this later period reflect both OHV activity as well as significant land use management and vegetation restoration initiatives implemented by CDPR to mitigate dust emissions and control invasive species. With more frequent photo coverage in recent years, responses of the landscape following implementation of Particulate Matter Reduction Plans (PMRP) associated with the SLO-APCD Rule 1001 “Coastal Dunes Dust Control Requirements” of 2011 and the State of California Stipulated Order of Abatement (SOA) in 2018 are also quantifiable.

The main objective of the report is to document and analyze historical changes in vegetation cover and related dune landforms within ODSVRA to help inform development of baseline conditions for restoration and dust emissions mitigation strategies in the future 2022 ARWP. In particular, it is important to establish what the state of vegetation cover was prior to, and since, the management of ODSVRA by CDPR and related changes in plant cover with sanctioned OHV activity and camping in the dunes. These results can also inform assessment of landscape changes

associated with more recent management and restoration activities in response to PMRP activities and act as a tool for identifying future treatment locations and methods.

2. Methods

An extensive dataset of aerial photography for the Oceano Dunes region was obtained from the UCSB Library Geospatial Collection[1], CDPR, and the National Agriculture Imagery Program (NAIP) website[2] consisting of 19 individual years of imagery taken between 1939 to 2020 (Table 1). Due to limitations resulting from limited coverage, image projection, size, and/or shadowing, three image years were omitted from the analysis, leaving a total of 16 image years. The imagery datasets for 1930 to 1985 are composed of a mosaic of individual aerial photos (tiles). The aerial photo tiles for 1930 to 1978 were received as digital scans from the UCSB Library and processed using Agisoft Metashape and standard historic imagery photogrammetric methods[3]. The 1985-1998 aerial photo tiles were scanned and processed by CDPR staff. The rest of the imagery used in this report (2005-2020) are in a digital orthophoto mosaic format (one tile) downloaded from different sources. The 1994, 1998, and 2007 images were received from CDPR, however, their sources are uncertain (see Table 1). The 2005 and the 2010 to 2020 images were downloaded from NAIP (Table 1).

For each image year between 1930 and 1985, photo tiles required local alignment to one another, typically completed with a simple shift or 2nd order transformation. Once all tiles were aligned, clipped shapefiles were created for each to remove cataloging data from the edges, interior portions of each tile were extracted, and the resulting images were then loaded into a raster mosaic of the study area as a file geodatabase in the Geographic Information System (GIS) software ArcGIS Pro. During this step, the tiles were manually assessed and layered so that rasters (digital image grid cells or pixels) with darker, more pronounced, sharper features were on top of those with lighter, or less pronounced features. This also allowed for continual assessment and correction of tile alignment. This alignment and orthorectification step is important as slight misalignments and planar tilt issues can produce appreciable errors in positioning and measurements of ground features. The final mosaic was then exported to a single digital (tiff) file for each photo year.

[1] University of California Santa Barbara Library geospatial collection of aerial photography is available at: https://www.library.ucsb.edu/geospatial/aerial-photography

[2] National Agriculture Imagery Program (NAIP) is available at: https://www.fsa.usda.gov/programs-and-services/aerial-photography/imagery-programs/naip-imagery/

[3] Carvalho, R.C., Kennedy, D.M., Niyazi, Y., Leach, C., Konlechner, T.M., Ierodiaconou, D., 2020. Structure-from-motion photogrammetry analysis of historical aerial photography: Determining beach volumetric change over decadal scales. Earth Surface Processes and Landforms 52, 2540–2555. https://doi.org/10.1002/esp.4911

For all image processing, a 2020 USDA National Agricultural Imagery Program (NAIP) geotiff was used as a reference layer, to which all photo years were compared and aligned. Some photo years (e.g., 1960s-70s) exhibited significant differences in the presence and/or alignment of key anchor features from the 2020 NAIP image (e.g., infrastructure features that were not present in earlier imagery), so these photo years were aligned using orthomosaic images from the early 1990s with high georectification accuracy and common anchor features. The oldest images (e.g., 1930s-1940s) were referenced to the best georectified images from the 1960s. In this way, locational precision for all years was cross-referenced to the position of the high resolution, geolocationally constrained 2020 NAIP imagery by using alignment features from closer years.

Table 1 contains metadata of all imagery datasets used in this report, including image resolution (i.e., pixel or raster grid cell size in m), also known as the ground sampling distance (GSD) of the imagery, as well as the number of image tiles used to create the mosaic of the final image file (.tiff). Transformation type refers to the way in which each raster cell was aligned with its real-world location through manual refinement and the selection of static ground control points (GCPs) between images. Of several methods available in ArcGIS Pro, polynomial and spline transformations were found to have the most accurate corrections for the datasets used. This accuracy is reported through the total root mean square (RMS) forward-inverse error, which expresses the projected uncertainty (in pixels), relative to the GCPs and the transformation type for each image set[4]. Pixel depth refers to the range of values that a raster cell type can store. For example, an unsigned 8-bit raster type can store 256 digital values between 0-255. The band number for each raster is a reference to how many layers of data are stacked to produce the raster dataset. Three band types were used in this study, including a single-band (grayscale) dataset for older imagery through 1978, and three- or four-band imagery in the later datasets. Three-band imagery expresses visual color (red-green-blue or RGB) wavelengths. Four-band imagery expresses the visual spectrum in the first three (RGB) bands and an additional near-infrared (NIR) band. The NIR spectrum is particularly useful for mapping, assessing, and extracting vegetation from multispectral imagery[5].

The aligned mosaic image datasets for each year were then classified using the supervised (sampling-based) classification wizard in ArcGIS Pro to identify vegetation and non-vegetation pixels using areas (and spectral signatures of color or grayscale) of known cover identified by the analyst. Classification results were then quality checked by visual inspection to identify wrongly classified pixels, then these cells were manually re-classified using the Pixel Editor tool. For each year, vegetation cover was calculated by area (km^2 and acres) and percentage cover (%).

[4] ArcGIS Pro helpdesk- https://pro.arcgis.com/en/pro-app/latest/help/main/welcome-to-the-arcgis-pro-app-help.htm

[5] Yichun Xie, Zongyao Sha, Mei Yu, Remote sensing imagery in vegetation mapping: a review, Journal of Plant Ecology, Volume 1, Issue 1, March 2008, Pages 9–23, https://doi.org/10.1093/jpe/rtm005

This report focuses on three analytical zones (regions) within a broader sub-region of the ODSVRA, as presented in Figure 1:

- the OHV riding area, border as in 2013,
- the North Oso Flaco foredune complex located north of Oso Flaco Creek,
- the South Oso Flaco dune complex, which includes both foredune and backdune areas south of Oso Flaco Creek.

The ODSVRA sub-area was set as the area south of Arroyo Grande Creek due to limited photo coverage across most years north of this area. The northern areas also contribute minimally to dust emissions due to the limited extent of open sand fetch and typically moist beach surfaces. Of note, this sub-area also includes the Pismo Dunes Natural Preserve (light blue area in Figure 1) that is technically not part of the ODSVRA. The preserve area is considered a subunit of Pismo State Beach, which is administered by the Oceano Dunes District of State Parks. The broader ODSVRA sub-area is approximately 17 km^2 (4215 acres), or about 74% of the total area managed by the Oceano Dunes District, and 85% of the ODSVRA park unit.

An additional portion of the southernmost area of ODSVRA was also excluded from the analysis (hatched area in Figure 1) due to changes in surface water features and human land use/infrastructure (agriculture, roads, buildings) over the years. These southern excluded areas total approximately 0.9 km^2 (238 acres), which is less than 4% of the total ODSVRA area. Furthermore, two years of imagery had limited photo coverage within the ODSVRA sub-area and, thus, the total area for the calculations differs slightly between years (Table 2).

The OHV riding area used for this report (1584 acres) is per the border of 2013 and includes both the open riding area and the vegetation islands. Since 2013, this area has been changed following implementation of various PMRP.

Both the North and South Oso Flaco areas were analyzed to provide comparison to vegetation dynamics within an area of the ODSVRA that has not seen significant OHV riding for decades (since at least 1982) and, as such, provides insights on a less disturbed and more developed state of vegetation cover and dune geomorphology. The borders of these areas (gray and brown Figure 1) were chosen due to hydrological changes of the Oso Flaco Creek over the image years.

Within each of the analytical zones (ODSVRA sub-area, OHV riding area, South Oso Flaco) a separate calculation was conducted for only the foredune zone, defined as the area in which foredune vegetation typically exists in the region, extends about 400m inland from the high water mark (dashed purple line in Figure 1). This zone was identified by the average depth of foredunes from Oso Flaco to near Pavillion Hill. North Oso Flaco area is entirely within the fordedune zone. In addition, this report also analyzed changes within a focus area of the new foredune restoration

sites, established in February 2020, located within the riding area between post markers 4-6 (pink line in Figure 1).

It is also important to note that invasive plant species are present in ODSVRA and have influenced vegetation cover over time. In the early 1900s, European beach grass (*Ammophila arenaria)* and ice plant (*Carpobrotus edulis*)[6,7] were planted to stabilize sand and dunes around the former La Grande Beach Pavilion. Currently, there are still areas within the ODSVRA and Pismo Dunes Natural Preserve that contain these species, as well as invasive South African Veldt grass (*Ehrharta calycina*), which is found in backdune areas. Invasive weeds have resulted in increased plant cover and foredune stabilization in ODSVRA. However, since 2009 different removal methods for invasive species have been used (e.g., burning, herbicides, hand-pulling)[8] at various locations.

The classified vegetation raster datasets were used to calculate changes in plant cover over time using the Raster Calculator and Change Detection tools in ArcGIS. From these maps, positive and negative changes were calculated as % values between subsequent image years and over different time periods. For change calculations between years that had limited image coverage, the analysis was conducted only on the area of overlap (union) in both image years.

For this report, we focused on three time periods that relate to different land management intervals:

1. 1939-1985: effectively characterizes landscape response during the interval preceding the management of ODSVRA by CDPR, which began in 1982,
2. 1985-2012: captures landscape changes during the management of ODSVRA by CDPR prior to adoption of SLO-APCD Rule 1001 (2011) and related PMRP, and
3. 2012-2020: reflects responses of the ODSVRA landscape following implementation of dust mitigation efforts and PMRP from Rule 1001 and the eventual state SOA (2018).

In addition to these three management intervals, we also characterize changes over the entire 1939 to 2020 period, and between 1939 and 2012. To the best of our knowledge, the 1939 imagery represents a time prior to OHV activity in the area, and comparison to modern 2020 imagery provides understanding of changes following multiple decades of OHV activity. The period between 1939 and 2012 represents these changes in vegetation prior to the SLO-APCD

[6] Guiton-Austin, L. (2011). As cited by Harris, W. California Geological Survey Report, 1 November 2011. "In consideration of Draft Rule 1001 proposed by the San Luis Obispo County Air Pollution Control District: An analysis of wind, soils, and open sand sheet and vegetation acreage in the active dunes of the Callendar Dune Sheet, San Luis Obispo County, California.

[7] Bonk. M. 2010. Mapping Invasive Beachgrass And Veldt Grass In Oceano Dunes Svra Using Multispectral Imagery. CDPR internal report.

[8] Glick, R., ODSVRA, Personal communication, October 2021

Rule 1001 (2011) and related PMRP. All change calculations are presented in Table S2 in the supplementary materials.

We take into consideration that the vegetation cover change rates and percentages presented in this report are influenced by image quality (Table 1). The pixel size (resolution), number of bands, and the overall image condition, generate inaccuracies in vegetation cover classifications and change calculations between the image years. For example, comparing two images with a quality difference can result in some loss of information. In order to address these inaccuracies we conducted thorough manual inspections of the change maps to prevent misclassified pixels.

Due to the limited image cover (Table 2), we were unable to use the oldest imagery available from 1930 in historical change comparison analysis, and thus, this was done using the 1939 image. To verify the classification of vegetation in this early imagery, the 1939 scene was compared to the 1930 imagery (Figure S1). We found very low differences between the years with less than 7% change (4.1% positive and 2.6% negative) in the total overlapping area of ODSVRA, most of which occurred along the margins of backdune areas (Figures S1 and S2). Some of these changes might also relate to seasonality as the 1930 orthophoto was taken at the end of summer (21 August) while the 1939 imagery was taken in the spring (2 May). All vegetation cover calculations performed for this study are presented in Table S1 in the Supplementary materials at the end of the report.

Table 1. *Imagery available for ODSVRA including metadata and source. Not all available years were used for the analysis due to issues with image projection, size, and/or shadowing that posed limitations for land cover classification (^ gray rows = years not analyzed for the report). Asterisk(*) indicates years with limited image coverage (see Table 2).*

Year	Collection date	Resolution (m)	Number of Tiles	Control Points	Transformation Type	Total RMS Forward-Inverse Error (m)	Source	Pixel Depth/Type	Band Number	Mosaic Size (GB)
1930*	Aug-21	0.794	16	12	Spline	0.000	UCSB Library - Geospatial Collection –C-1125A	8 bit unsigned	1	0.299
1939	May-02	0.832	9	27	Spline	0.023	UCSB Library - Geospatial Collection – AXH-1939-ARMY	8 bit unsigned	1	0.136
1949	Mar-31	0.894	NA	24	Spline	<0.001	UCSB Library - Geospatial Collection – AXH-1949	8 bit unsigned	2	0.568
1956	Sep-10	0.937	27	17	3rd Order Polynomial	0.172	UCSB Library - Geospatial Collection –AXH-1956	8 bit unsigned	1	0.617
1960^	Jul-12	0.790	6	13	3rd Order Polynomial	0.125	UCSB Library - Geospatial Collection – HA-GH	8 bit unsigned	1	0.131
1966	Dec-27	1.057	3	NA	NA	NA	UCSB Library - Geospatial Collection – HB-JT	8 bit unsigned	1	0.063
1971*	Jun-13	1.141	14	8	2nd Order Polynomial	NA	UCSB Library - Geospatial Collection – HB-SM	8 bit unsigned	1	0.039
1978	Sep-23	1.856	24	9	2nd Order Polynomial	0.001	UCSB Library - Geospatial Collection – USDA-40-06079	16 bit unsigned	1	0.068
1985	May-14	0.149	13	NA	NA	NA	Source unknown – received from CDPR	16 bit unsigned	3	18.980
1994	Feb-28	0.500	1	10	2nd Order Polynomial	0.004	Source unknown – received from CDPR	16 bit unsigned	3	0.879
1998	May-15	0.200	1	12	3rd Order Polynomial	0.036	Source unknown – received from CDPR	8 bit unsigned	4	16.420
2005	Jun-26	1.000	1	11	2nd Order Polynomial	<0.001	NAIP	8 bit unsigned	3	0.524
2007 *^	Jun-01	0.300	1	10	2nd Order Polynomial	0.001	Source GlobeXplorer – received from CDPR	8 bit unsigned	3	3.320
2010^	Aug-26	1.001	4	11	Spline	0.005	NAIP	8 bit unsigned	4	1.010
2012	May-19	1.000	1	11	2nd Order Polynomial	0.003	NAIP	8 bit unsigned	4	0.697
2014	Sep-24	1.000	1	11	2nd Order Polynomial	NA	NAIP	8 bit unsigned	3	1.640
2016	Aug-07	0.601	1	11	2nd Order Polynomial	0.002	NAIP	8 bit unsigned	4	1.800
2018	Sep-13	0.600	1	0	None	0.000	NAIP	8 bit unsigned	4	0.826
2020	Jun-07	0.600	1	0	Reference	0.000	NAIP	8 bit unsigned	4	1.830

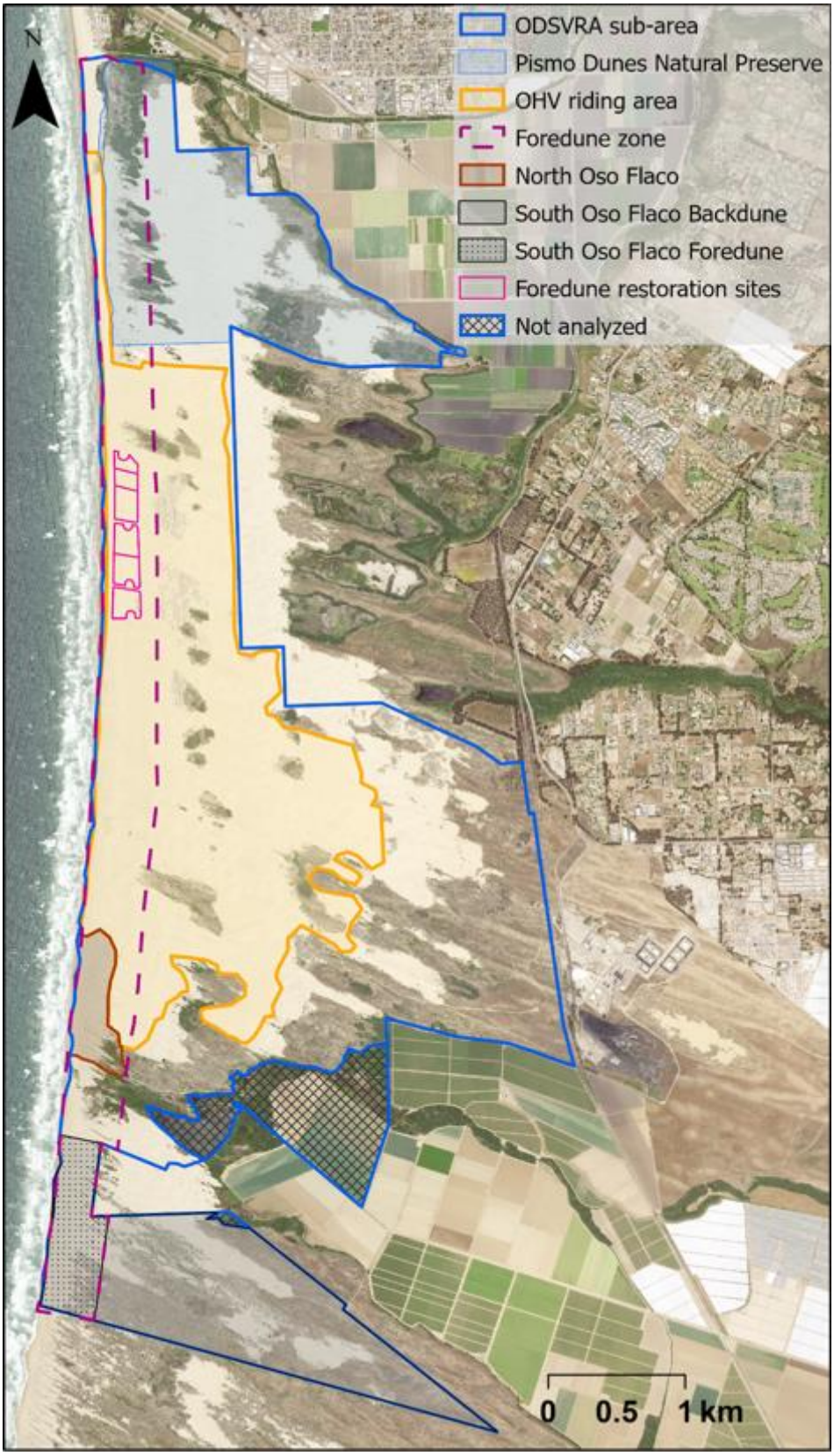

Figure 1. Boundary polygons of the different analytical regions used in the historical vegetation cover change analysis. Orthophoto source from NAIP 2020 (see Table 1).

Table 2. List of image years with limited photo coverage of the ODSVRA sub-area, OHV riding area, and the Oso Flaco area (foredune and backdune) in acres and as a percentage (%). Overall, the sub-area of the ODSVRA is approximately 4215 acres, the OHV riding area is 1584 acres, and the Oso Flaco total area is 577 acres. For specific locations of missing coverage, see Figures S3 and S10 in the supplementary materials.

Area missing						
	ODSVRA sub-area		OHV Riding area		Oso Flaco area	
Year	(acres)	(%)	(acres)	(%)	(acres)	(%)
1930	1108	23.3	338	21.4	0	0.0
1971	135	3.2	0	0.0	129	21.8
Area analyzed						
	ODSVRA sub-area		OHV Riding area		Oso Flaco area	
Year	(acres)	(%)	(acres)	(%)	(acres)	(%)
1930	3107	73.7	1245	78.6	577	100
1971	4080	96.8	1584	100	451	78.1

Our findings (values and maps) were also compared to those derived in previous undocumented analyses by CDPR[9]. For this comparison, we examined differences within the OHV riding area in four image years (1939, 1978, 2014, 2020) that were also analyzed by CDPR for an internal reporting exercise. Unfortunately, due to different methods for georeferencing the images, there was no geometric way to compare differences in vegetation patterns for the 1939, 1978, and 2014 maps. We were, however, able to compare the total calculated areas (acres) of vegetation cover between the CDPR reports and our findings. The CDPR reports showed slightly higher values by roughly 3% for 1939 and 2020 images (i.e., 60 and 51 acres, respectively) and by 0.5% (8 acres) for the 1978 images. The 2014 vegetation cover estimates showed essentially negligible differences (<0.1% or 3 acres) between the reports. The greater differences likely result from different methods in the land cover classification process and related quality assurance checks, which can generate uncertainties. Although the magnitude of difference in estimates between these results is relatively small, the location and pattern of differences is notable. For example, in our analysis of the 2020 vegetation cover, the specific locations (pixels) of every shrub, tree, and herbaceous plant were identified systematically by the supervised classification in the GIS, then the pixels were reviewed manually for discrepancies. The CDPR report appears to have taken a different approach by contouring the area around the vegetation as polygons (Figure 2) and, in doing so, included temporary straw cover in the classification in some areas (Figure 3). Our analysis did not include straw cover, only plants, even if they were growing in older straw cover.

[9] Glick, R., ODSVRA,, Personal communication, 2021.

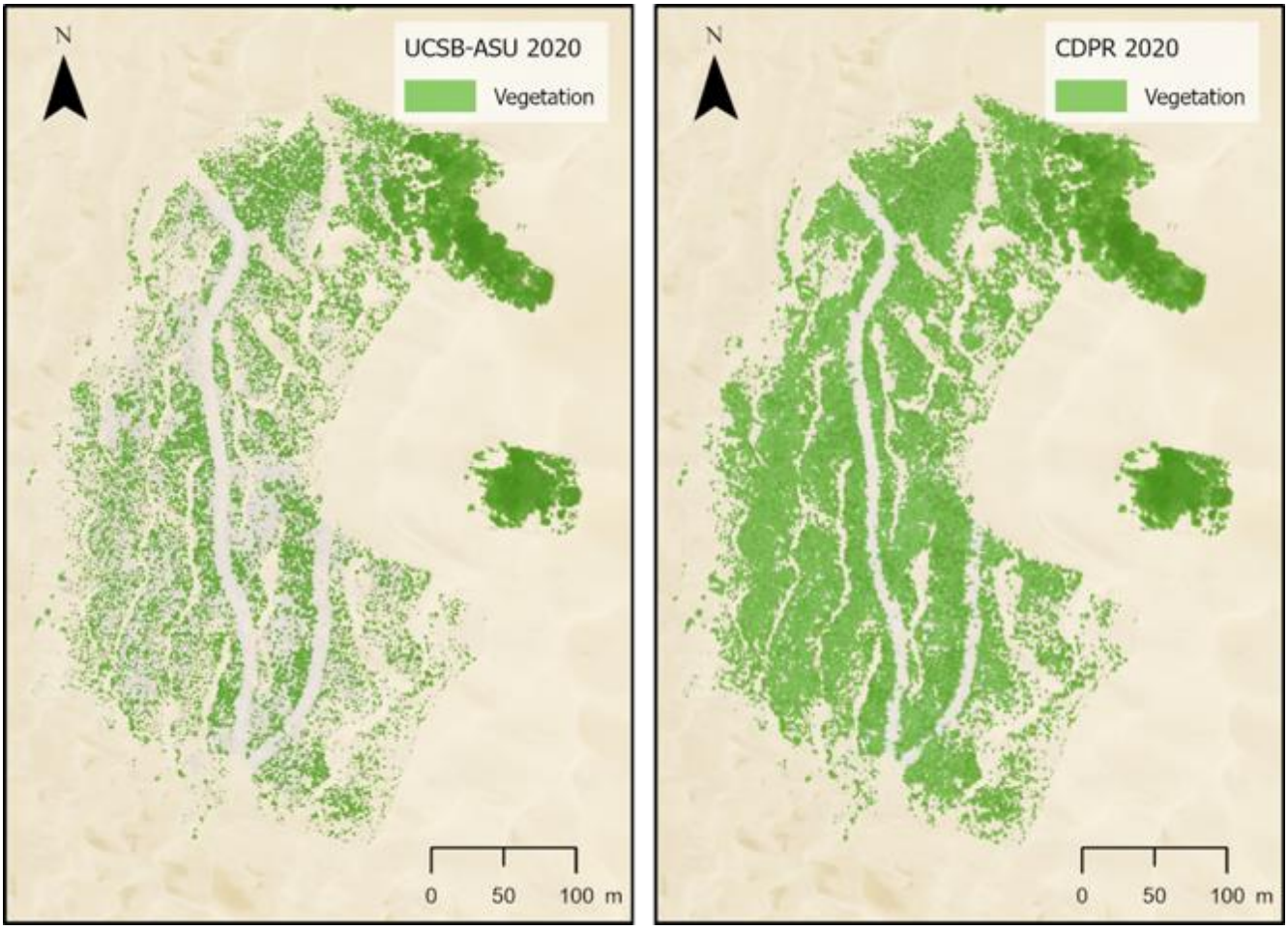

Figure 2. Vegetation cover analysis comparison between the CDPR report (Right) and the current report (Left) for 2020 imagery.

In addition, we tried to compare our findings to those presented in a 2011 report by the California Geological Survey (CGS)[10] that examined vegetation cover change between the 1930s and 2010 (Figure S19). In the CGS report, the 1930s dataset used was a combination (mosaic) of image tiles from both 1930 and 1939, while in this report we used tiles only from a single year (1939) that covered the entire sub-area of the ODSVRA. In addition, there were quality issues with the imagery for 2010 that did not allow for proper alignment and classification, so we were unable to conduct a direct comparison of vegetation cover area to the CGS report. A more general comparison of our 1939-2010 results to the CGS change map shows roughly similar plant cover identification (Figures S19 and S20), yet our calculated areas of change are significantly smaller, which could result from different classification methods, multi-year image mosaicing issues, and/or differences in analytical boundaries.

[10] Harris, W.J. 2011. An analysis of wind, soil and open sand sheet and vegetation acreage in the active dunes of the Callender dune sheet, San Luis Obispo County, California. Department of Conservation, California Geological Survey. 10p.

Figure 3. Vegetation cover analysis comparison between the CDPR report (pink) and the current report (green) for 2020 imagery. The arrows indicate areas where there is a straw treatment that was classified by CDPR as vegetation and by UCSB-ASU as non-vegetated area.

3. Results

3.1. Total vegetation cover

Vegetation cover maps for each individual year are presented in the supplemental Figures S3-S18 and the calculated plant coverage by area (km^2 and acres) and percentage values are summarized in Table 3 and Figure 4. The results show that there is a general positive trend of increasing vegetation cover over the years within the analyzed sub-area of the ODSVRA, especially after the mid 1980s (Blue in Figure 4). Between the early years of 1939 and 1949, there was a slight decrease in plant cover (from

25 to 24%), followed by a gradual increase in vegetation on the dunes up to the mid-1960s (27%). Between the 1960s and 1980s, plant cover declined to values close to that of 1949 (between 1001 and 1033 acres, or around 24%, see values in Table 3 and Table S1). This trend then shifts to a gradual increase in vegetation after 1978 to a peak value of 37% (1569 acres) in 2012.

Within the OHV riding area, vegetation cover is generally much lower than in the broader ODSVRA sub-area and the post-1960s decline in cover is more pronounced with a steady reduction from a peak value of about 196 acres (12%) in 1966 to only 61 acres (4%) in 1985 (orange in Figure 4). After 1985, a slow gradual increase in plant cover was observed in the OHV riding area to 128 acres (8%) by 2020, which remains approximately 67 acres below the peak value in 1966, when the decline in cover began. This does not include the new 48-acre foredune restoration site, however, which did not exist when the 2020 NAIP imagery was captured. As of 2021, plant cover within the foredune restoration area had an average of approximately 2.7%[11], as discussed further in section 3.2 below.

The South and North Oso Flaco areas (light gray and brown in Figure 1, respectively) were also analyzed to provide comparison to vegetation dynamics areas of the ODSVRA that have not seen significant OHV riding for decades (since at least 1982 in S. Oso Flaco). As such, these sites provide insights on a less disturbed and more developed state of vegetation cover and dune geomorphology. At South Oso Flaco, plant cover is substantially higher than other areas of the ODSVRA, showing a general positive trend (Figure 4) from 37 % in 1930 to 66% in 2012 (212 and 373 acres, respectively). Between 1930 and 1949, there was a small decline in plant cover to a historic low of 34% (197 acres). In contrast, plant cover in the OHV riding area has not exceeded 13% over the period of analysis. The area analyzed at South Oso Flaco represents approximately 14% of the total ODSVRA sub-area, yet it contains 14-34% of the vegetation within the park. For comparison, the OHV riding area is just over 37% of the ODSVRA sub-area but contains only 6-18% of the total vegetation, depending on the year.

The North Oso Flaco foredune complex shows a gradual trend similar to the OHV riding area with an increase in vegetation up to the late 1960s, from less than 1% in 1930 to almost 11% in 1966, which then declined to 5% in 1985. Following 1985 plant cover increased to a peak of 24% in 2012, , and after that plant cover declined but remained over 19%. The North Oso Flaco site consists only of foredune vegetation, which is generally more exposed to disturbance (natural and anthropogenic), yet following 1987 the plant cover at this site is consistently higher than that in the OHV riding area, which also includes large backdune vegetation.

[11] Hilgendorf, Z., Turner, C., & Walker., I.J. 2021. UCSB-ASU 2020-2021 ODSVRA Foredune Restoration UAS Survey. Report from UCSB and ASU submitted to CDPR.

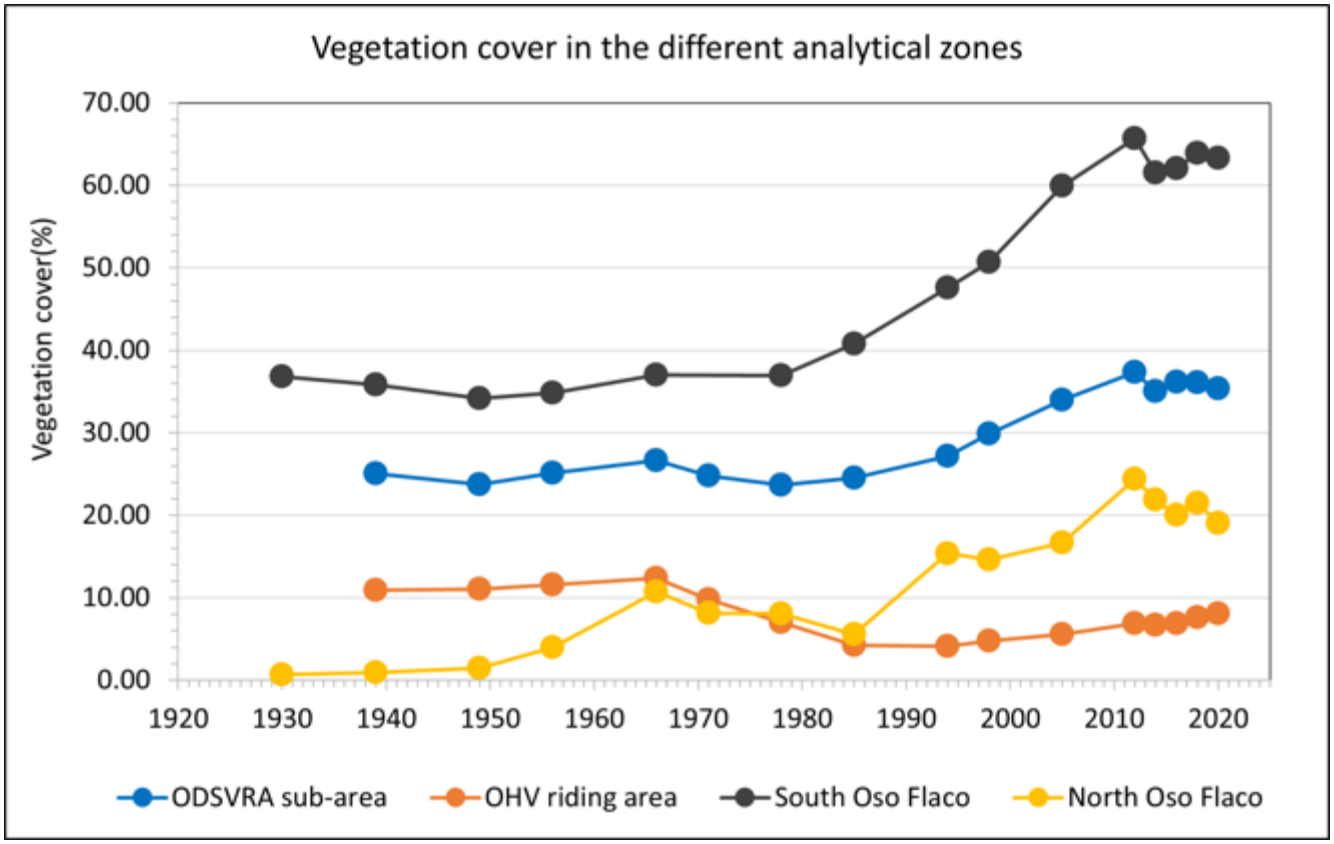

Figure 4. Time series of total vegetation cover (foredune + non-foredune vegetation in Table 3) as a percentage (%) of the ODSVRA sub-area at large (blue), the OHV riding area (orange), South Oso Flaco area (gray), and North Oso Flaco (yellow, foredune vegetation only). Percent cover values are derived as a proportion of the respective areas of each analytical region. Due to limited imagery coverage (Table 2), the 1930 photo year was not included in the ODSVRA sub-area and OHV riding area curves, and 1971 was not included for South Oso Flaco (gray).

Table 3. Calculated land cover values for vegetation and non-vegetated areas from each image year in the ODSVRA sub-area, OHV riding area, South Oso Flaco , and the North Oso Flaco area. Values are provided for vegetation in the foredune zone and for other back dune areas (see boundaries in Figure 1). Asterisk (*) represents limited imagery for 1930, 1971, and 1985 (Table 2), resulting values are derived from smaller areas than outlined in Figure 1. All values presented are in relation to the entire area of each analyzed zone (to a total of 100%). Values relative to specific areas within each of these broader areas (e.g., foredune zones) are shown in Figure 5 (Section 3.2) and provided in Table S1 (supplementary materials).

		ODSVRA sub-area			OHV riding area			South Oso Flaco			North Oso Flaco	
		Vegetated		Non vegetated	Vegetated		Non vegetated	Vegetated		Non vegetated	Vegetated	Non vegetated
		Foredune	Backdune		Foredune	Backdune		Foredune	Backdune		Foredune	
1930*	km² (acres)	0.07 (16)*	3.37 (832)*	9.14 (2258)*	0.03 (8)*	0.48 (118)*	4.53 (1120)*	0.02 (6)	0.84 (207)	1.48 (365)	0.002 (0.4)	0.28 (68)
	%	0.52*	26.79*	72.69*	0.63*	9.46*	89.91*	0.95	35.83	63.21	0.69	99.31
1939	km² (acres)	0.13 (32)	4.14 (1023)	12.78 (3159)	0.05 (12)	0.07 (161)	5.71 (1411)	0.01 (6)	0.83 (204)	1.50 (371)	0.003 (0.7)	0.28 (68)
	%	0.76	24.29	74.95	0.77	10.16	89.08	0.45	35.35	64.2	0.95	99.05
1949	km² (acres)	0.23 (57)	3.82 (944)	13.01 (3214)	0.08 (19)	0.63 (157)	5.70 (1408)	0.02 (5)	0.78 (192)	1.54 (380)	0.004 (1)	0.27 (68)
	%	1.34	22.4	76.25	1.18	9.89	88.93	0.84	33.32	65.84	1.49	98.51
1956	km² (acres)	0.33 (82)	3.95 (977)	12.78 (3159)	0.07 (16)	0.68 (167)	5.67 (1401)	0.03 (7)	0.78 (194)	1.52 (376)	0.01 (3)	0.26 (66)
	%	1.94	23.17	74.89	1.03	10.56	88.41	1.30	33.52	65.18	3.96	96.04
1966	km² (acres)	0.45 (111)	4.09 (1011)	12.52 (3093)	0.10 (24)	0.70 (172)	5.62 (1388)	0.08 (19)	0.79 (195)	1.47 (364)	0.03 (7)	0.25 (61)
	%	2.64	23.99	73.37	1.51	10.85	87.64	3.28	33.71	63.00	10.72	89.28
1971*	km² (acres)	0.37 (90)*	3.86 (955)*	12.26 (3035)*	0.08 (19)	0.55 (1336)	5.79 (1430)	N/A	0.82 (203)*	0.97 (240)*	0.02 (6)	0.25 (63)
	%	2.21*	23.41*	74.38*	1.19	8.56	90.25	N/A	45.82*	54.18*	8.1	91.9
1978	km² (acres)	0.40 (99)	3.64 (899)	13.02 (3218)	0.04 (11)	0.41 (100)	5.96 (1473)	0.07 (17)	0.79 (196)	1.47 (364)	0.02 (6)	0.26 (63)
	%	2.34	21.32	76.34	0.68	6.33	92.98	3.02	33.9	63.08	8.09	91.91
1985	km² (acres)	0.45 (110)	3.73 (922)	12.88 (3183)	0.02 (4)	0.25 (62)	6.14 (1517)	0.10 (24)	0.86 (211)	1.38 (342)	0.02 (4)	0.26 (65)
	%	2.61	21.88	75.51	0.28	3.93	95.79	4.15	36.61	59.24	5.53	94.46
1994	km² (acres)	0.50 (125)	4.11 (1016)	12.40 (3065)	0.01 (2)	0.25 (63)	6.15 (1519)	0.11 (26)	0.99 (244)	1.20 (298)	0.02 (5)	0.26 (64)
	%	2.97	24.16	72.87	0.16	3.98	95.87	4.62	42.97	52.41	7.34	92.66
1998	km² (acres)	0.54 (133)	4.54 (1122)	11.94 (2950)	0.02 (4)	0.29 (71)	6.11 (1509)	0.11 (28)	1.05 (260)	1.13 (280)	0.04 (10)	0.24 (59)
	%	3.17	26.68	70.15	0.25	4.49	95.26	4.85	45.86	49.29	14.62	85.38
2005	km² (acres)	0.70 (173)	5.08 (1254)	11.24 (2778)	0.02 (6)	0.33 (82)	6.05 (1496)	0.15 (38)	1.10 (250)	1.13 (280)	0.05 (11)	0.23 (57)
	%	4.12	29.83	66.05	0.37	5.20	94.43	6.66	44.04	49.29	16.63	83.36
2012	km² (acres)	0.81 (200)	5.54 (1369)	10.67 (2637)	0.04 (9)	0.40 (100)	5.97 (1475)	0.16 (40)	1.25 (309)	0.89 (219)	0.07 (18)	0.21 (52)
	%	4.75	32.56	62.69	0.60	6.31	93.09	7.12	54.36	38.52	24.41	75.95
2014	km² (acres)	0.69 (170)	5.28 (1304)	11.05 (2732)	0.04 (10)	0.39 (95)	5.98 (1479)	0.15 (36)	1.27 (313)	0.89 (219)	0.06 (15)	0.22 (54)
	%	4.05	31.00	64.95	0.64	6.01	93.35	6.34	55.14	38.52	21.87	78.13
2016	km² (acres)	0.70 (173)	5.24 (1296)	11.08 (2737)	0.04 (10)	0.40 (99)	5.97 (1475)	0.14 (34)	1.29 (318)	0.87 (216)	0.06 (14)	0.22 (55)
	%	4.12	30.81	65.08	0.64	6.25	93.11	6.04	55.98	37.98	20.00	80.00
2018	km² (acres)	0.68 (168)	5.46 (1348)	10.88 (2689)	0.04 (10)	0.45 (111)	5.92 (1463)	0.14 (36)	1.32 (327)	0.83 (205)	0.06 (15)	0.22 (54)
	%	3.99	32.06	36.95	0.63	7.00	92.37	6.27	57.60	36.12	21.46	78.54
2020	km² (acres)	0.64 (157)	5.37 (1328)	11.01 (2720)	0.04 (11)	0.47 (117)	5.89 (1456)	0.12 (30)	1.33 (330)	0.84 (208)	0.05 (13)	0.22 (55)
	%	3.74	31.58	64.68	0.67	7.4	91.93	5.27	58.05	36.68	19.05	80.95

3.2. *Changes in vegetation cover in the foredune zone*

As plant communities, geomorphology, and other ecological processes within foredune ecosystems are distinctly different from those in the larger transgressive dunes, parabolic dunes, and interdune areas in the broader ODSVRA landscape, a separate analysis of vegetation cover was conducted for the foredune zone (see Section 2 and Figure 1). Values presented in this section are specific to the foredune within each of the larger analytical regions and are not a proportion of the larger zones themselves (see values in Table S1).

Vegetation cover trends within the foredune zone (Figure 5) are generally similar to those within the broader ODSVRA sub-area and OHV riding areas described above (Figure 4). Peak values (and years) of foredune plant cover within ODSVRA, the OHV riding area, and at the South and North Oso Flaco reference sites are 21% (2012), 5% (1966), 36% (2012) and 24% (2012), respectively. Foredune vegetation cover within the entire ODSVRA sub-area shows a general increase over time, with high positive rates of change from a historic low in 1939 (3.3%) to 1966 (from 32 to 111 acres) and between 1998 and 2012 (133 to 200 acres). From 2012 to 2020, however, there was a net loss of 49 acres of vegetation (from 21% to 16% cover, blue in Figure 5), some of which results from removal of invasive grass species (e.g., *Ammophila breviligulata* or European beach grass) from foredunes in the northern area of the ODSVRA[12].

Within the OHV riding area, foredune vegetation shows an increase in cover from approximately 2.6% (12 acres) in 1939 to 5.3% (24 acres) in 1966 (orange in Figure 5B, Table S1). From 1966 to 1994, plant cover declined sharply to 0.5%, which is well below the historic 1939 value. Since 1998, vegetation cover has risen gradually to about 2.3% by 2020 (Figure 5).

It is important to note that all orthophotos from 2005-2020 were taken during the period of nesting for the Western Snowy Plover (March through September), which results in up to 70% of the foredune zone in the OHV riding area (or roughly 20% of the overall riding area) being closed to OHV traffic and camping for 7 months (see borders in Figure 7). The enclosure reduces the impact of human activity over the foredune area which may allow better conditions for plant establishment in that area. Since 2005, plant cover within the bird nesting enclosure increased from negligible to over 1% by 2012 (Figure S21). From the historic analysis, it seems that the last time vegetation cover was over 1% in this area was in the late 1970s, which is also a big decrease from the early 1930s when this area had over 10% vegetation cover (Figure S21).

At the South Oso Flaco reference site, foredune vegetation cover between 1939 and 1949 (2.4% and 4.3%, respectively) is comparable to that in the foredune zone of the OHV riding area (2.6% and 4.1%, respectively). After this, plant cover remains consistently and appreciably higher

[12] Glick, R., ODSVRA, Personal communication, 2021.

at Oso Flaco than in other foredune zones, especially in the OHV riding area (Figure 5). As in the larger ODSVRA sub-area, foredune vegetation cover at South Oso Flaco shows a positive trend over time to a peak in 2012. Comparatively then, Figure 5 indicates that foredunes at South Oso Flaco that were not subjected to the same amount of OHV activity as that in the nearby riding areas of ODSVRA (at least since 1982) have attained and maintained significantly higher vegetation cover, particularly between 1985 and 2005 (see also Table S1; Figures S3-S18). It is worth noting that the decrease in foredune plant cover following 2012 is partly related to CDPR efforts to remove invasive *Ammophila arenaria* and other weeds, mostly at South Oso Flaco[12].

North Oso Flaco had very low vegetation cover (less than 2%) up to the 1950s, then gradually rose to a peak of 10% in 1966. Following this, plant cover declined to 5% in 1985, then rose to a historic peak of 24% in 2012 (Figure 5). The North Oso Flaco area has been fenced to exclude OHV activity since 1982, which largely explains the rise in vegetation growth since 1985.

Although plant cover within the broader ODSVRA and in both North and South Oso Flaco sites has gradually increased over time, vegetation within the OHV riding area, and its foredune zone in particular, have shown steady declines since 1966 (Figure 5). This corresponds with an era of increasing recreational OHV activity in the region that began in the 1950s[13].

Another area of interest for detecting changes in foredune vegetation cover is within the newly implemented (2020) 48-acre foredune restoration site in the OHV riding area. (Figures 1, 5). Historical plant cover in this area shows a similar trend to that of the foredune zone in the larger OHV riding area with a decline in cover from almost 2% in 1949 to essentially zero cover in 1985. Since then there has been no detectable change in plant cover at the foredune restoration sites until after implementation of the restoration treatments in February 2020. The 2020 NAIP imagery used in this analysis does not reflect these treatments, however.

An independent report by UCSB and ASU[14] explores more recent changes in vegetation cover within the foredune restoration site captured from aerial UAS surveys between October 2019 and February 2021. The report shows that, as of February 2021, plant cover increased to an average of approximately 2% (ranging from 0.04 to 4.91%, depending on treatment type).

[13] Guiton-Austin, L. 2011. As cited by Harris, W. California Geological Survey Report, 1 November 2011. "In consideration of Draft Rule 1001 proposed by the San Luis Obispo County Air Pollution Control District: An analysis of wind, soils, and open sand sheet and vegetation acreage in the active dunes of the Callendar Dune Sheet, San Luis Obispo County, California.

[14] Hilgendorf, Z., Turner, C, Walker, I.J. UCSB-ASU 2020-2021 ODSVRA Foredune Restoration UAS Survey Report. 37p. Produced for CDPR-ODSVRA and published as Attachment 8 in the 2021 ARWP.

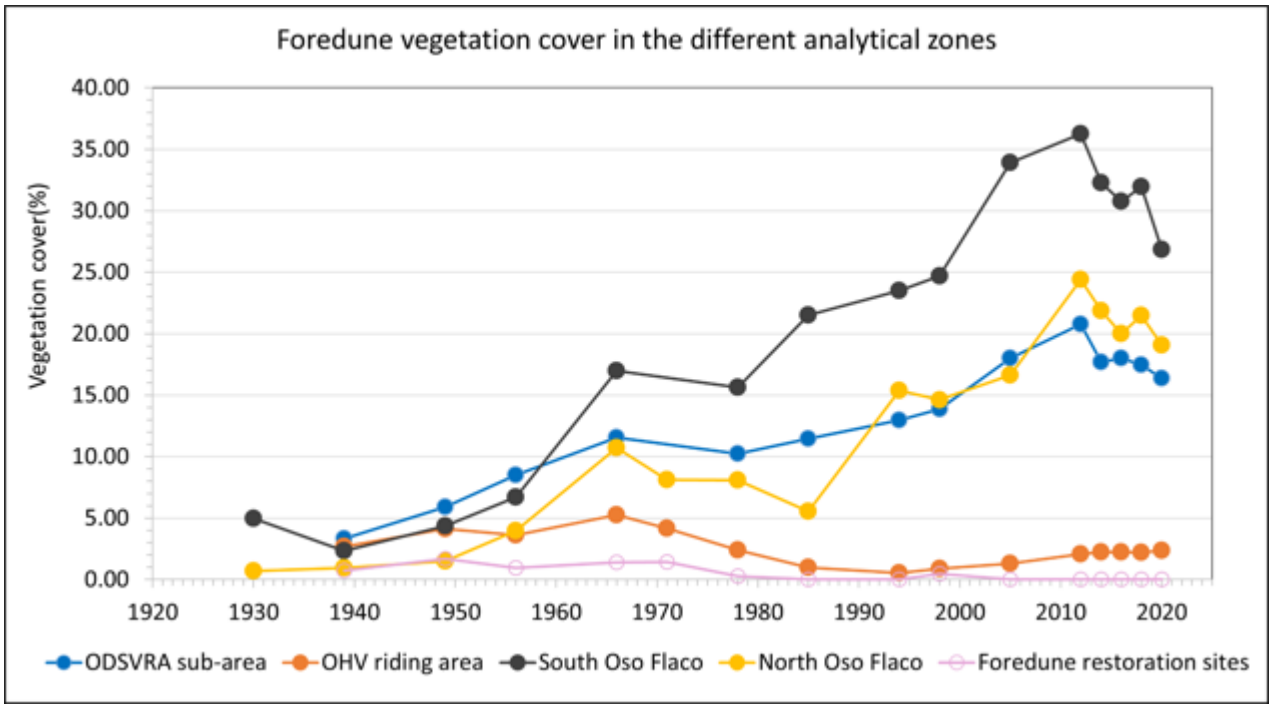

Figure 5. Percent vegetation cover within the foredune zone in the ODSVRA sub-area (blue), OHV riding area (orange), South Oso Flaco area (gray), and North Oso Flaco (yellow). Values are relative to areas of the foredune zone within each analytical zone (calculations in Table S1). Plant cover within the foredune restoration zone is shown for comparison (pink). Due to limited coverage of imagery (Table 2), the 1930 image was not included in the ODSVRA sub-area and OHV riding area curves, and 1971 was not included in the ODSVRA sub-area and South Oso Flaco analysis (gray).

3.3. Change detection between years

Changes in vegetation coverage between photo years are presented both as change maps (Figures S22-S35) and as plots of rates of positive or negative change over time (% yr^{-1}) (Figure 6), which generally reflect dynamism in plant cover over time. It is noted, however, that change calculations derived by comparing two points over time (i.e. two different image years) inevitably precludes interpretation of changes during the intervening years. This said, there is interpretive value in estimating rates of change between image years particularly given the varying intervals between the photos.

Figure 6 shows negative or positive change rates derived from the number of pixels that either lost or gained vegetation from the earlier image year, respectively, divided by the number of years between the images. All change calculations, including total change (sum of all changes, negative + positive) and net change (positive - negative) are presented in Table S2 in the supplementary material. Within the broader ODSVRA sub-area, there is an increasing trend in the total amount of change/year between the 1930s to the 1980s, with mainly negative changes (losses) in plant cover from 1966 to 1985, after which more positive changes (gains) occur (Figure 6A). Between 2012 to 2020, there is a large increase in the amount of total change, however, a large portion of this is negative, mostly between 2012-2016 (Figure 6A). Much of the negative change in these years occurs in areas that experienced removal of invasive species (e.g., the Pismo Dunes Natural Preserve and South Oso Flaco areas, see Figures S32, S33) between 2012 and 2015. In addition, some of the detected changes between 2012 and 2014 reflect the time of year when the imagery was taken. The 2012 orthophoto was taken in the middle of May (late spring) when vegetation is in full growth stage (and easier to identify and classify using aerial photo analysis), while the 2014 orthophotos were taken in late September at the end of the growing season, so there is potential for subtle seasonal differences based on time of photo acquisition (Table 1; Figure 6).

In the OHV riding area, there is a similar trend to the larger ODSVRA - between 1966 to 1985 the majority of changes were negative and after 1985 the changes were largely positive (Figure 6B). Between 1985 and 2005, the change rates are very small (<0.3% yr^{-1}) compared to other analytical zones. Most of the positive changes in the OHV riding area occur after 2005 (Figure 4) largely related to new plants along the margins of fenced vegetation islands, and foredune vegetation establishing in the seasonal bird nesting enclosure area (Figure 7; Figures S31-S35). The reduction of OHV disturbance offered by the seasonal bird nesting enclosures since 2005 corresponds with increases in foredune vegetation cover of about 1% with only 0.1% negative change between 2005 and 2020 (0.07% yr^{-1} and 0.01% yr^{-1}, respectively).

At South Oso Flaco, there is a similar net pattern in the total amount of change as in the other analytical zones (Figure 6C). However, up to 1971 there is generally a more balanced occurrence of positive and negative changes between most years. Following 1971, for the most part, there are more positive changes and between 2012 and 2020, the change rates increased to over 5% yr^{-1} (Figure 6C). Most of this change occurs around the edges of existing vegetation in both backdune and foredune areas (Figures 8). The backdune zone of South Oso Flaco shows mainly positive rates of change up to 2012 (Figure 8B). The South Oso flaco foredune zone shows a similar trend to the backdune area (Figure 8B), however, the rates of change in the foredune were much higher in all years (Figure 8A and 8B).

In the North Oso Flaco foredune complex, a positive trend of change occurs up to 1966, then shifts to more negative change rates up to 1985 (Figure 6D). Following the closure of the area in the early 1980s, North Oso Flaco showed a strong positive trend of increase. North Oso Flaco shows the highest amount of change between 2012 and 2020 compared to the other analytical zones, peaking at over 7% yr^{-1} of total change between 2012 and 2014 with mostly negative change between 2012 and 2016 (Figure 6D).

Figure 6. Positive, negative and net percent change per year (% yr^{-1}) in vegetation between successive imagery years in the entire ODSVRA sub-area (A), OHV riding area (B), South Oso Flaco area (C), and North Oso Flaco (D) relative to areas of each analytical zone. The negative change values were converted to negative numbers (less than zero) to represent the vegetation loss. Areas with no change between years are not shown (hence, values do not total 100%). Due to limited coverage of imagery, the 1930 was not included in the ODSVRA sub-area and OHV riding area change analysis (black X sign). In 1971 the limited image coverage in the ODSVRA sub-area and South Oso Flaco resulted in some missing data (see Table 2, Figure S10) and possible underestimates of change.

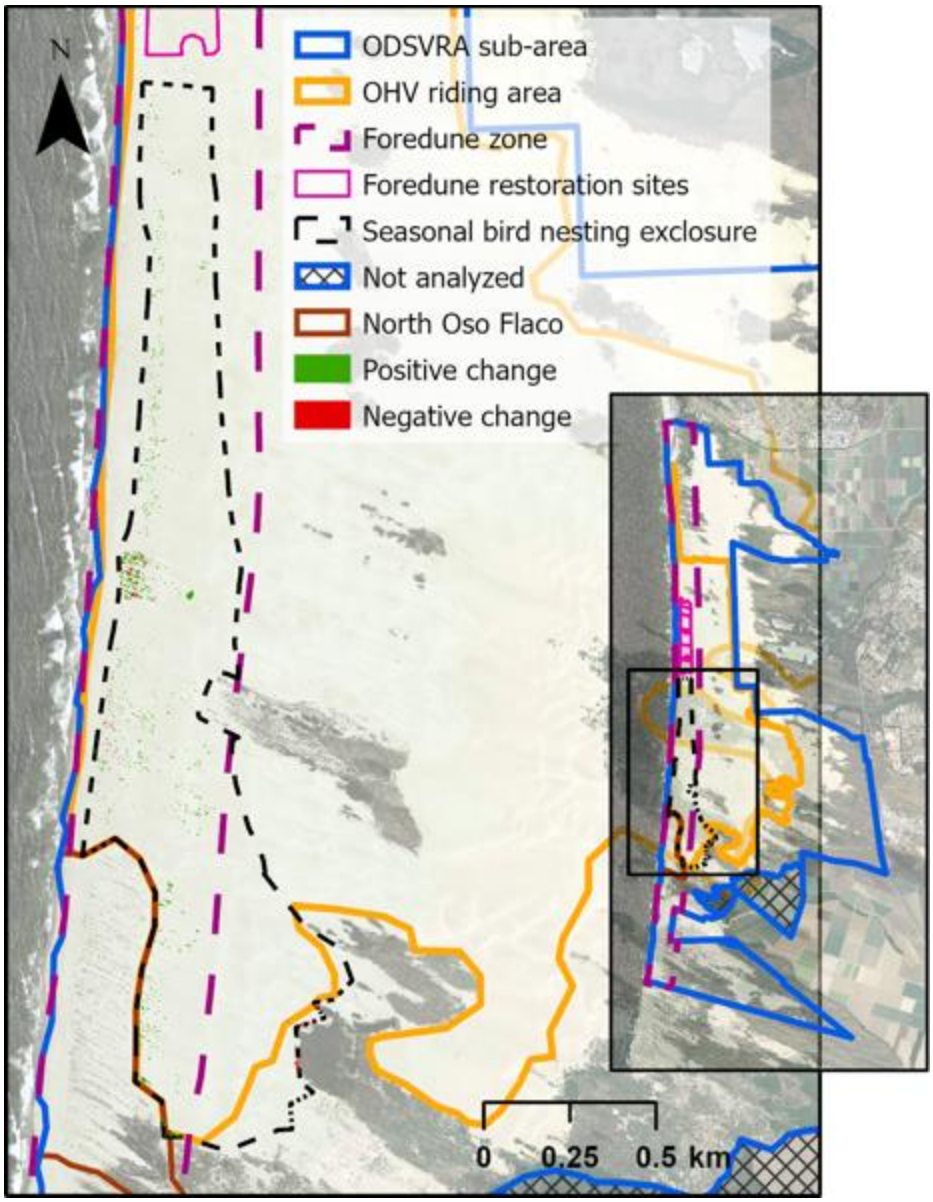

Figure 7. Change map between 2005 and 2020 of the seasonal bird nesting exclosure area (black dashed line) that have been fenced off to OHV activity since 1982[15]. Change map is shown on the 2005 orthophoto.

[15] Glick, R., ODSVRA,, Personal communication, 2021.

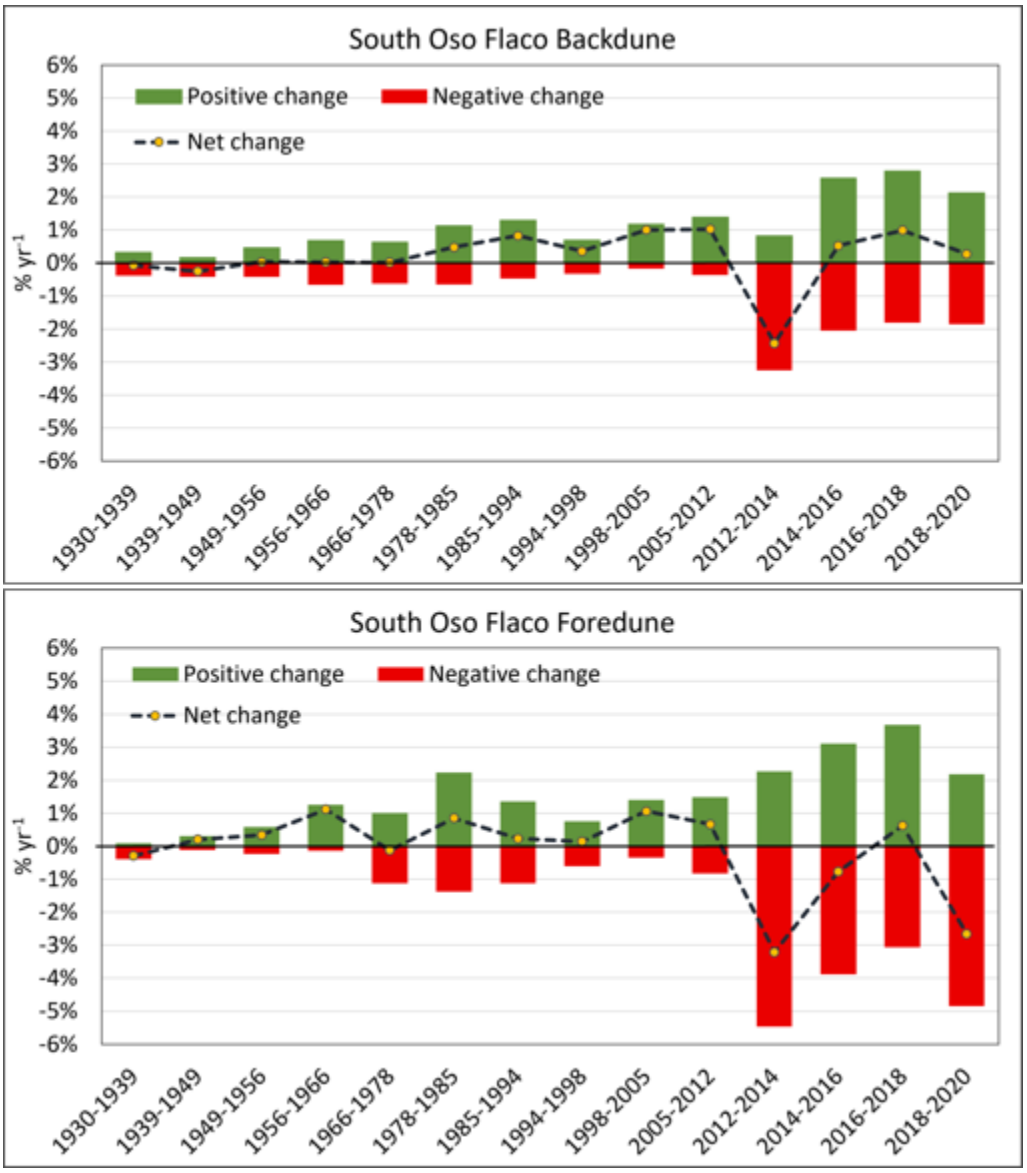

Figure 8. Positive, negative and net percent change rates (% yr^{-1}) in vegetation between successive imagery years in the South Oso Flaco backdune (A) and foredune (B) zones relative to areas of each analytical zone. The negative change values were converted to negative numbers (less than zero) to represent the vegetation loss. Areas with no change between years are not shown (hence, values do not total 100%). Net change (positive change - |negative change|) represent the overall trend of change between the image years. There was very limited coverage for 1971 and so this year was excluded and an analysis of 1966-1978 was done instead.

Figures 9-15 provide a focused analysis of vegetation changes during the three broader time periods identified in Section 2. During the 1939-1985 period, roughly prior to the management of ODSVRA by CDPR (in 1982) the total amount of change in the ODSVRA sub-area is relatively high at 18.72%, but this translates to a change rate of only 0.4% yr^{-1} (Figures 9A and 10, Table

S2). The majority of positive change appears mostly between 1966 and 1985 (Figure 6A). Between 1985 and 2012, this area showed increasing positive change rates in plant cover (1714.9% or 0.6355% yr^{-1}) with only 21.8% loss (0.07% yr^{-1}) (Figure 9A). Many of the areas of negative change between 1939 and 1985 showed subsequent vegetation growth in 2012 (Figures 9A, 10, 11). As above, most of this change occurred in areas subjected to restoration activities implemented by CDPR between 2005 and 2012 (Section 3.3; Figure 6). From 2012 to 2020, a comparatively low amount of total change was observed (8%) with equal amounts of positive and negative change (Figure 9A and 12), yet the rates of change were among the highest (total of 1% yr^{-1}).

Within the OHV riding area (Figure 9B), there is a declining trend in the total amount of change over time. From 1939 to 1985, there was a proportionately large negative change (9.2%) in plant cover in both foredune and backdune zones (Figures 10 and 13). From 1985 to 2012, there was a shift toward proportionately greater positive change (4.2%) with only 1.4% negative change (Figure 10B), mainly around existing vegetation islands in the backdune area (Figures 11 and 14). Between 2012 and 2020, the total amount of change in the riding area is relatively small (3.3%) and mostly positive (2.2%) (Figure 9B), resulting from vegetation growth in backdune restoration areas (straw treatments) implemented by CDPR (Figure 15). Rates of change are moderate (~0.2% yr^{-1}) for both 1939-1985 and 1985-2012 with only 0.2% yr^{-1} and 0.05% yr^{-1} negative change rates, respectively. Between 2012 and 2020 the change rate is slightly higher at 0.4% yr^{-1} with over 0.3% yr^{-1} positive change.

At South Oso Flaco, between 1939 and 1985, the total change in backdune and foredune areas was 22.5% with mostly gains (13.7%) (Figure 9C). Most of the losses occurred in the backdune area between 1966 and 1985 (Figures 6C, 8-10). Between 1985 and 2012, there was a high amount of total change of 31.7% (1.2% yr^{-1}), most of which (28.1%) was positive (Figure 9C) and occurred in the backdune zone and on the landward (eastern) side of the foredune, whereas higher vegetation loss is evident on the shoreward side of the foredune (Figure 11). Between 2012 and 2020, there was 12.1% total change, which is relatively low compared to previous years, but still high compared to other analytical zones (Figures 9) and at a faster rate of change (1.5% yr^{-1}) than the previous interval. Most of this change was vegetation loss (7.7%) in the Oso Flaco foredune zone and around existing vegetation in the backdune zone (Figures 9C, 12, 15). According to CDPR staff, some of this recent decline in plant cover at South Oso Flaco relates to removal of invasive grasses between 2009 and 2020.

The North Oso Flaco foredune complex shows a comparatively lower total amount of change between 1939 and 1985 (6.0%) with mostly positive changes (5.3%) (Figure 9D). The positive trend continued between 1985 and 2012, with a higher amount of total change (26% or 0.96% yr^{-1}), most of which (23.5%) was positive (Figure 9D). An invasive weed analysis performed by

CDPR in 2010[16] suggests that the North Oso Flaco area did not host any invasive species that were found in other foredune and backdune areas in the park. As such, the high positive changes between 1985 and 2012 can be attributed mostly to growth and expansion of native plants in the absence of vehicle activity and other anthropogenic disturbances. Between 2012 to 2020, however, there is mostly negative change in plant cover (11%) with only 3.6% gains.

For this report we used the 1939 orthophoto to represent an era prior to widespread OHV riding in the ODSVRA. Some accounts suggest that intensive riding in the area began in the 1950s[17]. Calculating changes in plant cover between 1939 and 2020 provides a comprehensive look at overall influences and changes that took place in the ODSVRA, including the combined impacts of land management by CDPR and the impact of OHV riding and other human activities over the last 9 decades. The results show that over this period there is a general increase in plant cover in the broader ODSVRA sub-area and in the North and South Oso Flaco reference areas (Figure 16A). In the ODSVRA, there is an overall increase of 17.8% plant cover vs. 7% loss. Most of the vegetation gain was in the backdune area and in the Pismo Dunes Natural Preserve, the broader South Oso flaco dune complex, and in backdune areas outside of the riding area (Figure 17 and S38). These areas were also found to be affected by growth of invasive weeds. According to a CDPR weed digitizing effort in 2010[16], invasive weeds (beach grass and veldt grass) in 2010 occupied less than 10% of the total vegetation cover within the broader ODSVRA sub-area (134 acres), about 14% of the plant cover in South Oso Flaco (310 acres), and 18% of the vegetation in the Pismo Dunes Nature Preserve (381 acres). It should be noted, however, that since 2010 there has been an increasing effort by the CDPR to remove invasive species in these areas.

[16] Bonk. M. 2010. Mapping Invasive Beachgrass And Veldt Grass In Oceano Dunes Svra Using Multispectral Imagery. CDPR internal report.

[17] Guiton-Austin, L. 2011. As cited by Harris, W. California Geological Survey Report, 1 November 2011. "In consideration of Draft Rule 1001 proposed by the San Luis Obispo County Air Pollution Control District: An analysis of wind, soils, and open sand sheet and vegetation acreage in the active dunes of the Callendar Dune Sheet, San Luis Obispo County, California.

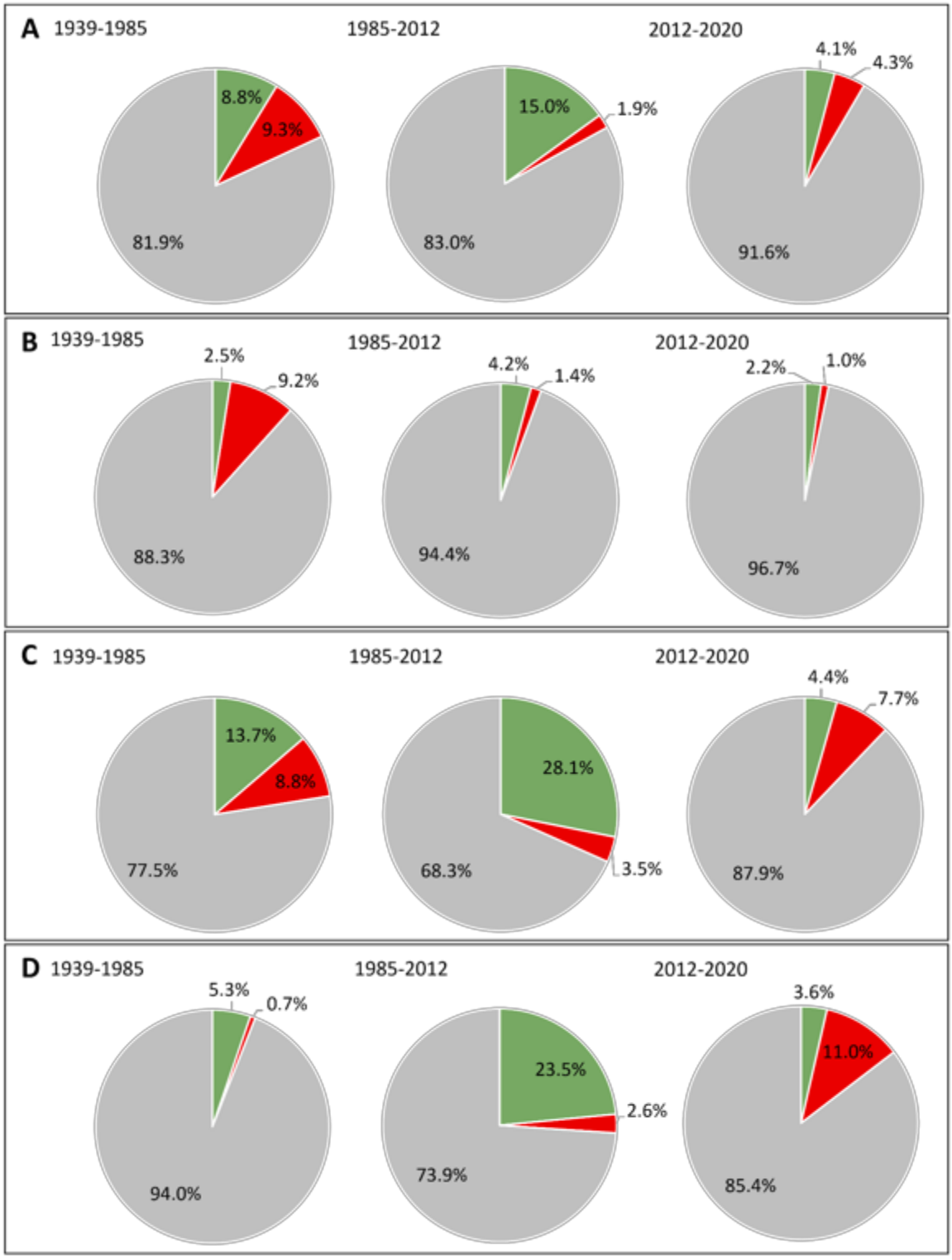

Figure 9. Change analysis (%) of vegetation cover in ODSVRA sub-area (A), OHV riding area (B), South Oso Flaco (C), and North Oso Flaco area (D) during three important management time intervals: i) 1939-1985, ii) 1985-2012, and iii) 2012-2020, as described in Section 2.

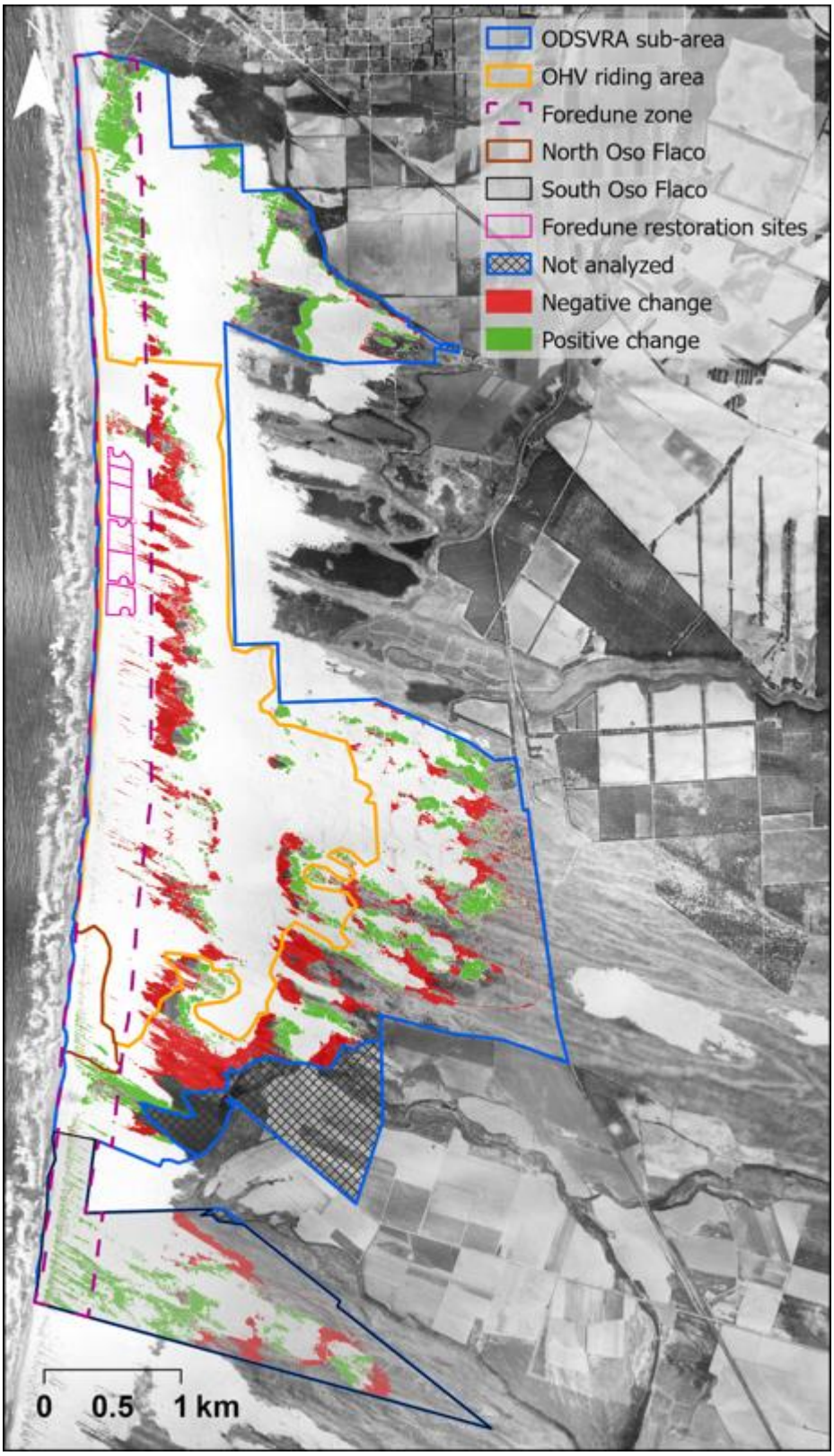

Figure 10. Change in vegetation between 1939 and 1985. Orthophoto from 1939.

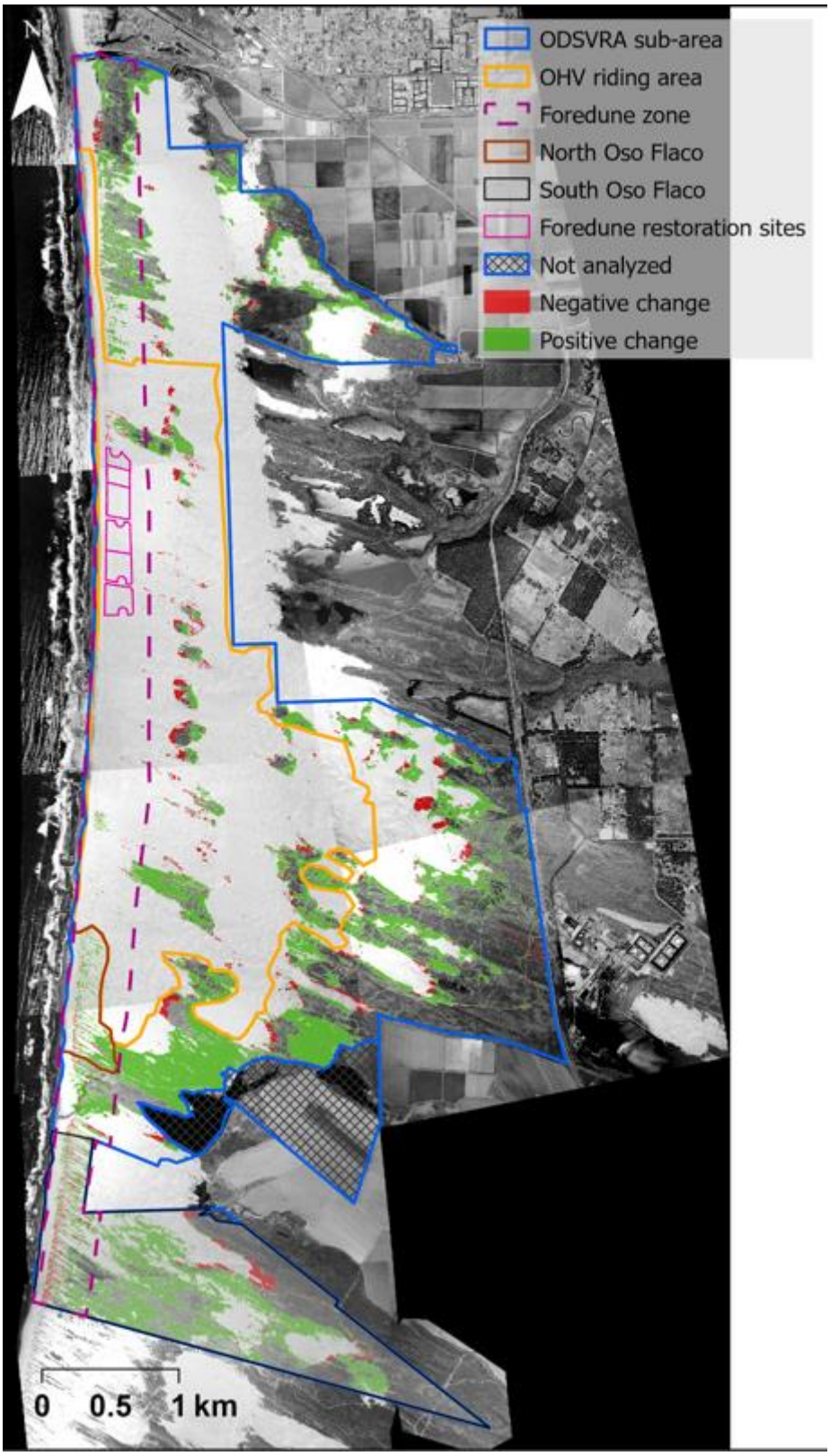

Figure 11. Change in vegetation between 1985 and 2012. Orthophoto from 1985.

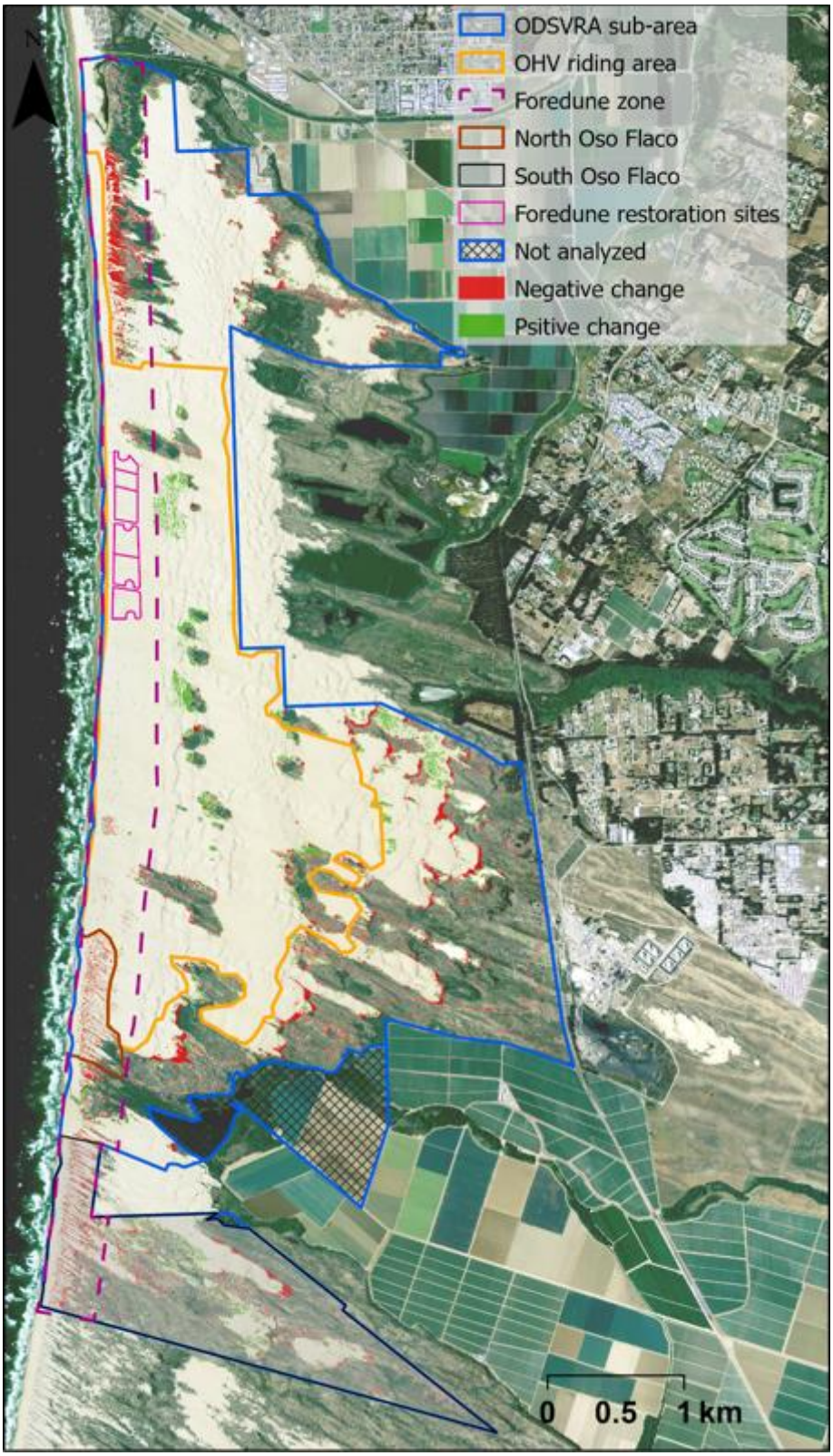

Figure 12. Change in vegetation between 2012 and 2020. Orthophoto of 2012.

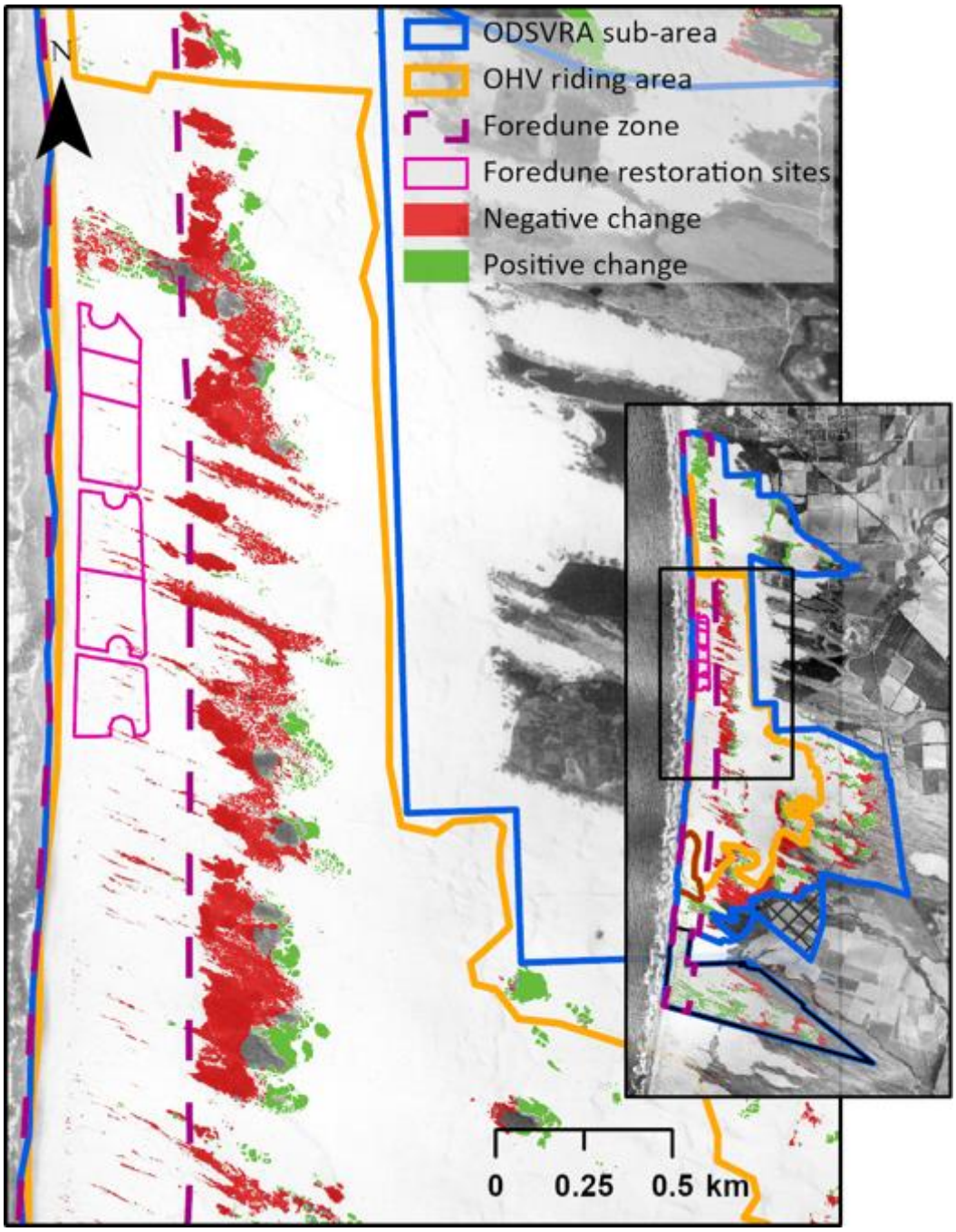

Figure 13. Close-up image of the change in vegetation cover around the foredune restoration sites between 1939 and 1985. Orthophoto from 1939.

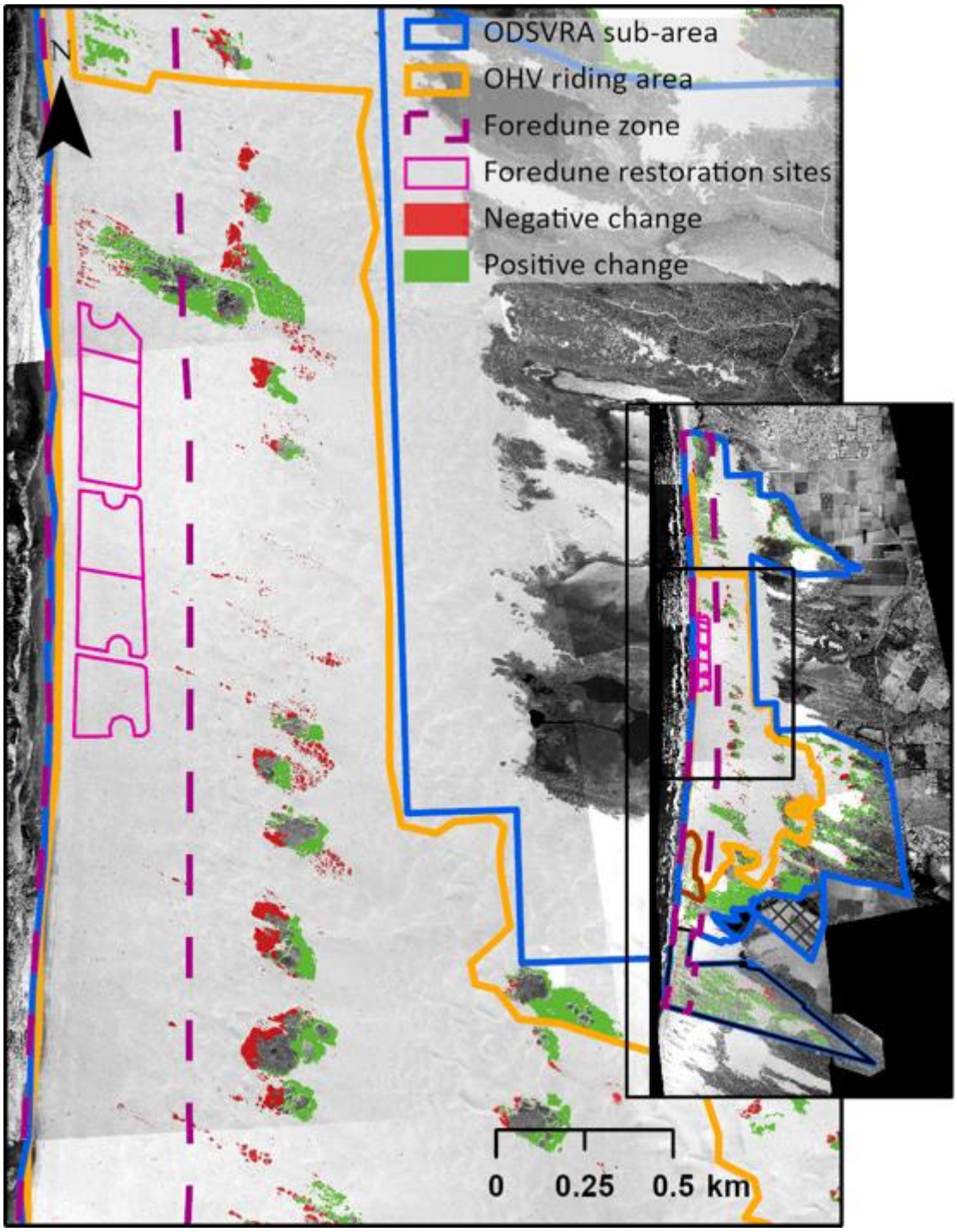

Figure 14. Close-up image of the change in vegetation cover around the foredune restoration sites between 1985 and 2012. Orthophoto from 1985.

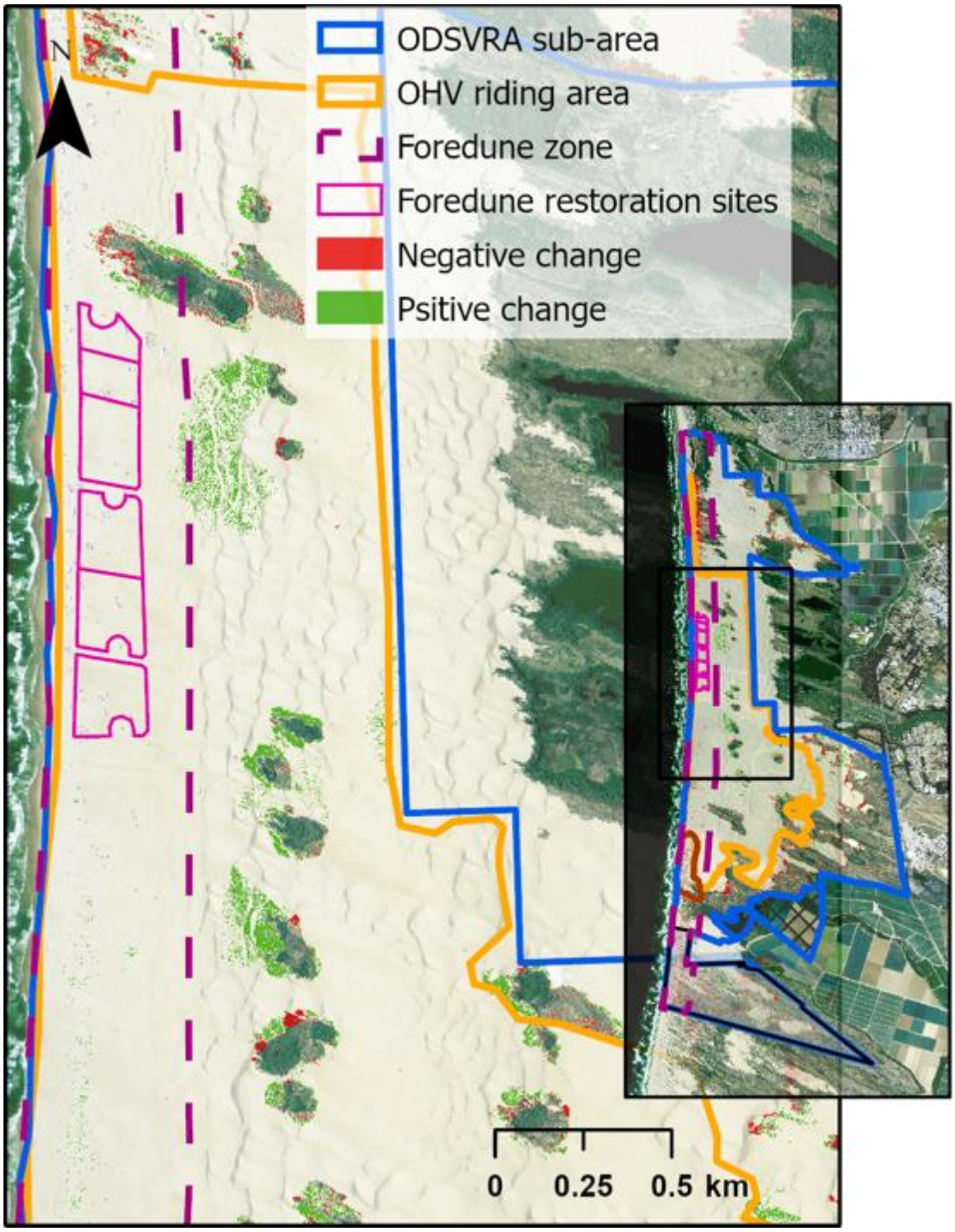

Figure 15. Close-up image of the change in vegetation cover around the foredune restoration sites between 2012 and 2020. Orthophoto from 2012.

Within the OHV riding area over the entire period of analysis, there are lower percentages of total change (13.5%) with mostly negative change (8.2%) in both the foredune and backdune zones (Figures 16A-18). Most of the negative changes occurred up to 1985 and were associated with the loss of hummocky nebkha and foredunes as well as vegetation in foredune swales (Figures 6 and 9B). Positive gains in plant cover in the OHV riding area occurred mostly in the backdune area within fenced vegetation islands (Figure 18).

The South Oso Flaco area showed significantly higher change rates (42%), with over 34% vegetation gain (Figure 16A) in both the backdune and the foredune zones. These gains are associated with limited OHV disturbance over at least the last 5 decades, as well as the growth and expansion of invasive weeds.

The more recently fenced North Oso Flaco area experienced significant increases (20%) in plant cover over the total period of analysis with only 0.7% loss (Figure 16B). The vast majority of plant growth occurred after the closure of the area for vehicle riding in 1982 (Figures 6 and 9) and is characterized mostly by hummocky nebkhas.

The analysis of changes between 1939 to 2012 provides an insight to the changes that occurred prior to the adoption of SLO-APCD Rule 1001 (2011) and related PMRP. The results show a similar trend of change in all analytical zones with slightly higher overall change values compared to the period between 1939 and 2020 (Figures 6B, S35 and S38, Table S2). These results match the trend of vegetation loss in North and South Oso Flaco and vegetation growth in the OHV riding area between 2012 and 2020 (Figures 4 and 9).

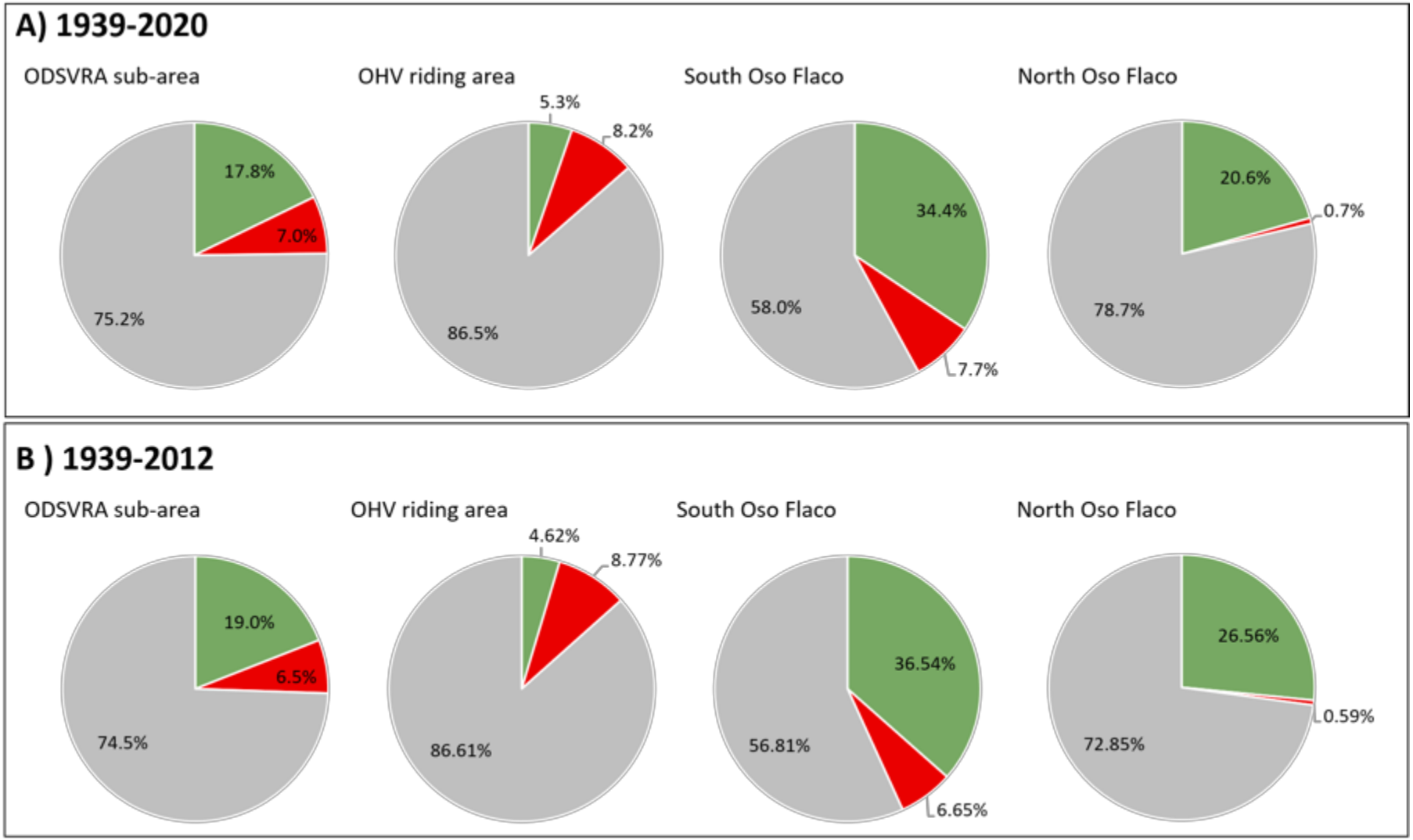

Figure 16. Change analysis (%) of vegetation cover in the ODSVRA sub-area, OHV riding area, and the South Oso Flaco area between A) 1939 and 2020, and B) 1939 and 2012. Positive change is presented in green, negative change in red, and no change in gray. data is in Table S2 in supplements.

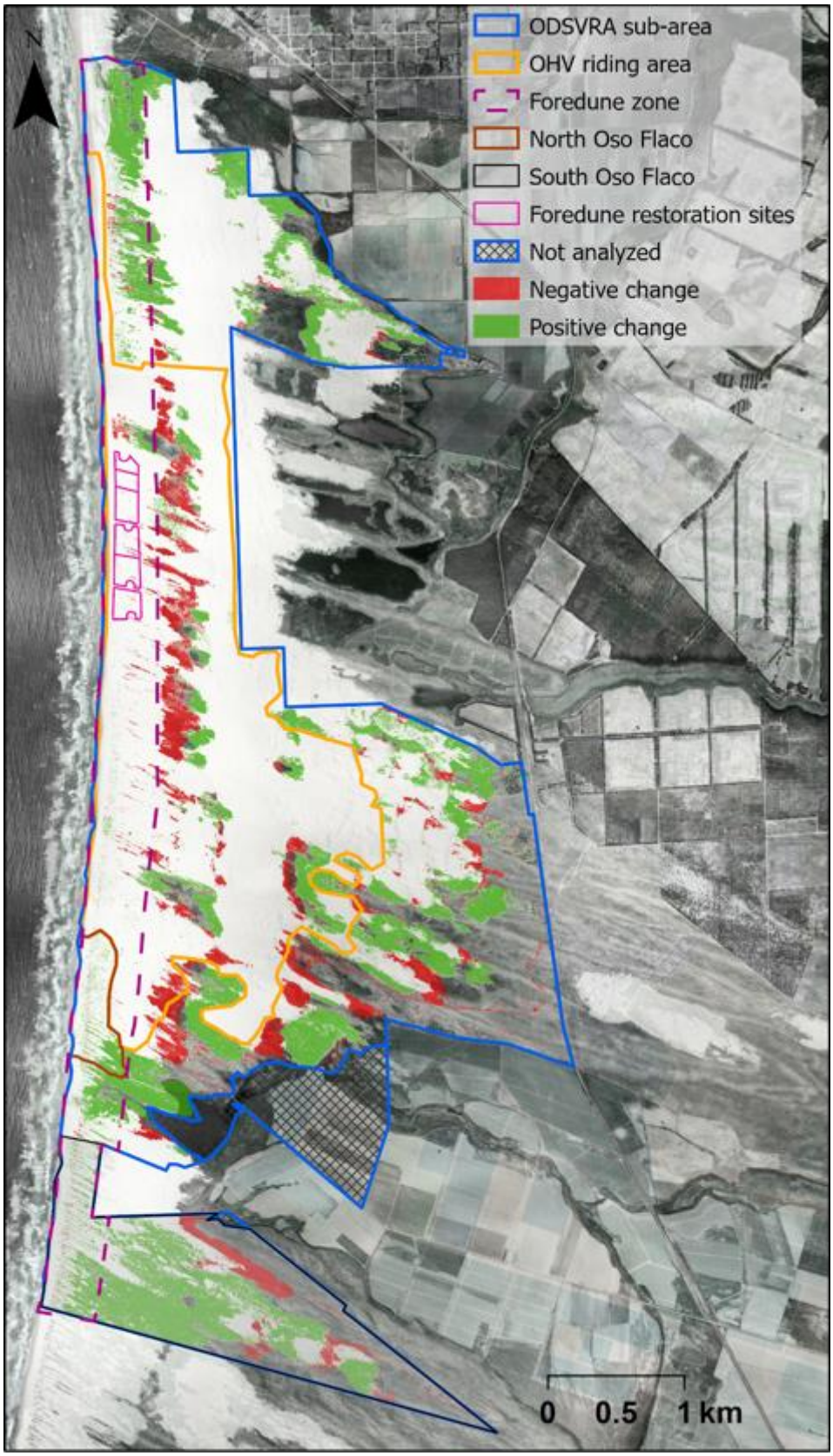

Figure 17. Change in vegetation between 1939 and 2020. Orthophoto from 1939.

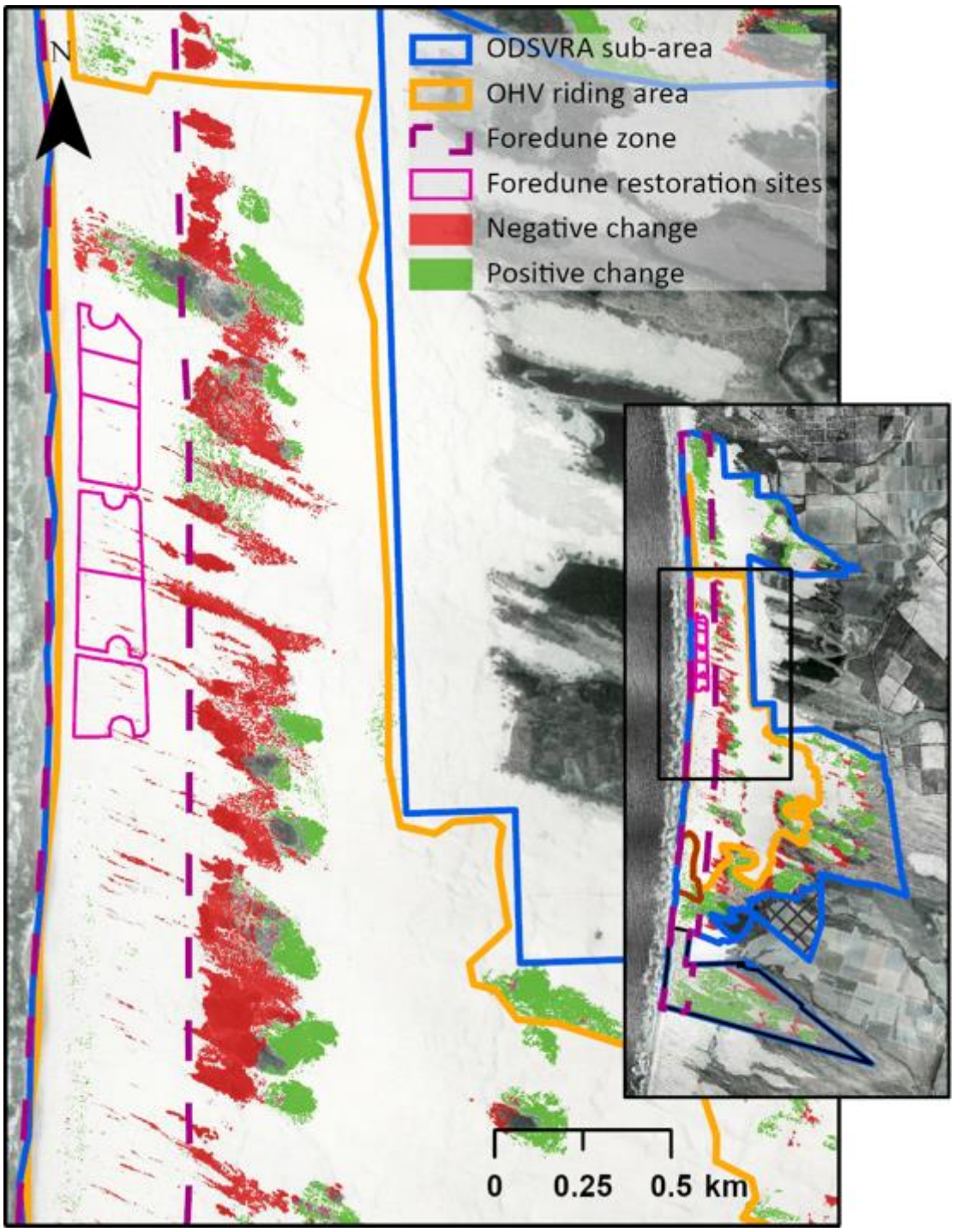

Figure 18. Close-up image of the change in vegetation cover around the foredune restoration sites between 1939 and 2020. Orthophoto from 1939.

4. Summary and Conclusions

As part of the 2020 ARWP, the CDPR requested a thorough analysis of historical changes in vegetation cover within the ODSVRA. This report provides a detailed analysis of the best available aerial photography of ODSVRA for 16 image years between 1930 and 2020 obtained from CDPR, the UCSB Library's Geospatial Collection, and the National Agriculture Imagery Program (NAIP). From this, plant cover was carefully and systematically classified and analyzed in a GIS software (ArcGIS Pro) to detect, quantify, and interpret changes and trends in vegetation cover.

To allow comparison between different management regions, the report focuses on three analytical zones within the sub-area of the ODSVRA south of Arroyo Grande Creek, ~75% of the total area of ODSVRA),

- the OHV riding area within the ODSVRA (c. 2013),
- the North Oso Flaco foredune complex, closed to OHV activity since 1982, serves as a reference site for mature foredunes,
- the South Oso Flaco dune complex within the ODSVRA boundary, including both foredune and backdune areas, which serves as a reference site for mature dunes that have not seen OHV activity since 1982,

In each analytical zone we also focused on the foredune zone, or the area where foredune vegetation would typically exist in the region, which extends ~400 m eastward/inland from the high-water mark. Another area of interest was the new (2020) foredune restoration sites, located within the foredune zone of the OHV riding area between post markers 4-6.

Plant cover maps and calculations (areas and %) were obtained for each analytical zone in all image years. Results show that vegetation cover trends within ODSVRA have varied over time and differ notably between the analytical regions. Within the broader ODSVRA sub-area, vegetation changes generally increased over time, ranging from 25% in 1939, to a peak of 37% in 2012, to just over 35% in 2020. In the OHV riding area, vegetation cover has been comparatively low across all years and declined appreciably from a peak value of 12% in 1966 to around 8% in 2020. After 1966 plant cover decreased to 4% in 1985 and remained low (<5%) until after 1988, when it began to gradually increase to the 2020 levels. The South Oso Flaco area shows a similar trend as the broader ODSVRA area, although with generally higher percentages. Plant cover at Oso Flaco was 37% in 1939, more than doubled to a peak of 66% by 2012, then remained over 60% up to 2020. The North Oso Flaco foredune area showed almost no plant cover in 1930 (0.7%), but has gradually increased over time, mostly after 1985, up to a peak of 24% in 2012.

Foredunes in the region are typically more sparsely vegetated than back dune environments and are characterized by a hummocky terrain of nebkha and elongated shadow dunes, blowouts, and narrow parabolic dunes, such as found at the South Oso Flaco reference site. Accordingly,

plant cover in the foredune zone of ODSVRA is generally less than that in the broader analytical zones over time, but shows similar trends. Foredune plant cover at Oso Flaco in 1939 was very low (2.3%), but increased by an order of magnitude to over 30% by the 2010s. For comparison, vegetation in the foredune zone of the OHV riding area had slightly higher cover (2.7%) in 1939, rose to a peak value of 5.4% in 1966, but then steadily declined to very low values >1% from 1985 to 1998. Since then, vegetation cover has increased slightly in the foredune zone of the OHV area to 2.4% by 2020, mostly due to new plants on the margins of fenced backdune vegetation islands and foredune vegetation establishing in the seasonal bird nesting enclosure.

Both North and South Oso Flaco areas have been fenced off to OHV traffic since roughly 1982 and, therefore, were selected as reference sites for plant cover and dune form in ODSVRA. The positive trend of plant growth over time and high percentages of cover in these areas vs. the OHV riding area attest to natural processes and responses of vegetation growth and dune development that could occur with limited anthropogenic disturbance. It is important to note, however, that some areas within the ODSVRA, including South Oso Flaco, are impacted by invasive species planted in the area during the early 1900s and, as such, plant cover percentages and dune stabilization could be higher than might be expected under natural conditions. Therefore, the specific cover values for South Oso Flaco provide a reference for relatively undisturbed areas in the ODSVRA, but they do not represent ideal natural conditions of this region. Unfortunately, there are no nearby dune systems that are pristine and undisturbed. Over the last decade CDPR have also conducted targeted efforts to remove invasive species in the ODSVRA particularly in backdune areas, South Oso Flaco, the Pismo Dunes Natural Preserve, and on some private land-holdings within and outside of the ODSVRA borders.

Although invasive grass species exist in ODSVRA, studies of sand dunes elsewhere in the world indicate a shift toward 'greening' (i.e., increased vegetation cover) over the last three decades[18,19,20,21] partly in response to climatic changes and enhanced preservation efforts. The results of this report are consistent with this global trend, yet they occur in the presence of intensive recreational use pressures, such as OHV riding and camping (sanctioned or otherwise) in various locations in the dunes. In part, the observed responses within ODSVRA are the result

[18] Ashkenazy, Y., Yizhaq, H., Tsoar, H., 2012. Sand dune mobility under climate change in the Kalahari and Australian deserts. Climatic Change 112, 901–923. https://doi.org/10.1007/s10584-011-0264-9

[19] Gao, J., Kennedy, D.M., Konlechner, T.M., 2020. Coastal dune mobility over the past century: A global review. Progress in Physical Geography: Earth and Environment 44, 814–836. https://doi.org/10.1177/0309133320919612

[20] Jackson, D.W.T., Costas, S., González-Villanueva, R., Cooper, A., 2019. A global 'greening' of coastal dunes: An integrated consequence of climate change? Global and Planetary Change 182, 103026. https://doi.org/10.1016/j.gloplacha.2019.103026

[21] Heathfield, D.K., & Walker, I.J. (2011). Analysis of coastal dune dynamics, shoreline position, and large woody debris at Wickaninnish Bay, Pacific Rim National Park, British Columbia. Canadian Journal of Earth Sciences, 48(7), 1185-1198. https://doi.org/10.1139/e11-043

of land use management and vegetation restoration efforts by CDPR since establishment of the park in 1982.

Detailed examination of change maps of negative (losses) or positive (gains) in plant cover over time show a large amount of change between 1966-1985, with negative change mostly in foredune areas and adjoining inland vegetation islands. Between 1998 and 2012, a large positive change occurred, mostly around existing vegetation islands, which corresponds partly with implementation of protective fencing and restoration projects in different areas outside the OHV riding area. Most positive changes in the OHV riding area were after 2005 and relate to new plants within the margins of fenced vegetation islands and foredune plants and nebkha development in the seasonal bird nesting enclosure between 2005 and 2020. In general, the vast majority of positive changes over the years in all analytical zones were within fenced areas with limited or no OHV activity, such as the seasonal bird nesting exclosures, fenced islands of existing plant cover, restoration project sites, and in the North and South Oso Flaco regions.

In terms of landscape responses during the identified management intervals, the period roughly preceding the establishment of the ODSVRA (1939-1985) saw a general decline in plant cover in the foredune and backdune of the OHV riding area (from 10.9 to 3.9% cover). Although cover increased between 1939-1966, it then declined until 1985 just as the ODSVRA was established. Between 1985 and 2012, there was mostly increasing plant cover with over 14% positive change in the broader ODSVRA sub-area, mainly around existing vegetation and other targeted restoration areas, particularly between 2005 and 2012. In the OHV riding area, plant cover increased mostly in fenced areas in backdune vegetation islands. From 2012 to 2020, there was a general decline in the amount of vegetation cover compared to previous intervals with 8% of total change in the ODSVRA sub-area. Some of this decline relates to invasive plant removal projects at the Pismo Dune Natural Preserve and Oso Flaco and most of the positive changes during this time related to backdune restoration areas implemented by CDPR.

It is clear that vegetation cover within ODSVRA has changed significantly over time and that the effects of OHV traffic, recreational activities, invasive species, and ecosystem restoration projects have collectively influenced the observed patterns and trends in varying ways and extents. Some of these effects are the result of aggregated impacts and, thus, are difficult to disentangle, while others are more clearly related to distinct activities in specific areas. It is important to note that the landscape that was inherited by CDPR when ODSVRA was established in 1982 had already experienced notable changes in vegetation cover related to unsanctioned OHV activity and other land use changes (e.g., agriculture, infrastructure development). Although it is beyond the scope of this report, it is also possible that plant communities at ODSVRA are also influenced by multi-decadal climatic changes similar to other coastal dune systems worldwide. Given the dynamic and compounded nature of forces that have shaped the dunes at ODSVRA, it

is essential to recognize that dune ecosystems and their plant communities are not static features of the landscape and that they will continue to evolve and reflect the changing conditions that shape their form and function. This poses a particular challenge for establishing management targets and restoration strategies in a landscape that has been subject to intensive OHV and recreation activities that destroy vegetation essential for dune development and reduction of dust emissions.

This report is intended to inform further discussions between CDPR, SAG, and SLO-APCD on how historic vegetation cover and change trends can be used to inform future dust mitigation strategies within ODSVRA. For instance, a reference point in time for 'pre-disturbance' or 'pre-CDPR management' conditions within the dunes would be useful for guiding dust emissions simulation modeling and revisiting the SOA target, which currently lacks a baseline condition. In addition, understanding the spatial distribution of plant communities and their changes through time in different disturbance settings is useful for refining decisions on the location and extent of future vegetation restoration dust mitigation strategies. It is anticipated that such discussions and related adaptive management decisions will help define ongoing vegetation for restoration and dust emissions mitigation strategies in the upcoming 2022 ARWP.

5. Supplements

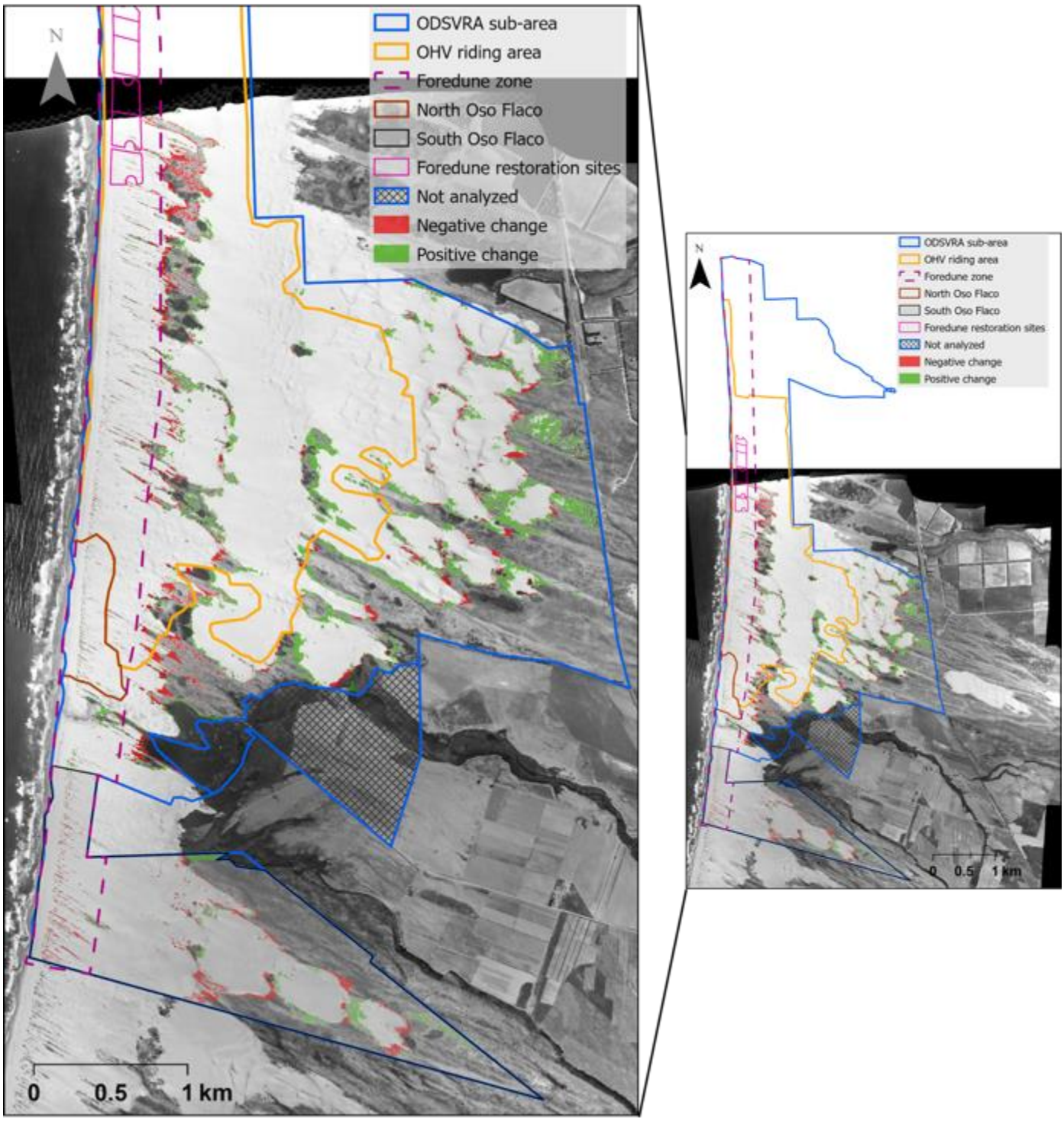

Figure S1. Vegetation change analysis results between 1930 and 1939. Positive change is in green, negative change is in red. Background orthophoto is from 1930.

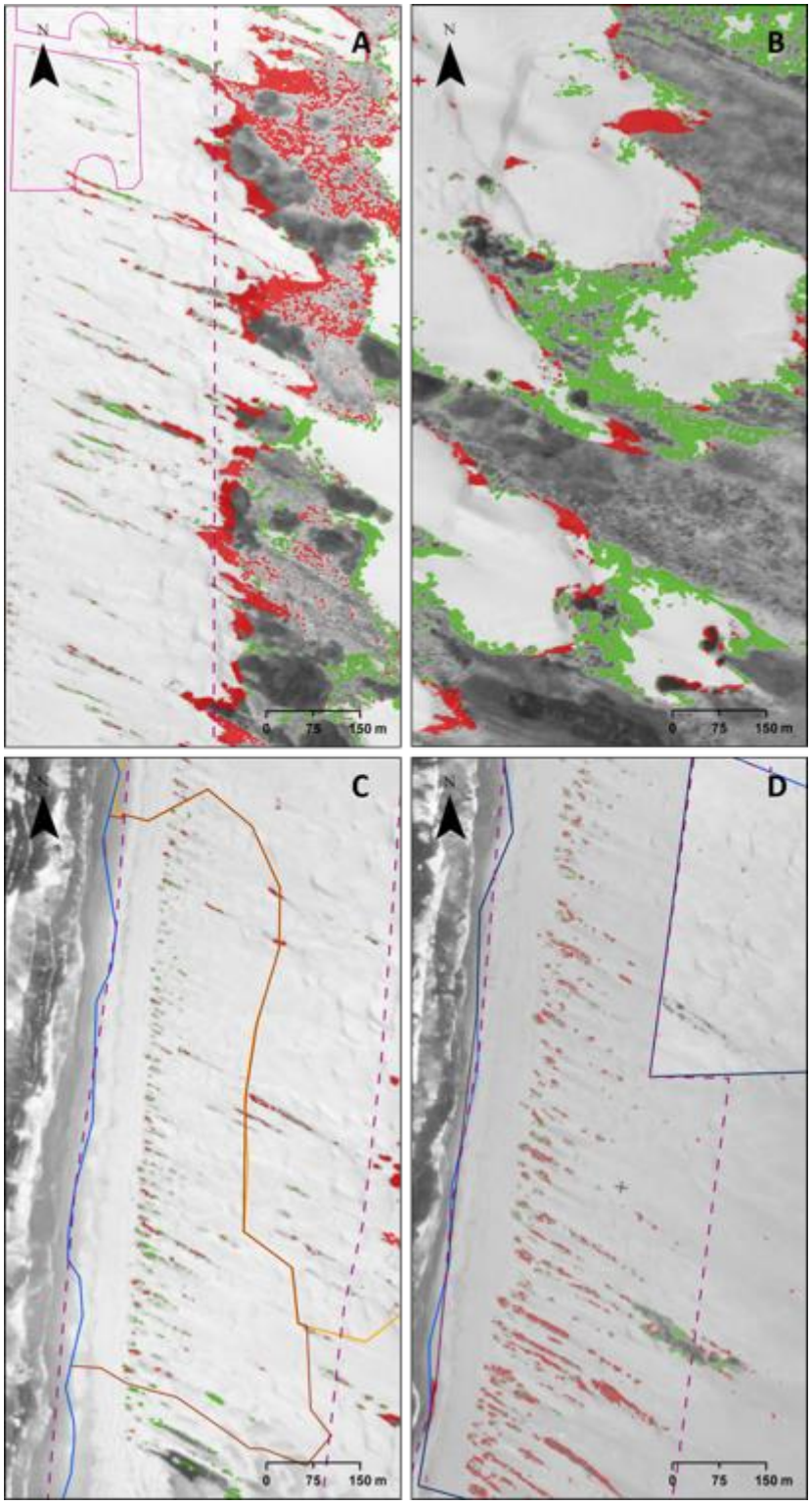

Figure S2. close-ups of vegetation change analysis results between 1930 and 1939 of the OHV riding area (A), backbude of the ODSVRA sub-area (B), North Oso Flaco (C), and South Oso Flaco (D). Positive change is in green, negative change is in red. Background orthophoto is from 1930.

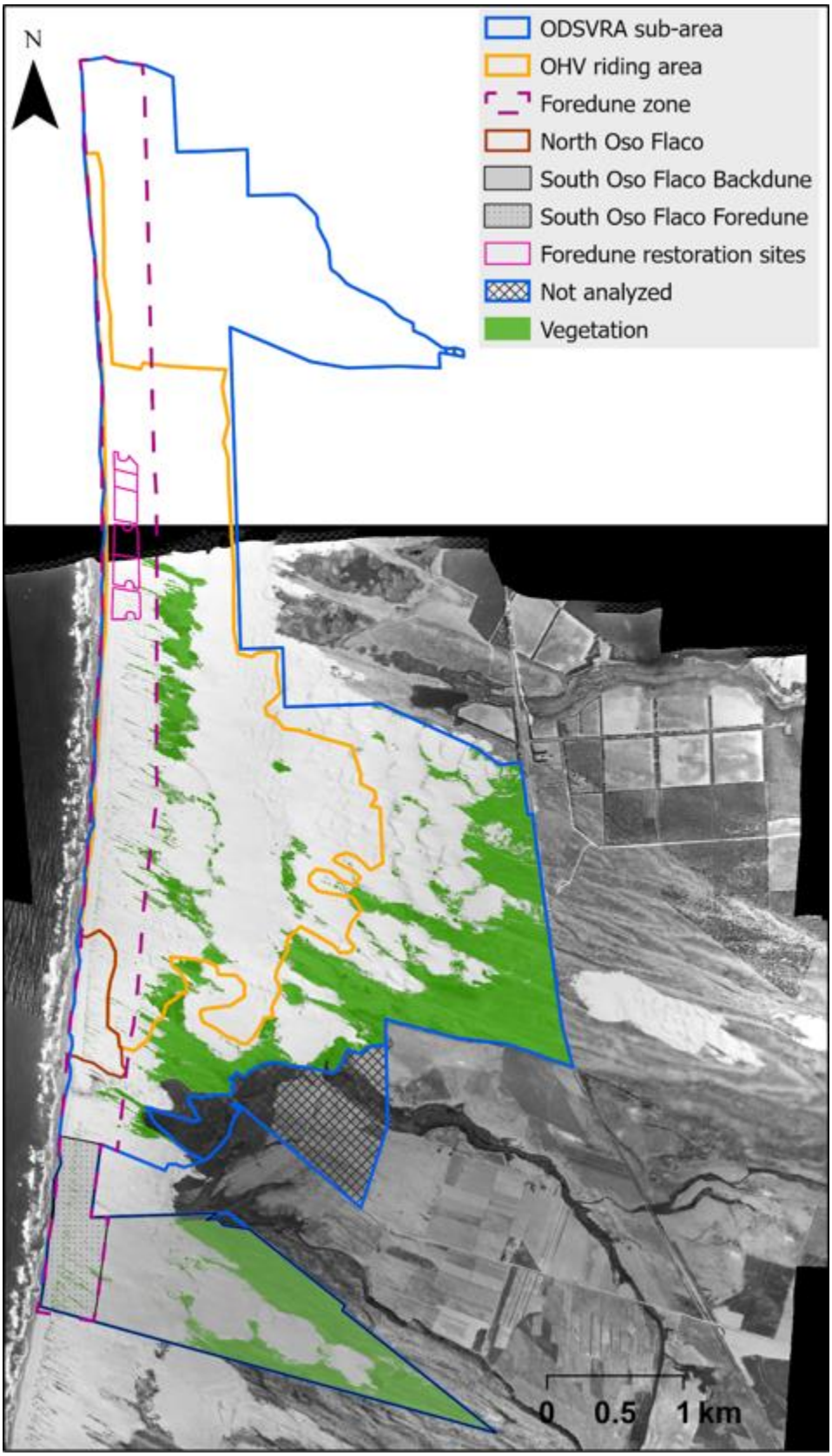

Figure S3. Vegetation cover map of 1930.

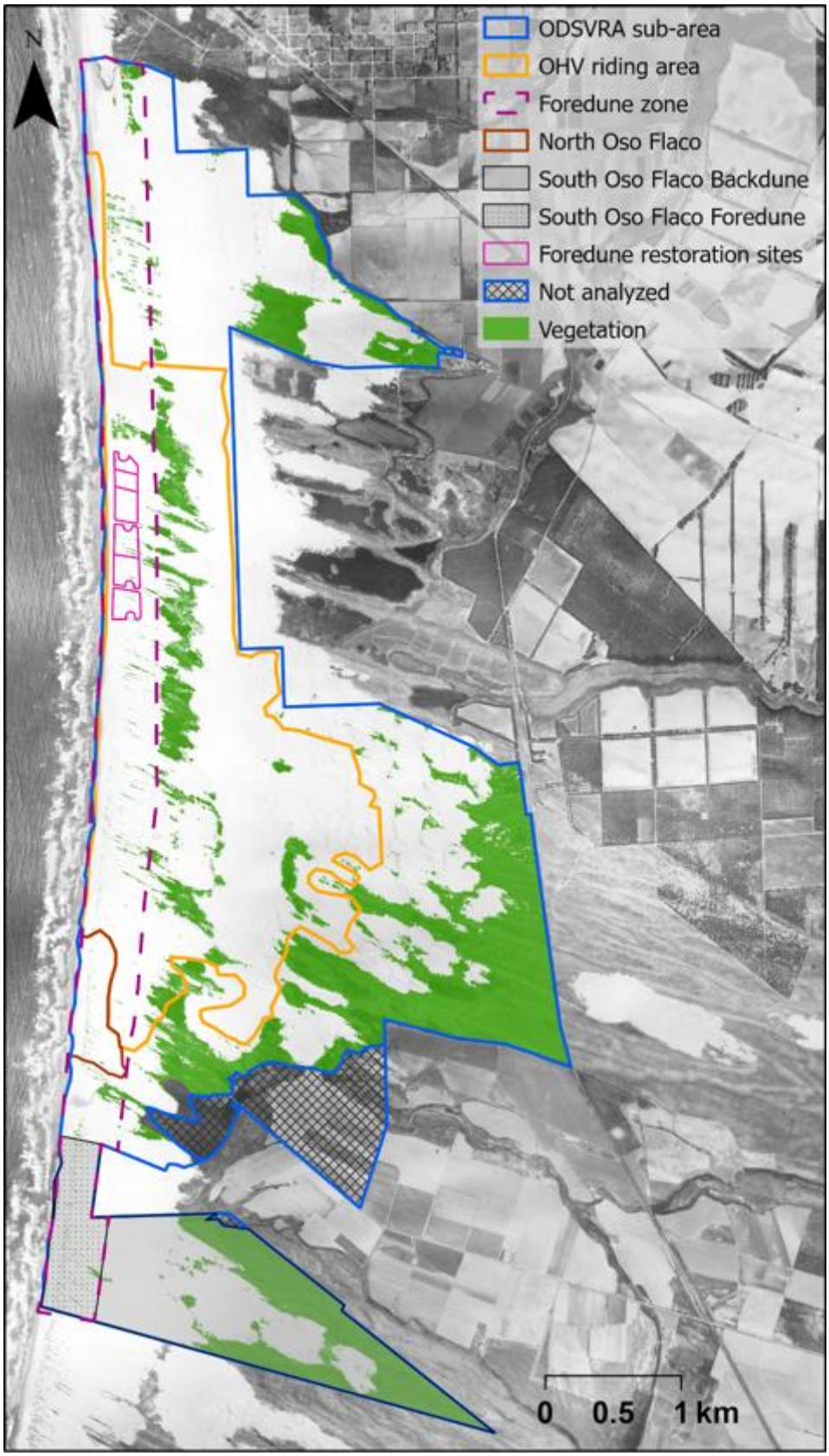

Figure S4. Vegetation cover map of 1939.

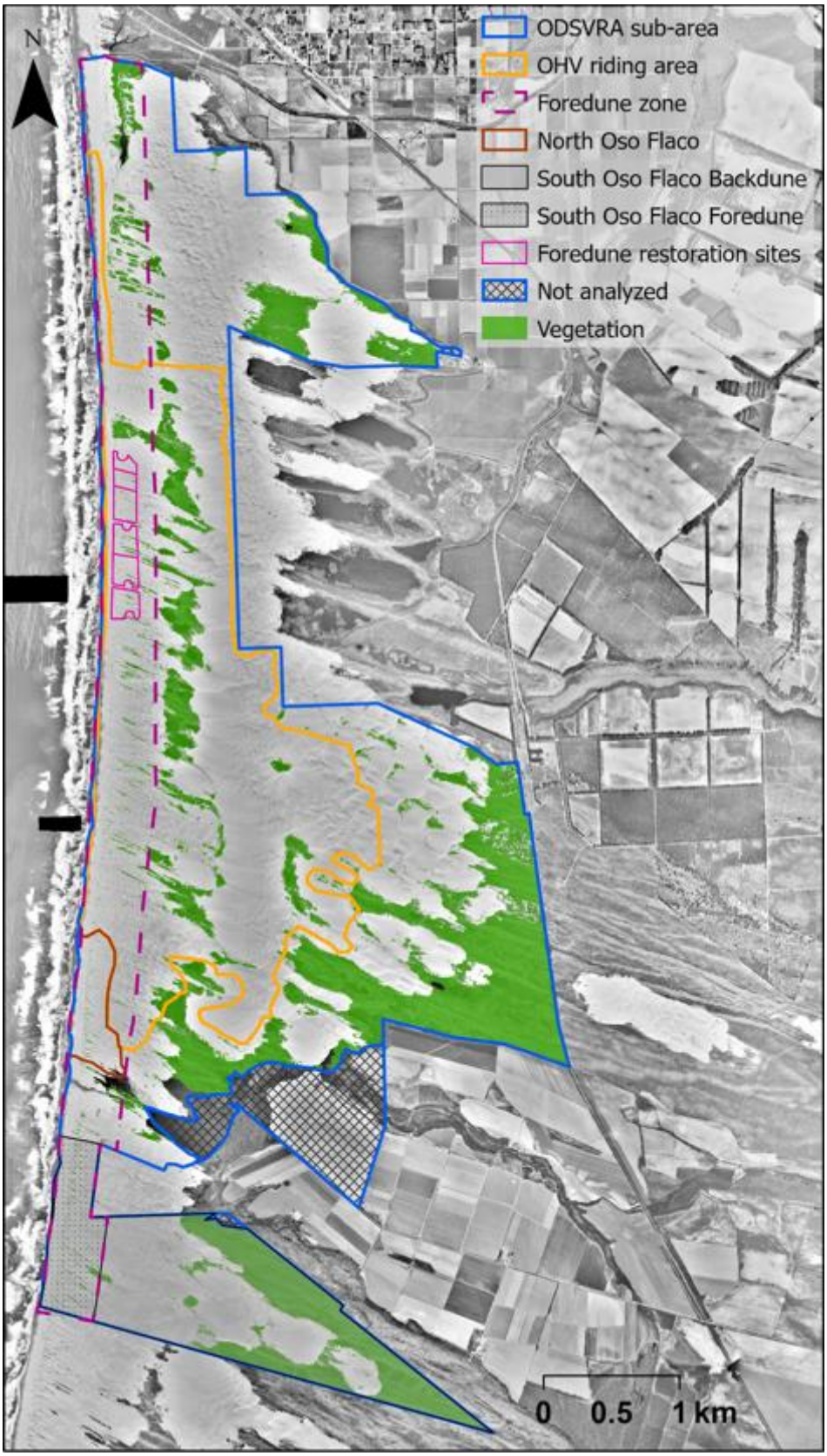

Figure S5. Vegetation cover map of 1949.

Figure S6. Vegetation cover map of 1956.

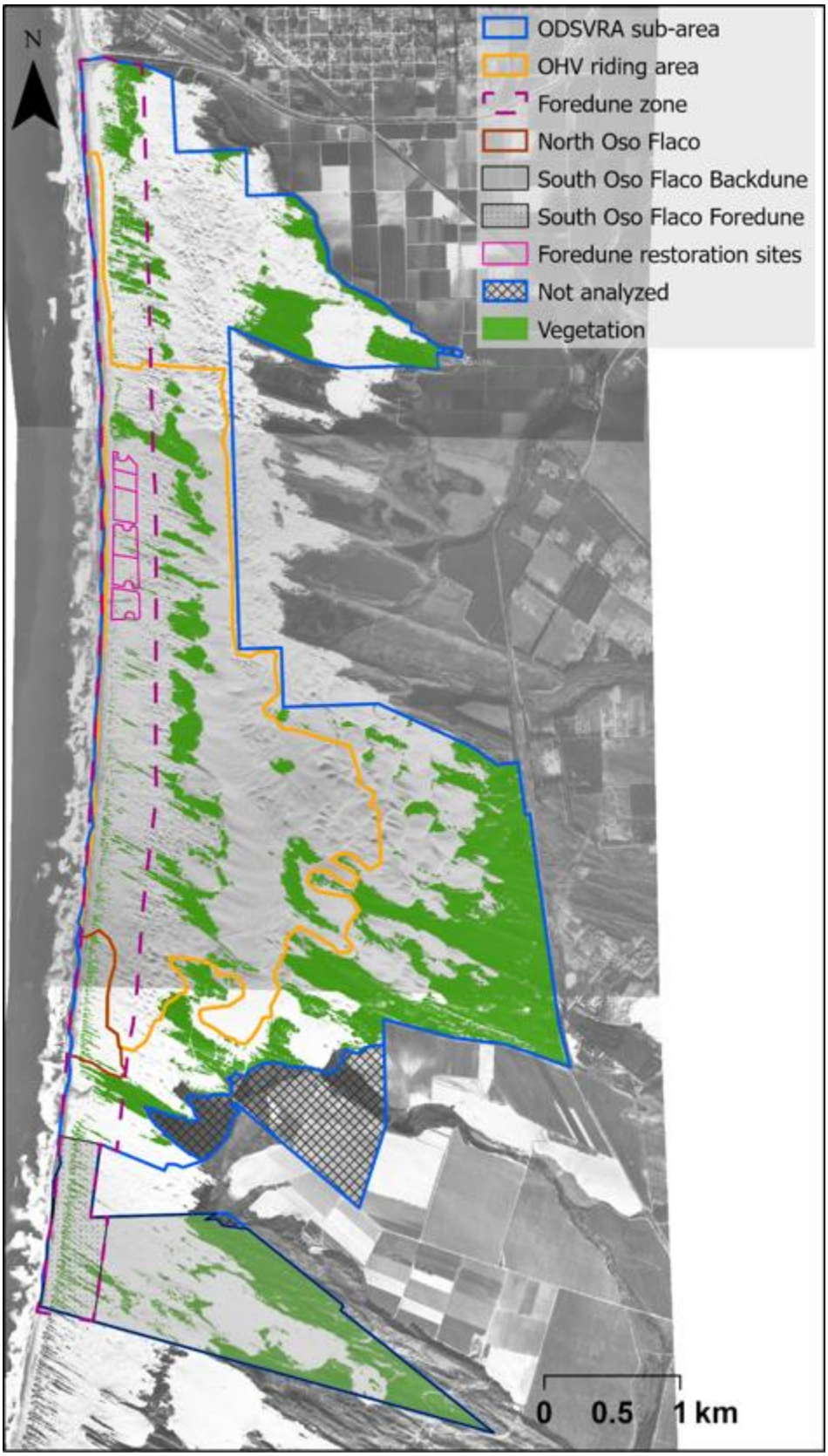

Figure S7. Vegetation cover map of 1966.

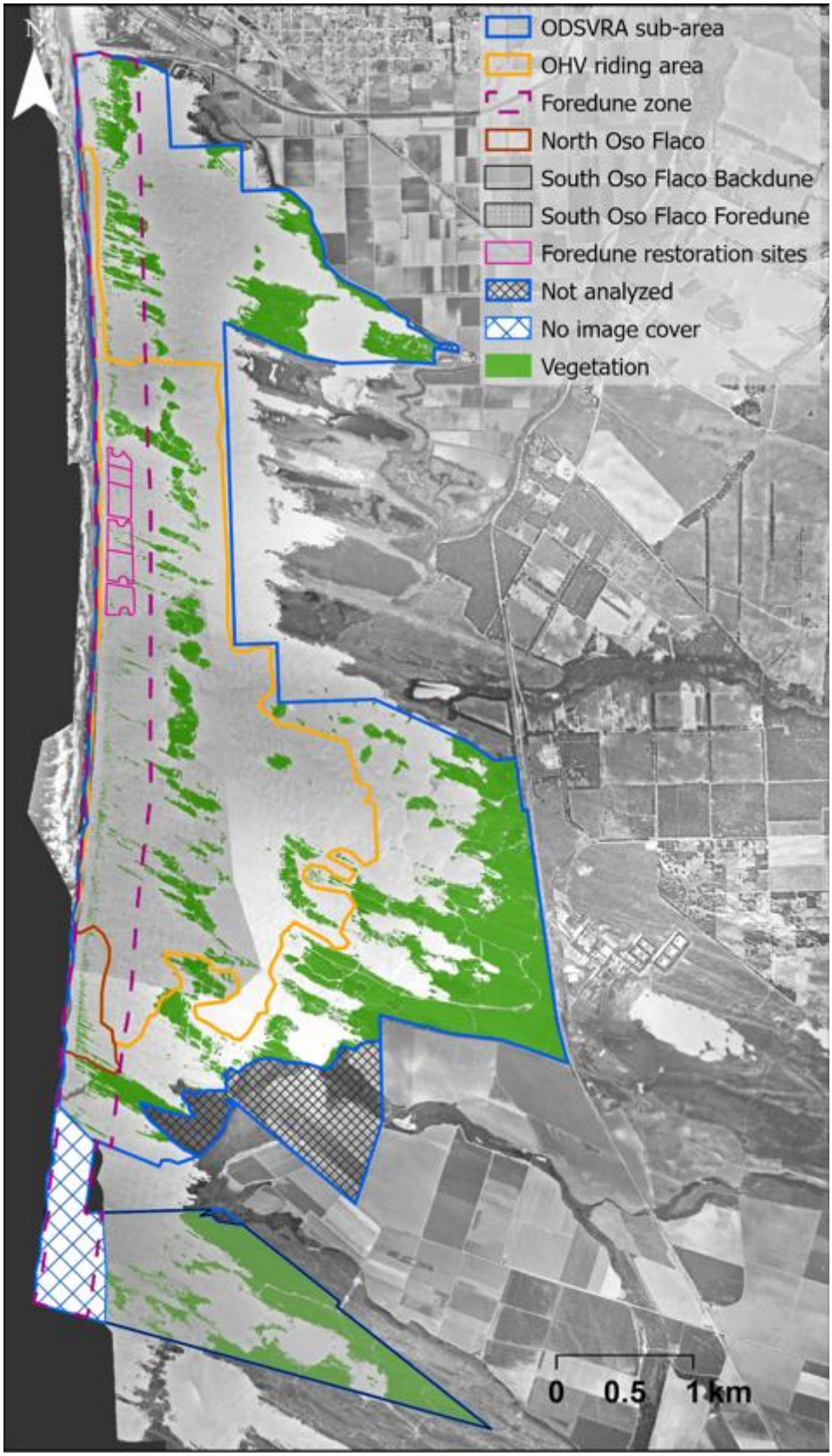

Figure S8. Vegetation cover map of 1971.

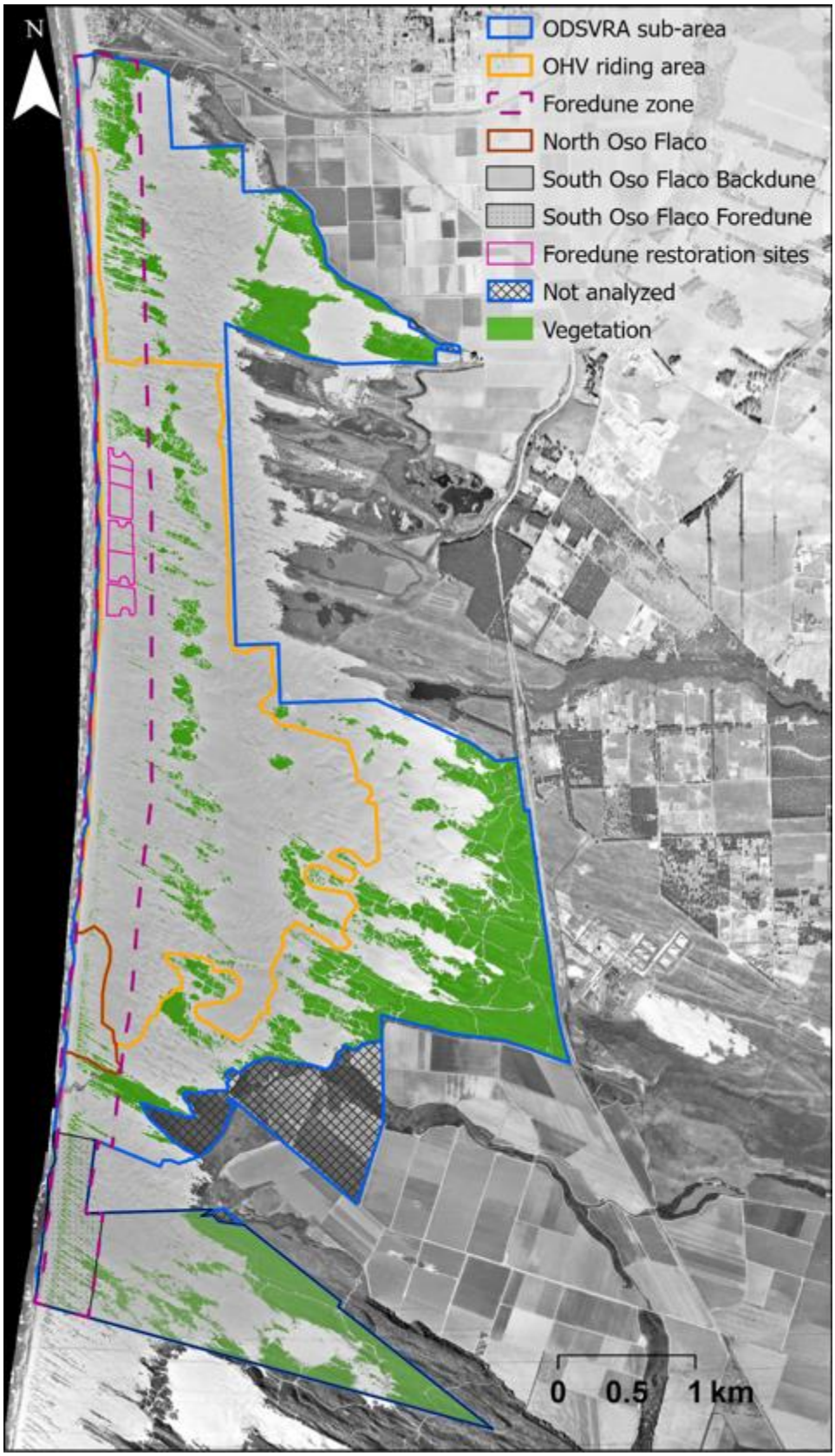

Figure S10. Vegetation cover map of 1978.

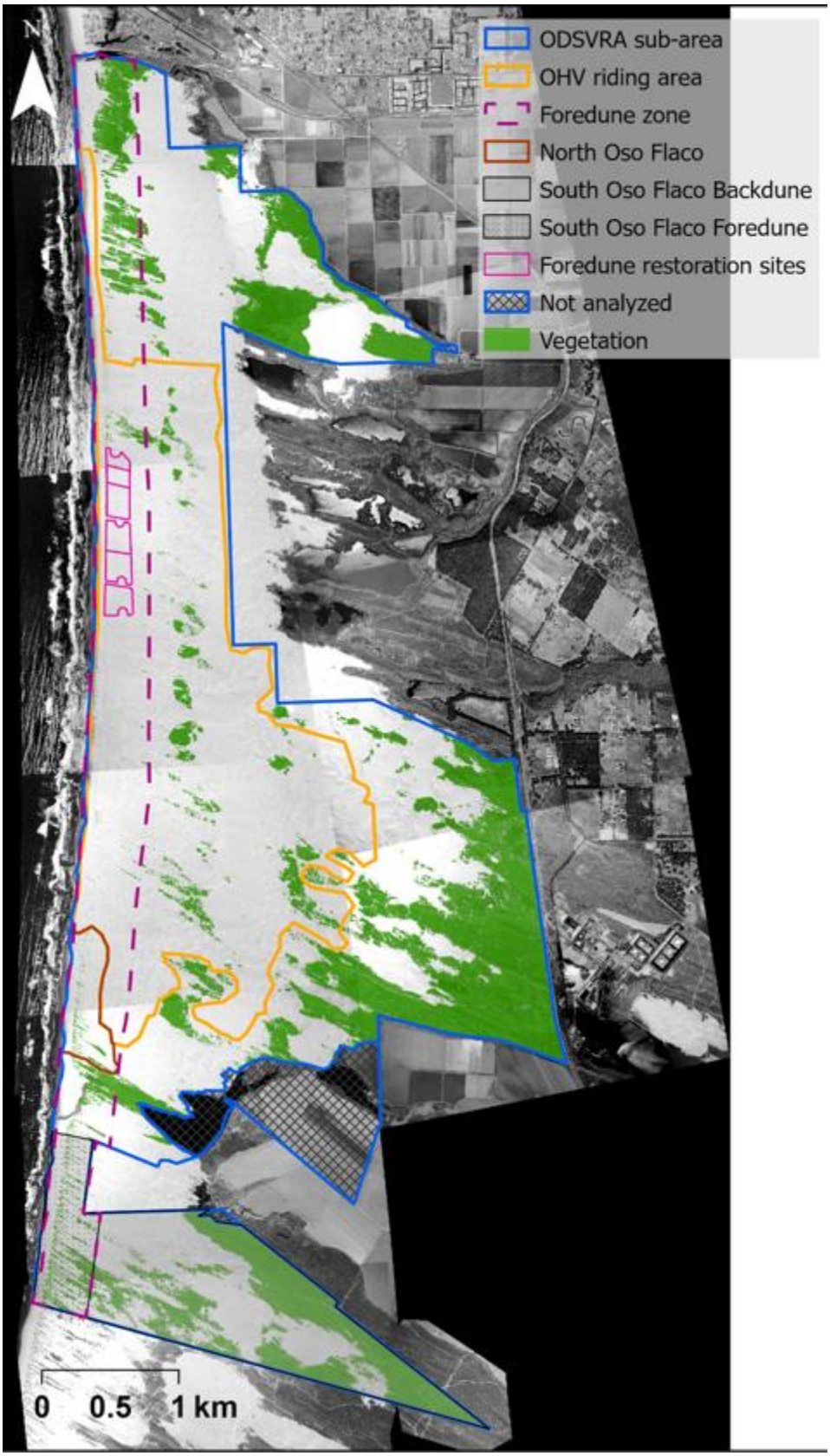

Figure S10. Vegetation cover map of 1985.

Figure S11. Vegetation cover map of 1994.

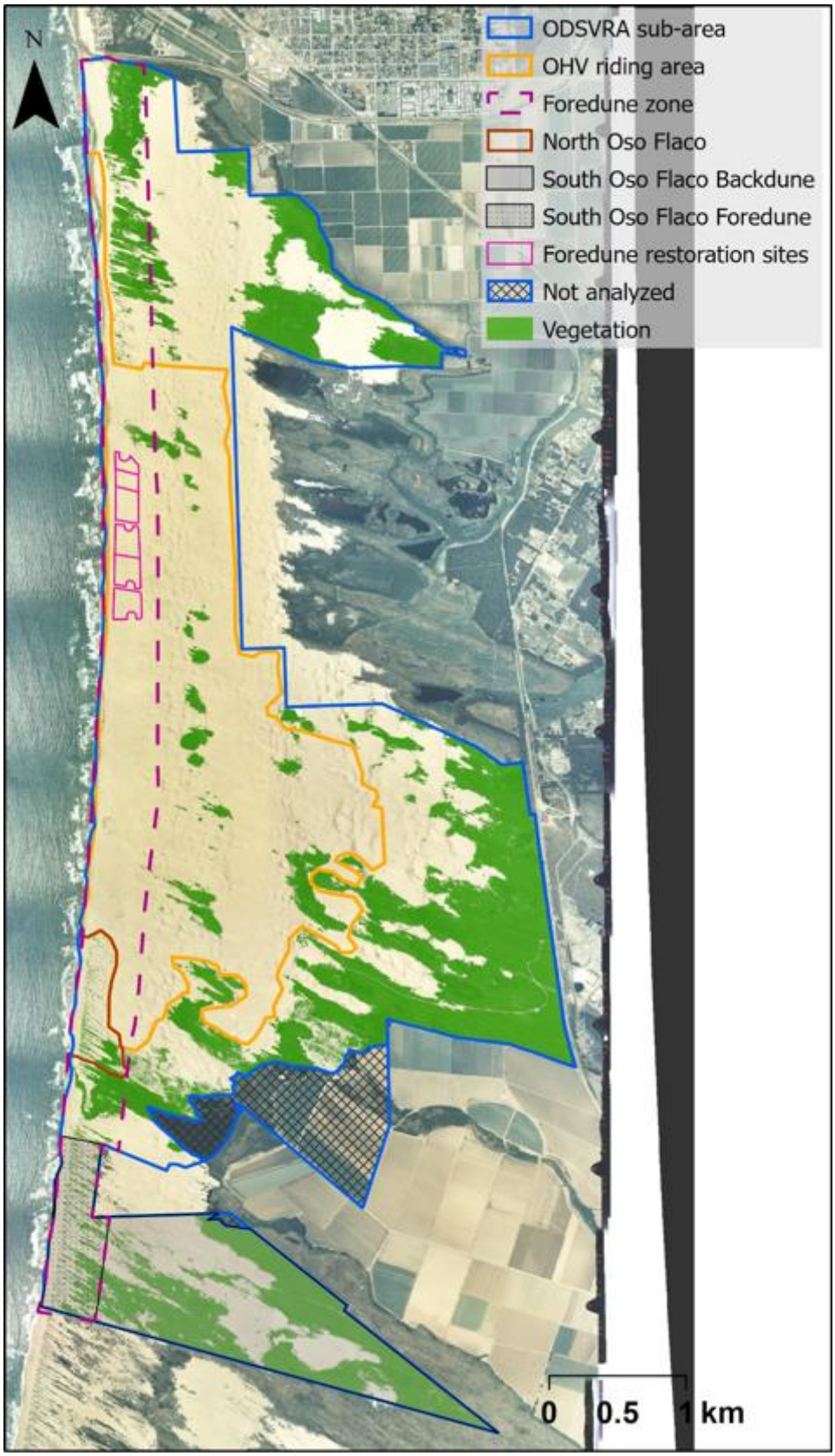

Figure S12. Vegetation cover map of 1998.

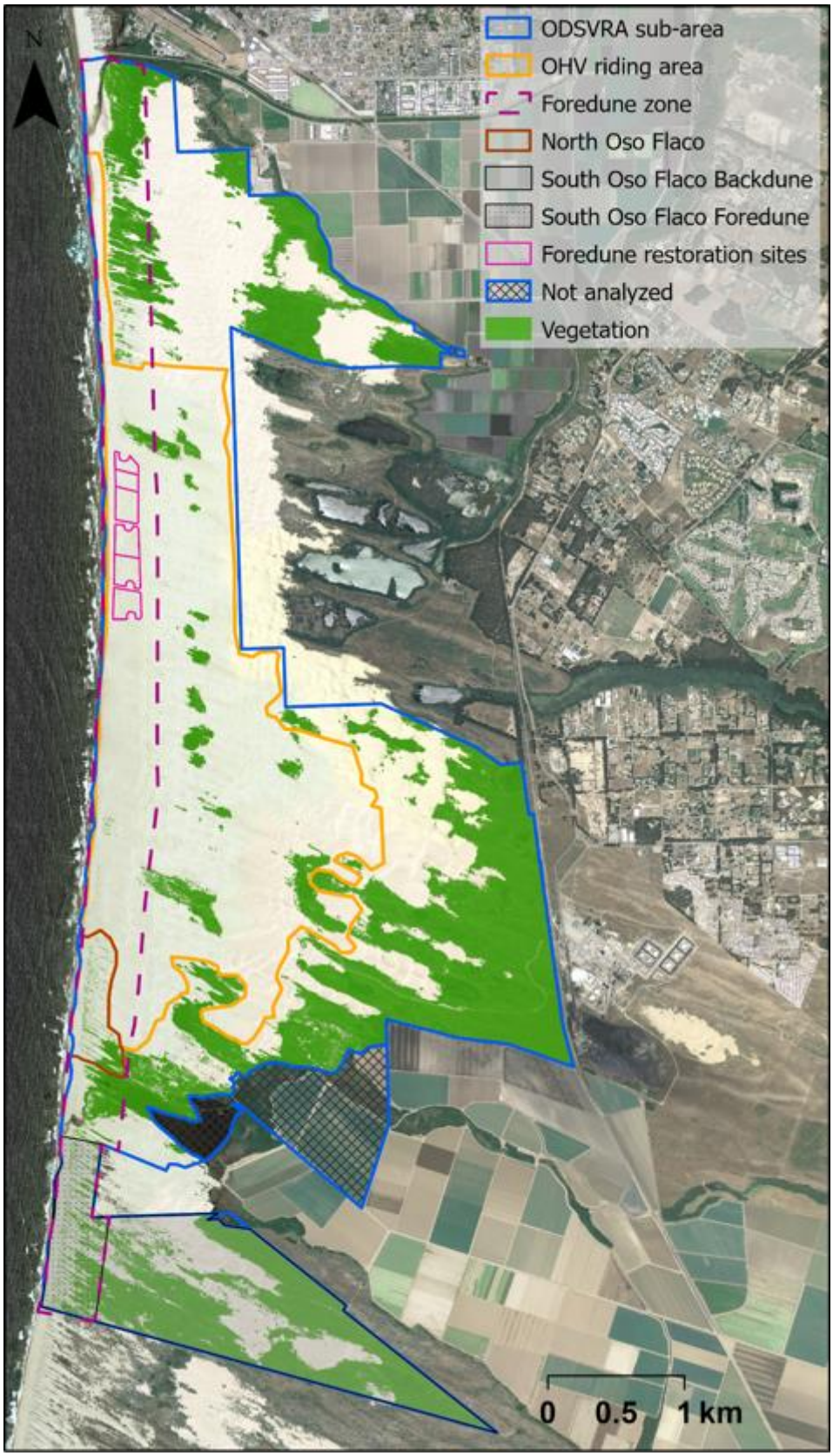

Figure S13. Vegetation cover map of 2005.

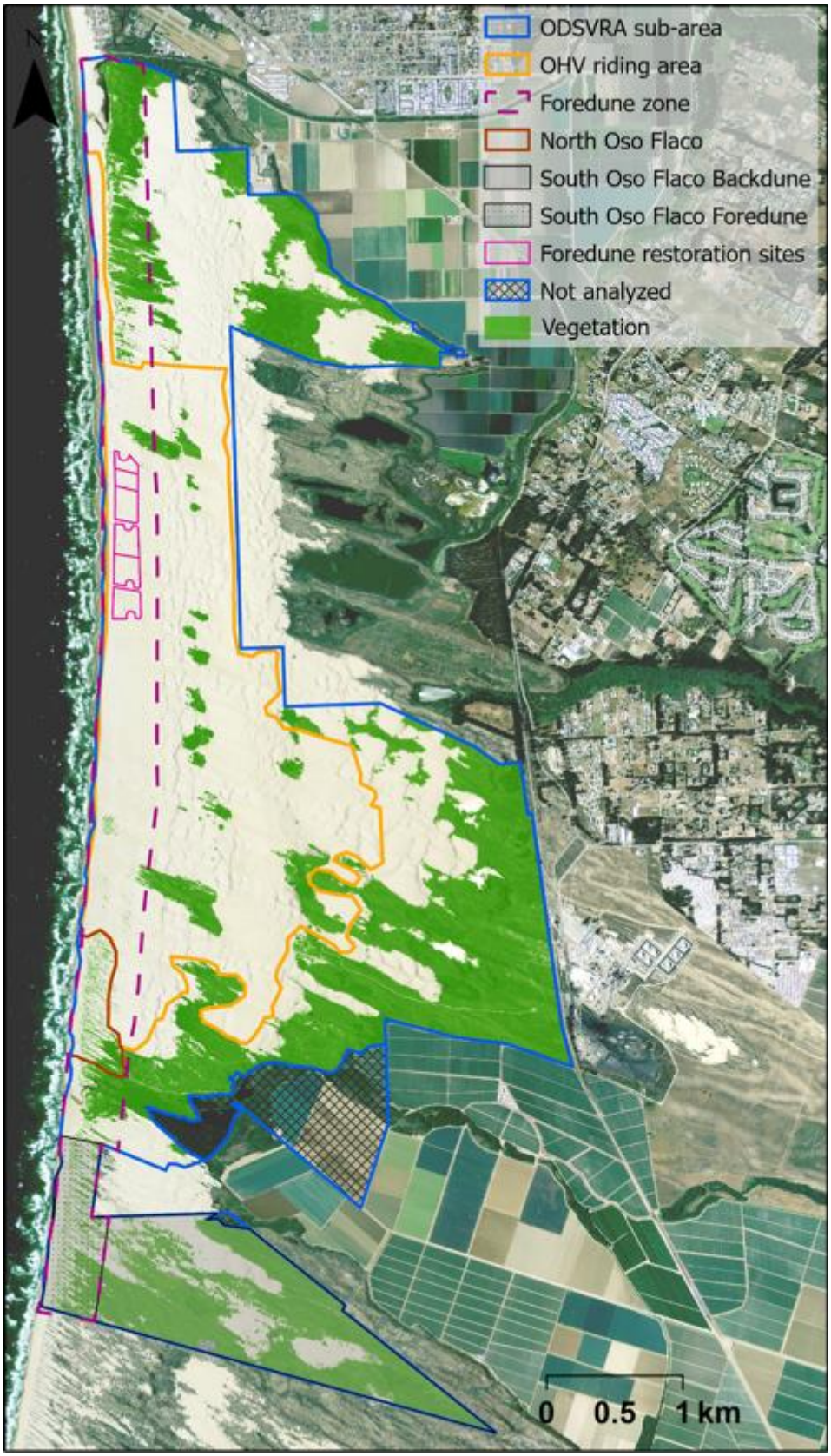

Figure S14. Vegetation cover map of 2012.

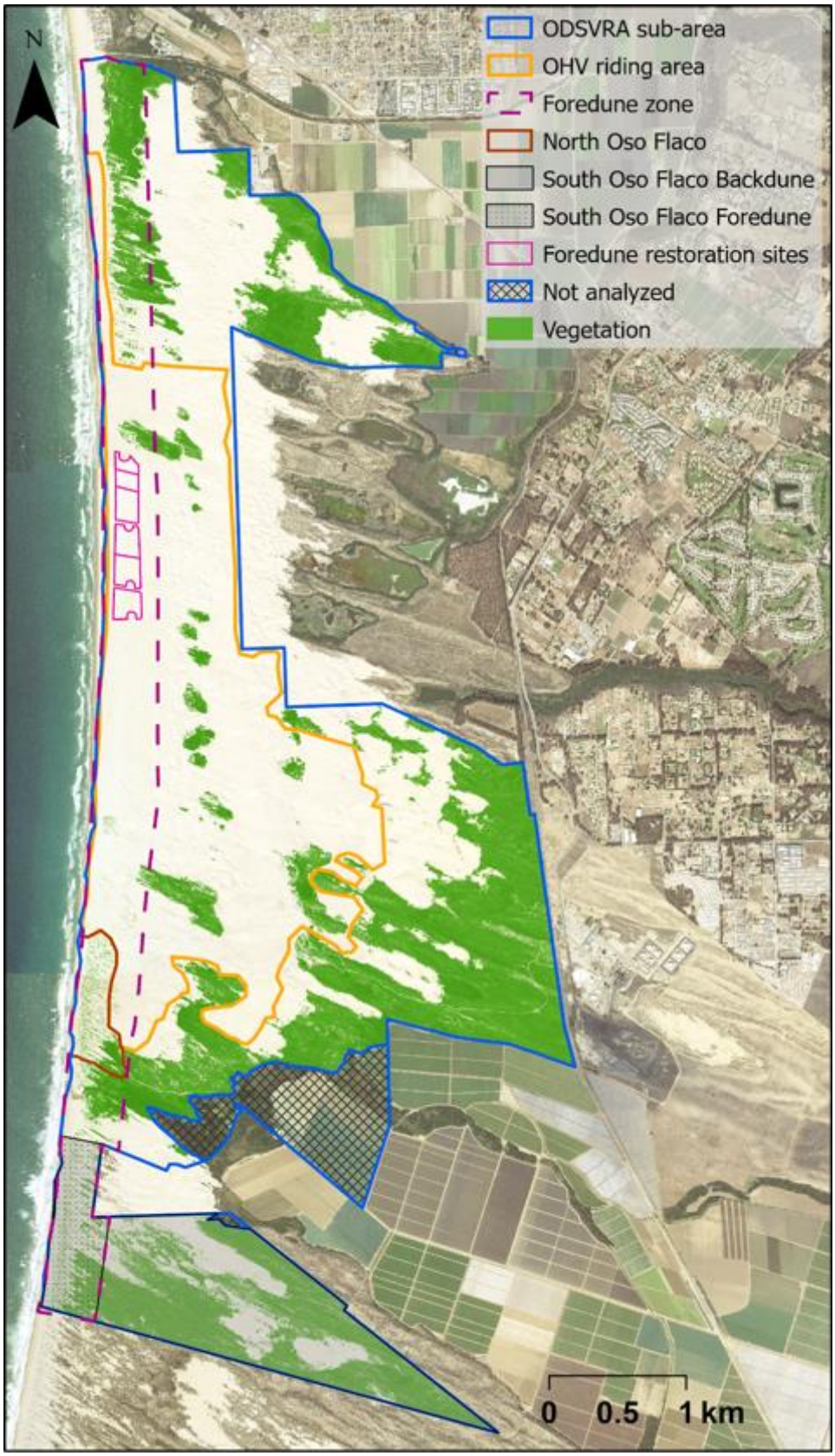

Figure S15. Vegetation cover map of 2014.

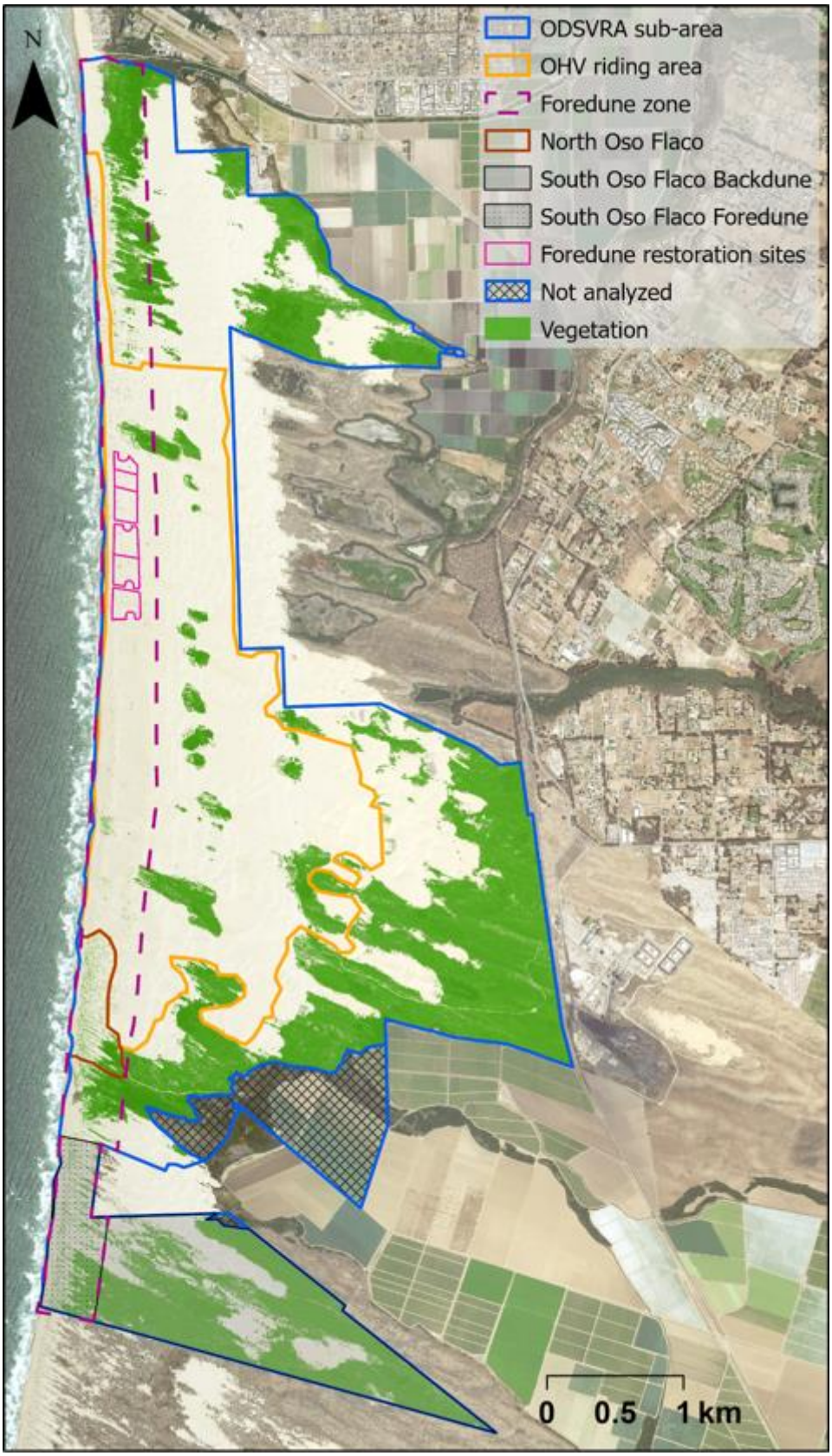

Figure S16. Vegetation cover map of 2016.

Figure S17. Vegetation cover map of 2018.

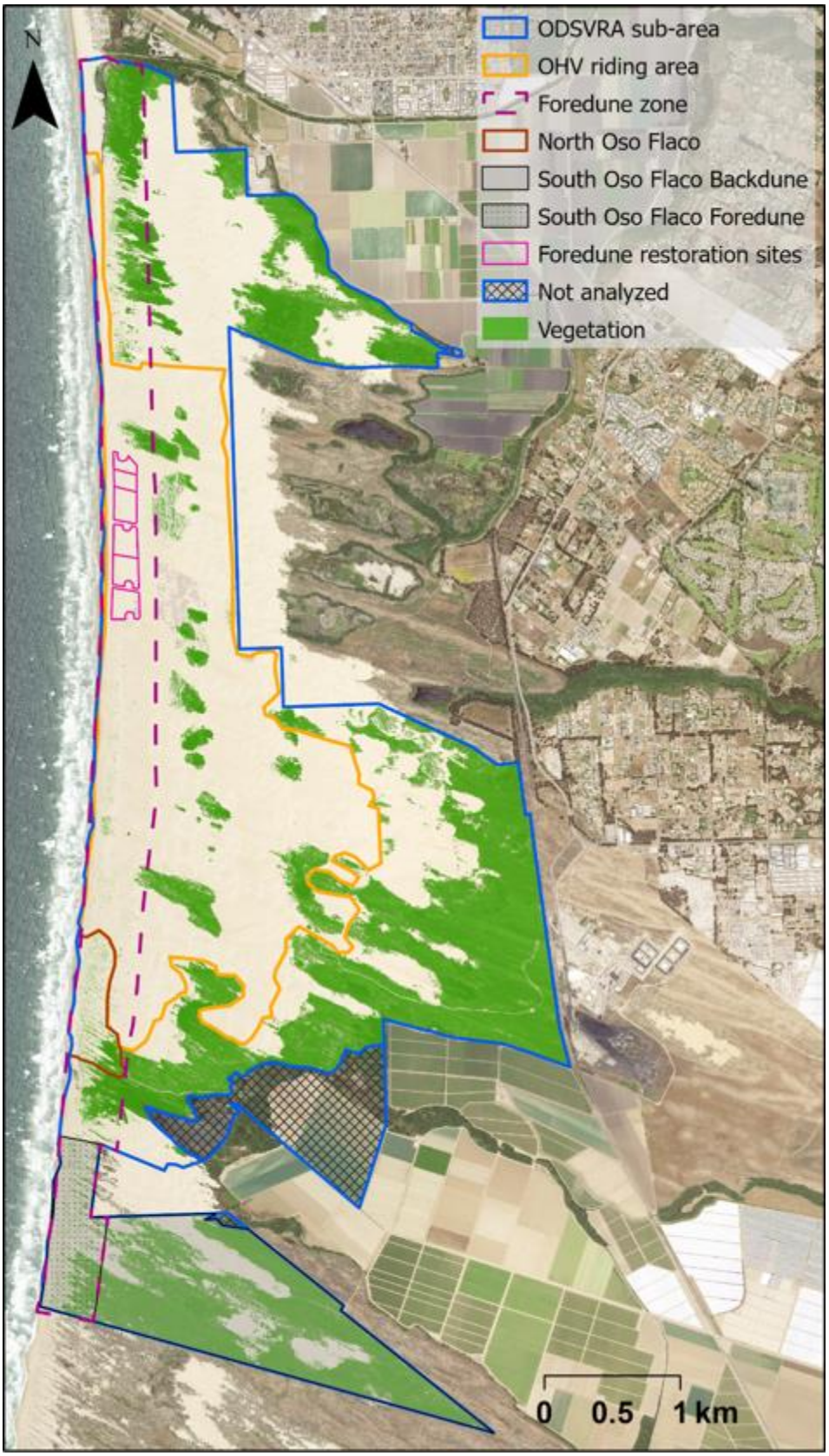

Figure S18. Vegetation cover map of 2020.

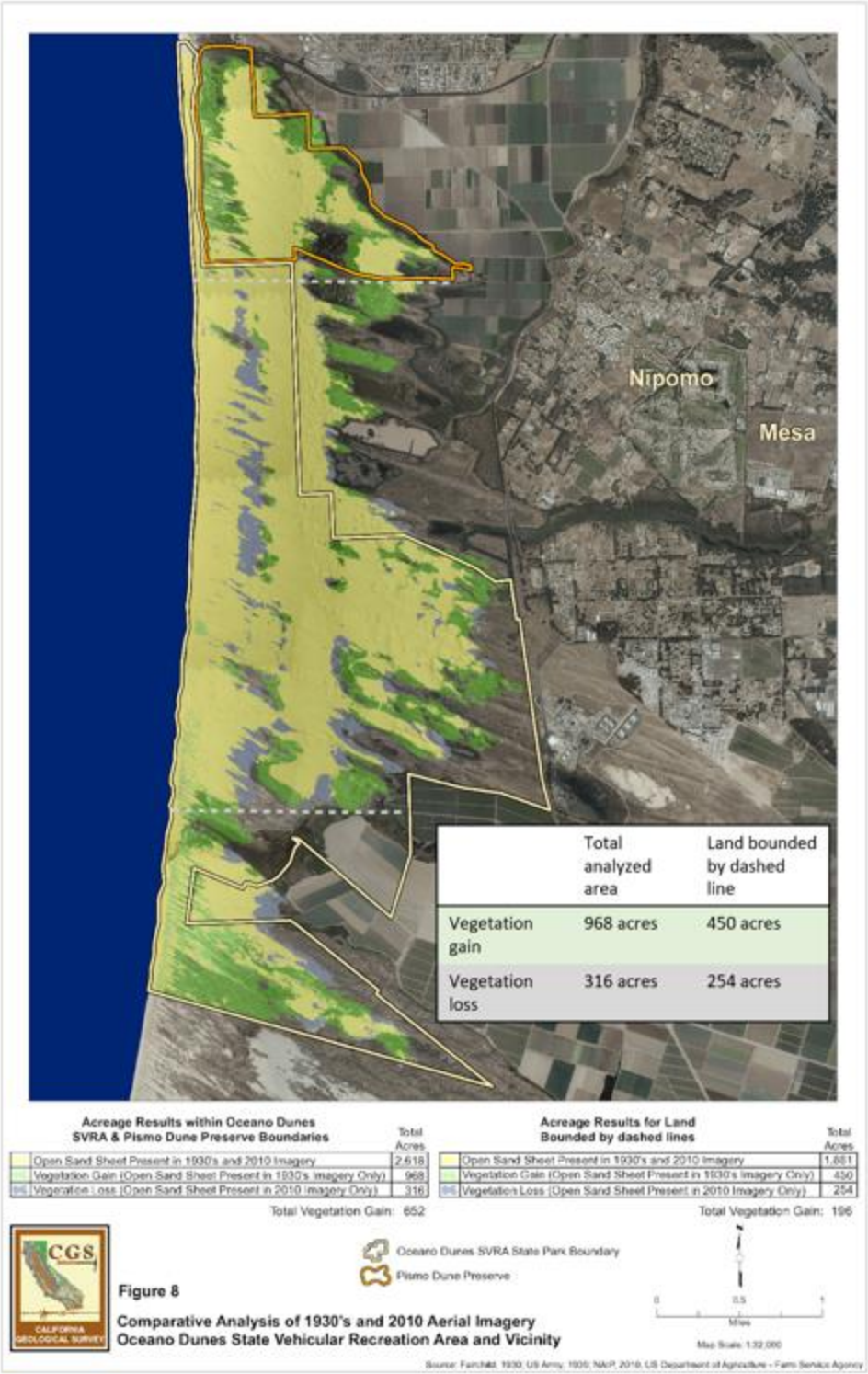

Figure S19. Sand and vegetation acreage results of the comparison between 1930's and 2010 presented in Figure 8 in the CGS report from 2011, positive change is in green, negative change in gray, open sand is in yellow in yellow (Harris, 2011).

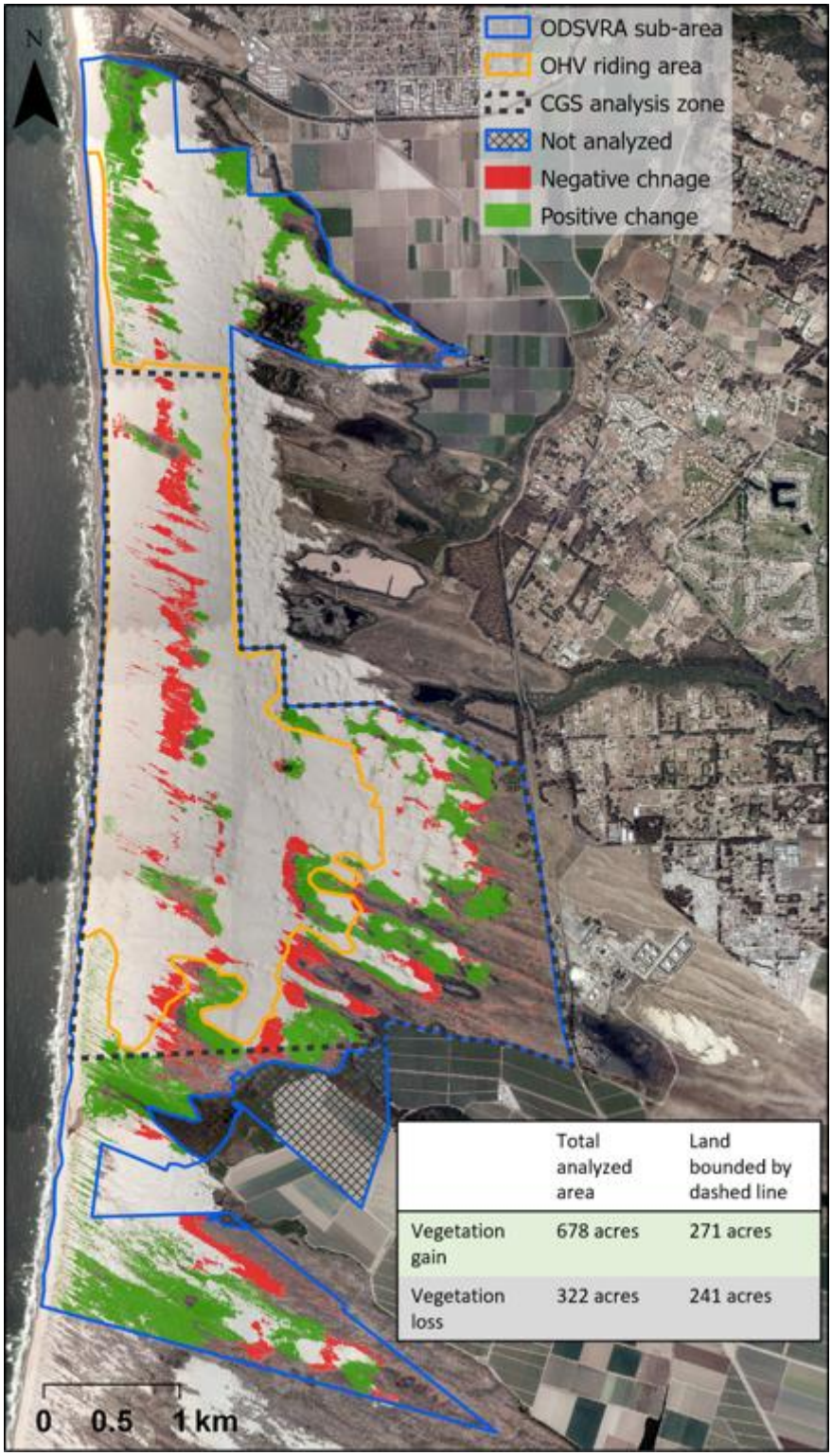

Figure S20. Vegetation change analysis results of the 1939 and 2010 UCSB-ASU analysis, positive change is in green, negative change is in red. Orthophoto background is from 2012. The grey dashed line represents the area for comparison with the CGS analysis.

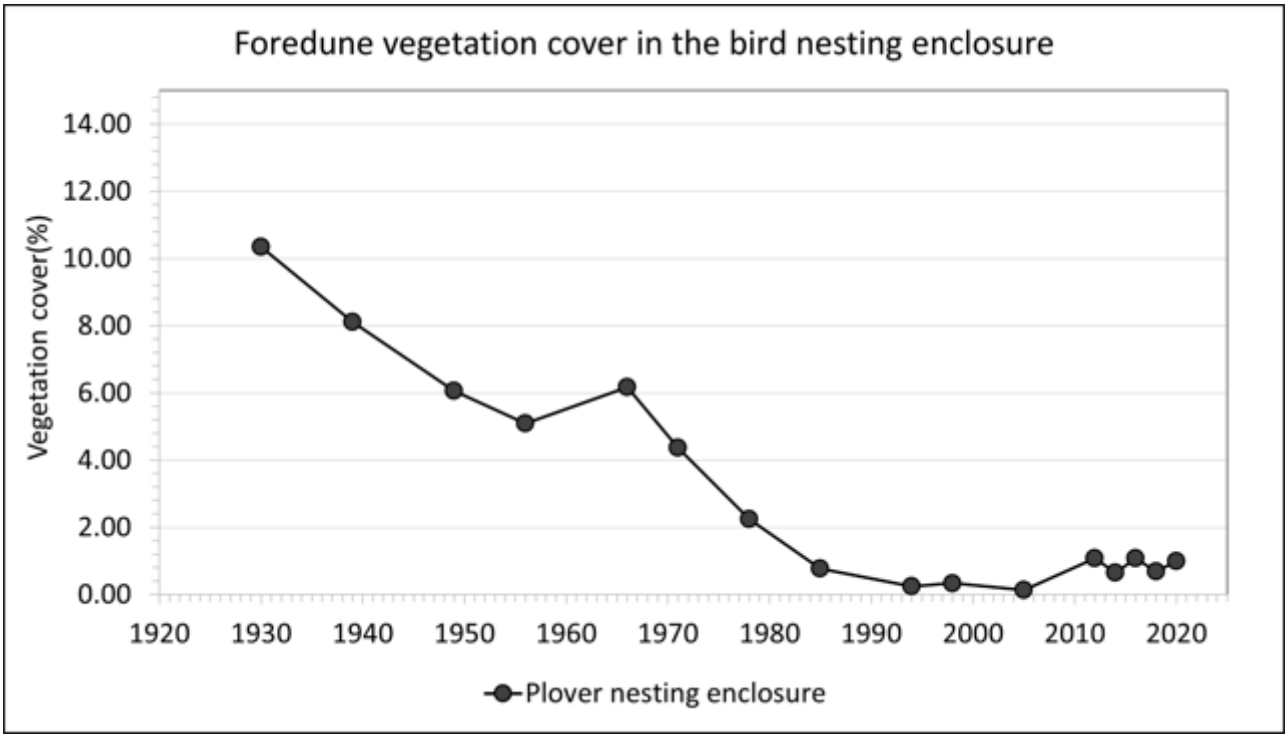

Figure S21. Percent vegetation cover within the seasonal bird nesting enclosure area (see borders in Figure 8). Vegetation cover percentages are related to the area of the analytical region.

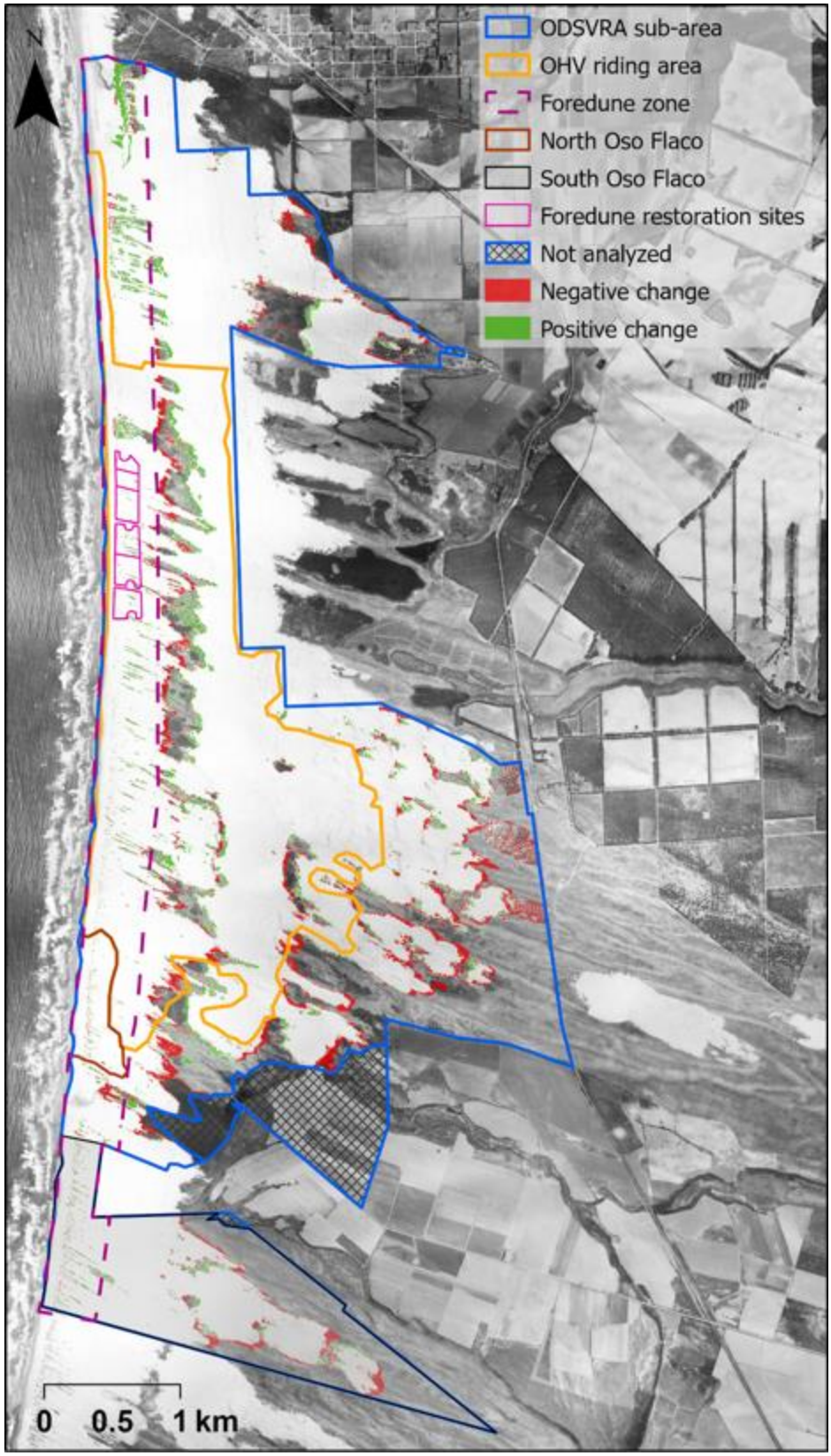

Figure S22. Vegetation change analysis results between 1939 and 1949. Positive change is in green, negative change is in red. Background orthophoto is from 1939.

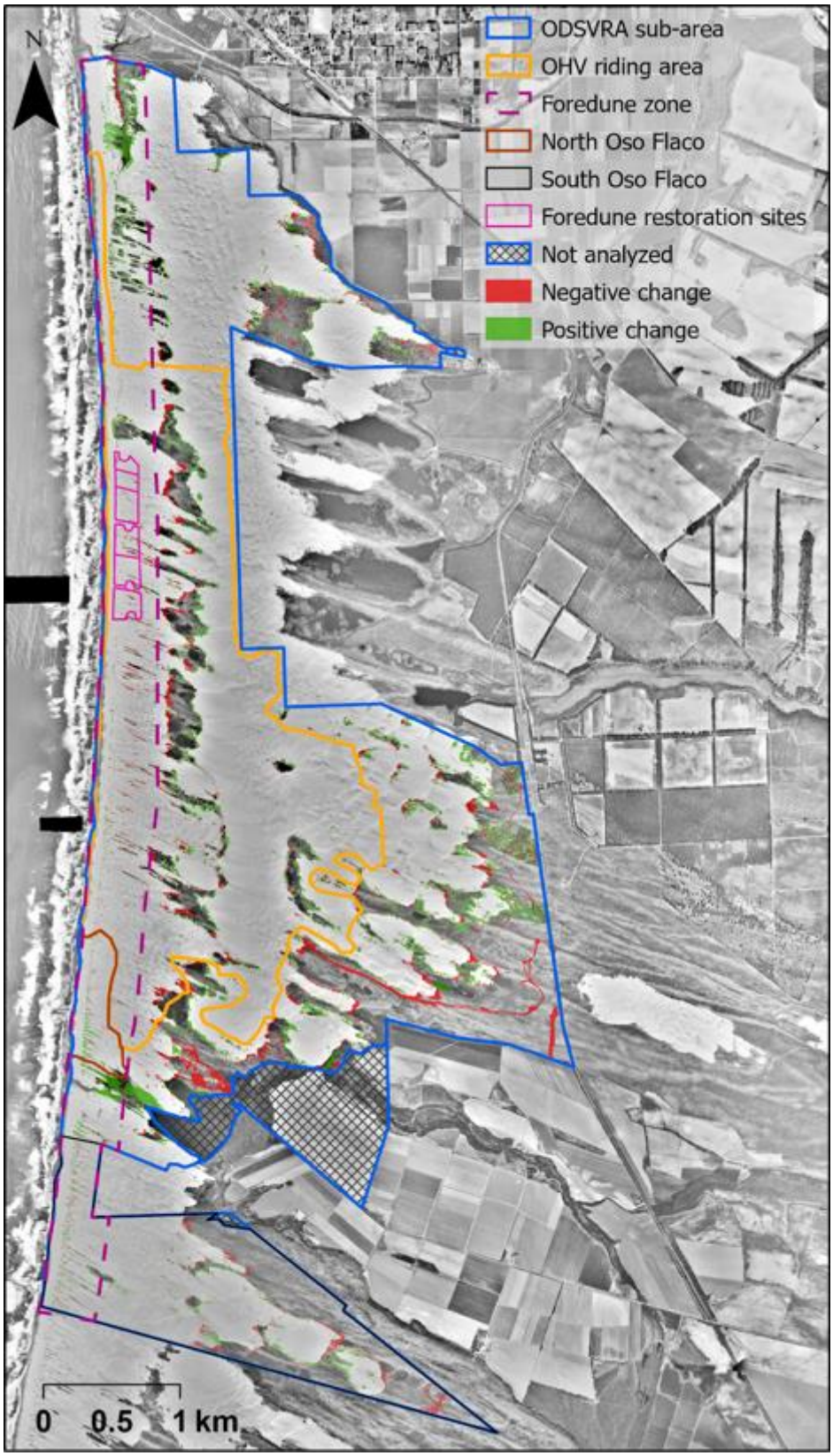

Figure S23. Vegetation change analysis results between 1949 and 1956. Positive change is in green, negative change is in red. Background orthophoto is from 1949.

Figure S24. Vegetation change analysis results between 1956 and 1966. Positive change is in green, negative change is in red. Background orthophoto is from 1956.

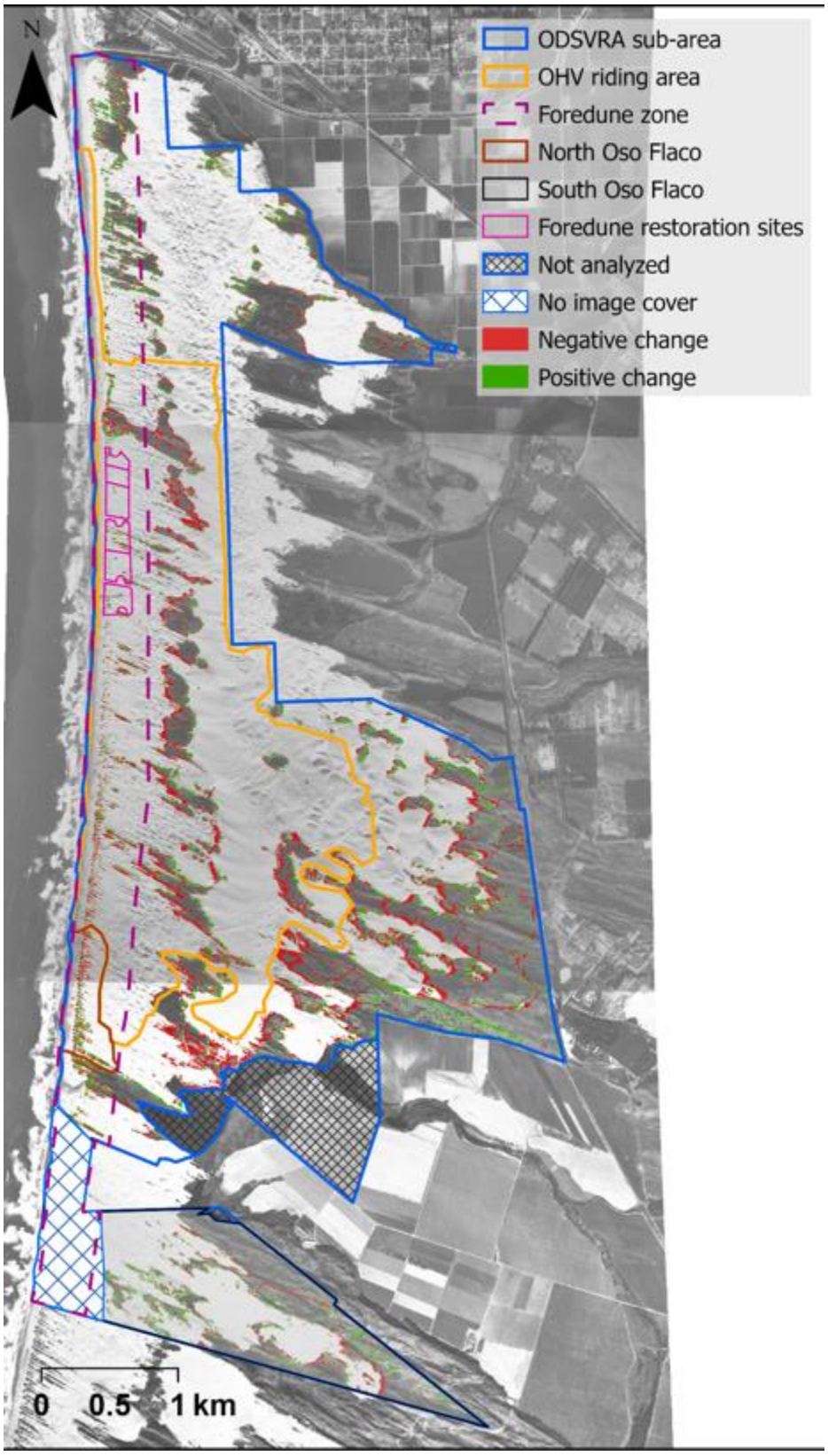

Figure S25. Vegetation change analysis results between 1966 and 1971. Positive change is in green, negative change is in red. Background orthophoto is from 1966.

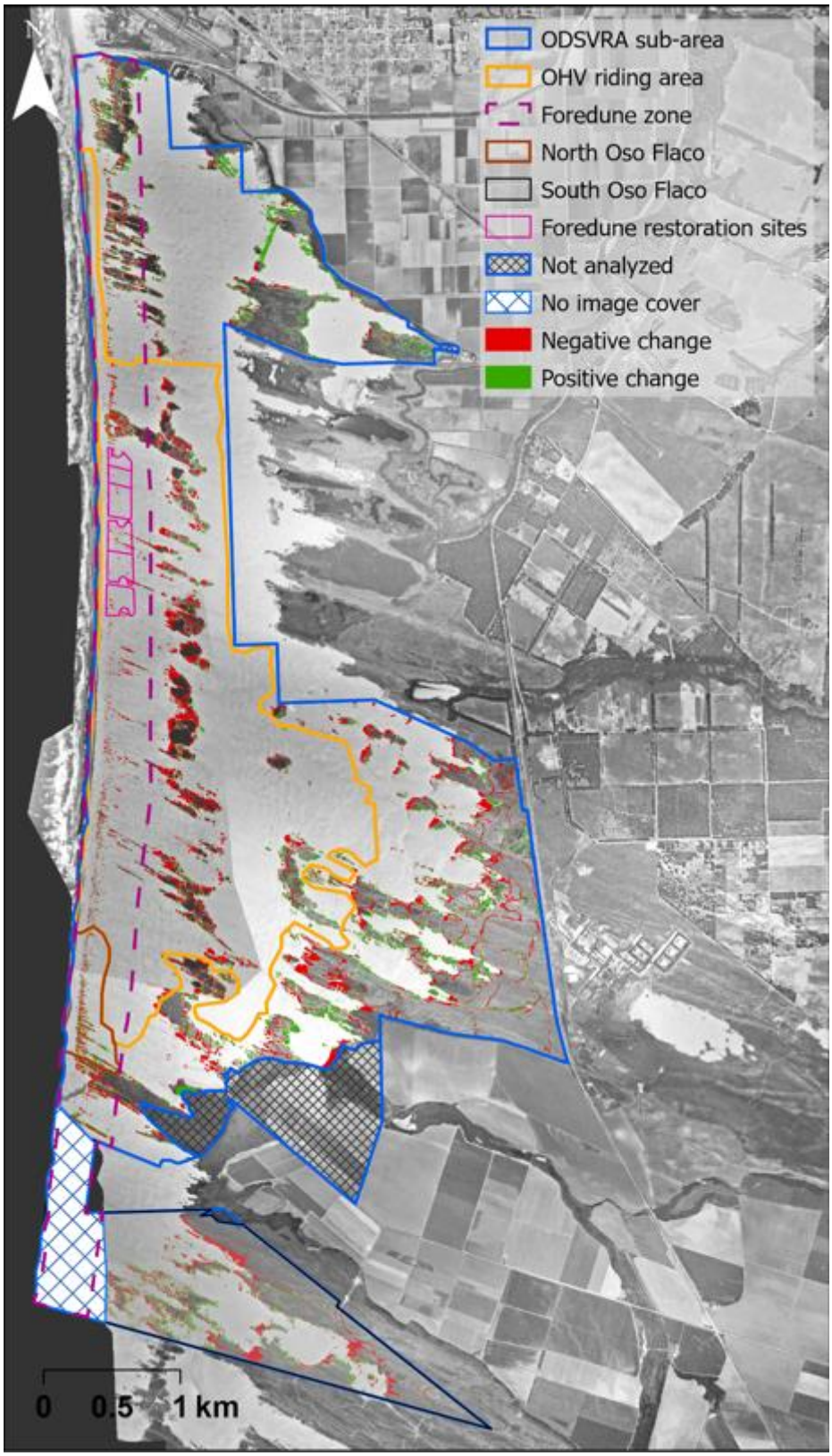

Figure S26. Vegetation change analysis results between 1971 and 1978. Positive change is in green, negative change is in red. Background orthophoto is from 1971.

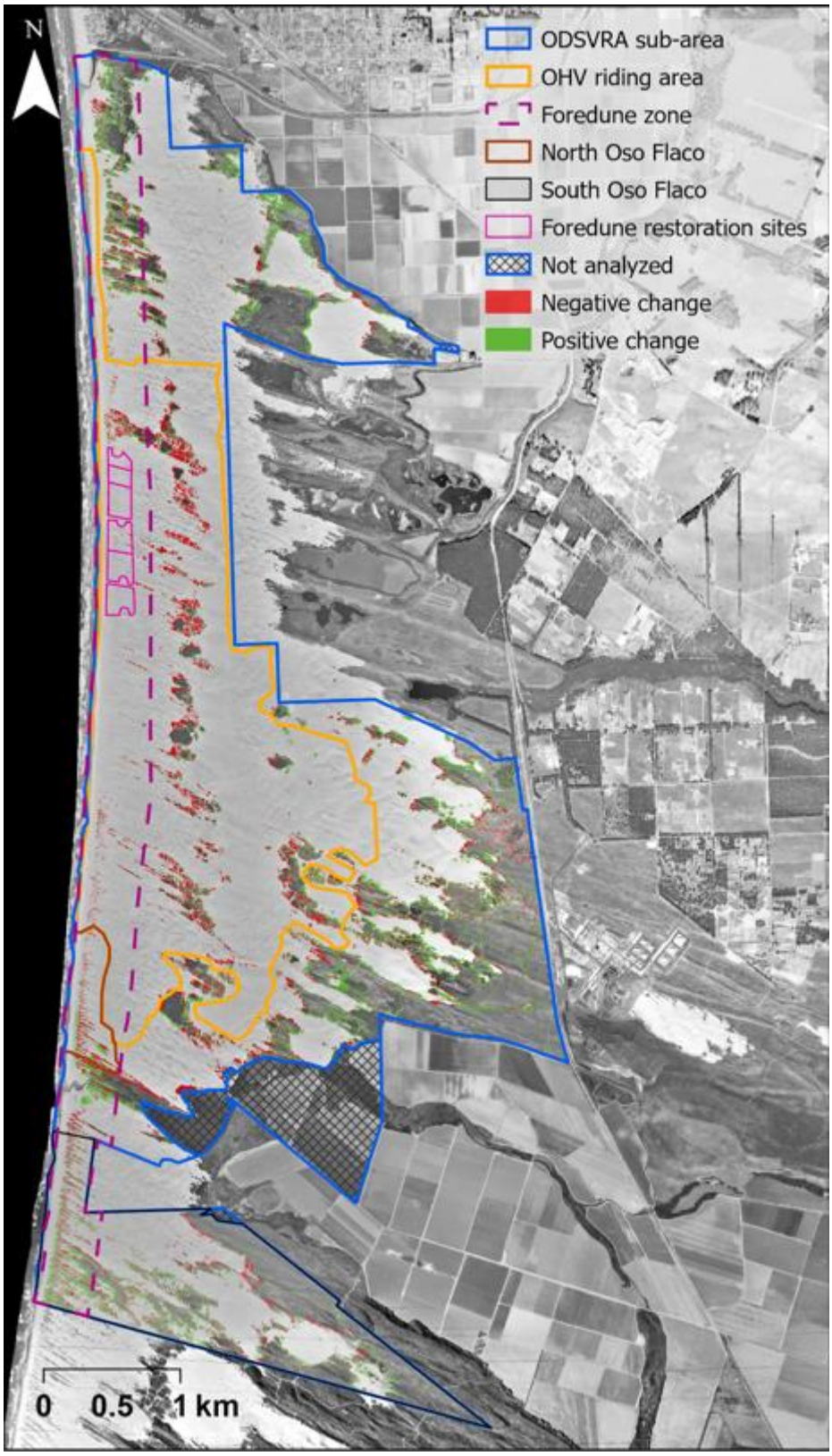

Figure S27. Vegetation change analysis results between 1978 and 1985. Positive change is in green, negative change is in red. Background orthophoto is from 1978.

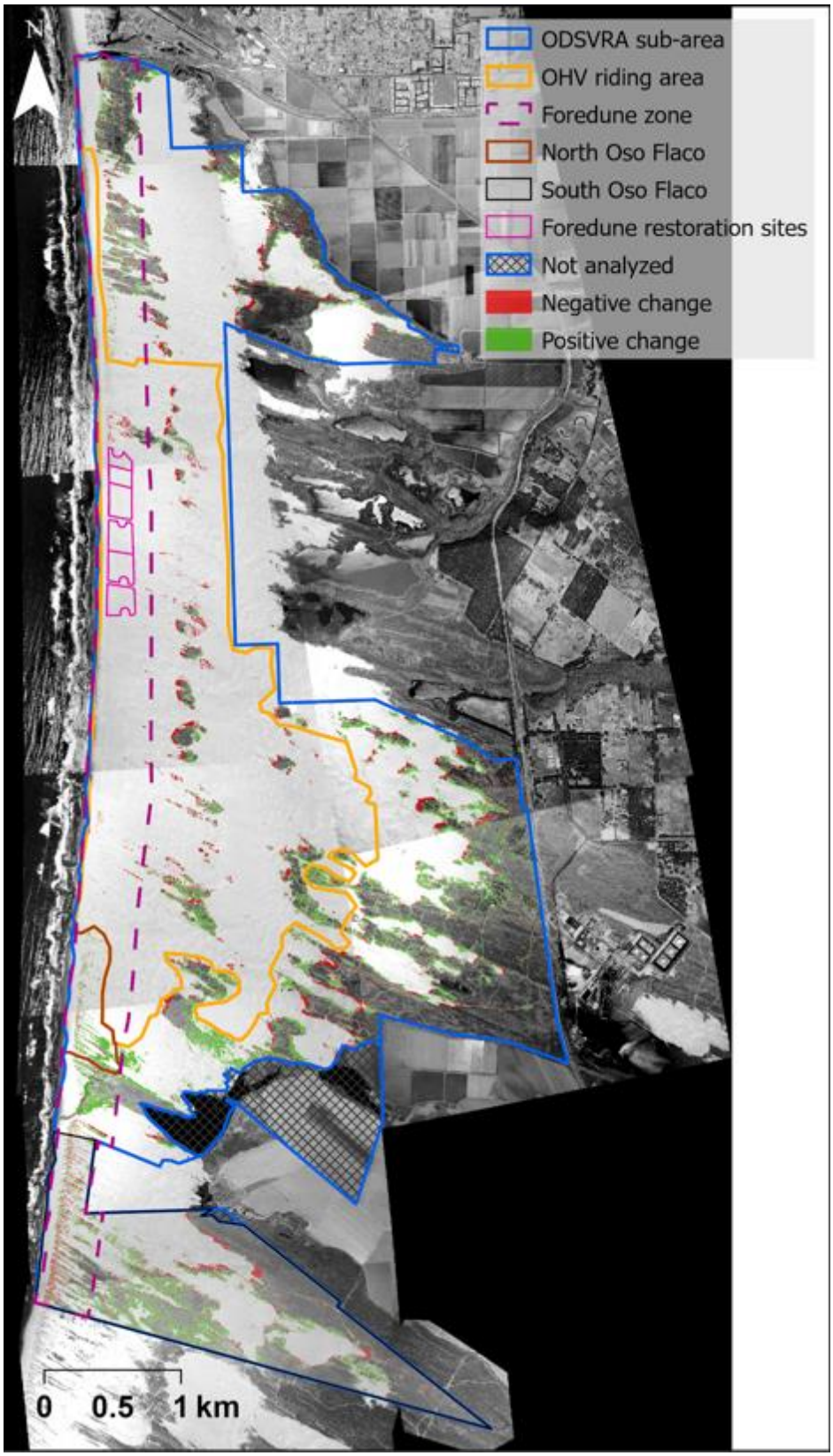

Figure S28. Vegetation change analysis results between 1985 and 1994. Positive change is in green, negative change is in red. Background orthophoto is from 1985.

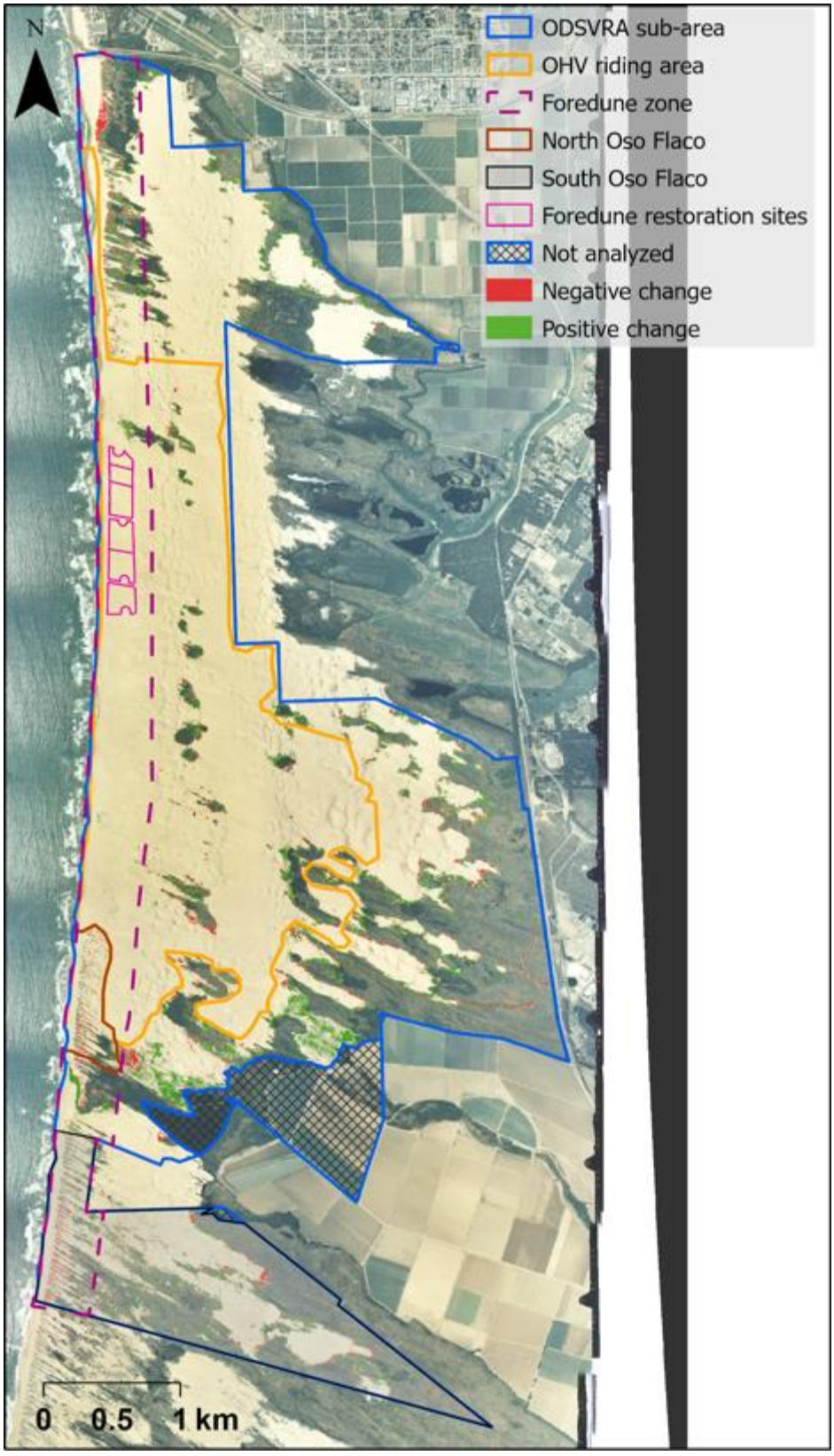

Figure S29. Vegetation change analysis results between 1994 and 1998. Positive change is in green, negative change is in red. Background orthophoto is from 1994.

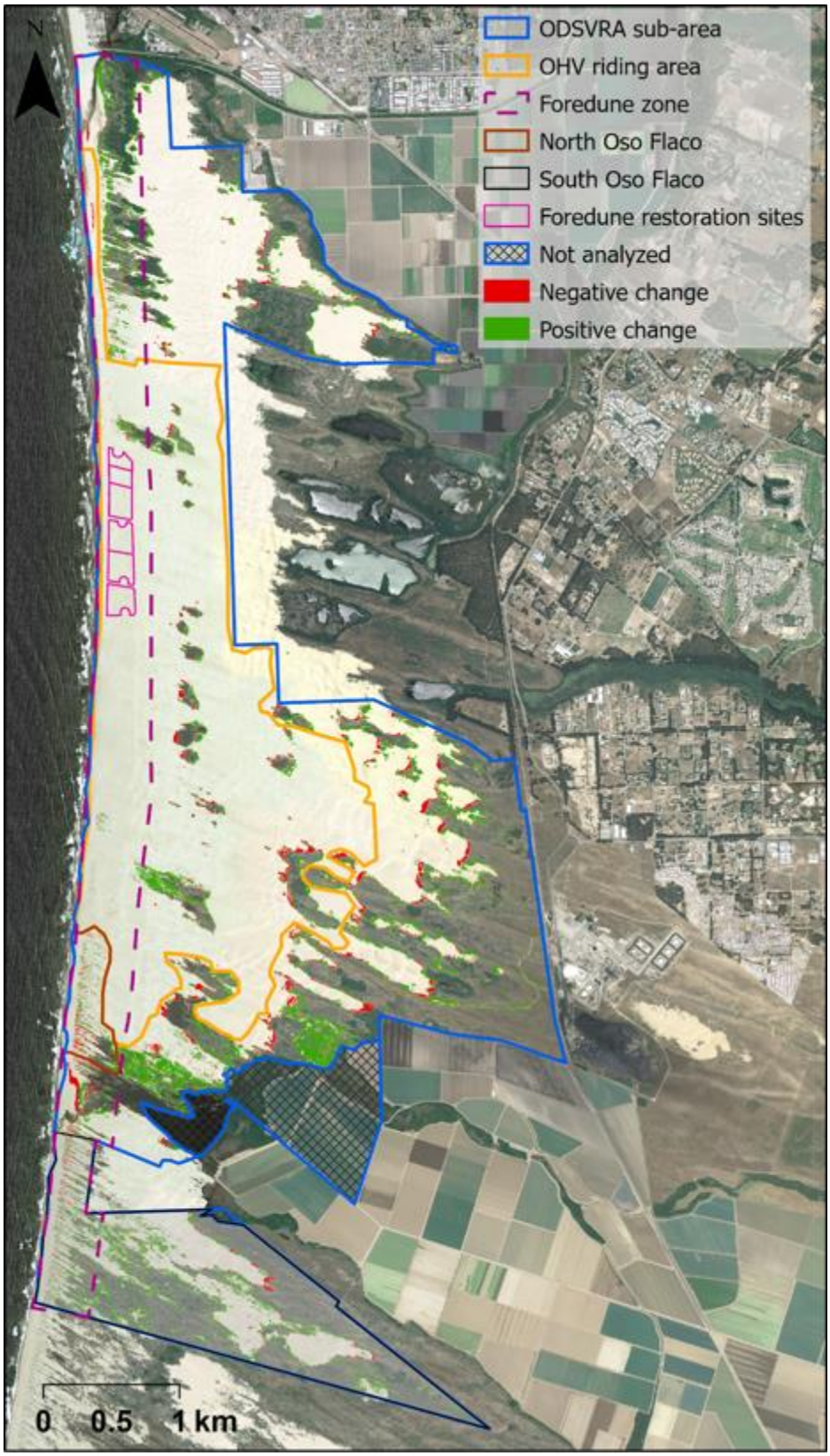

Figure S30. Vegetation change analysis results between 1998 and 2005. Positive change is in green, negative change is in red. Background orthophoto is from 1998.

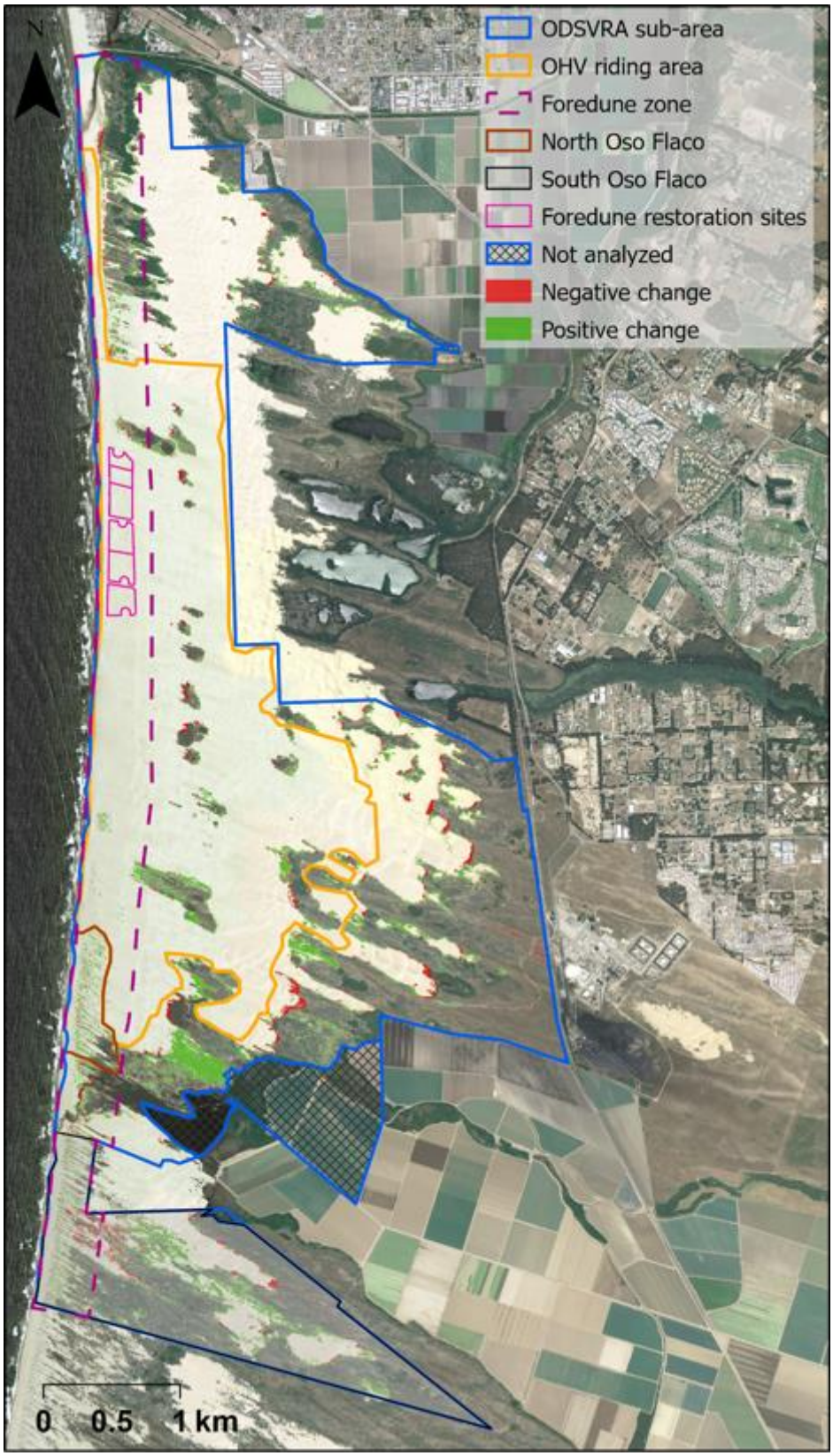

Figure S31. Vegetation change analysis results between 2005 and 2012. Positive change is in green, negative change is in red. Background orthophoto is from 2005.

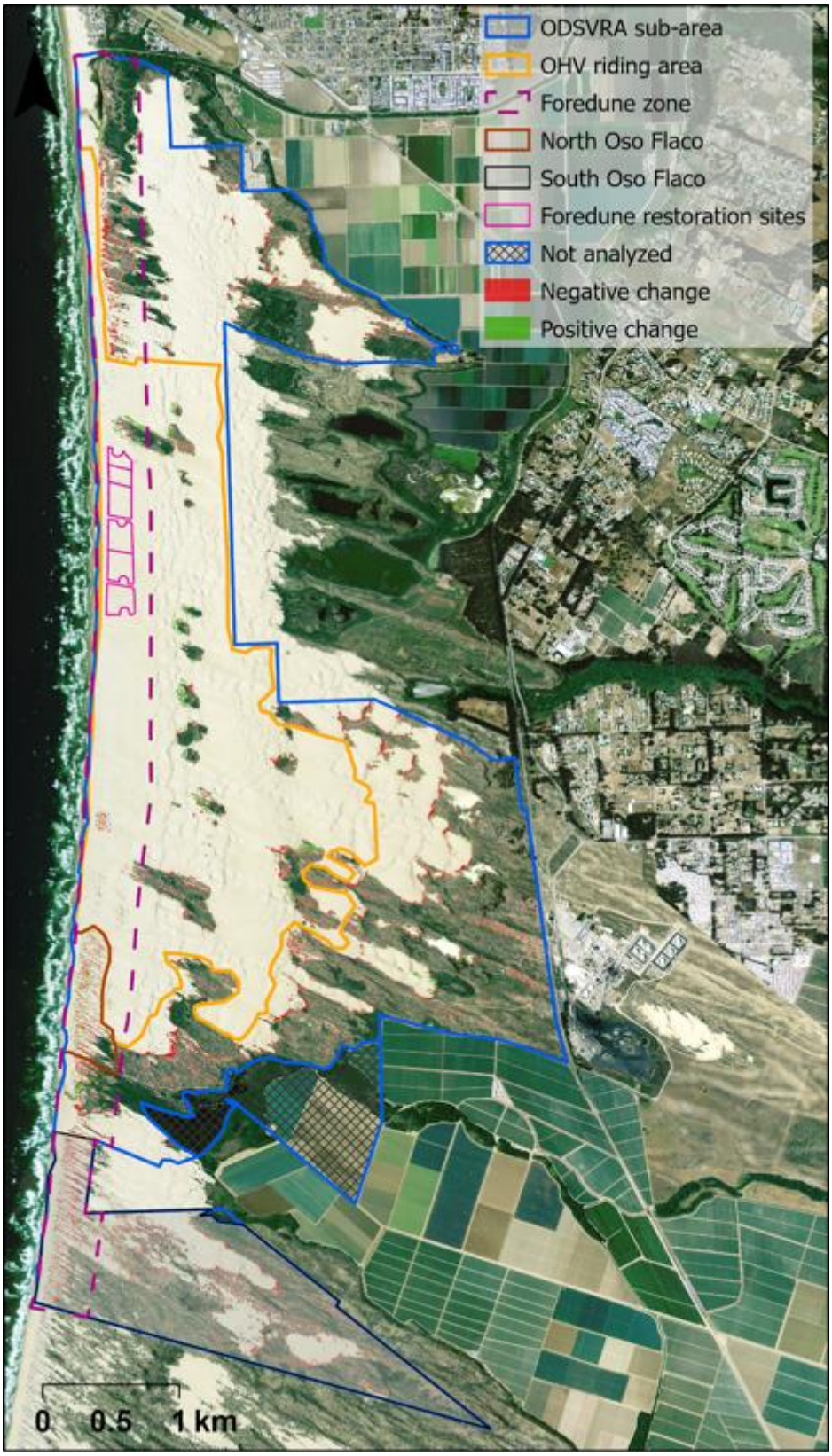

Figure S32. Vegetation change analysis results between 2012 and 2014. Positive change is in green, negative change is in red. Background orthophoto is from 2012.

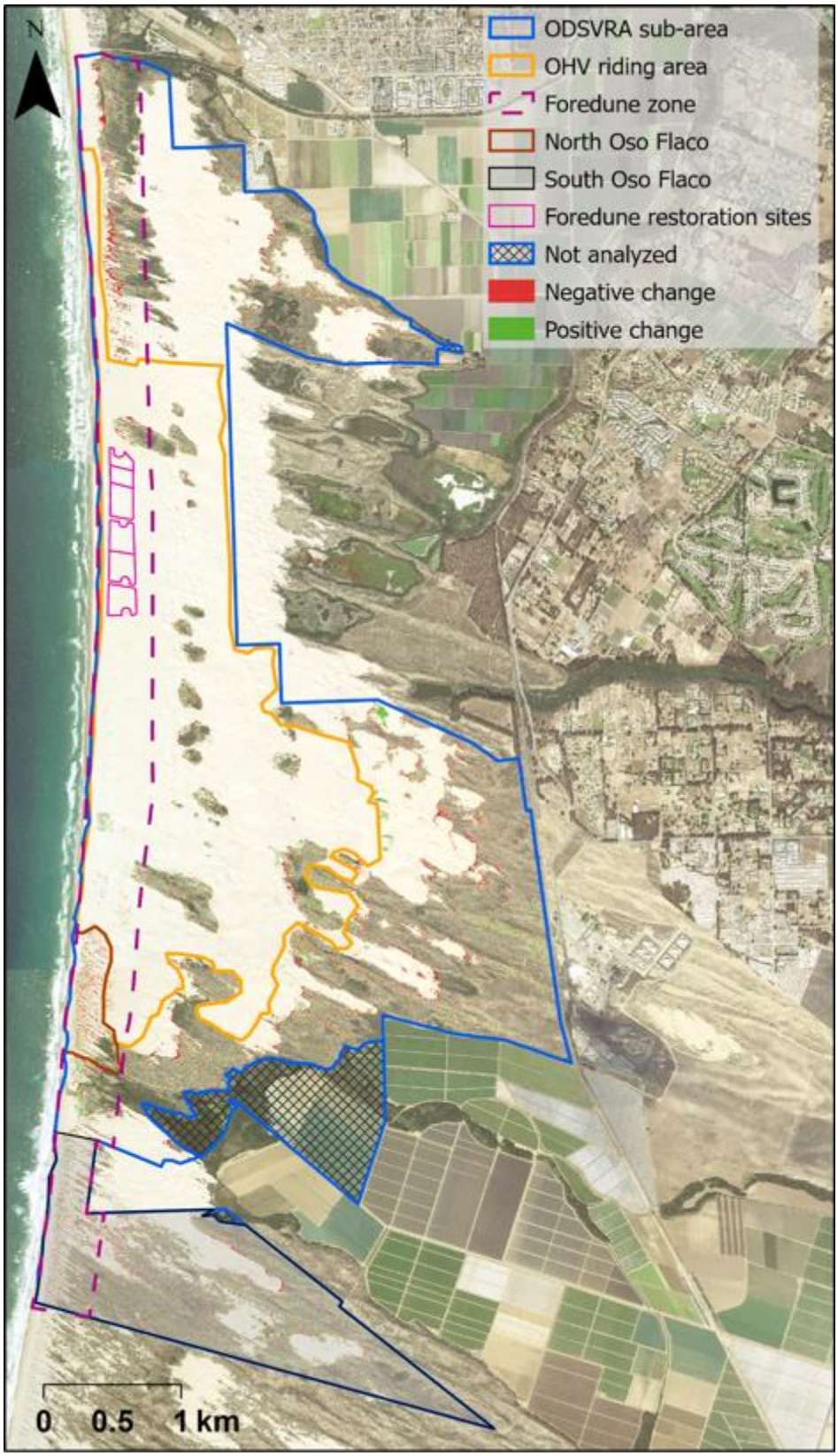

Figure S33. Vegetation change analysis results between 2014 and 2016. Positive change is in green, negative change is in red. Background orthophoto is from 2014.

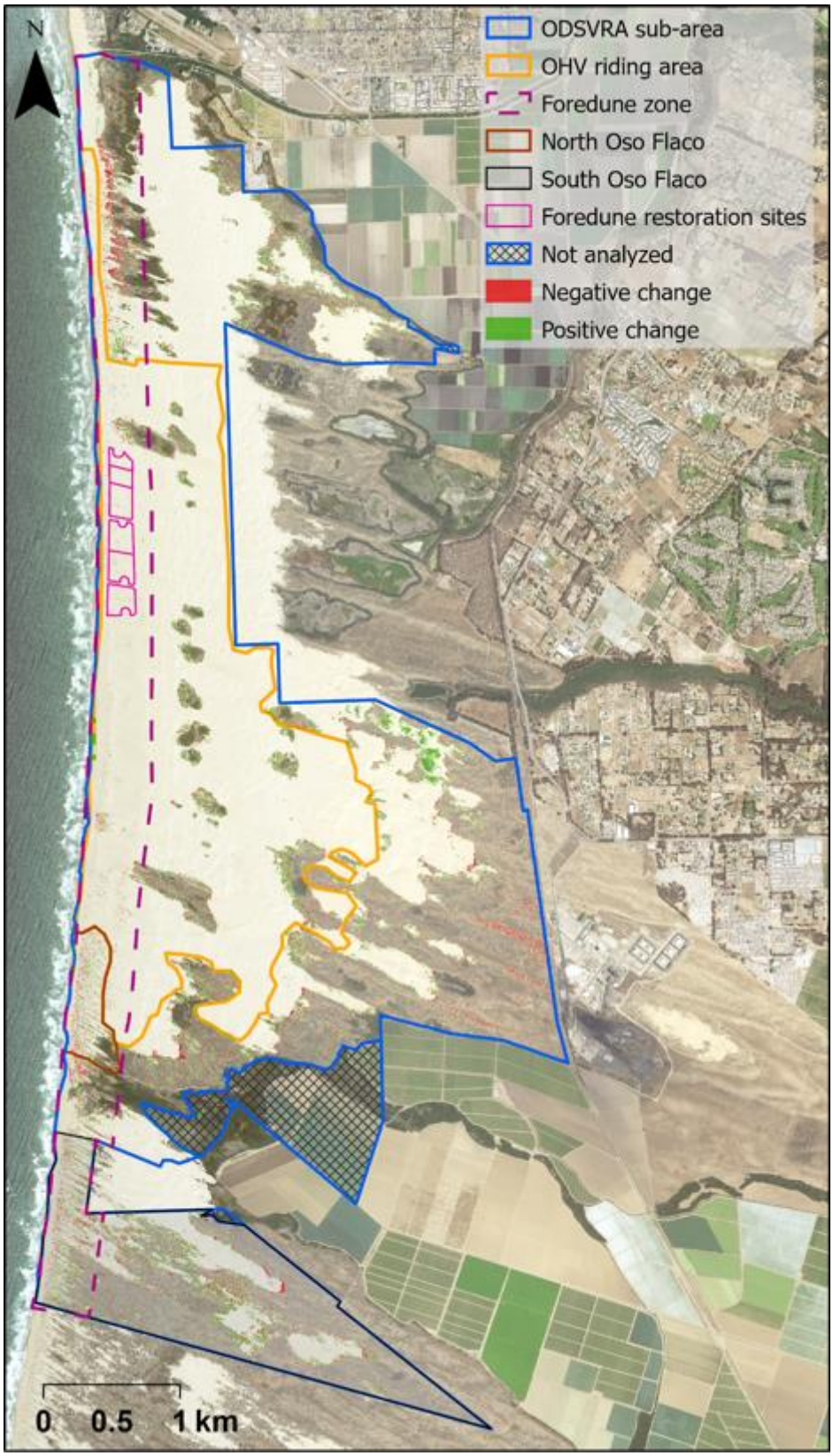

Figure S34. Vegetation change analysis results between 2016 and 2018. Positive change is in green, negative change is in red. Background orthophoto is from 2016.

Figure S35. Vegetation change analysis results between 2018 and 2020. Positive change is in green, negative change is in red. Background orthophoto is from 2018.

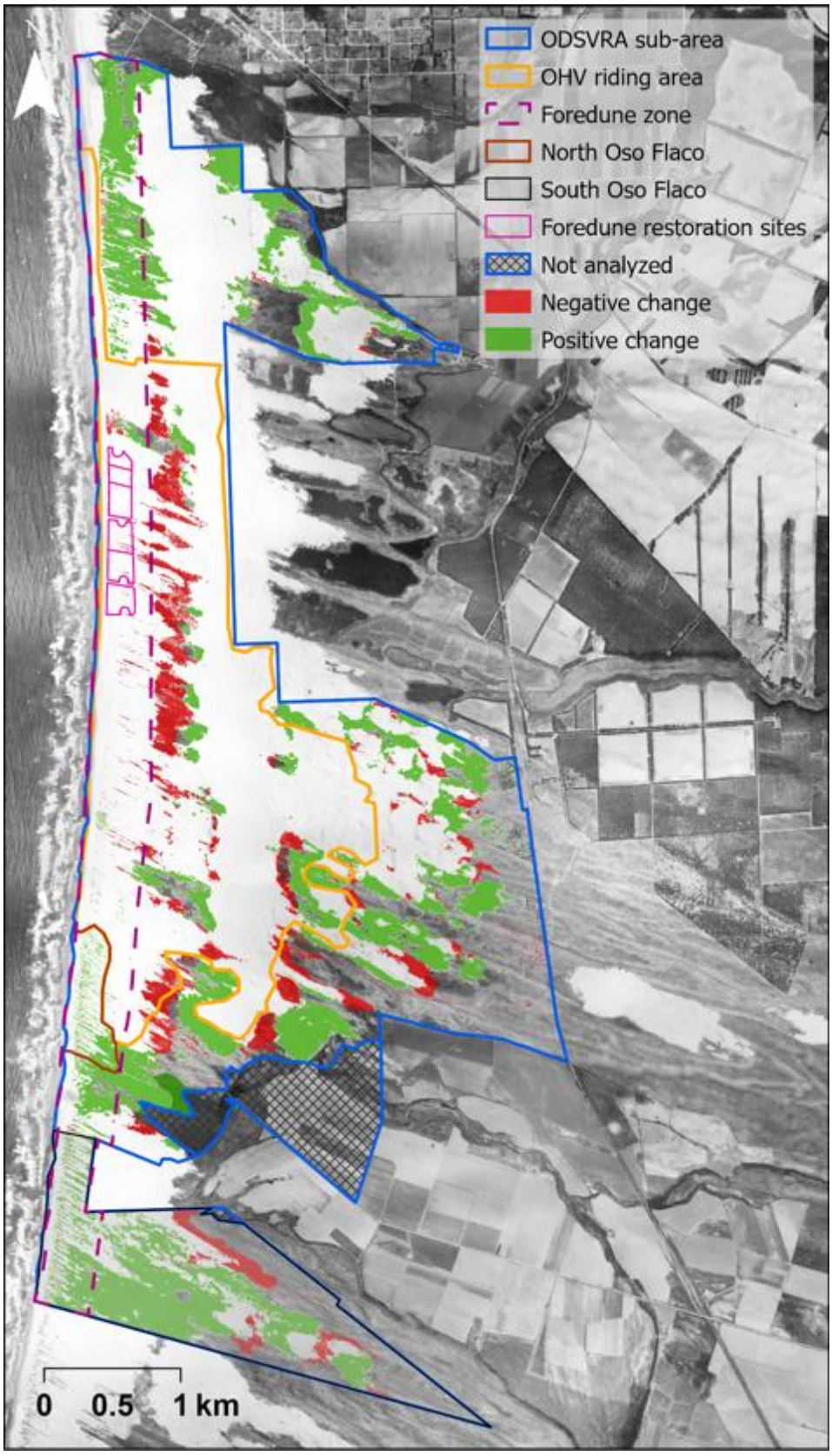

Figure S36. Change in vegetation between 1939 and 2012. Orthophoto from 1939.

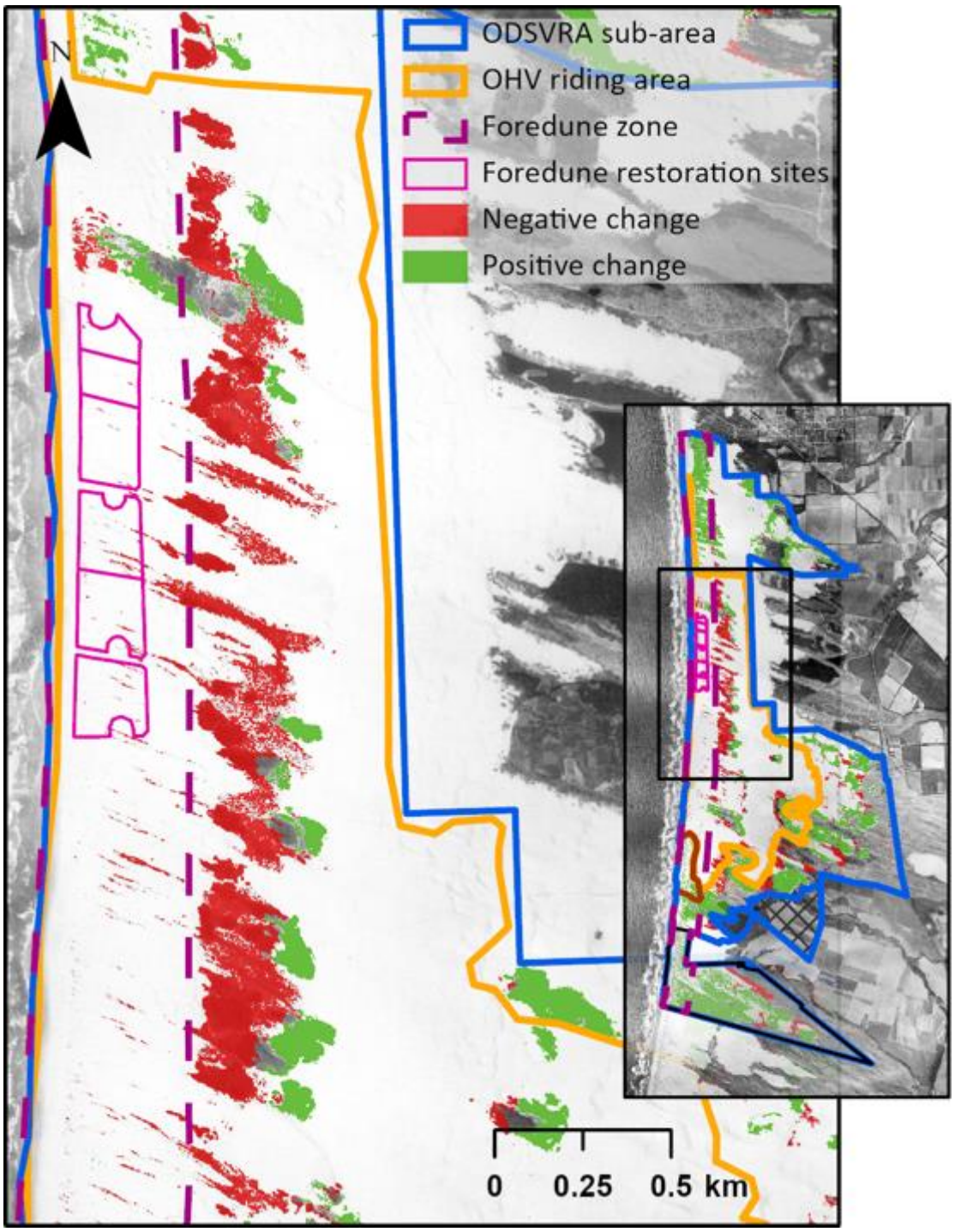

Figure S37. Close-up image of the change in vegetation cover around the foredune restoration sites between 1939 and 2012. Orthophoto from 1939.

Table S1. Calculated land cover values for vegetation areas from each image year, in the ODSVRA sub-area, OHV riding area, non riding area (ODSVRA sub-area minus the OHV riding area), and the Oso Flaco area. The vegetation cover (%) was calculated for the total area of each analytical zone and for the vegetation within the foredune zone (400 m from the shoreline) (see boundaries in Figures 1). The

area values are presented as km² (acres) and percentage values were calculated in relation to the different analytical zones. Asterisk (*) represents a lack of image cover and thus is calculated for smaller areas (see Table 2 and Figures S3, S8 and S10).

		ODSVRA sub-area	OHV riding area	Non-riding area	South Oso Flaco	Backdune South Oso Flaco	North Oso Flaco	Foredune ODSVRA	Foredune OHV riding area	Foredune South Oso Flaco	Plover nesting encloser	Foredune restoration sites
	Area analyzed km² (acres)	4215.03	1584.07	2630.96	577.29	465.73	68.56	961.90	453.23	111.56	311.42	94.96
1930*	Vegetation cover km² (acres)	3.43 (848)*	0.51 (125)*	2.93 (722)*	0.86 (212)	0.84 (207)	0.002 (0.5)	0.07 (16)*	0.03 (8)*	0.02 (6)	0.10 (26)	N/A
	% to analytical zone	N/A	N/A	N/A	36.79	44.41	0.69	N/A	N/A	4.96	10.34	N/A
1939	Vegetation cover km² (acres)	4.27 (1056)	0.70 (173)	3.57 (883)	0.84 (207)	0.83 (204)	0.003 (1)	0.13 (32)	0.05 (12)	0.01 (3)	0.08 (20)	0.003 (1)
	% to analytical zone	25.05	10.92	33.55	35.80	43.82	0.95	3.33	2.68	2.32	8.10	0.71
1949	Vegetation cover km² (acres)	4.05 (1001)	0.71 (157)	3.34 (826)	0.80 (197)	0.78 (192)	0.004 (1)	0.23 (57)	0.08 (19)	0.02 (5)	0.06 (15)	0.01 (2)
	% to analytical zone	23.75	11.07	31.38	34.16	41.31	1.49	5.88	4.13	4.34	6.06	1.67
1956	Vegetation cover km² (acres)	4.28 (1058)	0.74 (184)	3.54 (875)	0.81 (201)	0.78 (194)	0.01 (3)	0.33(82)	0.07 (16)	0.03 (7)	0.05 (12)	0.004 (1)
	% to analytical zone	25.11	11.59	33.24	34.82	41.55	3.96	8.49	3.61	6.71	5.09	0.96
1966	Vegetation cover km² (acres)	4.54 (1122)	0.79 (196)	3.75 (927)	0.86 (214)	0.79 (195)	0.03 (7)	0.45 (111)	0.10 (24)	0.08 (19)	0.06 (15)	0.005 (1)
	% to analytical zone	26.63	12.36	12.36	37.00	41.79	10.72	11.56	5.27	16.99	6.17	1.38
1971*	Vegetation cover km2 (acres)	4.23 (1045)*	0.63 (155)	3.60 (891)*	0.82 (203)*	0.82 (203)*	0.02 (6)	0.37 (90)*	0.08 (19)	N/A	0.04 (11)	0.01 (1)
	% to analytical zone	24.80	9.75	33.86	35.11	43.52	8.10	N/A	4.16	N/A	4.36	1.42
1978	Vegetation cover km² (acres)	4.04 (997)	0.45 (111)	3.59 (886)	0.86 (213)	0.79 (196)	0.02 (6)	0.40 (99)	0.04 (11)	0.07 (17)	0.02 (5)	0.001 (0.3)
	% to analytical zone	23.66	7.02	33.68	36.92	42.02	8.09	10.24	2.38	15.63	2.24	0.28
1985	Vegetation cover km² (acres)	4.18 (1032)	0.27 (67)	3.91 (965)	0.95 (235)	0.86 (211)	0.02 (4)	0.45 (110)	0.02 (4)	0.10 (24)	0.01 (2)	<0.001 (0.01)
	% to analytical zone	24.49	4.21	36.69	40.76	45.37	5.54	11.44	0.97	21.52	0.77	0.01
1994	Vegetation cover km² (acres)	4.62 (1141)	0.26 (65)	4.35 (1076)	1.09 (270)	0.99 (224)	0.04 (11)	0.50 (125)	0.01 (2)	0.11 (26)	0.002 (1)	<0.001 (0.01)
	% to analytical zone	27.13	4.13	41.03	47.59	53.48	15.37	12.97	0.54	23.51	0.24	0.01
1998	Vegetation cover km² (acres)	5.08 (1256)	0.30 (75)	4.78 (1180)	1.17 (288)	1.05 (260)	0.04 (10)	0.54 (133)	0.02 (4)	0.11 (28)	0.003 (1)	0.002 (0.4)
	% to analytical zone	29.85	4.74	45.03	50.71	57.07	14.62	13.86	0.88	24.70	0.33	0.47
2005	Vegetation cover km² (acres)	5.78 (1428)	0.36 (88)	5.42 (1339)	1.38 (340)	1.22 (302)	0.05 (11)	0.70 (173)	0.02 (6)	0.15 (38)	0.001 (0.3)	0.00 (0)
	% to analytical zone	33.95	5.57	51.09	59.90	66.25	16.64	18.01	1.30	33.92	0.13	0.00
2010	Vegetation cover km² (acres)	5.72 (1413)	0.39 (97)	5.33 (1316)	1.26 (310)	1.14 (283)	0.05 (13)	0.70 (172)	0.04 (9)	0.11 (28)	0.01 (1.38)	<0.001 (0.01)
	% to analytical zone	33.59	6.09	50.20	54.62	61.93	19.07	17.91	2.00	24.70	0.57	0.01

		ODSVRA sub-area	OHV riding area	Non-riding area	South Oso Flaco	Backdune South Oso Flaco	North Oso Flaco	Foredune ODSVRA	Foredune OHV riding area	Foredune South Oso Flaco	Plover nesting enclosure	Foredune restoration sites
	Area analyzed km^2 (acres)	4215.03	1584.07	2630.96	577.29	465.73	68.56	961.90	453.23	111.56	311.42	94.96
2012	Vegetation cover km2 (acres)	6.35 (1569)	0.44 (109)	5.91 (1460)	1.51 (373)	1.35 (332)	0.07 (17)	0.81 (200)	0.04 (9)	0.01 (3)	0.01 (3)	0.00 (0)
	% to analytical zone	37.31	6.91	55.68	65.66	72.85	24.41	20.76	2.09	36.24	1.07	0.00
2014	Vegetation cover km^2 (acres)	5.97 (1474)	0.43 (105)	5.45 (1369)	1.41 (346)	1.27 (313)	0.06 (15)	0.69 (170)	0.04 (10)	0.006 (2)	0.07 (17)	<0.001 (0.01)
	% to analytical zone	35.05	6.65	52.21	61.48	68.62	21.87	17.69	2.24	32.27	0.65	0.01
2016	Vegetation cover km^2 (acres)	6.15 (1520)	0.44 (109)	5.71 (1411)	1.43 (352)	1.29 (318)	0.05 (14)	0.70 (173)	0.04 (10)	0.14 (34)	0.01 (3)	0.00 (0)
	% to analytical zone	36.15	6.89	53.83	62.02	69.67	20.00	17.99	2.24	30.76	1.07	0.00
2018	Vegetation cover km^2 (acres)	6.14 (1516)	0.49 (121)	5.65 (1395)	1.47 (363)	1.32 (327)	0.06 (15)	0.68 (168)	0.04 (10)	0.14 (36)	0.007 (2)	<0.001 (0.01)
	% to analytical zone	36.05	7.63	53.22	63.88	71.69	21.46	17.46	2.21	31.95	0.68	0.01
2020	Vegetation cover km^2 (acres)	6.01 (1486)	0.52 (128)	5.49 (1358)	1.46 (360)	1.33 (330)	0.05 (13)	0.64 (157)	0.04 (11)	0.12 (30)	0.01 (2)	<0.001 (<0.01)
	% to analytical zone	35.32	8.07	51.79	63.32	72.24	19.05	16.36	2.35	26.83	0.99	0.00

Table S2. Calculated Absolute change (%) and change per year (% yr^{-1}) in vegetation areas between photo years, *in the ODSVRA sub-area, OHV riding area, and the North and South Oso Flaco areas. The positive and* negative change percentages are the percentage of pixels that *gained or lost vegetation from the previous year, respectively,* and were divided by the number of years between the images.

The total change is the cumulative change rate (positive + negative). Net change (positive - negative) represents the trend in change between the image year. *Asterisk (*) represents a lack of image cover and thus is calculated for smaller areas (see Table 2).*

Absolute change (%)																
	ODSVRA sub-area				OHV riding area				South Oso Flaco				North Oso Flaco			
	Positive change	Negative change	Total change	Net change	Positive change	Negative change	Total change	Net change	Positive change	Negative change	Total change	Net change	Positive change	Negative change	Total change	Net change
1930-1939*	N/A	N/A	N/A	N/A	N/A	N/A	N/A	N/A	2.49%	3.49%	5.98%	-1.00%	0.79%	0.53%	1.31%	0.26%
1939-1949	2.95%	4.23%	7.18%	-1.28%	3.31%	3.16%	6.47%	0.15%	1.93%	3.58%	5.51%	-1.65%	1.32%	0.78%	2.10%	0.54%
1949-1956	4.31%	2.94%	7.25%	1.36%	2.58%	2.06%	4.64%	0.51%	3.39%	2.73%	6.12%	0.66%	3.30%	0.84%	4.14%	2.47%
1956-1966	5.88%	3.95%	9.83%	1.93%	3.57%	2.77%	6.34%	0.79%	7.87%	5.63%	13.49%	2.24%	8.71%	1.66%	10.37%	7.04%
1966-1971*	3.77%	5.51%	9.28%	-1.74%	1.95%	4.65%	6.60%	-2.69%	6.30%	4.05%	10.35%	2.25%	6.91%	9.43%	16.34%	-2.52%
1971-1978*	3.30%	5.02%	8.32%	-1.72%	1.27%	4.01%	5.28%	-2.74%	5.30%	7.58%	12.88%	-2.28%	5.43%	5.37%	10.80%	0.06%
1978-1985	5.10%	4.25%	9.35%	0.85%	1.10%	3.90%	5.00%	-2.81%	9.38%	5.52%	14.90%	3.86%	4.31%	6.82%	11.13%	-2.50%
1985-1994	5.86%	2.83%	8.68%	3.03%	1.46%	1.66%	3.13%	-0.20%	11.84%	4.40%	16.24%	7.44%	12.90%	2.01%	14.91%	10.89%
1994-1998	4.21%	1.82%	6.03%	2.39%	1.15%	0.51%	1.66%	0.64%	6.29%	3.46%	9.75%	2.83%	4.53%	5.35%	9.88%	-0.83%
1998-2005	5.69%	1.61%	7.29%	4.08%	1.54%	0.68%	2.22%	0.86%	10.91%	1.81%	12.72%	9.11%	6.99%	4.79%	11.78%	2.20%
2005-2012	5.07%	1.49%	6.55%	3.58%	1.84%	0.46%	2.30%	1.37%	9.83%	3.13%	12.96%	6.70%	12.43%	2.30%	14.72%	10.13%
2012-2014	1.30%	3.71%	5.01%	-2.42%	0.81%	1.08%	1.89%	-0.26%	2.18%	7.34%	9.53%	-5.16%	5.29%	9.62%	14.91%	-4.32%
2014-2016	2.51%	2.54%	5.05%	-0.03%	1.03%	0.79%	1.82%	0.25%	5.34%	4.77%	10.11%	0.56%	5.80%	7.84%	13.64%	-2.04%
2016-2018	5.78%	2.11%	7.90%	3.67%	1.51%	0.68%	2.19%	0.84%	5.91%	4.07%	9.99%	1.84%	7.23%	4.93%	12.15%	2.30%
2018-2020	1.46%	1.01%	2.47%	0.45%	1.46%	1.01%	2.47%	0.45%	4.28%	4.84%	9.12%	-0.56%	4.31%	6.93%	11.23%	-2.62%
1939-1985	8.75%	9.32%	18.07%	-0.57%	2.48%	9.19%	11.67%	-6.72%	13.71%	8.75%	22.46%	4.96%	5.29%	0.70%	5.98%	4.59%
1985-2012	15.04%	1.95%	16.99%	13.09%	4.20%	1.42%	5.63%	2.78%	28.14%	3.53%	31.67%	24.60%	23.47%	2.58%	26.05%	20.89%
2012-2020	4.12%	4.33%	8.45%	-0.22%	2.23%	1.03%	3.26%	1.20%	4.42%	7.72%	12.14%	-3.30%	3.57%	11.03%	14.60%	-7.45%
1939-2012	19.02%	6.51%	25.53%	12.51%	4.62%	8.77%	13.39%	-4.15%	36.54%	6.65%	43.19%	29.89%	26.56%	0.59%	27.15%	25.97%
1939-2020	17.78%	7.00%	24.78%	10.78%	5.30%	8.24%	13.54%	-2.93%	34.39%	7.65%	42.05%	26.74%	20.64%	0.70%	21.34%	19.94%

Change per year (%yr^{-1})																
	ODSVRA sub-area				OHV riding area				South Oso Flaco				North Oso Flaco			
	Positive change	Negative change	Total change	Net change	Positive change	Negative change	Total change	Net change	Positive change	Negative change	Total change	Net change	Positive change	Negative change	Total change	Net change
1930-1939*	N/A	N/A	N/A	N/A	N/A	N/A	N/A	N/A	0.28%	0.39%	0.66%	-0.11%	0.09%	0.06%	0.15%	0.03%
1939-1949	0.29%	0.42%	0.72%	-0.13%	0.33%	0.32%	0.65%	0.01%	0.19%	0.36%	0.55%	-0.16%	0.13%	0.08%	0.21%	0.05%
1949-1956	0.62%	0.42%	1.04%	0.19%	0.37%	0.29%	0.66%	0.07%	0.48%	0.39%	0.87%	0.09%	0.47%	0.12%	0.59%	0.35%
1956-1966	0.59%	0.39%	0.98%	0.19%	0.36%	0.28%	0.63%	0.08%	0.79%	0.56%	1.35%	0.22%	0.87%	0.17%	1.04%	0.70%
1966-1971*	0.75%	1.10%	1.86%	-0.35%	0.39%	0.93%	1.32%	-0.54%	1.26%	0.81%	2.07%	0.45%	1.38%	1.89%	3.27%	-0.50%
1971-1978*	0.47%	0.72%	1.19%	-0.25%	0.18%	0.57%	0.75%	-0.39%	0.76%	1.08%	1.84%	-0.33%	0.78%	0.77%	1.54%	0.01%
1978-1985	0.73%	0.61%	1.34%	0.12%	0.16%	0.56%	0.71%	-0.40%	1.34%	0.79%	2.13%	0.55%	0.62%	0.97%	1.59%	-0.36%
1985-1994	0.65%	0.31%	0.96%	0.34%	0.16%	0.18%	0.35%	-0.02%	1.32%	0.49%	1.80%	0.83%	1.43%	0.22%	1.66%	1.21%
1994-1998	0.47%	0.20%	0.67%	0.27%	0.13%	0.06%	0.18%	0.07%	0.70%	0.38%	1.08%	0.31%	0.50%	0.59%	1.10%	-0.09%
1998-2005	0.63%	0.18%	0.81%	0.45%	0.17%	0.08%	0.25%	0.10%	1.21%	0.20%	1.41%	1.01%	0.78%	0.53%	1.31%	0.24%
2005-2012	0.72%	0.21%	0.94%	0.51%	0.26%	0.07%	0.33%	0.20%	1.40%	0.45%	1.85%	0.96%	1.78%	0.33%	2.10%	1.45%
2012-2014	0.65%	1.86%	2.50%	-1.21%	0.41%	0.54%	0.95%	-0.13%	1.09%	3.67%	4.76%	-2.58%	2.65%	4.81%	7.46%	-2.16%
2014-2016	1.26%	1.27%	2.53%	-0.01%	0.52%	0.39%	0.91%	0.12%	2.67%	2.39%	5.06%	0.28%	2.90%	3.92%	6.82%	-1.02%
2016-2018	2.89%	1.06%	3.95%	1.83%	0.76%	0.34%	1.10%	0.42%	2.96%	2.04%	4.99%	0.92%	3.61%	2.46%	6.08%	1.15%
2018-2020	0.73%	0.50%	1.24%	0.23%	0.73%	0.50%	1.24%	0.23%	2.14%	2.42%	4.56%	-0.28%	2.15%	3.46%	5.62%	-1.31%
1939-1985	0.19%	0.20%	0.39%	-0.01%	0.05%	0.20%	0.25%	-0.15%	0.30%	0.19%	0.49%	0.11%	0.11%	0.02%	0.13%	0.10%
1985-2012	0.56%	0.07%	0.63%	0.48%	0.16%	0.05%	0.21%	0.10%	1.04%	0.13%	1.17%	0.91%	0.87%	0.10%	0.96%	0.77%
2012-2020	0.51%	0.54%	1.06%	-0.03%	0.28%	0.13%	0.41%	0.15%	0.55%	0.96%	1.52%	-0.41%	0.45%	1.38%	1.82%	-0.93%
1939-2012	0.26%	0.09%	0.35%	0.17%	0.06%	0.12%	0.18%	-0.06%	0.50%	0.09%	0.59%	0.41%	0.36%	0.01%	0.37%	0.36%
1939-2020	0.22%	0.09%	0.31%	0.13%	0.07%	0.10%	0.17%	-0.04%	0.42%	0.09%	0.52%	0.33%	0.25%	0.01%	0.26%	0.25%

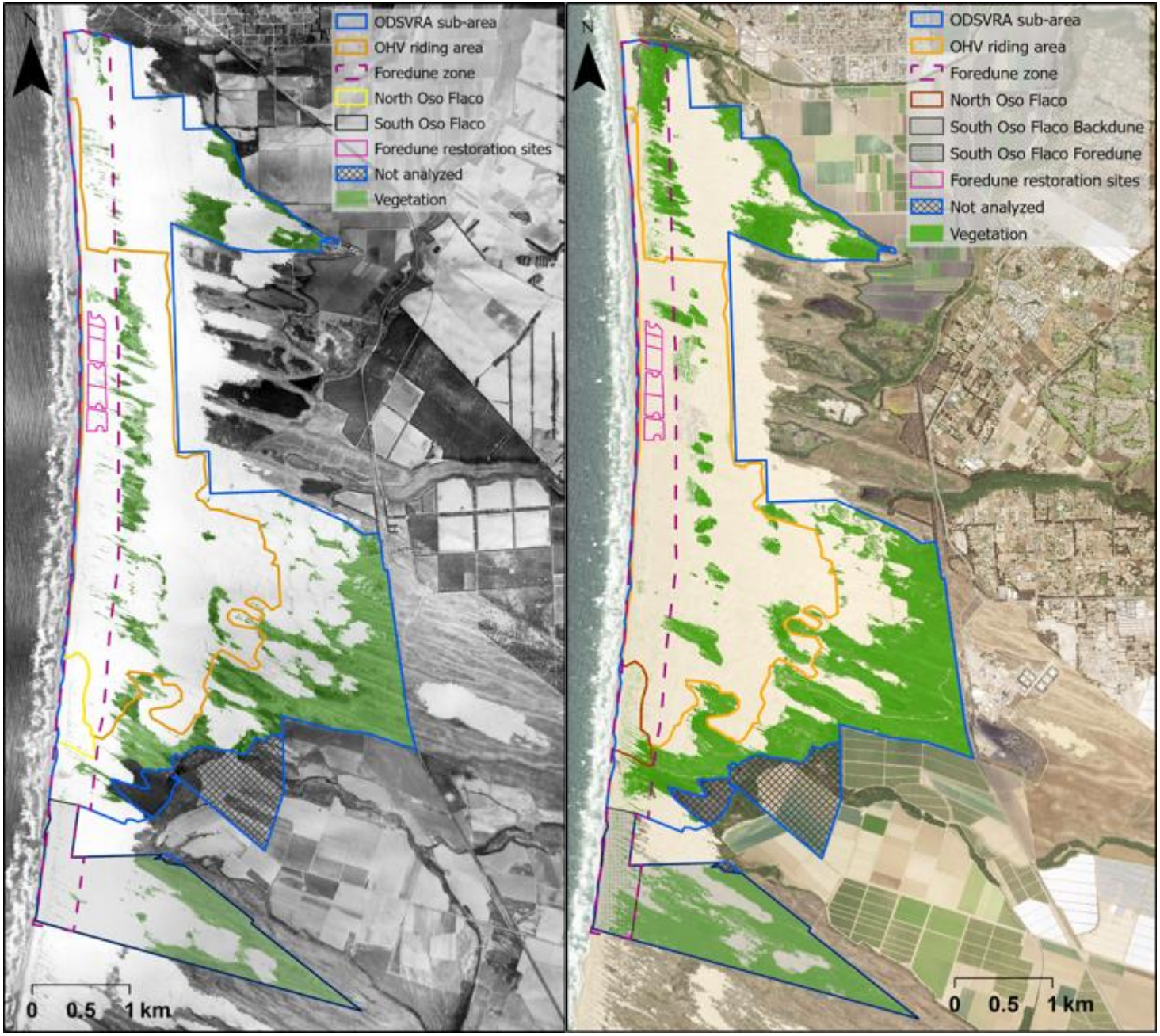

Figure S38. Vegetation cover comparison between 1939 (left) and 2020 (right) as presented in Figures S4 and S18.

ATTACHMENT 3

SAG (December 18, 2020). "Reevaluating the Stipulated Order of Abatement (SOA) Oceano Dunes PM10 dust mitigation target"

Reevaluating the Stipulated Order of Abatement (SOA) Oceano Dunes PM_{10} dust mitigation target
The Scientific Advisory Group (SAG)
December 18, 2020

This Stipulated Order of Abatement (SOA) requires that particulate matter reduction efforts undertaken at the Oceano Dunes State Vehicular Recreation Area (ODSVRA):

> 2b. "…be designed to achieve state and federal ambient PM_{10} air quality standards;" and
> 2c. "…[establish] an initial target of reducing the maximum 24-hour PM_{10} baseline emissions by fifty percent (50%), based on air quality modeling based on a modeling scenario for the period May 1 through August 31, 2013…"

SOA provision 2d allows that "[t]he estimate of emission reductions identified in 2c may be modified based on air quality modeling conducted by CARB or other modeling subject to the review of the SAG…."

The initial 50% emissions reduction target (SOA provision 2c) was developed by staff of the San Luis Obispo Air Pollution Control District (SLOAPCD) based on air quality monitoring downwind of the Oso Flaco section of the ODSVRA. Relative to the ODSVRA Riding Area, Oso Flaco experiences negligible disturbance from off-highway vehicles (OHVs). SLOAPCD staff found that the CDF air quality monitoring site, which is located downwind of the ODSVRA Riding Area, displayed a significantly higher frequency of exceedances of state and federal ambient PM_{10} air quality standards than the Oso Flaco monitoring station. SLOAPCD staff estimated that a 50% reduction in maximum 24-hour PM_{10} baseline emissions from the ODSVRA Riding Area would be required to achieve a similar frequency of PM_{10} exceedances at CDF as at Oso Flaco. Though such a 50% reduction target would not entirely eliminate exceedances of PM_{10} standards, it would achieve ambient PM_{10} concentrations similar to what would be expected for a naturally dusty undisturbed coastal dune environment.

The SAG supports the SLOAPCD's overall approach to establishing the SOA initial target for dust mitigation, but the SAG proposes the following changes to the specific methodology for defining the SOA target from estimates of ambient PM_{10} concentrations for undisturbed dune conditions:

1. Instead of using the Oso Flaco air quality monitoring site as the basis of comparison for the SOA target, make the comparison to the mass and/or concentration of PM_{10} dust produced under a "Pre-Disturbance Emissions Scenario" for the ODSVRA Riding Area itself. This Pre-Disturbance Emissions Scenario would be defined using existing information obtained between 2013 and 2019 about the known PM_{10} dust emissivity of representative undisturbed locations immediately adjacent to Riding Areas within the ODSVRA. Such undisturbed locations include the northern and southern Dunes Preserve areas and areas immediately to the east and south of the Riding Area. Based on geographical and particle size similarities, the PM_{10} emissivity in these Non-Riding Areas is assumed to be representative of conditions within the Riding Areas prior to disturbance by vehicles. In addition, the Pre-Disturbance Emissions Scenario would also incorporate known morphological characteristics of the ODSVRA prior to OHV disturbance, such as vegetated areas similar in size and position to those shown in old aerial photographs, which would be mapped onto the model emission surface and assigned zero emissivity. This method would allow simulation of pre- and post-disturbance PM_{10} emission conditions in the ODSVRA using known conditions from undisturbed active dune sites and knowledge of past land cover and landforms. In turn, this would eliminate concerns about the limited representativeness of the Oso Flaco site and related differences in wind, sediment, vegetation, and dust emission characteristics. The specific methodology for simulating the Pre-Disturbance Emissions Scenario has yet to be decided upon, but three methods have been developed and their relative merits are under discussion by the SAG in consultation with Parks and APCD staff.

2. As the basis for defining the new SOA target, use the Desert Research Institute (DRI) model to simulate ODSVRA Riding Area PM_{10} mass emissions and ambient PM_{10} concentrations for the Pre-Disturbance Emissions Scenario. Subject to further SAG discussions, such model results could then be used to set a new SOA target defined by: (1) ambient PM_{10} concentration at CDF and/or Mesa2; (2) spatially-averaged PM_{10} concentration for the full downwind catchment currently affected by ODSVRA Riding Area PM_{10} dust emissions; and/or (3) PM_{10} mass emissions, as per the approach of the existing SOA target. Options (1) and (2) represent a change from an emissions-based to a concentration-based SOA target. Option (3) retains a target based on a reduction in PM_{10} mass emissions. If this approach were chosen, then the existing SOA 50% mass emissions reduction target would be modified only if simulation of the Pre-Disturbance Emissions Scenario yielded a value that was statistically distinguishable from the existing target.

Preliminary analysis of PM_{10} dust emissivity collected during the 2013 PI-SWERL campaign supports this proposed approach. PI-SWERL measurements of PM_{10} dust emissivity are significantly lower for undisturbed ODSVRA Non-Riding Areas relative to equivalent disturbed ODSVRA Riding Areas. To affirm these findings, the SAG plans to extend this analysis to include data from additional PI-SWERL campaigns after 2013.

If Parks is supportive of this proposal to reevaluate the SOA target, these are the expected next steps:

(1) In consultation with the DRI modeling group, the SAG would prepare a detailed methodology for identifying the new SOA target. The SAG is already in agreement on the general approach, but specific methodological elements remain to be discussed.
(2) Based on the SAG's proposed methodology, the DRI modeling group would estimate the time and resources needed to undertake the proposed analysis. Preliminary discussions indicate that the proposed work is reasonably straightforward to perform, though a specific time estimate will depend on the final methodology agreed to by the SAG.
(3) If approved by Parks, DRI would carry out the proposed analysis. Then the SAG would review the model findings and potentially propose a modified SOA target as per provision 2d of the SOA.

ATTACHMENT 4

Gillies, J. A., Mejia, J., Furtak-Cole, E. (April 27, 2021). "Report to the SAG and Parks Evaluating the Potential for Developing a New Baseline Mass Emissions Rate and Target Reduction within the SOA"

Report to the SAG and Parks Evaluating the Potential for Developing a New Baseline Mass Emissions Rate and Target Reduction within the SOA

J.A Gillies, J. Mejia, and E. Furtak-Cole

The Science Advisory Group (SAG) requested, and California State Parks agreed, that DRI use available PI-SWERL emissivity data and the DRI emission/dispersion model to evaluate an alternative method to determine the target for mass emission reductions in the Stipulated Order of Abatement. The general approach to be evaluated is: what is the mass emissions from the ODSVRA for the 10 baseline days if the emissivity of the riding area was represented by the mean emissivity relationship for all non-riding areas? The assumption is that the mean non-riding area emissivity better represents the conditions for a non-OHV impacted dune system than is currently represented in the SOA that is based solely on PM_{10} and wind data air quality downwind of the Oso Flaco/southern dune preserve area. In the alternative method examined here, the mean emissivity of the non-riding area is assumed to be quantifiable based on the available PI-SWERL measurements made in the period 2013 to 2019 in areas where OHV activity was restricted. PI-SWERL tests made within the seasonal plover exclosure were excluded as this area has a period that allows OHV activity and period that excludes OHV activity.

The locations of PI-SWERL test areas that have occurred between 2013 and 2020 are shown in Fig. 1. The area within the red border in Fig. 1 is riding area and outside this border, non-riding. For the testing carried out at the ODSVRA the PI-SWERL was operated with a set sequence of target RPM values (2000, 3000, and 3500, named the "Hybrid 3500" test). For the Hybrid 3500 test, 60 s of clean air flush are followed by a linear "ramping" increase of the blade rotation from 0 RPM to 2000 RPM over the course of 60 s. The rotation rate of 2000 RPM is held constant for 60 s corresponding to the first constant RPM "step", followed by a ramping increase to 3000 RPM over 60 s. The second step at 3000 RPM is held for 90 s, followed by a 60 s ramp to 3500 RPM, which is also held for 90 s. Following this, power to the blade is cut and the cylindrical chamber is flushed with clean air for 60 s. Coordination of motor speed, air flow control, and data collection and logging from the dust monitor and control components is automated.

Each RPM step corresponds to constant shear stress, τ, values (or $\tau = \rho_{air}\, u_*^2$ where u_* is shear velocity, m s^{-1} and ρ_{air} is air density, kg m^{-3}). The RPM is converted to a u_* value using the relationship from Etyemezian et al. (2014):

$$u_* = C_1 \alpha^4 RPM^{C2/\alpha} \qquad (1)$$

where C1 is a constant (0.000683), C2 is a constant (0.832), and α, which has a value between 0.8 and 1 that varies with the surface roughness, and which was assumed equal to unity based on the surface roughness designation of smooth sand.

Dust emissions at each of the three steps where RPM is held constant are calculated by averaging the 1 s dust concentrations over the duration of the step and using:

$$E_i = \frac{(C_{DT,i} \times \frac{F_i}{60 \times 1000})}{A_{eff}} \qquad (2)$$

Figure 1. The Oceano Dunes and the ODSVRA, central coast California, USA, and the locations of the PI-SWERL tests carried out 2013-2020.

where E_i is the PM_{10} dust emissions in units of mg m^{-2} s^{-1} at the *i*th step, CDT,i is the average DustTrak PM_{10} in mg m^{-3}, F_i is the clean air flow rate (lpm) in (and out of) the PI-SWERL chamber, and A_{eff} is the effective area of the PI-SWERL annular blade (0.035 m^2 as recommended by Etyemezian et al., 2014).

From 2013 through to 2019, all or a portion of the measurement grid was revisited annually with the measurements typically completed in five days, weather permitting. The details of the sampling procedure through this time are provided in Mejia et al. (2019). A total of 2797 valid measurements of emissivity were available from riding areas and 1113 from non-riding areas between 2013 and 2019.

Each PI-SWERL Hybrid 3500 test results in three paired values of E and u_*, not all of which may pass a quality control screening.

Extensive quality control was conducted to ensure the integrity of the data collected with the PI SWERL. Collocations were conducted at the beginning, end, and every ten measurements, wherein both PI SWERL units were used in close proximity for three measurements. This allows field operators to diagnose problems in-situ and provides traceable measurements that can be used to quantify discrepancies between the instruments. Prior to averaging each of the three constant RPM Levels (2000, 3000, 3500), a median filter was run over the time series to remove noise from the PM_{10} sensor. For each measurement taken, visual quality control was conducted to flag any RPM levels with significant PM_{10} sensor or RPM sensor malfunction. This approach allows for individual RPMs to be removed in later analyses and serves as a check on values where the median filter may not have been sufficient to remove noise.

PI-SWERL Emissivity Data 2013-2019

The distribution of emissivity (E, mg m^{-2} s^{-1}) as a function of the three shear velocity (u_*, m s^{-1}) settings of the Hybrid 3500 test cycle of the PI-SWERL for the riding and non-riding areas of the ODSVRA amalgamated from 2013 to 2019 are shown in Figs. 2 and 3, respectively. For all the u_* set-points (i.e., u_* values corresponding to the three constant RPM values, 2000, 3000, 3500) the distribution of E for the seven years of data show skewed distributions (Figs. 2 and 3). As these data are skewed with a tail of high emissivity, a single factor Analysis of Variance (ANOVA) was used to determine if the distribution of E values for the same u_* were significantly different between the riding and non-riding areas. The results of these ANOVA tests are shown in Table 1. For each emissivity data pair for the same set-point u_* the non-riding area emissivity is statistically different from the riding area. This is based on the P values being less than 0.05 and the F values being greater than the F critical values. Also note is that the non-riding area E variances are at least one order of magnitude smaller than those from the riding area.

Table 1. ANOVA results comparing non-riding area emissivity distribution to riding area emissivity for data from 2013 to 2019.

Groups	u_* (m s^{-1})	Count	Sum E (mg m^{-2} s^{-1})	Mean E (mg m^{-2} s^{-1})	Variance	F	P-value	F crit
Non-Riding	0.38	372	11.158	0.030	0.001	75.299	1.2E-17	3.849
Riding	0.38	934	99.636	0.107	0.029			
Non-Riding	0.53	372	97.366	0.262	0.035	159.417	1.5E-34	3.849
Riding	0.53	934	677.750	0.726	0.488			
Non-Riding	0.61	369	97.366	0.262	0.035	114.573	1.1E-25	3.849
Riding	0.61	929	1326.372	1.428	1.321			

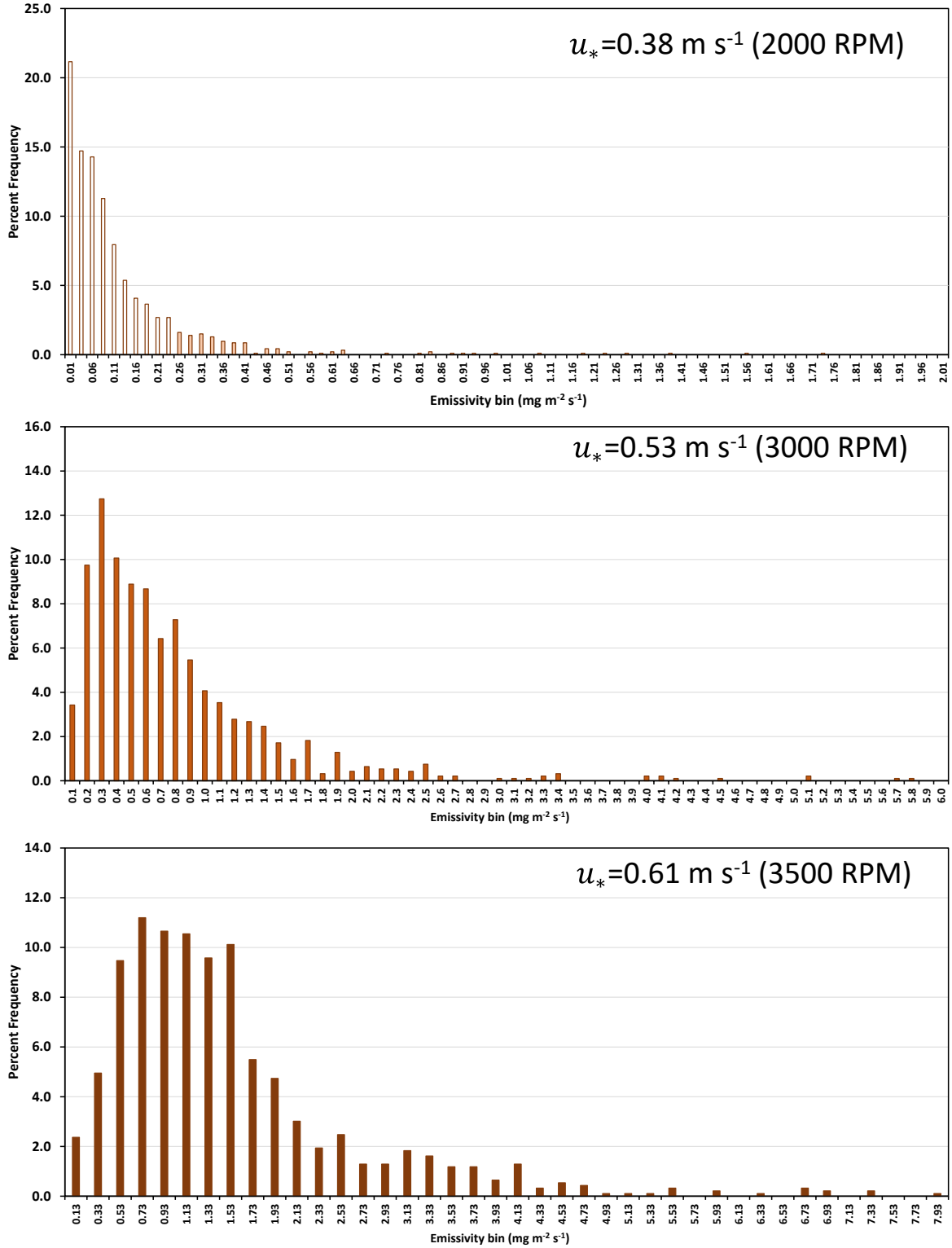

Figure 2. The distribution of emissivity (E, mg m^{-2} s^{-1}) as a function of the three shear velocity (u_*, m s^{-1}) settings for the riding areas of the ODSVRA amalgamated from 2013 to 2019.

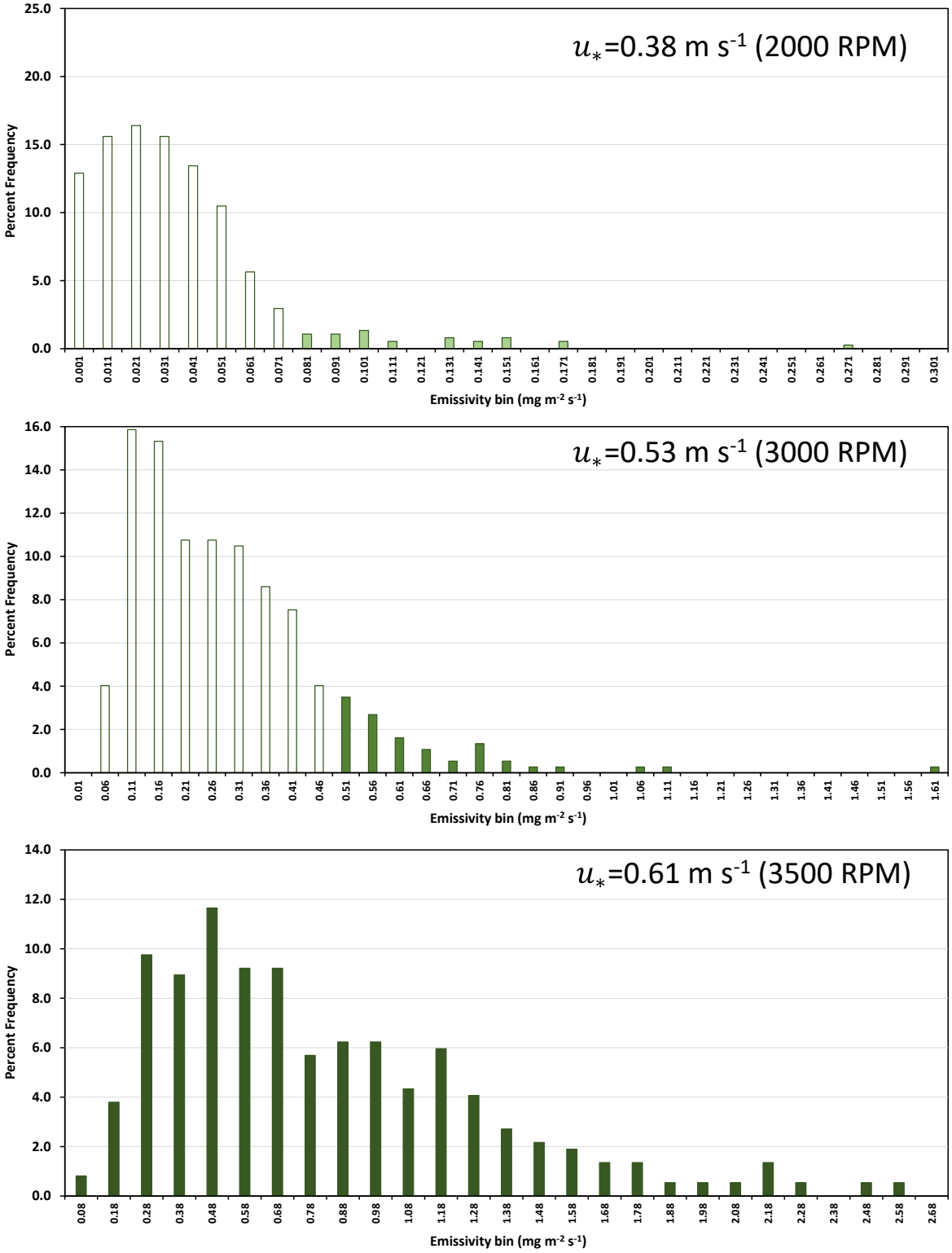

Figure 3. The distribution of emissivity (E, mg m^{-2} s^{-1}) as a function of the three shear velocity (u_*, m s^{-1}) settings for the non-riding areas of the ODSVRA amalgamated from 2013 to 2019.

Emissivity scales as a power function of u_* and the relation for the riding and non-riding area E data for 2013-2019 are shown in Fig. 4. The data represent the mean E at each of the u_* set points with the error bars representing the standard error of the estimate (i.e., standard deviation of the mean/(# observations-1)$^{0.5}$). The riding area, according to the PI-SWERL data, has greater emissivity than the non-riding area for equivalent values of u_*.

For evaluating the potential of the proposed alternative method to set a new baseline emissions target, the mean non-riding area emissivity relationship:

$$E\ (mg\ m^{-2}\ s^{-1}) = 21.51\ u_*^{6.85} \qquad (3)$$

was used to define the emissivity of the grid cells in the DRI emission/dispersion that are identified as being in the riding area (based on latitude/longitude and boundaries provided by California State Parks). All the non-riding area grid cells retained their emissivity relationships as defined by the 2013 PI-SWERL data and the associated extrapolation procedure. With the emissivity defined in each grid cell, the meteorology represented by the 10 established baseline days from 2013 was used to generate the wind shear (i.e., u_*) on each of the grid cells in the modeling domain.

The mass emissions rate expressed in tonnes of PM_{10} emitted in 24 hours for the ODSVRA based on the 2013 emissivity data and the mean non-riding emissivity relationship (Eq. 3) and the 10 baseline days of meteorology and the distribution of the emissions across space are shown in Fig. 5. The only masking done to identify zones of zero emissivity was for the vegetation islands that currently exist. The vegetation mask layer was received from Parks (T. Carmona, personal communication).

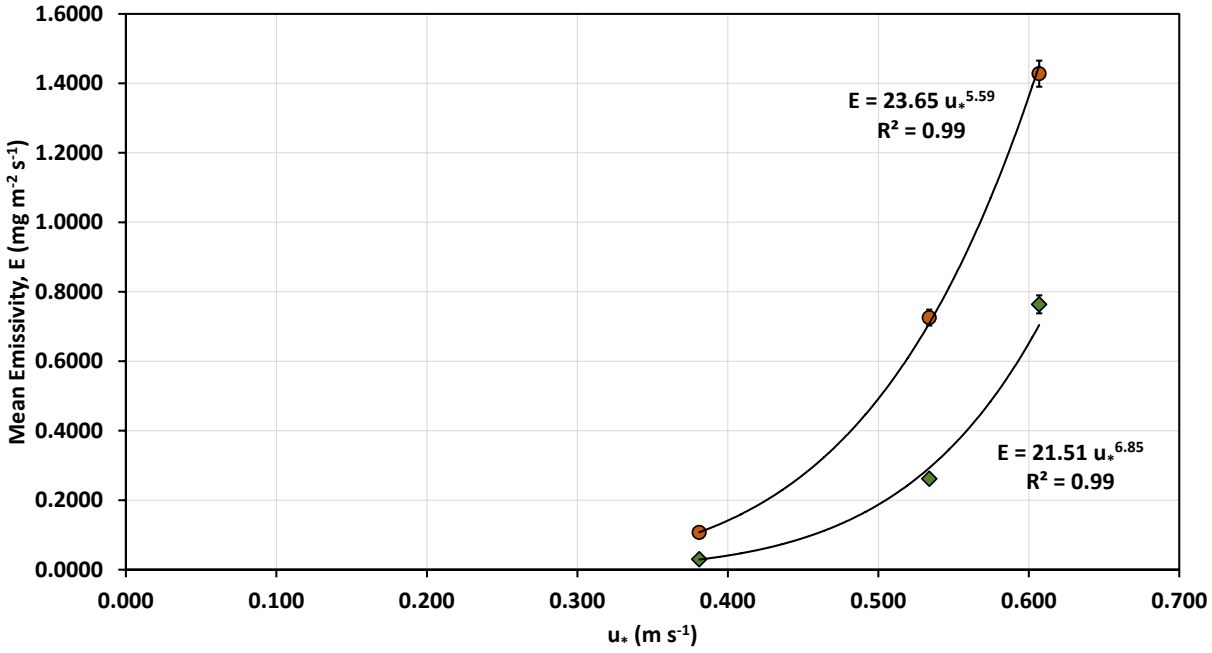

Figure 4. The relation between mean E (mg m^{-2} s^{-1}) and u_* (m s^{-1}) for the amalgamated data from 2013 to 2019 for the riding (orange circles) and non-riding areas (green diamonds). Error bars represent the standard error of the estimate (standard deviation/(#observations-1)$^{0.5}$).

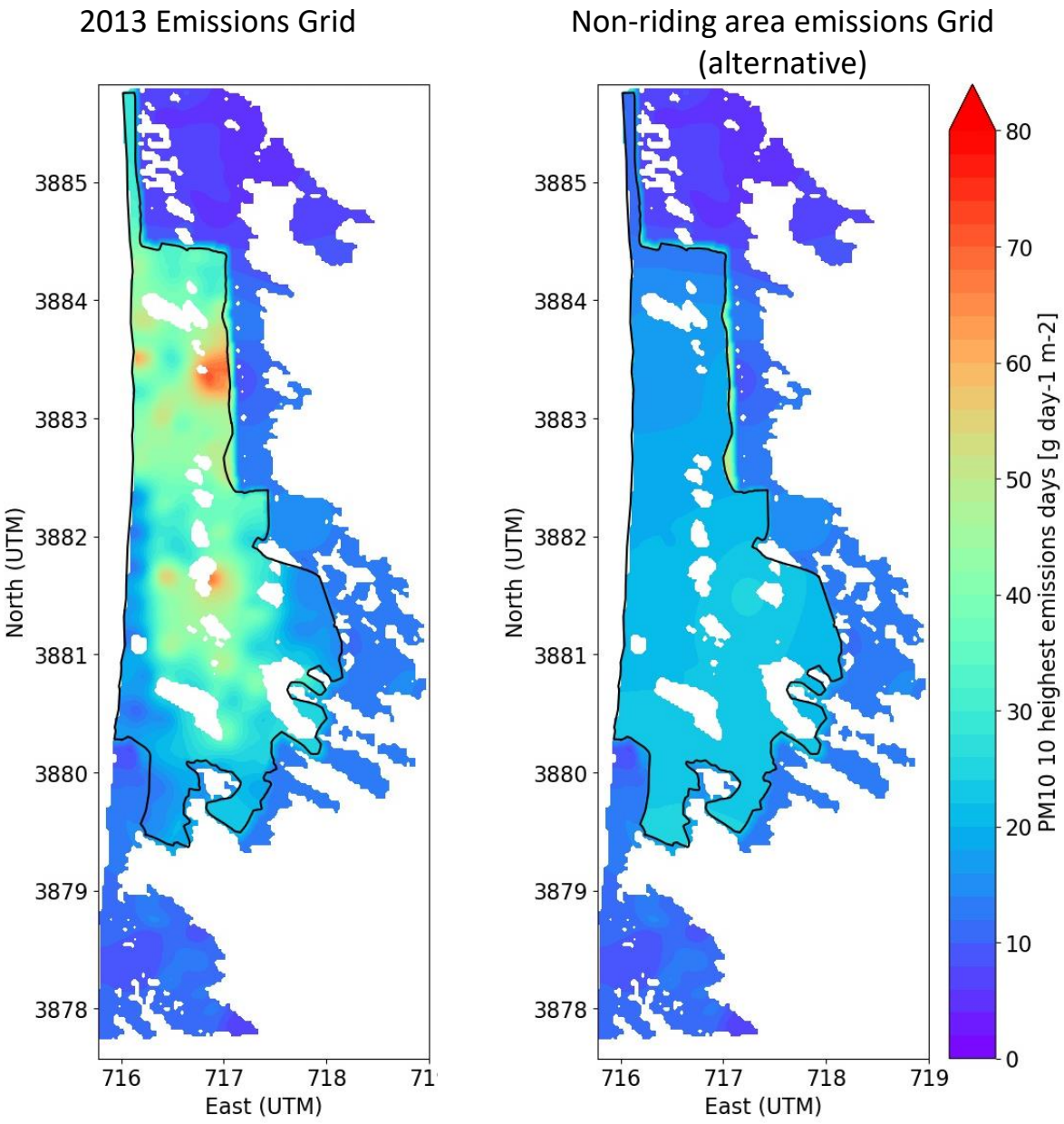

Figure 5. The mass emission maps for the 2013 emission grid based on 2013 PI-SWERL measurements and extrapolation (left panel) and for the alternative emission grid using Eq. 3 to define emissivity in the riding area (right panel). White areas represent the vegetation islands as they currently exist.

The mass emissions for the 2013 PI-SWERL emissions grid (Fig. 5, left panel) for the entire ODSVRA (riding+non-riding grid cells) is 263.1 tonnes/day and for the alternative emissions grid (Fig. 5, right panel) is 191.9 tonnes/day. The difference is 71.2 tonnes/day, which represents a percentage difference of 27.1% (lower) than the 2013 total mass emissions.

The current SOA, as implemented in the Particulate Matter Reduction Plan (PMRP) and Annual Reports and Work Plans (ARWPs), sets the reduction in mass emissions to be 50% less than the baseline for the riding area only, currently defined as 189.4 tonnes/day, making the current target 94.7 tonnes/day. The alternative approach target (118.2 tonnes/day [riding area only]) is 23.5 tonnes/day greater than the current target of 94.7 tonnes/day.

The alternative emission grid and the 10 baseline days of meteorology were also used to model the 24-hour mean PM_{10} concentrations at the two key receptor sites CDF and Mesa2. The pattern of PM_{10} concentrations across the modeling domain for the two emission grids are shown in Fig. 6. The lines defining the State 24-hour mean standard for PM_{10} of 50 µg m^{-3} and the Federal standard of 150 µg m^{-3} are defined in the maps by the black and gray lines, respectively.

The PM_{10} 24-hour mean concentrations for the 10 baseline days (measured and modeled) for the 2013 emission grid and the alternative emission grid for CDF and Mesa2 are shown in Table 2. For the meteorology of the 10 baseline days and the alternative grid, the modeled 24-hour mean PM_{10} concentrations for both measurement sites are still above the State standard of 50 µg m^{-3}.

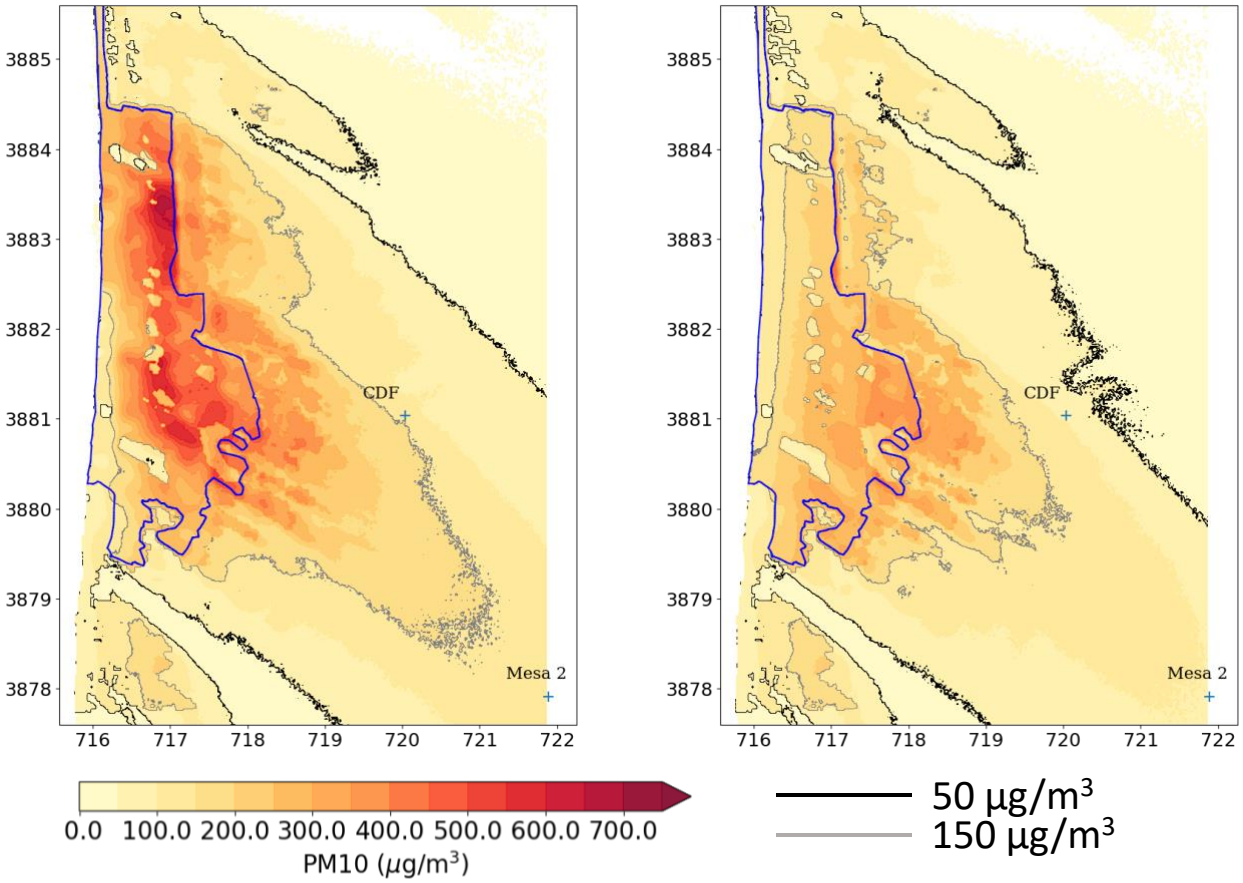

Figure 6. The modeled spatial distribution of PM_{10} using the DRI Lagrangian Particle Dispersion model, for the two emission grids. Left panel represents the 2013 emission grid and the right panel the mean non-riding alternative emission grid.

Table 2. Measured and modeled 24-hour mean PM_{10} at CDF and Mesa2 for the two emission grids for the 10 baseline days.

CDF	PM_{10} (μg m^{-3})	% Change (lower than observed)
Observed	128	
Modeled (2013 grid)	124	
Alternative grid	80	37.5
Mesa2		
Observed	95	
Modeled (2013 grid)	98	
Alternative grid	73	23.2

Implications of the Alternative Emission Grid with respect to Current and Projected Modeled Mass Emissions and PM_{10} Distribution with Dust Control Areas in Place

The results presented above reflect the emissivity for the ODSVRA based on the conditions of 2013 with the identified vegetation islands accounted for and no areas of dust control and for the alternative emission grid. These results can be compared with the most recent modeling of mass emissions and PM_{10} concentrations at key receptor sites CDF and Mesa2.

Table 3 shows the mass emission change scenarios for the current and alternative baseline and modeled effects of the acres of dust control in 2021. Considering only the riding area, modeling the effect on mass emissions assuming the dust controls as defined by Option 1 identified by Parks for 90 acres of additional dust controls for the 2020-21 ARWP, the total mass emissions for the 10 baseline days is 142.6 tonnes/day. This is 33% greater than the current 50% reduction target of 94.7 tonnes/day. For the alternate target mass emissions (118.2 tonnes/day), the modeled emissions from the riding area with Option 1 in place for 2021 (142.6 tonnes/day) is 17% greater.

In terms of PM_{10} concentrations at CDF and Mesa2 (Table 2) the modeled PM_{10} concentrations for CDF and Mesa2 are 80 μg m^{-3} and 72 μg m^{-3}, respectively, using the alternate emission grid. Under the high wind conditions of the 10, 2013 baseline days, an exceedance of the State Standard 24-hr mean PM_{10} is possible at both locations for the non-OHV impacted alternate emission grid.

In 2021 with 90 acres of dust control area as defined by Option 1 operating at 100% effectiveness (i.e., zero emissions), the modeled mean 24-hour PM_{10} for the 10 baseline days is 72 μg m^{-3} at CDF and Mesa2. The percentage difference between the PM_{10} concentrations for the alternate grid modeled values (i.e., CDF=80 μg m^{-3} and Mesa2=72 μg m^{-3}) and the Option 1 predictions (current emission grid, i.e., 2013, CDF=72 μg m^{-3} and Mesa2=72 μg m^{-3}) are 10% lower and equivalent for the concentrations at CDF and Mesa2, respectively. Under this model scenario, and given the uncertainties, the dust controls in place operating at 100% effectiveness, the mass emissions target and PM_{10} concentrations at CDF and Mesa2 computed using the alternate emission grid would be near compliance with an SOA based on the alternate emission grid. It needs to be noted, however, that assuming zero emissions from areas under dust control is not accurate and actual effectiveness will be less than 100%. The model predictions can be updated using more realistic control efficiencies.

Table 3. Mass emission change scenarios for the current and alternative baselines for 2020 and 2021 acres of dust control.

State of ODSVRA	Total Acres of Treatment	Total Mass Emissions Riding +Non-Riding area (tonnes/day)	Total Mass Emissions Riding area (tonnes/day)	50% Target Mass Emissions (Riding) (tonnes/day)	% Difference from Target
2013 (baseline)	0	263.5	189.4	94.7	
2020	224	213.9	155.3		39% (higher)
2021 (option 1 projected)	314	197.2	142.6		33% (higher)
				Alternate Target Mass Emissions (tonnes/day)	
2013 (alternate baseline)	0	191.9		118.2	
2020	224	213.9	155.3		24% (higher)
2021 (option 1 projected)	314	197.2	142.6		17% (higher)

Comments on the Scientific Justifications for the Alternative Approach for Establishing a New Baseline Mass Emissions in the SOA

Proposing a change to the SOA will demand a high degree of scientific justification to make the case to the Hearing Board and the APCD. We offer here some observations that support the case for proposing the change to this alternative method.

The North-South Gradient of Emissivity

There is strong evidence of a decrease in emissivity moving from north to south in the riding and non-riding areas of the ODSVRA. The mean emissivity relations for riding and non-riding areas (Fig. 4) can be disaggregated to examine for geographic influence on the emissivity across space. The emissivity data for the non-riding areas can be grouped as: northern dune preserve, areas east of the riding/non-riding boundary in the middle zone of the ODSVRA, and the southern dune preserve (Fig. 7). For each of the three zones an ANOVA test was done on the paired data for each set-point u_*. The ANOVA tests indicated that the mean emissivity values for each test u_* are significantly different between the geographic locations at the P=0.05 level, with the north having higher emissivity than the east and the south, and east higher than the south (Table 3).

The gradient of increasing emissivity towards the north in the non-riding area also is observed in the emissivity data for the riding area of the ODSVRA. This is demonstrated in Fig. 8, which shows the increase in mean emissivity as a function of latitude bins of 0.005 (decimal) degrees expressed as the increase in emissions when normalized to the southern-most measurement group for all available data (i.e., mean emissivity in latitude bin/mean emissivity in southern-most latitude bin) from 2013 to 2019.

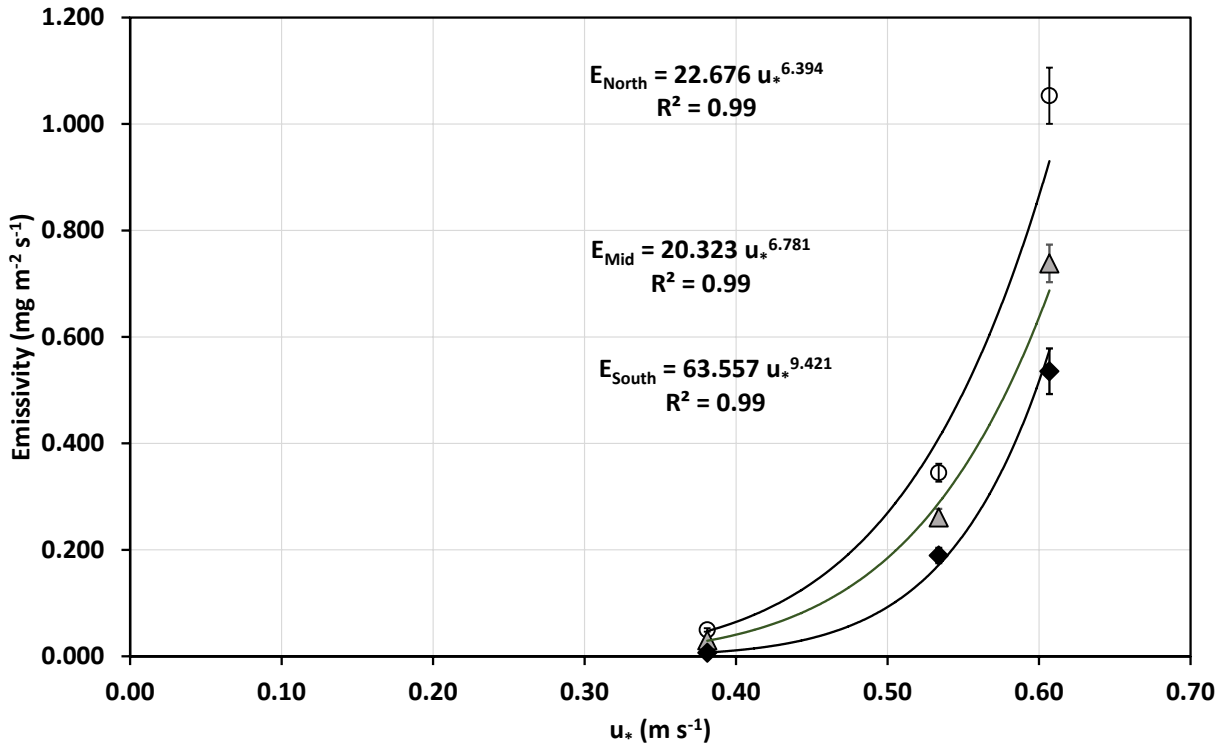

Figure 7. The relation between mean E (mg m^{-2} s^{-1}) and u_* (m s^{-1}) compared by geographic position for the non-riding areas: white circle, north; grey triangle, middle, black diamond, south. Error bars represent the standard error of the estimate (standard deviation/(#observations-1)$^{0.5}$).

Table 3. ANOVA testing, non-riding areas.

Groups	u_* (m s^{-1})	Test Count	Sum E (mg m^{-2} s^{-1})	Mean E (mg m^{-2} s^{-1})	Variance	F	P-value	F crit
North, Non-riding 2013-2019	0.381	101	5.016	0.050	0.001	24.472	1.32E-06	3.876
Middle, Non-riding 2013-2019	0.381	173	5.199	0.030	0.001			
North, Non-riding 2013-2019	0.534	101	34.850	0.345	0.029	26.672	4.68E-07	3.876
Middle, Non-riding 2013-2019	0.534	173	45.175	0.261	0.043			
North, Non-riding 2013-2019	0.607	101	106.368	1.053	0.279	26.672	4.68E-07	3.876
Middle, Non-riding 2013-2019	0.607	172	126.946	0.738	0.212			
Middle, Non-riding 2013-2019	0.381	173	5.199	0.030	0.001	39.260	1.66E-09	3.880
South, Non-riding 2013-2019	0.381	74	0.515	0.007	0.0001			
Middle, Non-riding 2013-2019	0.534	173	45.175	0.261	0.043	7.763	0.006	3.880
South, Non-riding 2013-2019	0.534	74	14.017	0.189	0.015			
Middle, Non-riding 2013-2019	0.607	172	126.946	0.738	0.212	11.173	0.001	3.880
South, Non-riding 2013-2019	0.607	73	39.088	0.535	0.132			
North, Non-riding 2013-2019	0.381	101	5.016	0.050	0.001	115.286	6.22E-21	3.896
South, Non-riding 2013-2019	0.381	74	0.515	0.007	0.0001			
North, Non-riding 2013-2019	0.534	101	34.850	0.345	0.029	45.528	2.18E-10	3.896
South, Non-riding 2013-2019	0.534	74	14.017	0.189	0.015			
North, Non-riding 2013-2019	0.607	101	106.368	1.053	0.279	52.182	1.57E-11	3.896
South, Non-riding 2013-2019	0.607	73	39.088	0.535	0.132			

This holds for each of the three test u_* values (Fig. 8). In each latitude bin for each test u_*, the emissivity represents the mean of all tests that fall within the bin.

As noted previously, the non-riding area PI-SWERL data (Fig. 7) indicate a north-south gradient of emissivity. Comparing emissivity between the riding and non-riding areas along a north-south gradient cannot be accomplished using a single increment of decimal degrees of latitude as the tests in the riding areas of the north and the south extend outside the latitude range of the riding area tests. To provide some indication of the difference between riding and non-riding emissivity north to south, the data are grouped into six latitudinal bins that pair the north and south non-riding area tests with a portion of the south and north riding area tests, respectively. Where there is latitudinal overlap among the riding and non-riding area tests, they are grouped in bins of 0.01 decimal degrees. The mean riding area emissivity normalized to the mean non-riding area in each latitudinal bin and for each u_* set point is shown in Fig. 9. In all cases, riding emissivity is greater than non-riding emissivity with the variability decreasing with increasing u_*. For the u_* set points of 0.53 and 0.61 m s^{-1} the ratio is approximately a factor of three for u_*=0.53 and a factor of two for u_*=0.61, with no strong signature of change as a function of latitude.

Within both riding and non-riding areas a north-south gradient of emissivity is observed, with higher emissivity in the north than in the south. In the riding area the gradient of emissivity is linear (Fig. 8), and this is likely due to the increase in mean grain size of the sand from north to south. In unpublished data, Gillies and Etyemezian (2014) reported that emissivity in the riding area of the ODSVRA, as measured with the PI-SWERL in 2013, increased with an increase in the proportion of the surface sand that was in the fine sand fraction (125-250 μm diameter). This north-south gradient of mean particle size is also present in the non-riding areas, and as Fig. 7 shows the non-riding areas also show a decrease in emissivity from north to south.

The argument could be made that the current method in the SOA neglects to account for these spatial characteristics of the dust emission system in the ODSVRA and over-emphasizes the importance of characterizing the non-OHV impacted dust emissions system as typified by the PM_{10} and wind conditions downwind of Oso Flaco/southern dune preserve. If the SAG and Parks agree to further evaluate this alternative approach to establishing a baseline mass emission rate, the alternative grid could be modified to create a north-south gradient of emissivity using the emissivity relationships presented in Fig. 7 and an agreed upon method that defines the application of a gradient.

Consideration should also be given to the vegetation and how it may have been distributed in pre-OHV impact times. The effect of vegetation cover on the total mass emissions and downwind PM_{10} can be modified in the model to reflect different amounts and distributions.

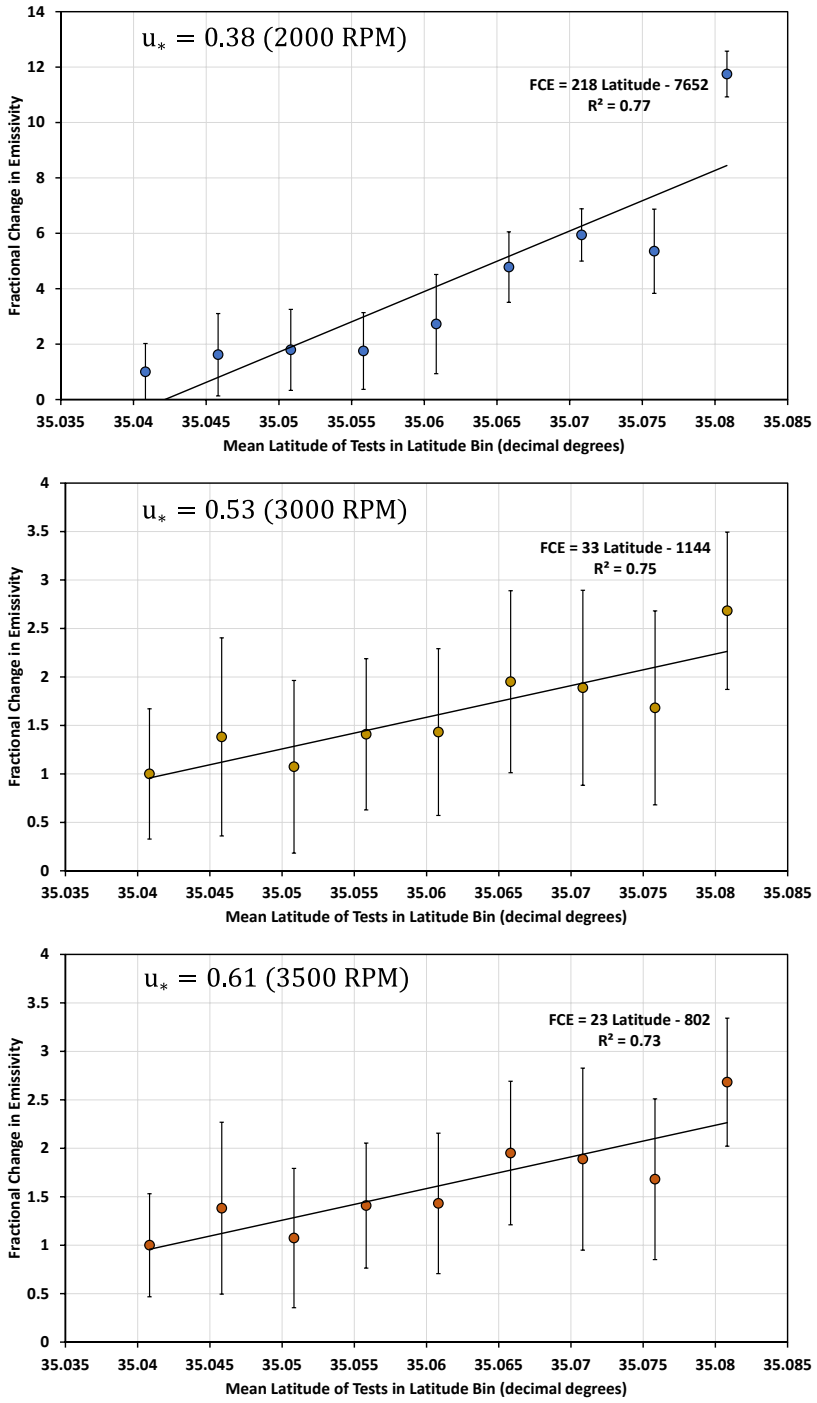

Figure 8. The fractional increase in emissivity as a function of position along the north (35.08 decimal degrees) to south (35.04 decimal degrees) gradient of the PI-SWERL tests in the ODSVRA riding area (2013-2019). Data represent mean emissivity in each latitudinal bin normalized to the mean emissivity in the southern-most latitude bin for the three PI-SWERL u_* set-points: 0.38 m s^{-1} (top panel), 0.53 m s^{-1} (middle panel), and 0.61 m s^{-1} (bottom panel). Error bars represent the coefficient of variation (standard deviation/mean).

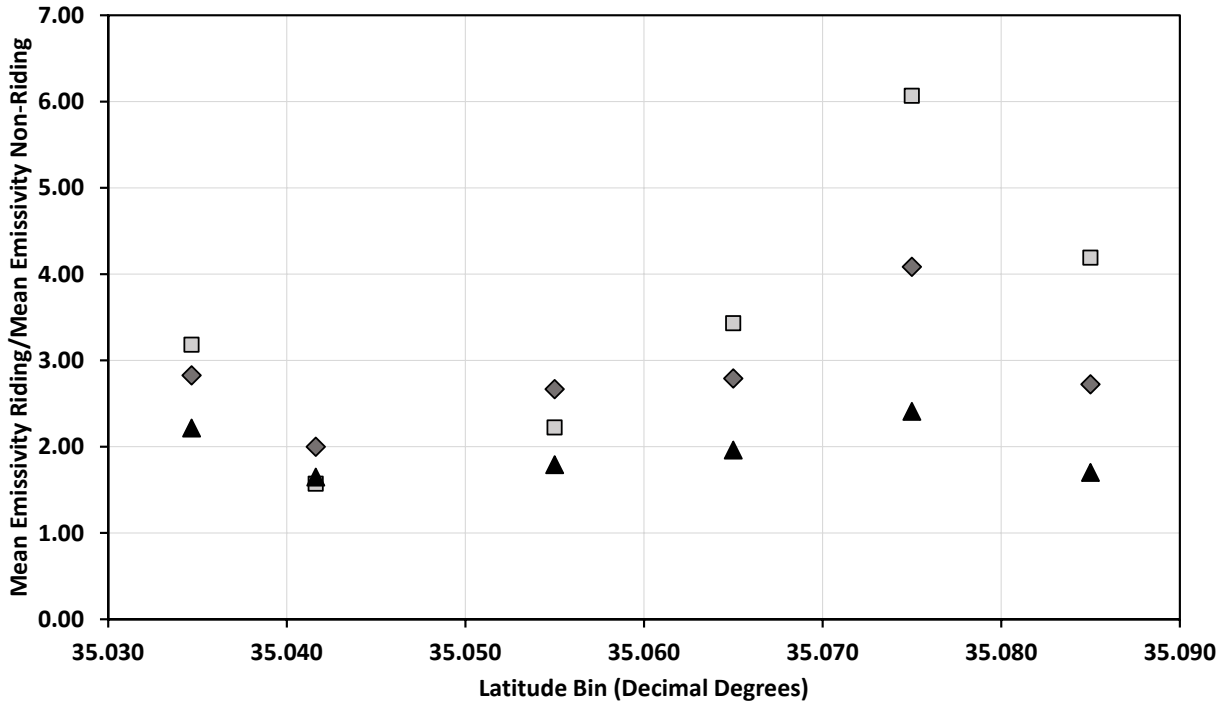

Figure 9. Mean emissivity in riding area normalized by mean emissivity of non-riding areas as a function of latitude 0.01 decimal degree bins. Symbols represent PI-SWERL u_* set points: square, 0.38 m s^{-1}; diamond 0.53 m s^{-1}; triangle, 0.61 m s^{-1}.

Cited Literature

Mejia, J. F., Gillies, J. A., Etyemezian, V. R., Glick, R. (2019). A very-high resolution (20 m) measurement-based dust emissions and dispersion modeling approach for the Oceano Dunes, California, Atmospheric Environment, 218, https://doi.org/10.1016/j.atmosenv.2019.116977

Etyemezian, V., Gillies, J.A., Shinoda, M., Nikolich, G., King, J., Bardis, A.R. (2014). Accounting for surface roughness on measurements conducted with PI-SWERL: evaluation of a subjective visual approach and a photogrammetric technique. Aeolian Res 13, 35‐50. https://doi.org/10.1016/j.aeolia.2014.03.002.

Gillies, J.A., Etyemezian, V. (2014). Wind and PM_{10} Characteristics at the ODSVRA from the 2013 Assessment Monitoring Network. Report prepared for California State Parks, ODSVRA and OHMVR, Pismo Beach and Sacramento, CA.

ATTACHMENT 5

Gillies, J.A., Mejia, J. (July 2020). "Model Verification Based on 2013 Measurements and 2013 Emission Grid and 2013 Wind Field for the 10 Baseline Days," Report prepared for CDPR by DRI

Model Verification Based on 2013 Measurements and 2013 Emission Grid and 2013 Wind Field for the 10 Baseline Days

J.A. Gillies and J. Mejia, DRI

This draft report presents measurements of PM_{10} made across the spatial domain of the ODSVRA as well as external to the ODSVRA, i.e., at CDF and Mesa2 and model-estimated values at the same locations for the environmental conditions defined by the 10 baseline days. The comparison between measured and modeled values is made to provide an evaluation of the veracity of the DRI dust emission and dispersion model (Mejia et al., 2019) prediction with available measurements.

2013 In-Park E-BAM 24 Hour PM_{10} versus Modeled 24 Hour PM_{10}

A comparison of the 24 Hour PM_{10} versus modeled 24 Hour PM_{10} for in-Park E-BAMs located at positions denoted as T1C, T2c, T3C, and T4B was carried out as part of the model verification procedure as requested by Parks, for Baseline-defined days. The E-BAM data used to derive the 24-hour mean PM_{10} was coded in the database as PM10_LC_Corr, which is defined in the metadata as: one hour concentration of particulate matter with a diameter of 10 micrometers or less, with correction factors applied. Upon review of the observed data the confidence in the measurements at T1C was low for the E-BAM, as the values were considerably lower than the T2C values by a factor of 4, so no comparison was carried out for this site. Due to instrument malfunction not all 10 Baseline days are available at each Station. Some of the available Baseline days did not have all 24 one hour data records.

Figures 1, 2, and 3 show the observed (E-BAM measured) 24-hour mean values compared with model estimates for the same positions for all available baseline days as measured at the identified locations on the four transects that were operated in 2013. The locations (latitude and longitude), distances between transect monitoring positions and their elevation above sea level are listed in Table 1.

Table 1. The positional data for the measurement locations where E-BAM and MetOne particle profilers were deployed in 2013. Meteorological data were collected at these positions as well.

Transect ID	Latitude	Longitude	Distance from Shoreline (m)	Elevation (m)
T1A	35.088257	-120.6235	700	17.95
T1B	35.087615	-120.6216	893	29.05
T1C	35.086687	-120.6186	1185	21.15
T2A	35.071805	-120.6263	409	13.09
T2B	35.070713	-120.6243	628	19.04
T2C	35.069508	-120.6193	1101	32.35
T3A	35.056977	-120.6261	500	19.64
T3B	35.052712	-120.6181	1365	34.31
T3C	35.048821	-120.6076	2420	24.31
T4A	35.023906	-120.6269	859	18.6
T4B	35.021225	-120.6218	1411	37.28
T4C	35.018632	-120.6173	1913	37.08

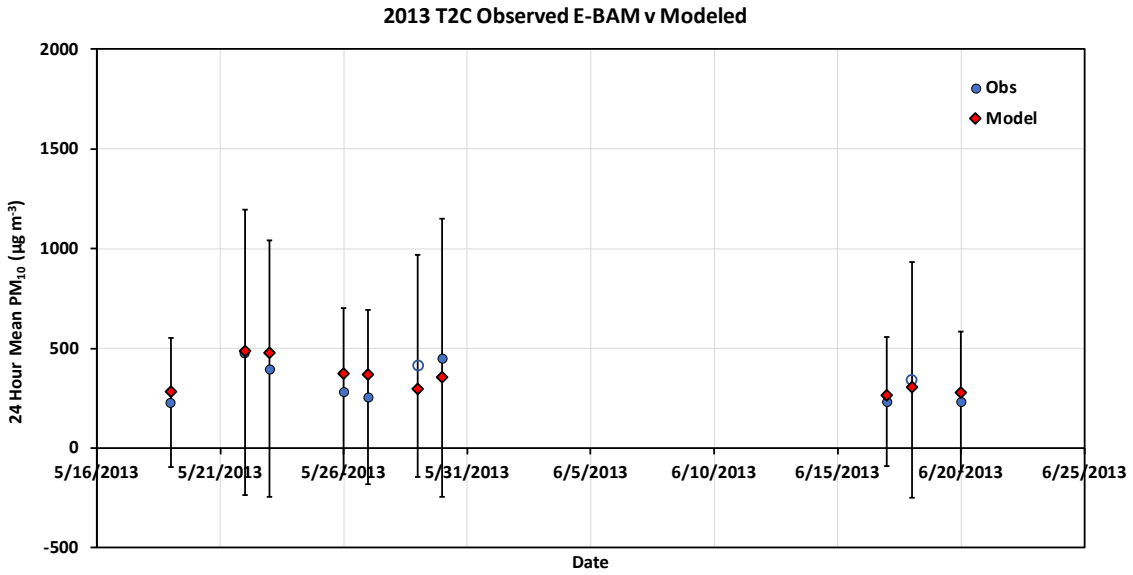

Figure 1. Observed 24 hour mean PM_{10} at Station T2C. Note the large standard deviation of the mean observed value as indicated by the error bars. This is due to the wide range of PM_{10} values observed during the 24 hour period on these dust-event days. Open blue circles indicate missing hours in the observational data record for estimating the mean. Error bars are not shown for the modeled values.

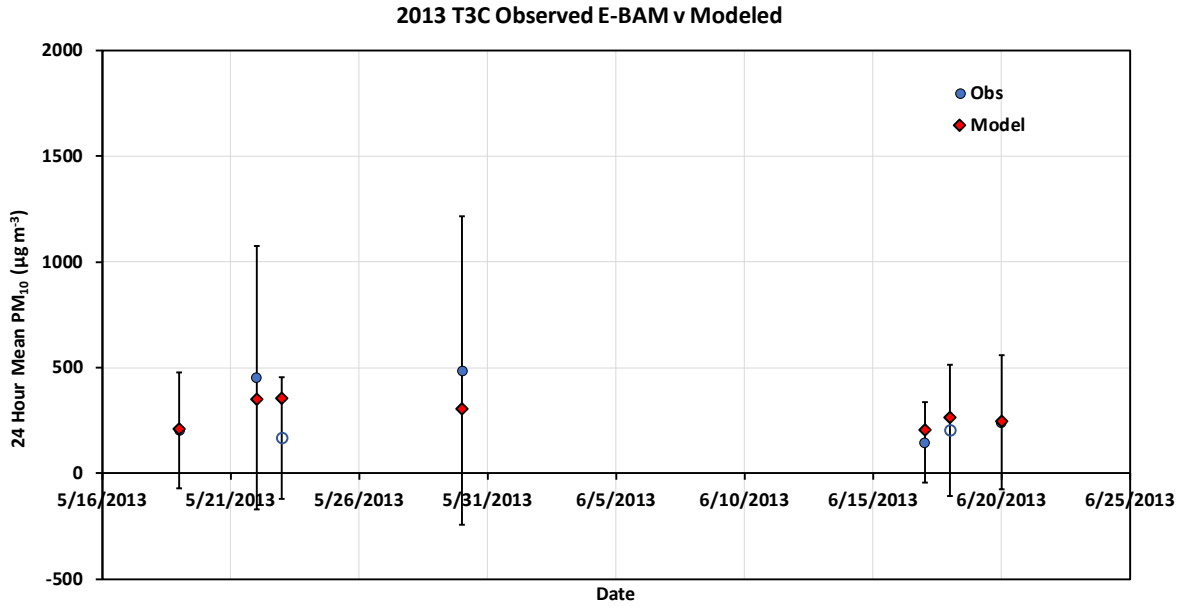

Figure 2. Observed 24 hour mean PM_{10} at Station T3C. Note the large standard deviation of the mean observed value as indicated by the error bars. This is due to the wide range of PM_{10} values observed during the 24 hour period on these dust-event days. Open blue circles indicate missing hours in the observational data record for estimating the mean. Error bars are not shown for the modeled values.

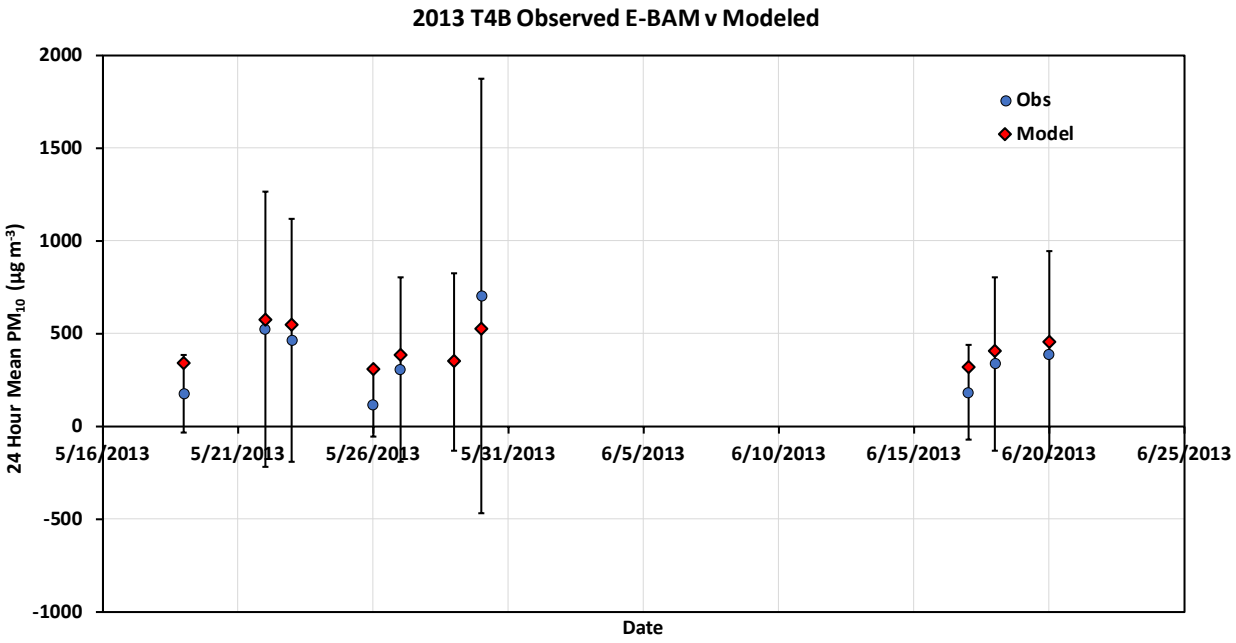

Figure 3. Observed 24 hour mean PM_{10} at Station T4B. Note the large standard deviation of the mean observed value as indicated by the error bars. This is due to the wide range of PM_{10} values observed during the 24 hour period on these dust-event days. Error bars are not shown for the modeled values.

For the three Stations, T2C, T3C, and T4B, the mean of all available 24-hour PM_{10} concentration values are compared with the mean of the model-predicted 24-hour PM_{10} concentration values (Fig. 4). The ratio of observed to modeled for the baseline days with valid observations are, respectively, 0.95 (±0.23), 0.97 (±0.38), and 0.80 (±0.27). For all Stations combined the mean value of the observed to modeled ratio is 0.90 (±0.29). Based on model verification criteria used by the US EPA, these values exceed the EPA's criteria of a factor of two being acceptable when comparing measured and modeled values. The analysis presented here provides confidence that the DRI model is operating in a predictive capacity at a high level of performance. It should also be noted that the in-Park monitoring locations are subject to much greater dynamic conditions than those downwind of the Park with both emission and dispersion occurring coincidentally. Downwind of the Park away from the active sand sheets only dispersion and particle deposition are affecting the mass concentration of PM_{10}.

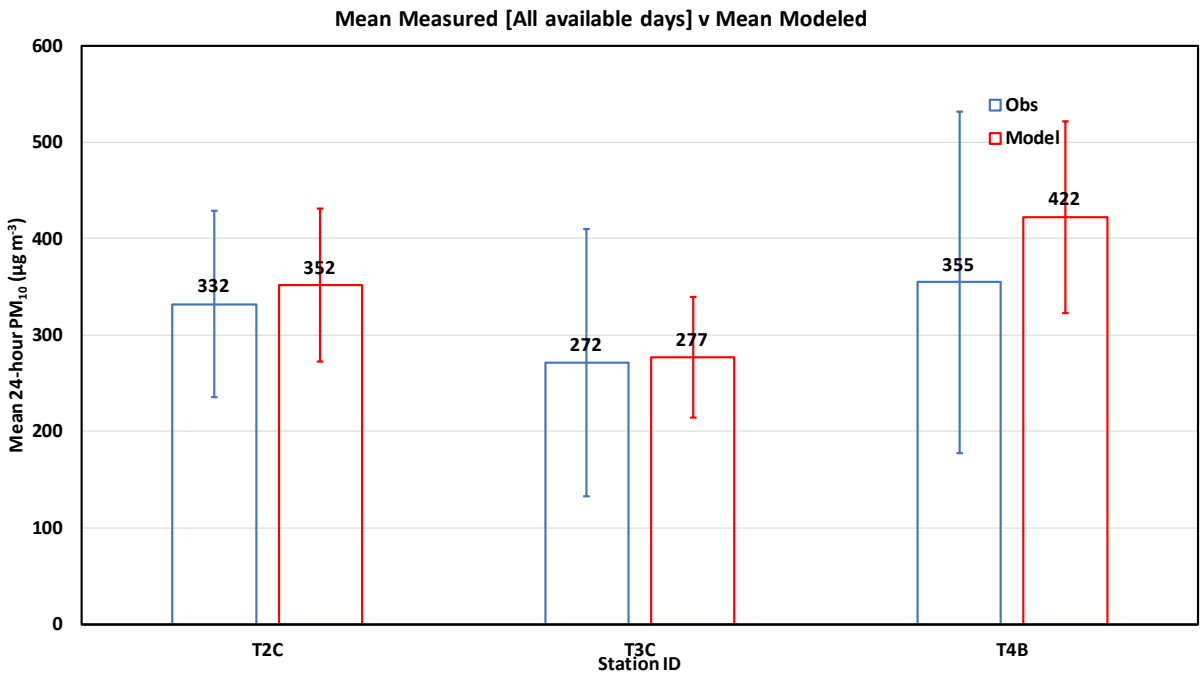

Figure 4. Comparison of the mean observed value (E-BAM measured) and the mean modeled value for the available Baseline days.

2013 In-Park MetOne Particle Profiler 24 Hour PM_{10} versus Modeled 24 Hour PM_{10}

During the 10 defined Baseline Days, MetOne instruments were operational at T1B, T1C, T2B, T2C, T3A, T3B, T3C, T4A, T4B, and T4C. As reported by Etyemezian et al. (2013) there were issues associated with these data, most notably substantial periods of data loss. Due to this loss of data some of the defined baseline days do not have full 24-hour records so the mean values are affected by this. As PM_{10} can vary several orders of magnitude during a 24-hour period, the loss of a few hours of data can dramatically affect the calculated mean value.

In 2013 there was no calibration of the MetOne instruments against a BAM as has been carried out in subsequent years. In 2013, the particle size bins reported by the MetOne instrument were used to reconstruct a PM_{10} proxy by assuming the counts per unit volume of sample air in each size bin i (Ci) are attributed to a single particle size (with diameter Di) in that size bin; the volume of an individual particle with diameter Di is calculated and multiplied by an assumed density (2.6 g/cm^3–that of silica) and then multiplied by the counts per unit volume of air. This converts the counts from that size bin into mass per unit volume of air associated within that size bin. The results for all size bins that represent particles with aerodynamic diameter smaller than 10 microns are added together to obtain the "reconstructed" PM_{10}. In subsequent years where collocation with BAM and mass-based concentration measurements were carried out, the process of converting MetOne particle count data to BAM-corrected PM_{10} values has provided a more robust method to more accurately represent PM_{10} levels using MetOne instruments.

Acknowledging that the 2013 MetOne particle profiler data are compromised by data loss and are not adjusted to BAM-corrected values, comparisons of the measured and modeled values for sites T1C, T2C, T3C, and T4B are presented in Figures 5, 6, 7, and 8. These represent the eastern-most measurement positions along the four transects of instrumented towers that were set up in 2013.

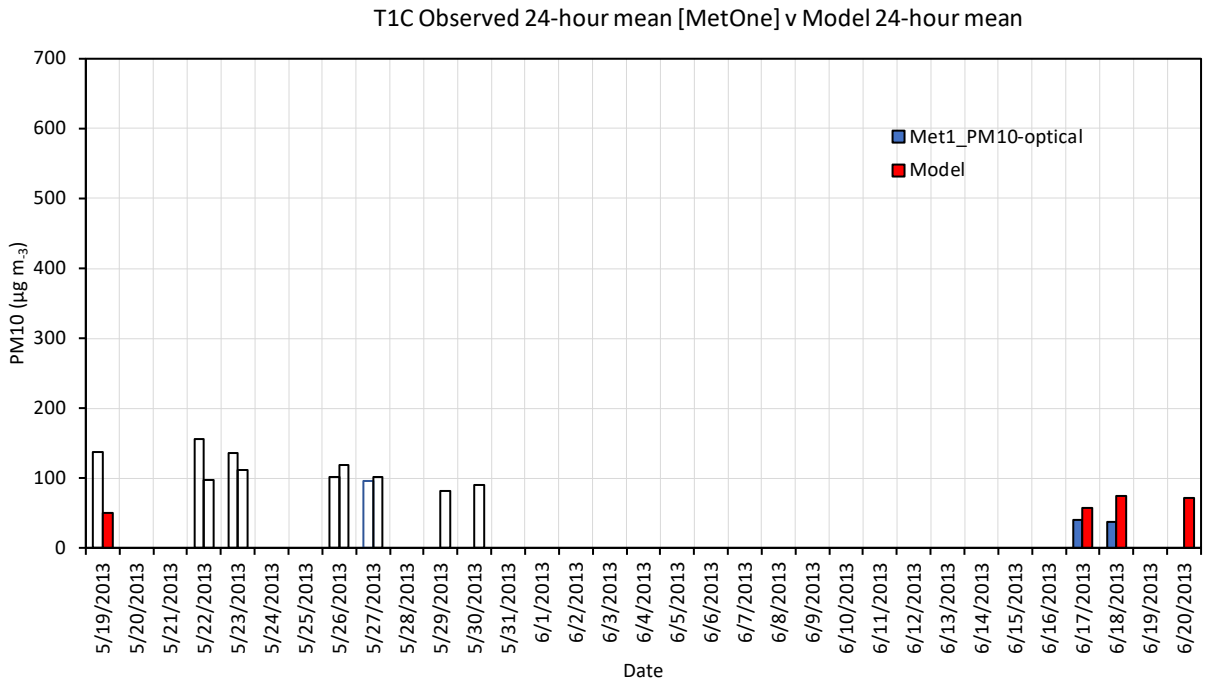

Figure 5. MetOne estimated 24-hour mean PM_{10} and model-generated 24-hour mean PM_{10} estimates for site TIC. White bars indicate that the mean value is based on less than 24 hours of measured data.

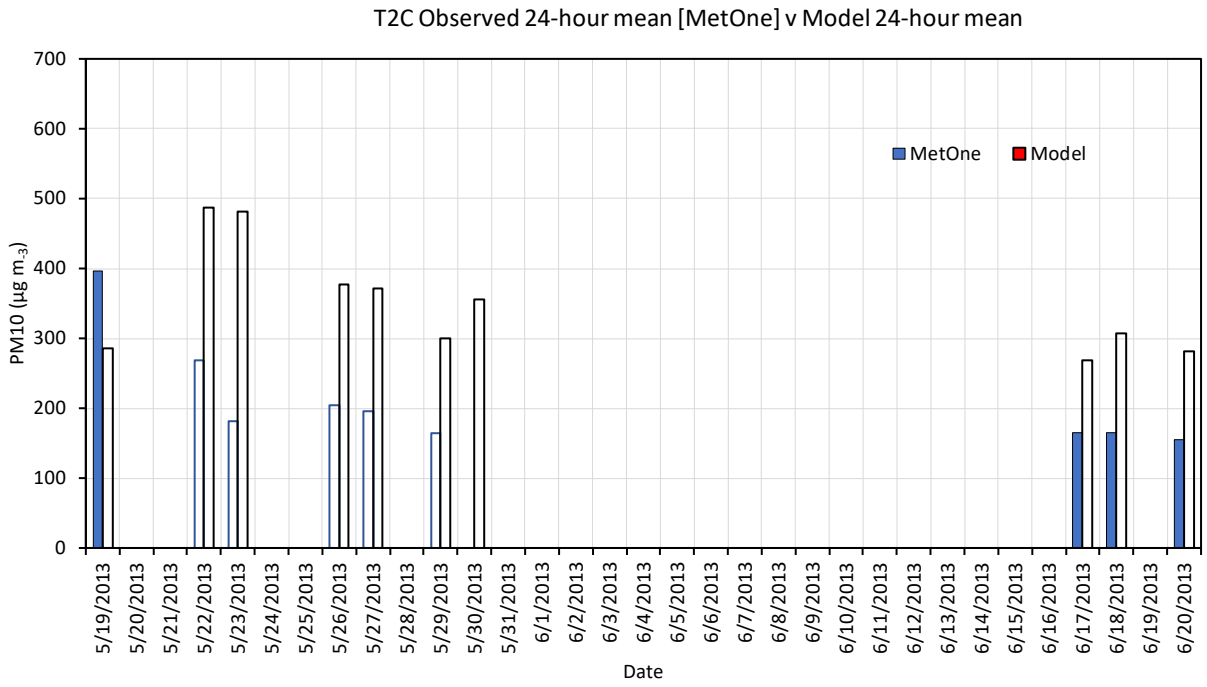

Figure 6. MetOne estimated 24-hour mean PM_{10} and model-generated 24-hour mean PM_{10} estimates for site T2C. White bars indicate that the mean value is based on less than 24 hours of measured data.

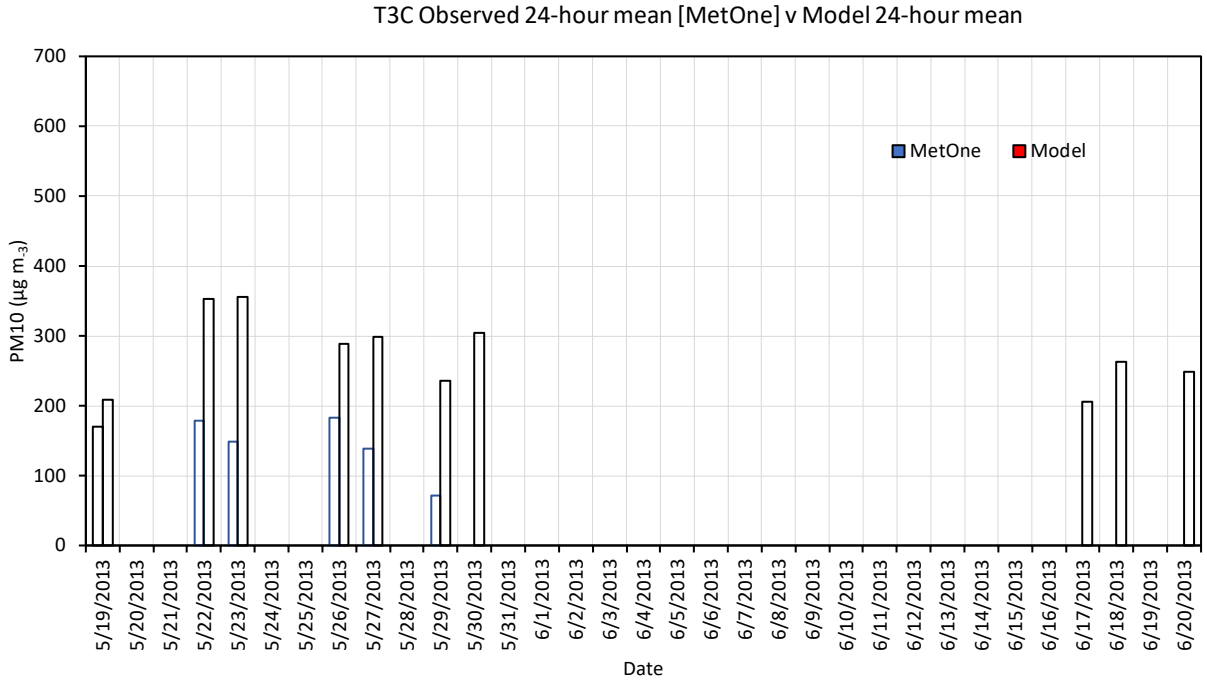

Figure 7. MetOne estimated 24-hour mean PM_{10} and model-generated 24-hour mean PM_{10} estimates for site T3C. White bars indicate that the mean value is based on less than 24 hours of measured data.

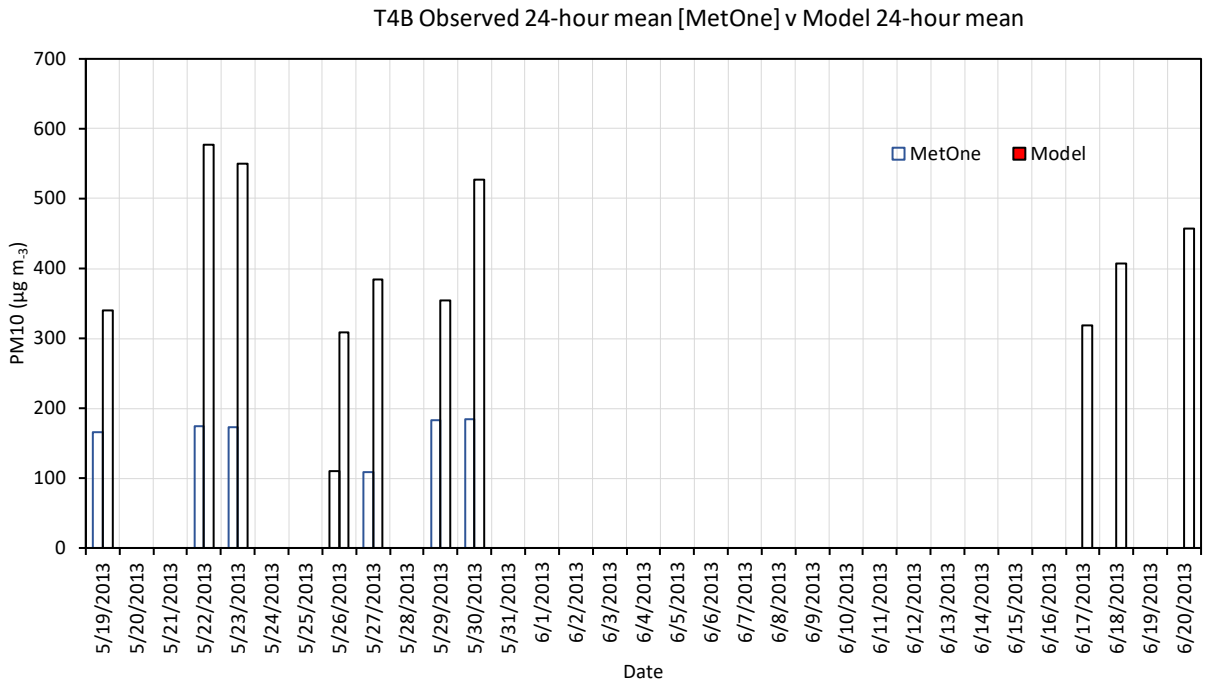

Figure 8. MetOne estimated 24-hour mean PM_{10} and model-generated 24-hour mean PM_{10} estimates for site T4B. White bars indicate that the mean value is based on less than 24 hours of measured data.

As these Figures show, the observed mean values are for many of the baseline days based on an incomplete 24-hour data record, with some days having less than half a day of hourly records. In general, the MetOne instruments are lower than the modeled values.

Table 1 shows the baseline days and the ratio of modeled:observed for all the other available stations on the 2013 transects. A clear pattern of modeled exceeding measured is not observed when examining all the Stations on the transects (6 out of 10 do have modeled>observed) (Fig. 9).

Table 1. Baseline days and the ratio of modeled:observed for all the other available stations on the 2013 transects.

	T1B	T1C	T2B	T2C	T3A	T3B	T3C	T4A	T4B	T4C
5/19/2013	0.19	0.37	0.77	0.72	0.38	1.13	1.22	0.32	2.06	0.30
5/22/2013	0.34	0.62	1.36	1.81	0.53	1.78	1.97	0.50	3.30	0.39
5/23/2013	0.46	0.82	2.03	2.66	0.59	2.21	2.39	0.45	3.17	0.38
5/26/2013	0.88	1.18	0.94	1.84	0.50	1.52	1.58	0.51	2.81	
5/27/2013	0.74	1.05	1.50	1.89	0.66	2.38	2.15	0.43	3.53	
5/29/2013	0.22		1.12	1.83	1.01	3.94	3.27	0.47	1.95	
5/30/2013									2.85	
6/17/2013		0.71		1.63						
6/18/2013		0.50		1.86						
6/20/2013				1.82						
Mean (all)	0.47	1.06	1.29	1.78	0.61	2.16	2.10	0.45	2.81	0.35
Std Dev	0.28	0.54	0.45	0.49	0.22	0.98	0.71	0.07	0.61	0.05
Mean (no missing hours)	0.47	0.75	1.29	1.51	0.52		1.22	0.42	2.81	0.34
Std Dev	0.28	0.34	0.45	0.53	0.20			0.13		0.06
<24 1 hour of observations in mean										

In our most recent measurements that collocate MetOne instruments with the in-Park BAM, we observe that the MetOnes under-represent the BAM-measured PM_{10} (Fig. 10) (also the case for observed previous colocation exercises, e.g., dust chamber and colocation with BAM at CDF), which suggests that the 2013 MetOne data are lower than would be observed if the recent protocols for converting their values to BAM-corrected were applied. This could, in part, explain some of the discrepancy between measured and modeled values. Due to the poor data recovery and the previously-applied method to convert MetOne particle count data to PM_{10}, and the lack of calibration using colocation with a BAM, using the MetOne observed to modeled values as a means to verify model performance is not robust for the 2013 data set.

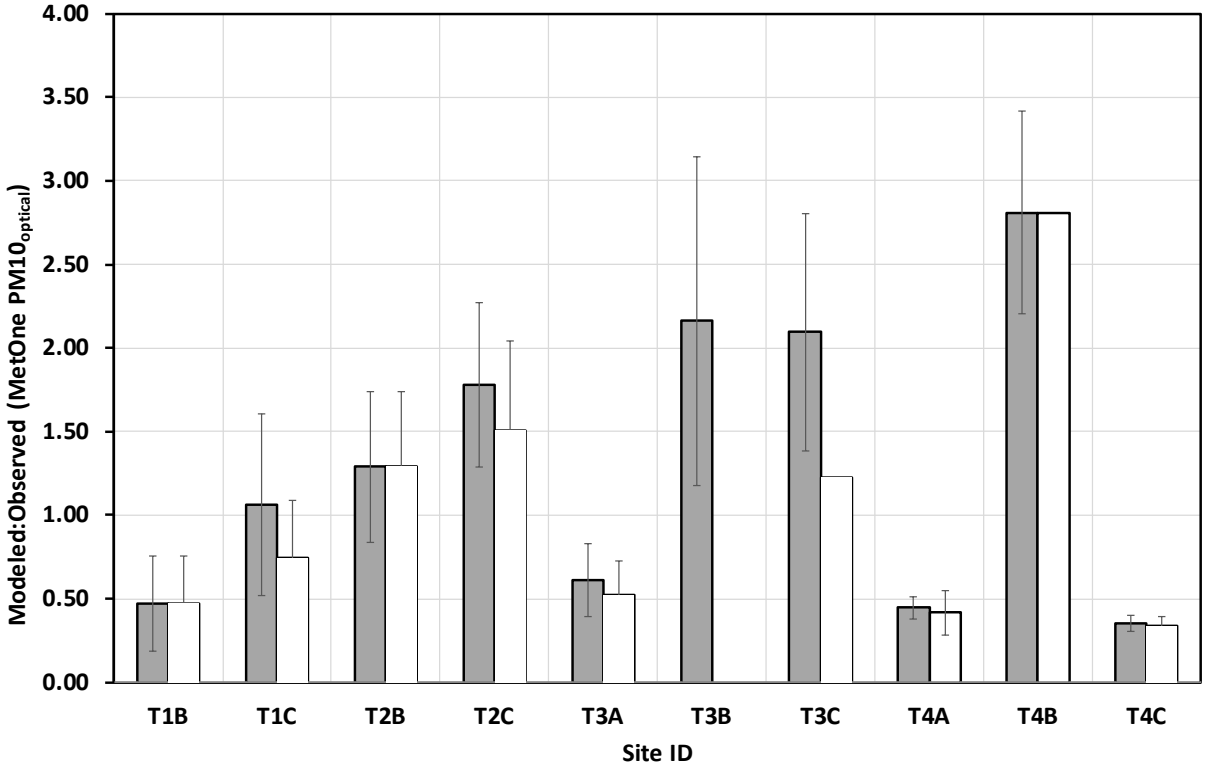

Figure 9. The mean Modeled:Observed ratio for the available stations on the 2013 measurement transects for the available baseline days. Gray bars indicate all available data were used and white bars signify the mean ratio value is based on baseline days with all 24 hours in the observation data.

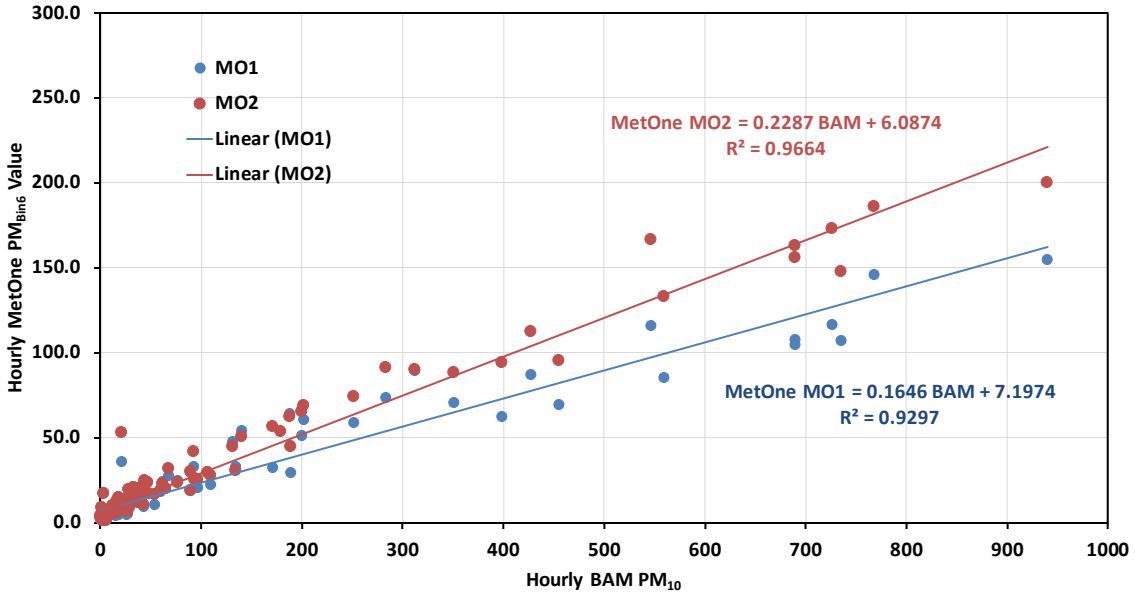

Figure 10. Recent colocation data (June 2020) comparing MetOne instruments with the in-Park BAM showing that MetOne instruments under-report PM_{10} compared to the BAM and need to be corrected by approximately a factor 4 to match BAM values.

2013 BAM 24 Hour PM_{10} versus Modeled 24 Hour PM_{10}, CDF and Mesa2

The comparison of the BAM-measured mean 24-hour PM_{10} and the model-predicted mean 24-hour PM_{10} values for the CDF and Mesa2 locations for the 10 baseline days are shown in Figs. 11 and 12. For clarity the measured and modeled mean 24-hour PM_{10} values shown in Figs. 11 and 12 are provided in Table 2.

The greatest percentage difference between a measured and modeled value is 36.5% (05-19-2013, CDF), with the average considering both sites being 17% (±11%), based on the absolute values of the % difference for each baseline day. The mean value of the observed to model-predicted value ratios for the 10 baseline days are 1.09 (±0.26) and 0.97 (±0.25) for CDF and Mesa2, respectively. The close agreement between the (SLOCAPCD quality assured/quality controlled) measured and the DRI model-predicted values verifies that the DRI model is performing at a level much greater than is accepted by the US EPA when using models for predicting the magnitude of scalar quantities (such as PM).

The comparison of observed versus modeled will be carried out for 2019 and 2020 once all data are available. Principally the data needed for modeling are the 2019 and 2020 SODAR data.

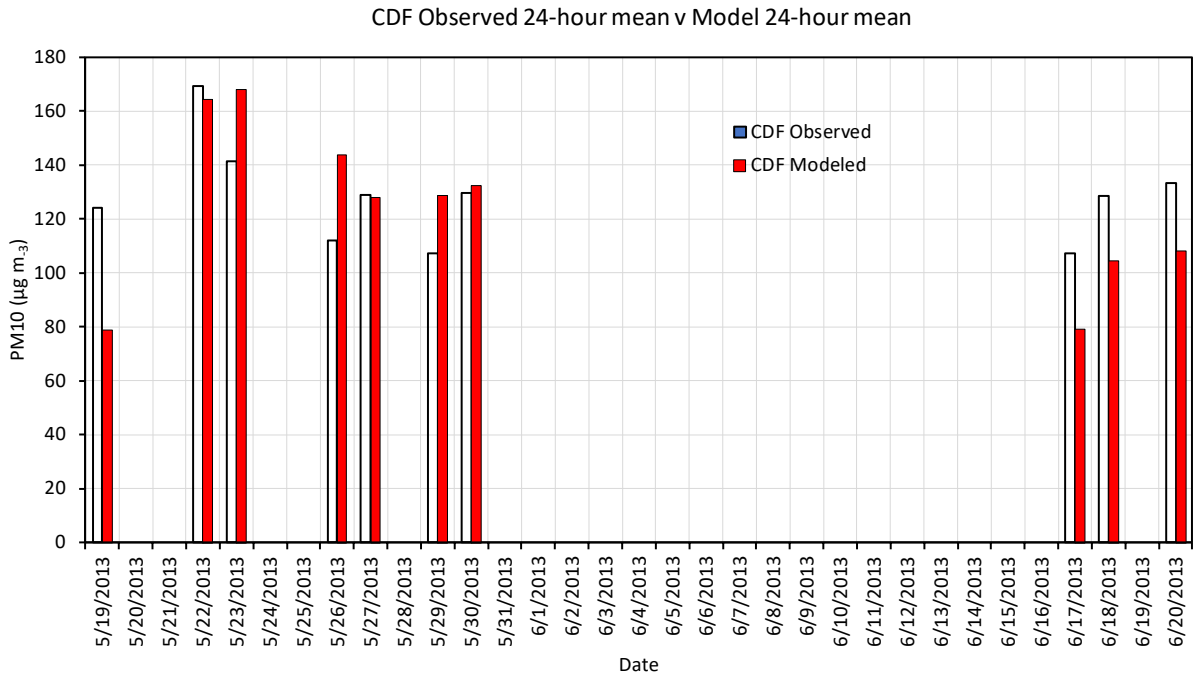

Figure 11. Comparison of the mean PM_{10} 24-hour observed value and the mean modeled value for the 10 Baseline days at the CDF site based on 2013 winds and 2013 emission grid.

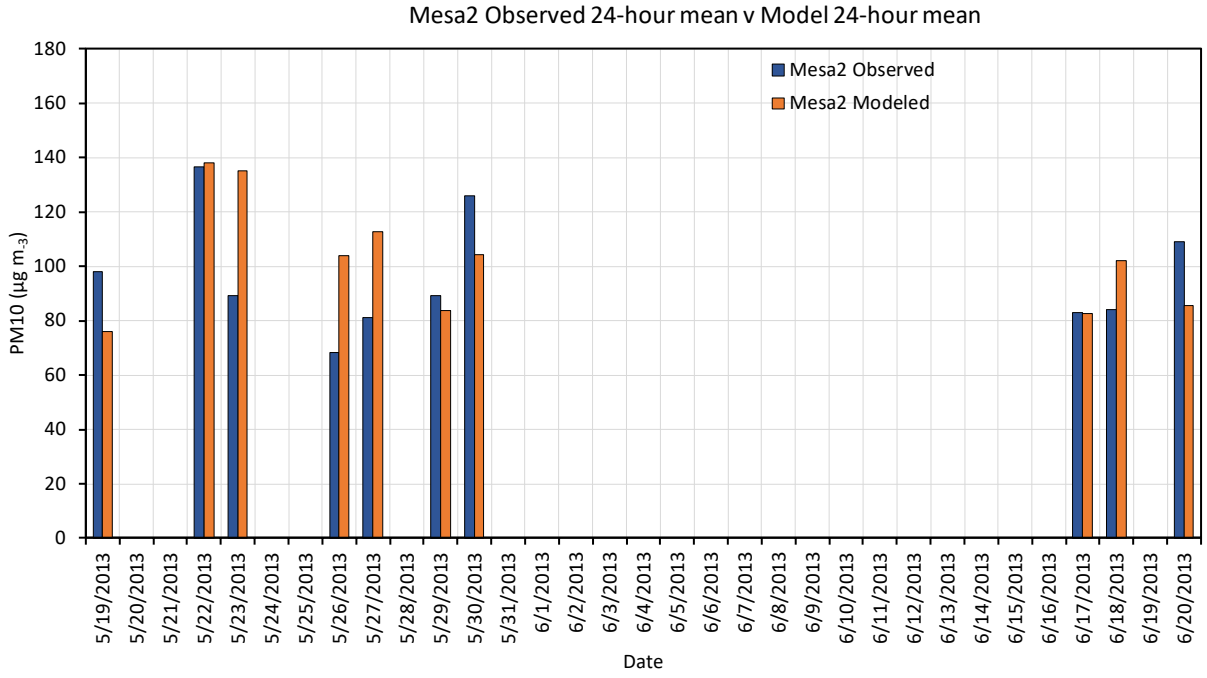

Figure 12. Comparison of the mean PM_{10} 24-hour observed value and the mean modeled value for the 10 Baseline days at the Mesa2 site based on 2013 winds and 2013 emission grid.

Table 1. Measured and modeled mean 24-hour PM_{10} values for the 10 Baseline Days.

	CDF (µg m^{-3})		Mesa 2 (µg m^{-3})	
Date	**Obs**	**Mod**	**Obs**	**Mod**
5/19/2013	124	79	98	76
5/22/2013	169	164	137	138
5/23/2013	141	168	89	135
5/26/2013	112	144	68	104
5/27/2013	129	128	81	113
5/29/2013	107	129	89	84
5/30/2013	130	133	126	104
6/17/2013	107	79	83	82
6/18/2013	129	104	84	102
6/20/2013	133	108	109	85
Mean	128	124	96	102
Std. Dev	18	31	21	22

References

Etyemezian, V., J. Gillies, G. Nikolich (2013). Analysis of Met One Aerosol Particle Profiler (APP) data from the Oceano Dunes, 2013. Report of 12/11/2013 to Parks.

Mejia, J.F., J.A. Gillies, V. Etyemezian, R. Glick (2019). A very-high resolution (20 m) measurement-based dust emissions and dispersion modeling approach for the Oceano Dunes, California. *Atmospheric Environment*, 218, 116977, doi: 10.1016/j.atmosenv.2019.116977.

ATTACHMENT 6

Furtak-Cole, E., Gillies, J., Walker, I., Hilgendorf, Z. (December 2, 2021). "Quantifying the value of a coastal foredune for wind erosion and dust emissions through numerical simulation"

Quantifying the value of a coastal foredune for wind erosion and dust emissions through numerical simulation

E. Furtak-Cole, J. Gillies, I. Walker, Z. Hilgendorf

December 2, 2021

Executive Summary

Under the advisement of the Science Advisory Group (SAG), a plan was developed and undertaken by Parks to investigate establishing a foredune system along a portion of the ODSVRA as a method to reduce PM_{10} mass emissions and the mass concentration of PM_{10} downwind of the ODSVRA.

The reason for establishing a foredune system is the expectation that it offers an opportunity to enhance control of dust that originates by wind erosion processes within the ODSVRA by reducing sand flux through the area the foredunes occupy and through their modulation of the wind flow within and downwind that results in conditions of lower shear stress than would be present in a flat, sloping beach. Lower shear stress conditions will result in a decrease in dust emissions. Resolving the effect of mature foredunes on the sand transport and dust emissions via experimentation would be a difficult undertaking, prohibitively expensive, and disruptive to Park operations. An effective means to evaluate the effect of foredunes on the system is to use Computational Fluid Dynamic modeling.

The goal of the modeling is to evaluate how the presence of a mature foredune system could alter the dynamics of the saltation and dust emission system in the near shore zone of the ODSVRA. We assume that the Oso Flaco foredune provides a suitable analog for representing a mature foredune system that could be established in the ODSVRA. The CFD model was implemented in the finite volume toolbox openFOAM using a Digital Elevation Model provided by UCSB and ASU to define the topography. Boundary conditions (i.e., the characterization of the incoming flow properties) were derived from wind speed and direction measurements collected upwind and at four locations within the Oso Flaco foredune test area.

The key results of the simulations are:

- Excellent agreement was observed between the measured and simulated ratio, downwind wind speed/upwind (i.e., beach) wind speed, providing confidence in the modeling results.
- Very little flow separation is observed for the nebkhas (vegetation-topped mounds) in the foredune indicating a very aerodynamic system. In contrast, the nonvegetated transverse dunes show zones of significant flow separation at the dune crests with zones of re-circulation on the lee-side slip faces.
- Plants exert considerable control of the shear stress distribution within the foredune, sheltering the sand surface underneath and in their lee.
- The integrated shear across the area beginning approximately 300 m from the shoreline through to the end of the sampling domain is lower for the actual geometry than for the geometry with no foredune present (areas are of equivalent size).

- For the boundary condition tested in these simulations, removal of the foredune would result in an 8.2% increase in integrated shear on the test area.
- In the lee of the foredune a zone of shear is created that reaches a minimum at the downwind border of the foredunes and then increases non-linearly with increasing downwind distance. The shear stress at the surfaces reaches approximately 90% of its potential (downwind) value 50 m behind the foredune, returning to its full potential value approximately 250 m behind the foredune.

1 Introduction

Under the advisement of the Science Advisory Group (SAG), a plan was developed and undertaken by Parks to investigate establishing a foredune system along a portion of the ODSVRA as a method to reduce PM_{10} mass emissions and the mass concentration of PM_{10} downwind of the ODSVRA. Six restoration methods are being evaluated to determine which method will result in the most rapid evolution to a foredune system that closely approximates the naturally occurring foredune system along this area of the central California coastline in terms of form and ecological function. The reason for establishing a foredune system is the expectation that it offers an opportunity to enhance control of dust that originates by wind erosion process within the ODSVRA by reducing sand flux through the area the foredunes occupy and through their modulation of the wind flow within and downwind that results in conditions of lower shear stress than would be present in a flat and sloping beach. Lower shear stress conditions will result in a decrease in dust emissions.

The presence of the foredune creates a perturbation in the wind flow coming onshore that affects the wind and sand transport processes due to its complex topography and vegetation on the space it occupies. In addition, the perturbation to the flow is expected to modulate the flow to some distance downwind of the foredune that also reduces sand flux and dust emissions. Collecting sufficient data using measurement techniques to characterize the effects of the foredunes on dust emissions presents a formidable undertaking that would be of considerable expense due to the needed instrumentation, labor, and time required. An alternative approach is to use Computational Fluid Dynamic (CFD) modeling to characterize the flow conditions associated with the movement of wind from the beach, through the foredunes, and to some distance downwind. From this type of simulation, relations can be established to aid in defining how the foredune roughness modulates the flow across space to infer how its presence affects dust emissions as compared to zones of the beach area at the ODSVRA that are currently lacking these types of forms.

CFD models provide complex analysis of fluid flow based on conservation of mass and momentum by resolving the Navier-Stokes equations using finite volume or other methods in three dimensions. The Navier-Stokes equations describe the motion of viscous fluids and arise from Newton's second law (i.e., the acceleration of an object depends directly upon the net force acting upon the object, and inversely upon the mass of the object). The Navier–Stokes equations are used to describe the physics of many phenomena of scientific and engineering interest including the flow of wind over surfaces.

Using CFD to provide realistic simulations requires that careful attention be given to the model boundary conditions (i.e., the correct velocity, pressure, and turbulence properties of the incoming flow) and a reasonable representation of the topography over which the air flows. It is also desirable to have measurements from within the modeling domain to compare with model-derived values to provide confidence that the model has achieved a simulation that is a realistic representation of the real-world conditions. It needs to be noted that all models are a simplification and cannot capture all the complexities of turbulent fluid flow over complex roughness forms.

Here we report on CFD modeling of the air flow and shear stress production for a portion of the mature foredunes in the ODSVRA known as the Oso Flaco Dunes that lie south of the plover exclosure area (Fig. 1). This area is interpreted as having relatively mature foredunes that, to the best of our knowledge, are representative of a foredune complex that would be typical of this part of the Central California coast that developed naturally or developed following the removal of OHV activity. The goal of the modeling is to evaluate how the presence of a mature foredune system could alter the dynamics of the saltation and dust emission system in the near shore zone of the ODSVRA. In this Report we describe the data used in the CFD model (implemented in the finite volume toolbox openFOAM), the measurements made for defining the boundary conditions and model verification, the computational methods defined in openFOAM, and the analysis undertaken to characterize how the presence of a foredune like Oso Flaco could potentially modulate wind erosion and dust emissions if it was present in the beach areas of the ODSVRA where it is currently absent.

Figure 1: The Oso Flaco foredune test site location.

2 Methods

2.1 Digital Elevation Model of the Oso Flaco Foredune

Detailed imagery of the ODSVRA was acquired using an unmanned aerial system (UAS) operated by UCSB and ASU. The acquired images were processed by ASU to produce digital elevation models (DEM) for various regions of the Park including the Oso Flaco foredunes. The constructed DEM has an accuracy level that resolves topographic details to 10 cm of resolution. The dataset from February of 2021 was selected to construct the DEM for the Oso Flaco dunes, as it most closely matches the time period when measurements of wind flow through the dunes were acquired in May 2021 (see Section 2.2).

To be used in a CFD simulation, additional processing was performed on the topographic dataset for the Oso Flaco foredune region of interest. A GeoTIFF of the region was exported to a point cloud, which was made into a 3D surface using 2D Delaunay triangulation. A GeoTIFF is a public domain metadata standard that allows georeferencing information to be embedded within a Tag Image File Format (TIFF). The GeoTIFF was used to create a topographic representation of the surface that is used to create the computational finite volume mesh (see Section 3.2) for the CFD simulation. This surface can be seen in Fig. 2 (top panel).

Two additional topographies were created to simulate surface shear stress patterns on relevant hypothetical surface forms, for comparison with surface shear stresses on the actual surface. In the first, the foredune is effectively flattened to a gently sloping surface. This is accomplished in the DEM by slicing a rectangular region covering the foredune out of the 3D point-cloud (Fig. 2, top panel). An in-house code was written to re-assign elevation values to the rectangular region, based on inverse distance weighting (IDW). The same 2D Delaunay process is then used to create a 3D surface. The result is a smooth gently sloping surface from the shoreline to the area where the large transverse dunes are located. This sloping surface, shown in the middle panel of Fig. 2, is the result of spatially interpolating the edges of the clipped areas together. In the second scenario, a horizontal sloping surface is created behind the foredune (Fig. 2, bottom panel). This is accomplished by clipping the point-cloud and interpolating a transition zone behind the foredune, which smoothly transitions the foredune topography to a flat plane. The height of this plane is 4.2 m above sea level (ASL), which is based on the average height of the beach.

2.2 Atmospheric Measurements

A measurement campaign was carried out to acquire vertically resolved wind speed and turbulence parameter data upwind of the Oso Flaco foredune and at four positions along a roughly west to east transect through the foredunes. Three sonic anemometers were mounted on two 3.05 m (10 ft) towers to collect 3-dimensional wind speed data (*u*-horizontal, *v*-spanwise, *w*-vertical) at 10 Hz. The anemometers were mounted on the towers with their sampling volumes positioned at approximately 0.025 m, 1.56 m and 3.26 m above the surface (Fig. 4). These data were used to set the boundary conditions and for model verification. One tower was installed upwind of the foredunes. The second tower was moved through the foredune but left in position for short periods of time (approximately 30 minutes). The

Figure 2: 3D representation of the topography of the mature Oso Flaco foredune test area (top panel) and two hypothetical geometry scenarios: the land surface with the foredune flattened (middle panel), and the surface with a flat region behind the foredune with the transverse dunes flattened (bottom panel).

geographic positions of the towers and a summary of time periods for which measurements were taken are shown in Table 1.

Table 1: Locations and durations for velocity profiles measured with the sonic anemometer towers.

Name	Long.	Lat.	Day	Start	End
upwind	-120.6329372	35.0378334	20-05-2021	8:45:00	24:00:00
P1	-120.6319444	35.0380164	20-05-2021	09:40:46	10:51:25
P2	-120.6309242	35.0374855	20-05-2021	11:18:00	11:49:20
P3	-120.6301323	35.0372208	20-05-2021	12:09:29	12:41:16
P4	-120.6296373	35.0367	20-05-2021	13:08:02	13:46:00

Figure 4: Tower configuration for data collected with the sonic anemometers.

Sufficient wind velocity data were collected to build an inlet boundary condition and verification points for numerical simulation. An average velocity profile was constructed over the range of instrument heights by averaging wind speeds for the time period 1:00 PM to 2:00 PM on 05-20-21. The average wind speed for this hour represents a wind speed that is above the threshold for saltation for most of the ODSVRA. A log-law velocity profile was fit to values from the three sonic anemometers, to provide velocity boundary values extending to a height of 100 m above ground level (AGL). A corresponding turbulence intensity, *TI*, profile was created by linearly interpolating calculated values between the three anemometers and extending the value at the 3.23 m anemometer to the top of the computational domain (50 m AGL). A profile of turbulent kinetic energy *k* is calculated from the average velocity *u* and *TI* as,

$$k = \frac{3}{2}(uTI^2) \qquad (1)$$

The specific dissipation rate ω can then be calculated as:

$$\omega = C_{\mu}^{0.75}\,\frac{k^{0.5}}{l} \qquad (2)$$

where the constant C_{μ}=0.09, and the turbulence length scale is taken to be *TI* = 5. The kinematic energy eddy viscosity can be calculated as:

$$v_t = 0.31 \frac{k}{\omega} \qquad (3)$$

Values of u, k, ω and v_t are needed as boundary condition inputs for the CFD simulation. Profiles of u and TI are shown in Fig. 5. Zero-gradient pressure was used at the inlet, solid, side, and top walls, while a fixed value of zero was applied at the exit. Slip velocity (no friction) was applied to the top and side walls, a zero velocity condition was applied to the ground, and the outlet was given a zero gradient condition.

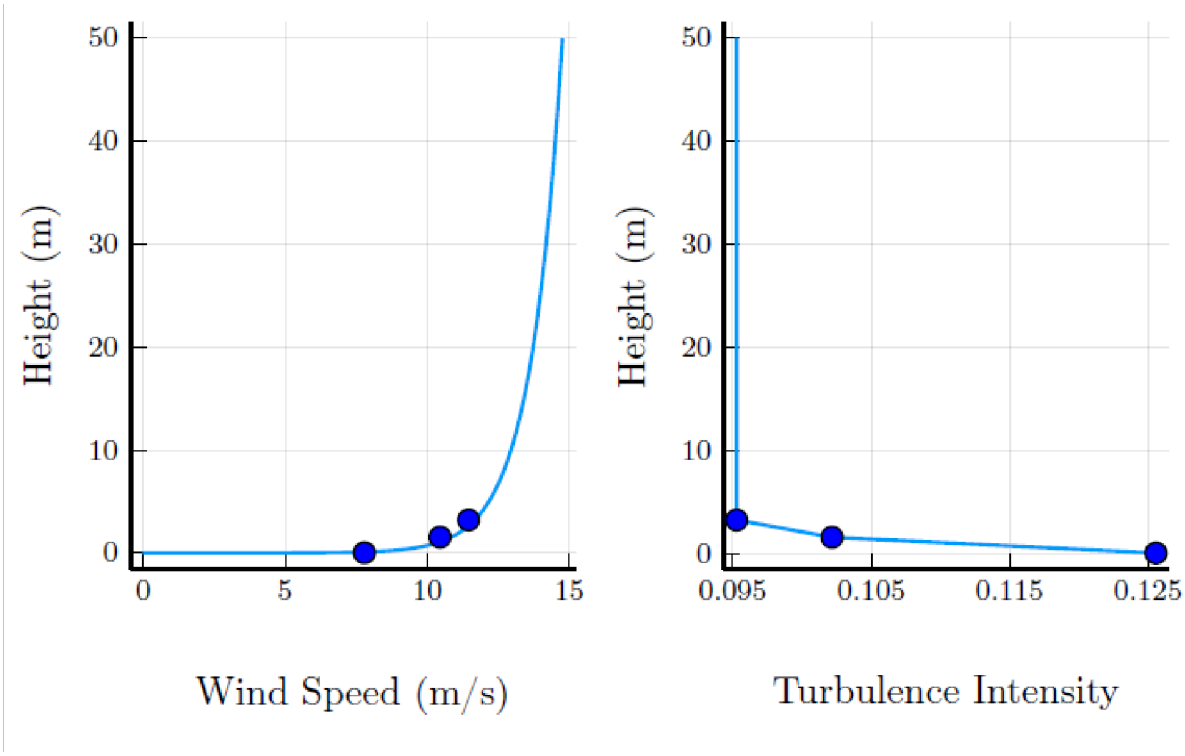

Figure 5: Profiles of u (left) and TI (right) were constructed for the inlet boundary condition. Blue circles represent the near surface measurements from the sonic anemometers.

2.3 Computational Methods

Simulations were performed by numerically solving the steady-state incompressible Navier Stokes equations:

$$\rho u \nabla u = -\nabla p + \rho g + \mu \Delta u \qquad (4)$$

$$\nabla u = 0 \qquad (5)$$

where, u is horizontal velocity, p is pressure (Pa), g (9.81 m s^{-2}) is the acceleration due to gravity, and μ is fluid viscosity (Pa s). Turbulence modeling was performed with a Menter's shear stress transport (SST) turbulence model. This model was chosen for its low sensitivity to the vertical dimension above the surface ($y+$), as the large and complex domain of interest presents a difficult meshing problem.

The computational domain is a 900 m × 200 m × 100 m prism, rotated to align with the prevailing wind direction along the 900 m fetch. An angled plane was used to cut the inlet boundary, ensuring that the inlet boundary condition is applied across the beach at a uniform elevation. An illustration of the domain imposed over the topography can be seen in Fig. 6. A domain height of 100 m was chosen to minimize flow acceleration that may occur due to changes in cross-sectional area caused by the topography. The selected height exceeds five heights of the largest topographic feature in the domain.

Meshing was performed with the CFmesh utility. A maximum cell size of 10 m was applied in the upper atmosphere, which is not a region of interest, to conserve computing resources. Cells are progressively refined with decreasing elevation to 0.5 m within 10 m of the ground. Below 10 m seven additional mesh layers were defined with the lowest at ground level (i.e., the bottom of the lowest mesh touches the surface). This lowest mesh layer has a cell width of 0.02 m. Total cell counts for the simulations performed vary by topography but are on the order of 20 million per simulation.

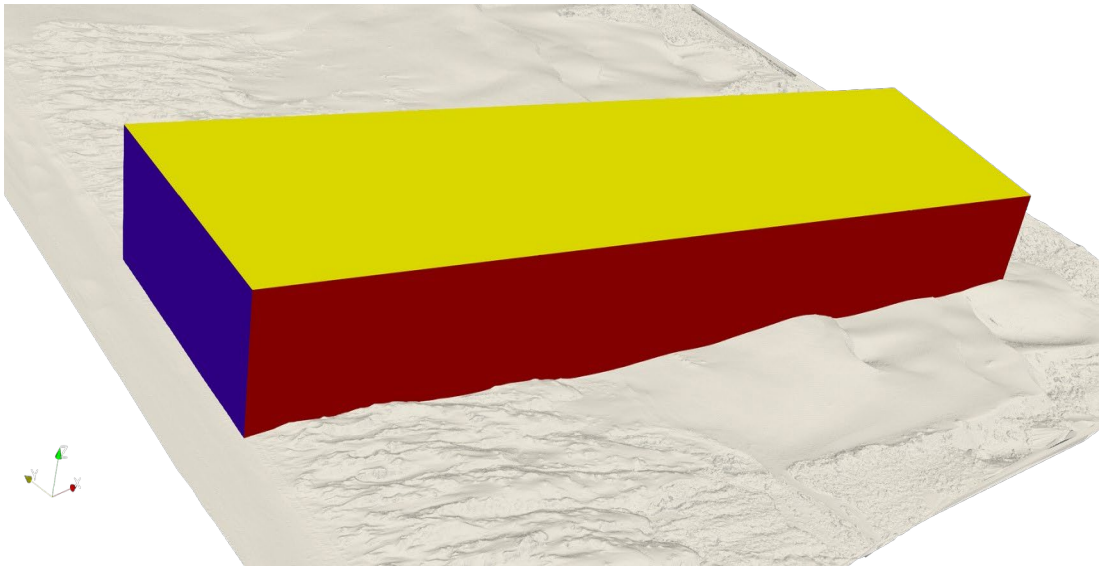

Figure 6: An illustration of the computational domain imposed over the topography. The angled inlet is shown in blue to apply the inlet boundary conditions on the beach across a uniform distance in front of the foredune.

3 Results

3.1 Model Verification

Verification of model results was performed by extracting velocity predictions from the simulation that match the tower locations and anemometer heights and comparing those values with the sonic anemometer measurements. The dataset measured in the field comes from two towers: one stationary tower positioned at the boundary of the computational domain on the beach, and a second that was moved throughout the day. A map of the tower locations can be seen in Figure 7. Consequently, a direct verification (i.e., value predicted to

value measured) cannot be carried out at the second tower locations for the time period that was used to construct the boundary condition. Thus, we compare the ratio of upwind velocity to the velocity measured at the mobile tower for the measurements and the simulation. This is possible, as the upwind tower was in operation for the entire period of time. Thus, validation points are not compared directly against the boundary condition, but additional data collected at the location of the boundary. For the highest sonic anemometer, located 3.26 m above the ground, this ratio for the measured and simulated results is shown in Table 2.

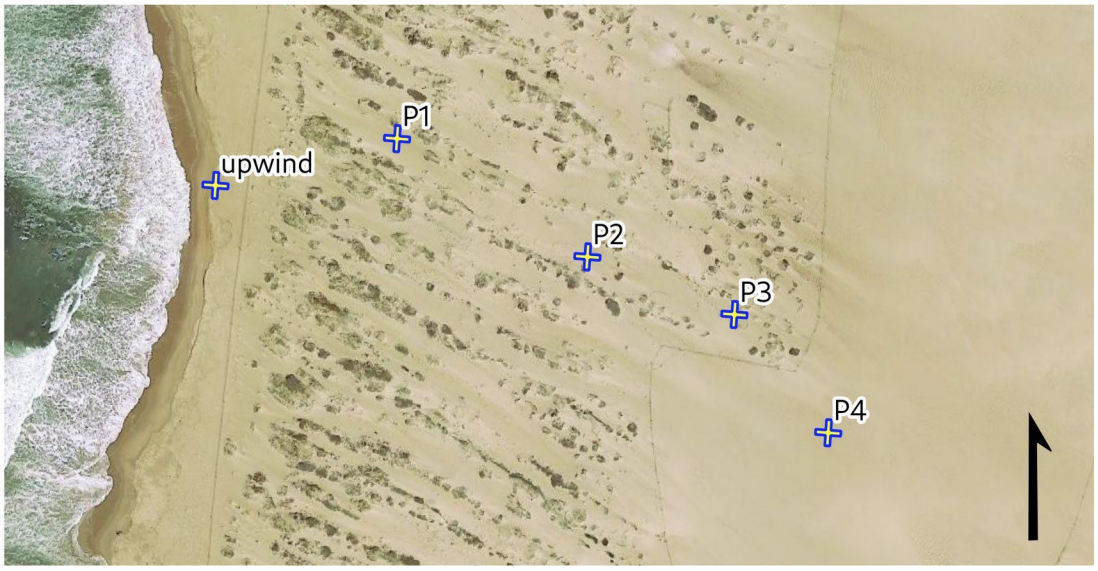

Figure 7: A map of tower locations. The "upwind" tower was fixed, while a second tower was moved to locations P1-P4 throughout the day.

Excellent agreement is observed between the measured and simulated ratio. This ratio serves as a verification that the measured and modeled wind speeds between the two locations in a specified period of time are closely matched even for differing atmospheric conditions. It is important to note that the measurement data were collected in a natural wind field, which varied in both intensity and direction through time and were made in the lee of dune structures that often exceeded the height of the highest sonic anemometer. In contrast the simulated results are modeled as a steady-state condition. Thus, an average relative error of 11.5% is an exceptional result for work outside of a controlled environment as would be found, for example, in a wind tunnel experiment. Moreover, the simulated results show a decrease in the ratio with distance into the foredune, which matches the measured results and classical boundary-layer theory.

Table 2: Validation results: modeled and measured wind speed ratios: downwind (in dunes)/upwind (beach). P1 is the measurement position in the foredunes closest to the beach and P4 is furthest from the beach.

	P1	P2	P3	P4
Simulated	0.952	0.866	0.835	0.749
Measured	0.964	0.706	0.897	0.886

3.2 Wind Flow and Shear Stress Across the Oso Flaco Test Section

Surface shear stress is created by the fluid, i.e., air, interacting with the surface topography which the CFD calculates using the Navier-Stokes equations and the set boundary conditions. A visualization of the magnitude of this force on the foredune and back dune topography is shown in Fig. 8. As seen in the upper panel of Fig. 8, the foredune has small areas where the highest shear stresses are observed (i.e., the red colored areas). On the western edge of the foredunes these represent the vegetated areas of the nebkhas (vegetation-topped mounds), which are the first major obstacle encountered by the inlet wind profile. The low area behind the complex foredune form is a region of lower shear. Past this area in the lee of the foredune where the bare sand surface begins to rise in elevation, the shear begins to increase again as a function of increasing downwind distance (lower panel of Fig. 8).

To illustrate the pattern of air flow over the foredunes and further downwind, the model can be used to generate near-wall streamlines that represent the movement of neutrally buoyant particles released into the flow at a height of 10 cm above the ground surface. As the simulations are steady-state, these can also be interpreted as being average path-lines for air molecules. Visualizations of the streamlines for the foredune and non-vegetated dune system behind the foredune can be seen in Fig. 9. This visualization provides insight into the different aerodynamics of the two dune systems. The individual nebkhas of the foredune show very little flow separation, indicating for the most part a very aerodynamic system. In contrast, the non-vegetated transverse dunes show zones of significant flow separation at the dune crests with zones of re-circulation on the lee-side slip faces.

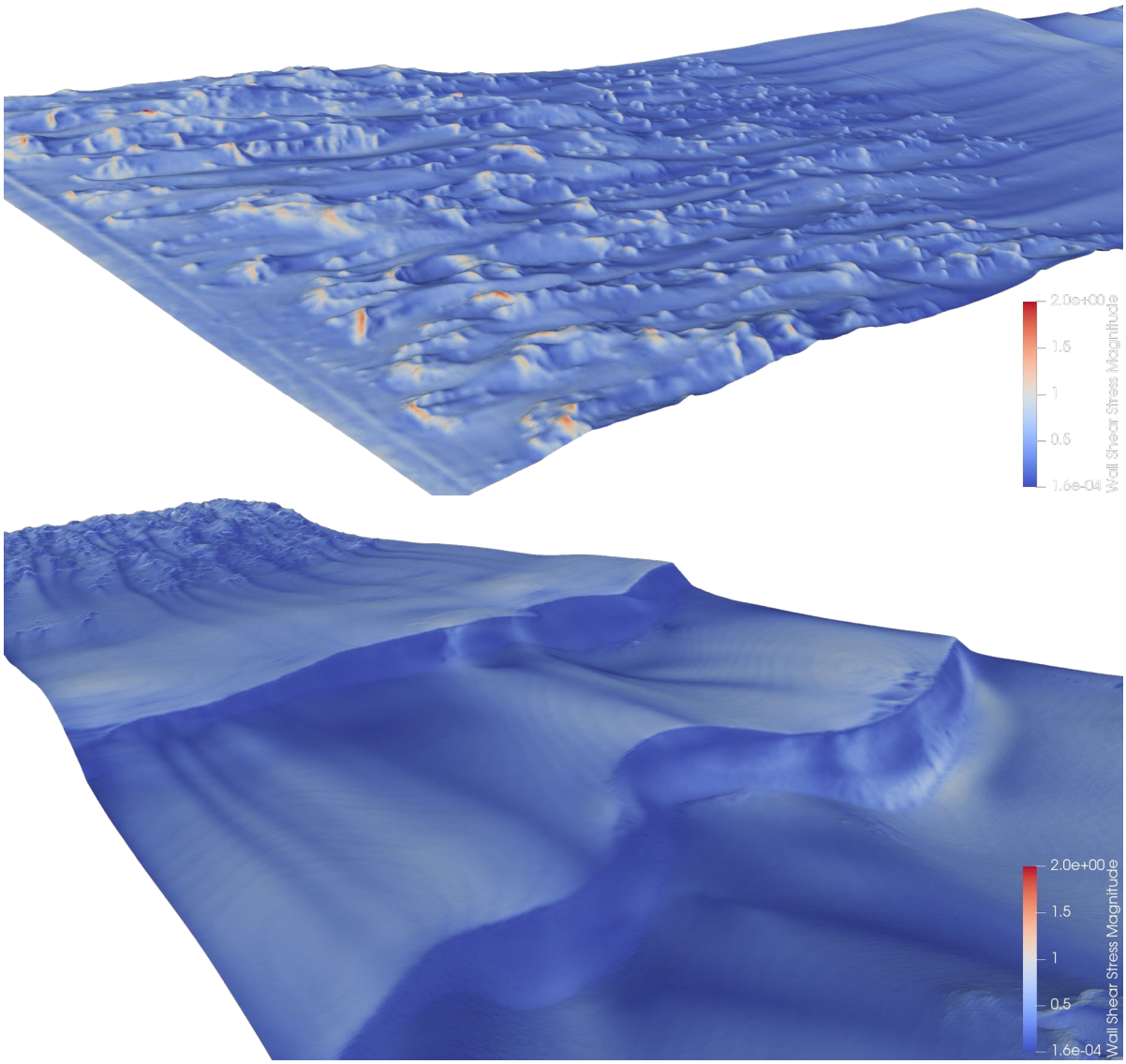

Figure 8: Visualization of the shear stress generated on the topography of the Oso Flaco foredune test area. A view of the foredune looking downwind (left side is west, right side is east) is shown in the upper panel, while a view of the non-vegetated dune system looking upwind (left side of image is west, right side of image is east) is shown in the lower panel.

The aerodynamics of the two dune types motivates an investigation of the role of plants in the shear stress distribution of the foredune. It is obvious from Fig. 8 that the foredune nebkhas receive large amounts of shear, and the low areas between them less so, despite the lack of flow separation. A raster vegetation mask of the foredune was created from spectral data acquired with the ASU/UCSB UAS. A map of this raster is shown superimposed over the magnitude of shear stress in Fig. 9. This image illustrates how plants exert considerable control of the shear stress distribution on the foredune. Areas of high shear are stabilized

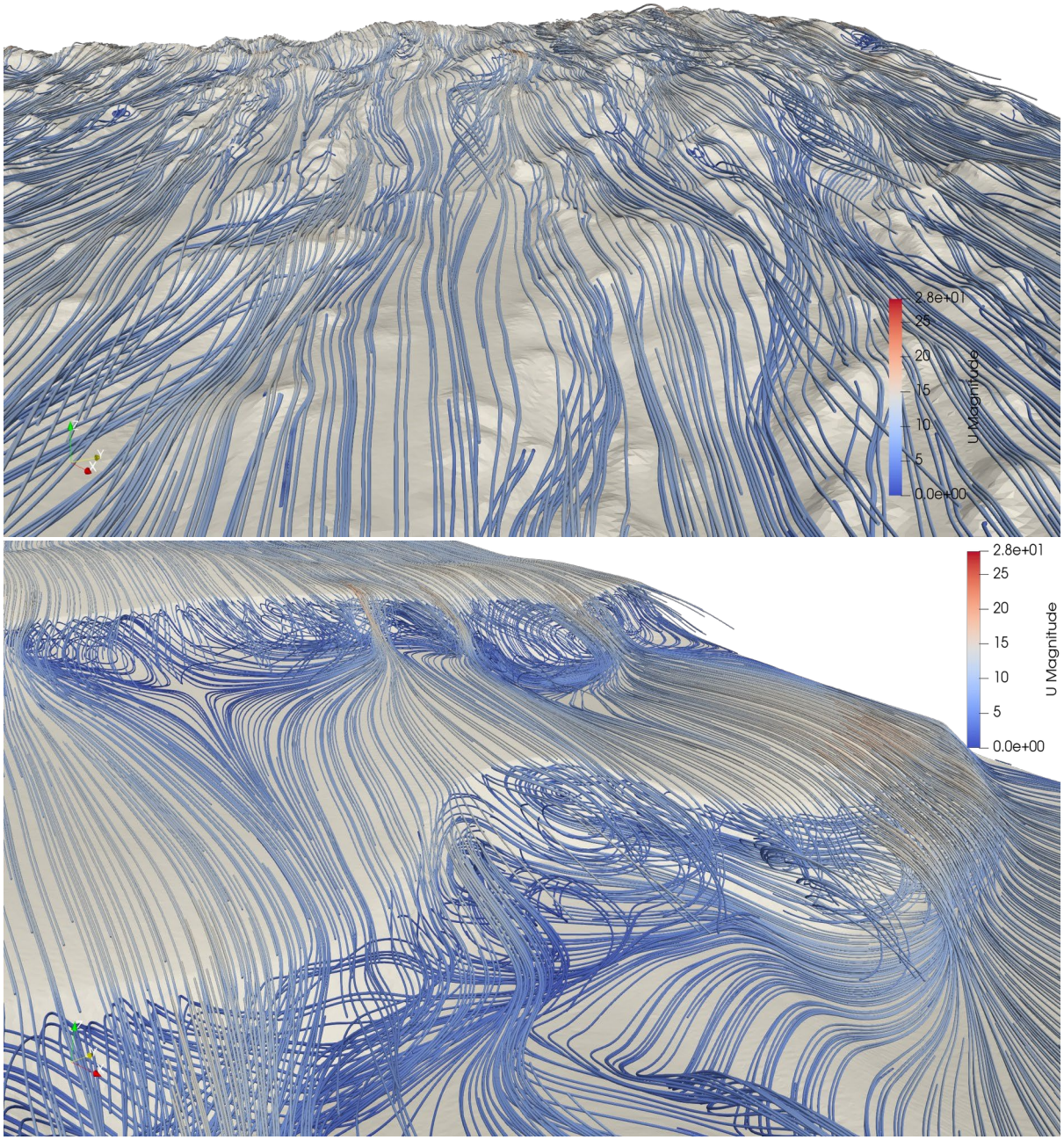

Figure 9: Upper panel: Near-wall streamlines are shown at the foredune, viewed looking upwind (top of image is west [upwind], bottom of image is east [downwind]). Lower panel: Near-wall streamlines are shown for the non-vegetated dune behind the foredune (top of image is west [upwind], bottom of image is east [downwind]).

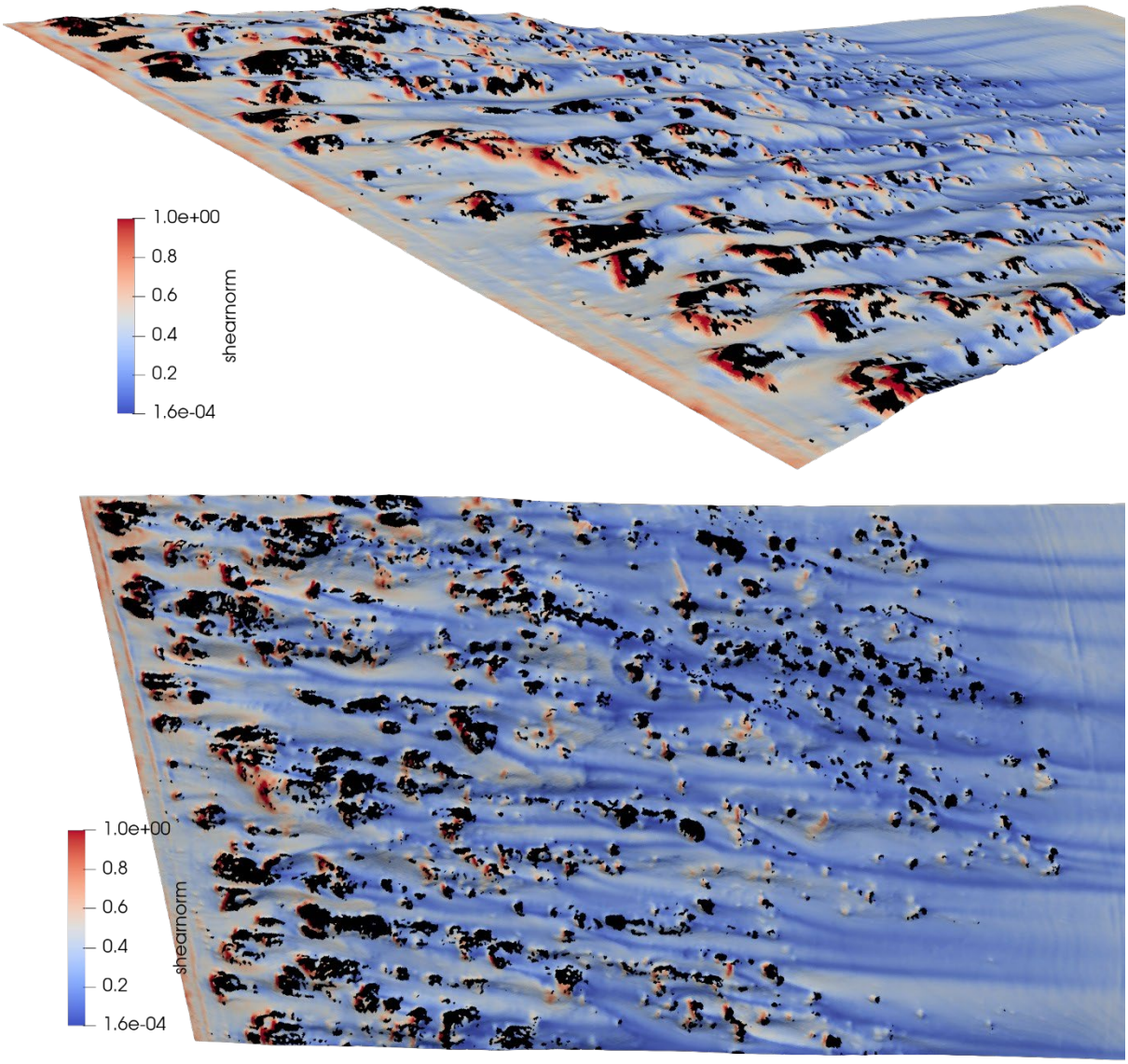

Figure 10: Two views of the Oso Flaco dune test area with a raster vegetation mask of the foredune vegetation superimposed on the foredune shear stress magnitude map. Black denotes locations of vegetation at 10 cm scale. The upwind boundary of the simulation is shown at the left of the image, with flow from left to right.

against entrainment and transport of sand by plants protecting the ng surface (e.g., Wolfe and Nickling, 1983; Gillies et al., 2010, Mayaud and Webb, 2017). In the lee of the vegetation an area of protection, characterized by low shear, is created on the bare ground.

3.3 The Aerodynamic Value of the Foredune

The presence of the foredune inevitably creates aerodynamic effects that affect the shear stress magnitude and distribution within the foredune complex and downwind of the foredunes. However, these are difficult to quantify in field studies, as the foredune cannot be flattened for a paired study. In simulation this can be achieved without high costs or environmental damage. This motivated the creation of the geometry shown in the middle panel of Fig. 2, where the foredune has effectively been flattened, and replaced with a smooth sloping surface, similar to what the shoreline of the ODSVRA looked like prior to 2019, when the foredune restoration project was established. Shear created by the simulation of flow over the Oso Flaco test surface is shown in Fig. 8 (the surface shown in Fig. 2, top panel), which we use to compare with the generation of shear stress across the same space for the hypothetical surface.

A comparison is achieved between surface geometries by performing a surface integration of shear (τ [Pa]. Note 1 Pa is equivalent to 1 N m^{-2} and $\tau=\rho u_*^2$ where ρ is air density [kg m^{-3}]) over each surface. In the first comparison the integral is computed over the rear sections of the two geometries (i.e., Fig. 2 top and middle panels) beginning approximately 300 m from the shoreline through to the end of the sampling domain in the east. The resultant integrated shear is 31,326 N for the unmodified geometry (Fig. 2 top panel), and 32,690 N for the geometry with no foredune upwind (Fig. 2 middle panel). The difference in shear can be attributed to changes in the wind field as it passes over the foredune or the absent foredune, with less energy extracted near the ground when the foredune is absent. For the boundary condition tested in these simulations, removal of the foredune resulted in a 4.4% increase in shear on the dune system for distance ≥300 m from the shoreline.

For the entire domain of the simulations, the integrated shear on the flattened geometry (i.e., all of Fig. 2 middle panel) was 56,530 N, which exceeds the integrated shear of the foredune geometry including the shear on the vegetation of 52,238 N (all of Fig. 2 top panel). This is notable, as the Oso Flaco (test area) foredune geometry has a higher surface area due to the complex topography. Moreover, the foredune topography is characterized by zones of high shear on the vegetated nebkhas, as seen in the upper panel of Fig. 8. For the boundary condition tested in these simulations, removal of the foredune would result in an 8.2% increase in shear on the equivalent sized area with no foredune present. In addition to significant shelter effects behind the foredune, the total effect of the foredune topography is a reduction in shear compared to a flattened surface.

The vegetation on the nebkas produces areas of high shear stress, but critically the area underneath vegetation is protected from this shear. Removing the areas of shear associated with the presence of the vegetation, as it represents areas where sand transport and dust emissions have a low probability of occurrence due to the protection afforded by the vegetation, further decreases the integrated shear on the Oso Flaco test surface (Fig. 2 top panel). The area-integrated shear excluding shear generated on the vegetation is 47,570 N. The total integrated shear on the geometry with the foredune flattened (Fig. 2 middle panel) is 15.8% higher than on the Oso Flaco test surface (Fig. 2 top panel). There is a significant increase in protection due to the presence of the vegetation. For the entire modeling domain

the plant cover is approximately 9%. Within just the foredunes the plant cover is approximately 16%.

3.4 The PM_{10} Emission Reduction Value of the Foredune

The shear stress analysis can be extended to evaluate how the different shear stress conditions on the actual and hypothetical surfaces affect PM_{10} mass emissions. An evaluation is made for the emissivity conditions represented by the mean riding area and mean non-riding area emissivity relations (DRI, 2021). Previous monitoring with the PI SWERL instrument has demonstrated higher emissions in the La Grande Tract as compared to Oso Flaco (Gillies and Etyemezian, 2015; Gillies et al., 2021). The average emissions (E, mg m^{-2} s^{-1}) relation for the riding area as a function of shear velocity u_* (m s^{-1}) is:

$$E = 23.65(u_*)^{5.59}, \quad (6)$$

The average emissions relation for the non-riding area as a function of shear velocity u_* is:

$$E = 21.51(u_*)^{6.85}. \quad (7)$$

The model derived shear values (τ) were converted to u_* (remember, $\tau=\rho u_*^2$ where ρ is air density [kg m^{-3}]) and then integrated across the surface areas of the actual and hypothetical geometries. The total integrated emissions are in units of mg s^{-1}. Total emissions and the corresponding total shear force are shown in Table 3. The third scenario of an unmodified topography (i.e., Oso Flaco test surface, Fig. 2 top panel) shows significantly lower emissions than the scenarios that neglect vegetation sheltering or have a flattened foredune. Total emissions calculated with the non-riding emissions curve are approximately half those calculated with the riding area emissions curve in all cases.

Table 3: Shear and total integrated emissions for the surfaces with the foredune flattened (Scenario 1), the unmodified surface neglecting the effects of plant cover (Scenario 2), and the unmodified surface with zero emissions from areas that are vegetated (Scenario 3).

	Scenario 1	Scenario 2	Scenario 3
Total Shear Force (N)	56530	52238	47570
Riding Total E (mg s^{-1})	163412	159654	134683
Non-riding Total E (m g s^{-1})	89458	88384	70387
Riding Total E (mg m^{-2} s^{-1})	.972	.950	.802
Non-riding Total E (mg m^{-2} s^{-1})	.533	.526	.419

3.5 Foredune Downwind Sheltering Effects

Being able to quantify the sheltering effects of the foredune will be a useful tool for planning remediation projects and evaluating secondary effects on dust emission on the lee side. This is the motivation for the geometry that situates a flat plane behind the foredune, as seen in the bottom panel of Fig. 2. As the actual shear on a given land surface may vary widely depending on the topography behind the foredune, the flat surface offers the best scenario for a generalized result. Shear stress was calculated from a simulation run for this surface using the boundary conditions outlined in Section 2.3. A plot of the average shear stress on the foredune followed by the flat surface (Fig. 2, bottom panel) is shown in Fig. 11. Note that the averaging is across the width of the modeling domain at each length interval along the west to east transect and not just along a narrow corridor through the foredune. The recovery of this relation beginning at zero on the figure (i.e., 0 on the x-axis) illustrates the sheltering behind the foredune. Figure 12 shows the shear stress relation past the foredune (i.e., 0 on the x-axis) in Fig. 11 normalized against the maximum shear stress, which occurs ≈300 m past the end of the foredune. Figure 12 shows that in the lee of the foredune a zone of shear is created that reaches a minimum at the zero point and then increases non-linearly with

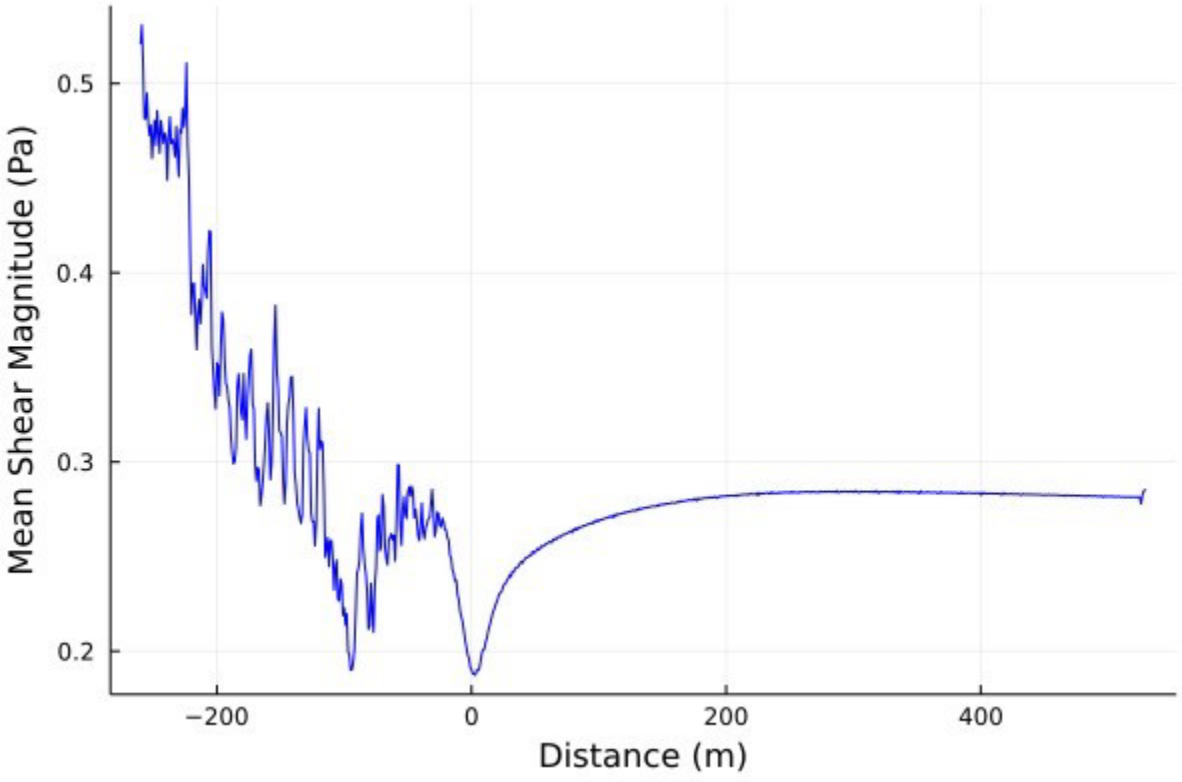

Figure 11: Mean shear magnitude as a function of distance in the freestream direction for the geometry shown in Fig 2., bottom panel. The leeward edge of the foredune is located at x = 0.

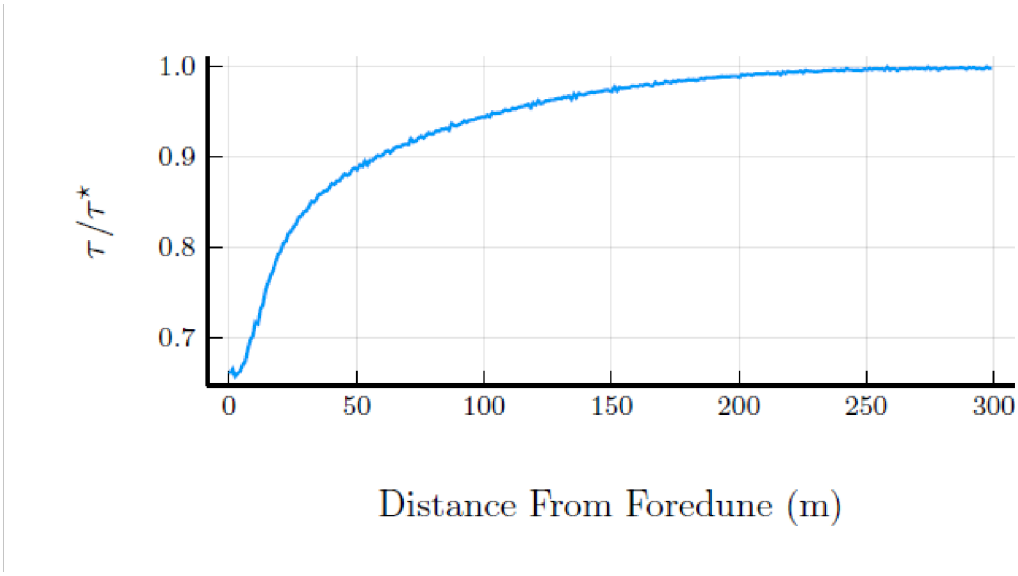

Figure 12: Mean shear τ normalized by maximum shear τ^* as a function of distance.

increasing downwind distance. The shear stress at the surfaces reaches approximately 90% of its potential value within a 50 m of fetch behind the foredune.

The shear stress along the west to east length of the domain for the Oso Flaco foredune test area (Fig. 2 top panel) and the geometry with the foredune flattened (Fig. 2 middle panel) are compared with Fig. 11 in Fig. 13.

Figure 13 provides a clear indication of the value of a foredune similar to Oso Flaco to modulate surface shear stress that favors a lower production of dust emissions when compared to the condition of an absent foredune. As a first approximation of the potential secondary effect of the foredune on dust emissions specifically in their lee, a recommendation is to apply the relation shown in Fig. 12 to the grid cells in the DRI dispersion model to modulate the CALMET estimated shear velocities from the zero point in Fig. 13 through to a distance equivalent to the start of the large transverse dunes.

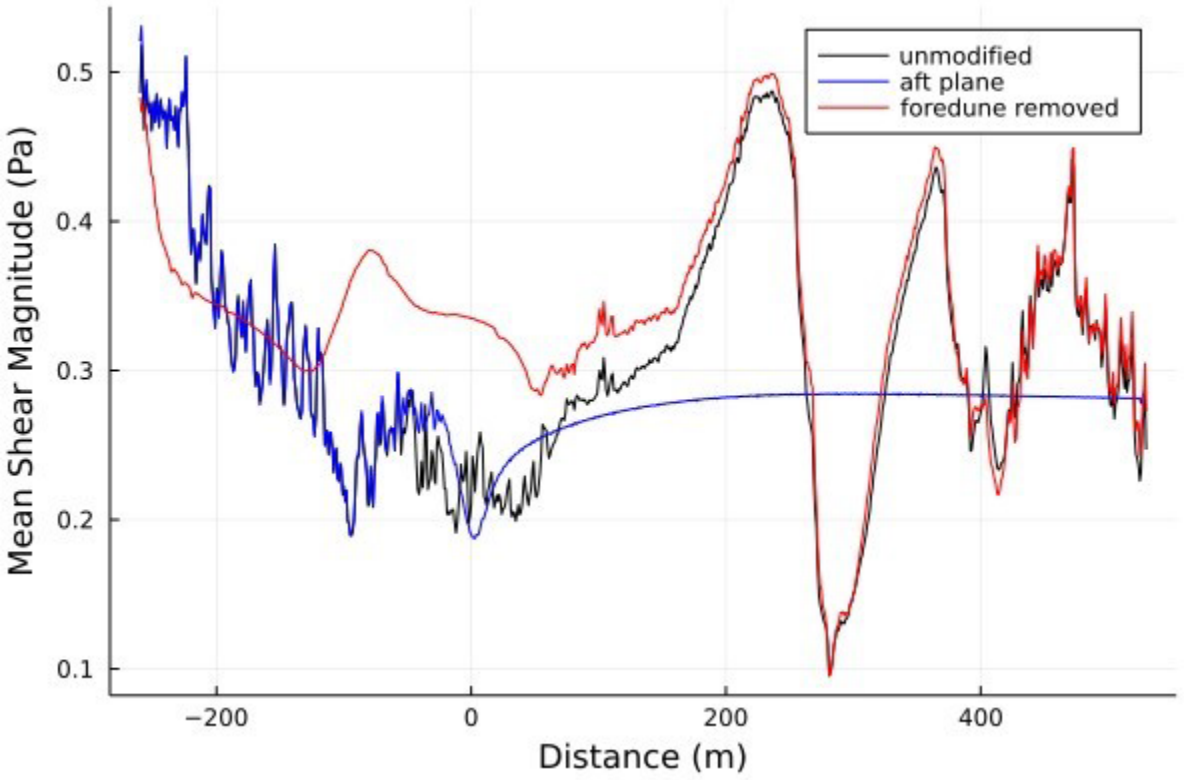

Figure 13: Mean shear magnitude as a function of distance in the freestream direction for the Oso Flaco geometry (Fig. 2, top panel represented by black line), the geometry with the foredune flattened (Fig. 2, middle panel represented by red line), and the geometry with the foredune followed by a sloping sand surface (Fig. 2, bottom panel represented by blue line). The downwind edge of the foredune is located at $x = 0$.

References

Gillies, J.A., Etyemezian, V., 2015. Addendum to the PI-SWERL Report of Etyemezian et al. (2014) Particle Size Distribution Characteristics and PI-SWERL PM_{10} Emission Measurements: Oceano Dunes State Vehicular Recreation Area. Report prepared by the Desert Research Institute for Off-Highway Motor Vehicular Recreation Division, California State Parks, 1725 23rd Street, Suite 200, Sacramento, CA 95816, July 13, 2015 (available upon request).

Gillies, J.A., E. Furtak-Cole, G. Nikolich, V. Etyemezian (2021). The role of off highway vehicle activity in augmenting dust emissions at the Oceano Dunes State Vehicular Recreation Area, Oceano CA. *Atmospheric Environment X* (accepted).

Gillies, J. A., W. G. Nickling, and N. Lancaster (2010), Vegetative roughness controls on wind erosion: a shear stress partitioning approach, paper presented at *Ninth International Conference on Dryland Development: Sustainable Development in the Drylands – Meeting the Challenge of Global Climate Change*, Alexandria, Egypt, 2010.

Mayaud, J. R., and N. P. Webb (2017), Vegetation in drylands: Effects on wind flow and aeolian sediment transport, *Land*, 6(64), doi:10.3390/land6030064.

Wolfe, S. A., and W. G. Nickling (1993), The protective role of sparse vegetation in wind erosion, *Prog. Phys. Geogr*., 17, 50-68.

Appendix A: CFD Development and Processing

The following summary contextualizes the scope of producing quality CFD results:

- Each simulation takes 4800 core-hours of computing.
- Approximately 15 Julia codes were written to process the input and output of data.
- Over 30 meshes were produced before the final configuration was set.
- Each simulation produces velocity and pressure at >20 million points within the modeling domain.
- Output from each simulation is ≈98 GB of data.

A typical CFD workflow is shown as a flowchart in Fig. A1. The process begins with creation of a surface geometry, which requires creation of a 3D surface from a Digital Elevation Model (DEM). Next a mesh is designed to discretize the domain for the solver. The solver and post processing utilities are run on a computing cluster (University of Utah). The simulation output is checked for integrity. The mesh is then re-designed to increase the quality of the result, and the processes is repeated. When sufficient quality is achieved, based on evaluation of model convergence metrics, additional post processing with custom codes and visualization tasks are performed. A cross section of the computational mesh is shown in Fig. A2, which needed to be carefully designed to resolve turbulent flow features over the topography.

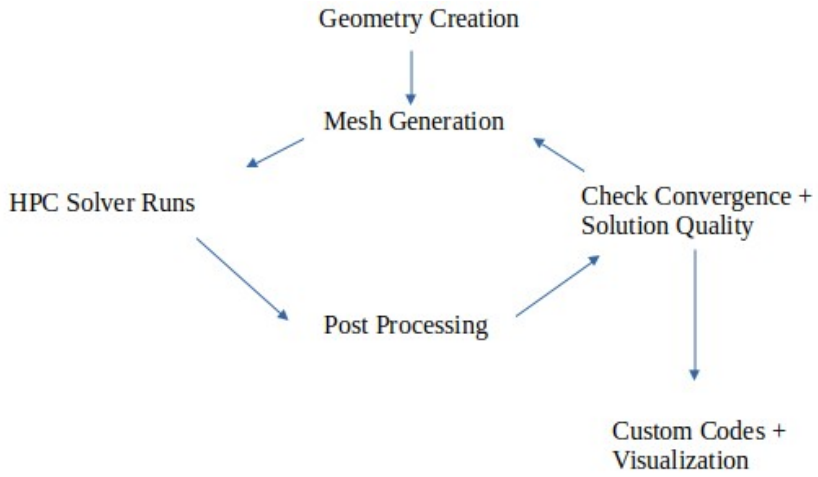

Figure A1. The workflow process for developing and processing the CFD.

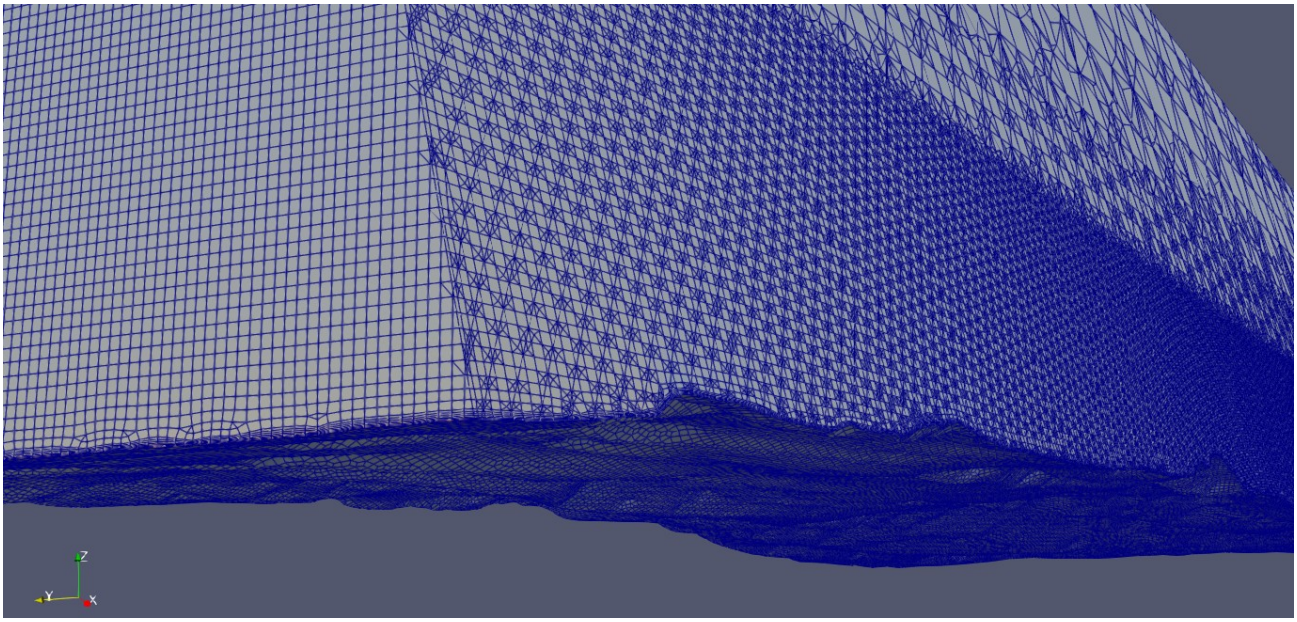

Figure A2. A cross section of the computational mesh developed for the Oso Flaco foredune test area.